Modeling Compressive Stress Distributions at the Interface between a Pallet Deck and Distribution Packaging

Jiyoun Yoo

Dissertation submitted to the faculty of the Virginia Polytechnic Institute and State University in partial fulfillment of the requirements for the degree of

Doctor of Philosophy
in
Wood Science and Forest Products

Joseph R. Loferski, Chairman
Marshall S. White, Co-Chair
Daniel P. Hindman
Surot Thangjitham

September 8, 2011
Blacksburg, VA

Keywords: Compressive stress distributions, Pallet decks, Packaging, Beam on an elastic foundation, Pallet and packaging stiffness, Joint fixity, Modeling, Testing, Modulus of Elasticity, Rotation modulus

Modeling Compressive Stress Distributions at the Interface between a Pallet Deck and Distribution Packaging

Jiyoun Yoo

(ABSTRACT)

Three components, a pallet, packaging, and material handling equipment, of the unit load portion of the supply chain are physically and mechanically interacting during product storage and shipping. Understanding the interactions between two primary components, a pallet and packaging, in a unit load is a key step towards supply chain cost reduction and workplace safety improvement. Designing a unit load without considering physical and mechanical interactions, between those two components, can result in human injury or death caused from a unsafe workplace environment and increased supply chain operating costs, due to product damage, high packaging cost, disposal expense, and waste of natural resources.

This research is directed towards developing predictive models of the compressive stress distributions using the principle of the beam on an elastic foundation and experimentally quantifying the compressive stress distributions. The overall objective of this study is to develop a model that predicts compressive stress distributions at the interface between a pallet deck and packaging as a function of: pallet deck stiffness, packaging stiffness, and pallet joint fixity. The developed models were validated by comparison to the results of physical testing of the unit load section. Design variables required for modeling included Modulus of Elasticity (MOE) of pallet deckboards, Rotation Modulus (RM) for nailed joints, and packaging stiffness.

Predictive models of the compressive stress distributions were non-uniformly distributed across the interface between pallet deckboards and packaging. Maximum compressive stresses were observed at the deckboard ends over stringer segments. All predictive compressive stress

distributions were influenced by pallet deck stiffness, packaging stiffness, and joint fixity. The less the joint fixity the greater the pallet deck deflection. The stiffer deckboards are more sensitive to joint fixity. For predictive compressive stress distribution models, the measure of the stress concentrations was the Compressive Stress Intensity Factor (SIF), which was the ratio of the estimated maximum compressive stress to the applied stress. Less stiff pallets and stiffer packaging resulted in greater SIF for all end condition models. SIF was reduced by stiffer joint, stiffer pallet deck and more flexible packaging. The stiffer the pallet deck and pallet joint the greater the effective bearing area. The lower stiffness packaging resulted in the greater effective bearing area with all three packages. The predicted effective bearing area was more influenced by pallet deck stiffness than the packaging stiffness.

The developed prediction models were validated by comparison to experimental results. All prediction models fell within 95% confidence bounds except the 3/8-inch deck with free ends and 3/4-inch deck with fixed ends. The difference between predicted and measured results was due to a limitation in pressure sensor range and test specimen construction for the free end model and fixed end model, respectively.

The results show effects of pallet deck stiffness and packaging stiffness on SIFs with percentage changes ranging from 2 to 26% (absolute value of change) for all three end conditions. The sensitivity study concluded that changing both pallet deck stiffness and packaging stiffness more significantly influenced the SIFs than bearing areas.

Table of Contents

List of Figures

Unless otherwise stated, all images are property of the author.

List of Tables

CHAPTER 1

1.0 Introduction

Since the 1940s, the pallet has been used as a fundamental device in the transportation and storage of consumer and industrial products in a unit load form. Products are arranged and restrained to a pallet to be stored, picked up, and moved between two locations as a single mass in the unit load form (White & Hamner, 2005). A typical unit load is comprised of corrugated shipping containers stacked on a pallet and stabilized with plastic stretch wrap. Three components, a pallet, packaging, and material handling equipment, of the unit load portion of the supply chain physically and mechanically interact during product storage and shipping.

Today, more than 450 million new pallets are manufactured annually in the United States. It is estimated that 1.9 billion pallets, of which approximate 95 percent are wooden, are currently in use throughout the United States (White et al, 2006) (FPInnovation™ , 2009). In the United States, approximately 90 percent of packaged products are shipped on pallets. Recently, due to the Free Trade Agreement (FTA), there has been a rapid increase in global transportation and distribution within which packaging plays an important role in protecting products from various hazards in static and dynamic environments of unit load handling. Packaging accounts for the largest component, 35 to 40 percent, of municipal solid waste in the United States (Liu & Liptak, 1999). Unfortunately, due to poor or improper packaging, about $10 billion of product damage occurs annually in the U.S. during the distribution cycle of the supply chain (Clancy, 1988). Materials handling related injuries resulted in 25 percent of all occupational injuries, with over half of those linked to packaging failure (White & Hamner, 2005). Excess or unnecessary packaging, inappropriately designed pallets, and unsafe work-places are responsible for product damage and human injury or death.

Commercial computer software programs such as PDS®, TOPS® and CAPE® have been used to

aid the pallet industry and packaging designers over the past few decades. PDS® provides prediction models of pallet design performance, and TOPS® and CAPE® allow users to optimize packaging use in terms of cost and space utilization. However, these programs do not predict structural performance of interactive unit load components in the entire unit load system. No models for both geometric fit and structural performance of the interactive components have been developed.

Understanding the interactions between two primary components, a pallet and packaging, in a unit load design is a key step towards supply chain cost reduction and workplace safety improvement. The results of this study will have an impact on reducing other economic losses caused by inefficiencies in the use of pallets and packaging as well.

1.1 Problem Statement

In component-based unit load design, each component of the unit load material handling system is designed separately by an independent design community. Redesign of a single component can potentially influence the performance of other components, and therefore affect the function of the entire unit load system. Designing a unit load without considering physical and mechanical interactions between the three primary components can result in human injury or death and increased supply chain operating costs, due to product damage, high packaging cost, disposal expense, and waste of natural resources. The design integration of the three components determines the effectiveness and efficiency of the entire unit load system within the supply chain.

Vendor designers are responsible for reducing product cost by creating more efficient unitization of raw materials in the system. Raw material is the largest cost component of each of the three components to the unit load portion of supply chain. Reducing the raw material cost by redesigning the packaging, pallets, or material handling equipment is a key to reducing the entire supply chain cost.

Historically, for modeling convenience, it has been assumed that a uniformly distributed load reasonably represents the load distribution of boxed or bagged products. However, in reality, non-uniform stress distribution at the interface of pallet decks and distribution packaging are observed during product storage and shipping. Figure 1 presents non-uniformly distributed stresses and stress concentrations within a unit load. Stress concentrations occur at the interface of the shipping container and pallet stringers when the pallet deck bends under the weight of the load. The stress concentrations may lead to failure of either packaged products or a pallet, or both, while in storage. Measuring and predicting the non-uniform stress distributions and stress concentrations will allow supply chain operations to better optimize pallet and packaging designs. This research is directed toward experimentally quantifying stress distributions and developing predictive models of the stress distributions using numerical analysis.

1.2 Objectives

This study includes the following objectives:

- The overall objective of this study is to develop a model that predicts compressive stress distributions at the interface between a pallet deck and packaging as a function of:
    - Pallet deck stiffness
    - Packaging stiffness
    - Joint fixity

- Determine the effect of packaging stiffness on compressive stress distributions and pallet deck deflections
- Determine the effect of pallet deck stiffness on compressive stress distributions and pallet deck deflections
- Determine the effect of joint fixity on compressive stress distributions and pallet deck deflections

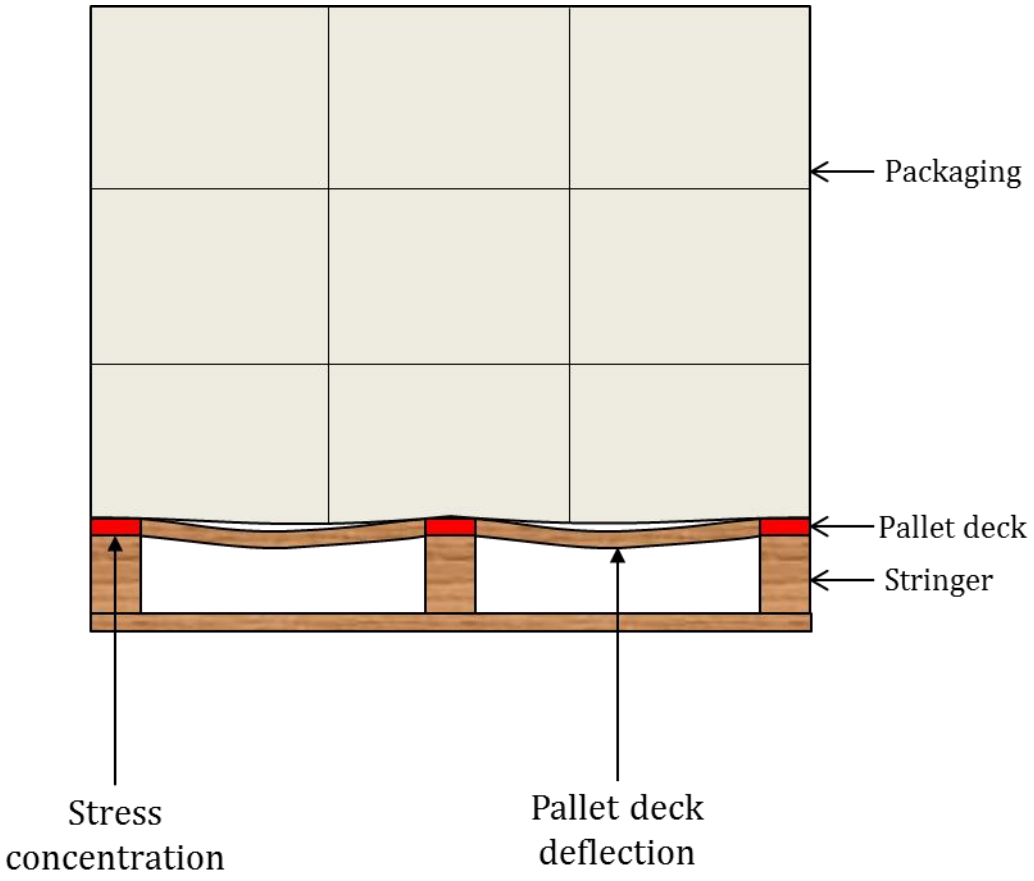

Figure 1. A schematic diagram of compression stress concentrations and non-uniform compression stress distribution between packaging and the pallet deck

1.3 Scope of Research

This dissertation explored mathematical models based on the principle of the beam on an elastic foundation that predict pallet deck deflections caused by the compression loads applied on the top of the packaging as well as stress distributions at a pallet deck/packaging interface. To validate the established models, several different simplified unit loads were tested. The scope of theoretical models developed in this research is:

- Differential equation solution based on the theory of beams on an elastic foundation is used to develop predictive models
- An one-dimensional beam element is used to develop models

The developed models were validated with the following scope of experimental study:

- Pallet deck stiffness: two different deck thickness
  - 3/4 inch
  - 3/8 inch
- Packaging: three different stiffness levels
  - Empty corrugated fiberboard container
  - 12 plastic bottles in a corrugated fiberboard container
  - 16 flour sacks in a corrugated fiberboard container
- Joint fixity: three joint conditions
  - Free ends
  - Semi-rigid joints (nailed)
  - Fixed ends (glued)
- 16 x 10 x 8 inch- RSC (Regular Slotted Container) C-flute single-wall corrugated box
- Pressure sensor type: two different sensitivities
  - 5 psi
  - 30 psi

- Floor stack support condition is exclusively considered for the pallet support condition simulated

The development procedures for the numerical models are described in the following chapters. Chapter 2 includes background information related to characteristics and modeling techniques for each of the unit load components. In chapter 3, input properties required for models are described and test procedures are presented to explain how the input values were determined. Chapter 4 describes the modeling methodologies used to obtain pallet deck deflection models and compressive stress distribution models. Experimental procedures used to verify the developed models and the results of a sensitivity study of independent design variables are described in chapter 5. Lastly, chapter 6 is a summary, conclusions and limitations of this research. Recommendations for future study are also discussed.

CHAPTER 2 LITERTURE REVIEWS

2.0 Introduction

In this chapter, section 2.1 focuses on a discussion comparing the advantages of systems-based design of unit loads to component-based design. The characteristics of pallet components under the stack support condition and the pallet joint stiffness are identified in section 2.2. Section 2.3 contains descriptions of the effect of load-bridging on pallet design. The general information from a previous study, which investigated modeling boxed products related to distribution packaging and corrugated containers, is described in section 2.4. The last section 2.5 examines the fundamental concept of beams on an elastic foundation theory and general solution of beam deflection on the elastic foundation.

2.1 Systems-Based Design of Unit Loads

There are three components to the unit load portion of product supply chains. These are: 1) pallets, 2) packaging containing products and 3) unit load material handling equipment. These components mechanically interact with each other throughout product distribution supply chains. A unit load is defined as a single item, a number of items, or a bulk material, that is arranged and restrained so that the load can be stored, picked up, and moved between two locations as a single mass (Tanchoco & Agee, 1980). A typical unit load comprises corrugated fiberboard containers with products stacked on a pallet and stabilized with plastic stretch wrap. The unit load system was developed to enable easy and efficient storage and distribution of products. Consequently, most consumer and industrial products are shipped in the unit load form. It is estimated that two billion or more unit loads are in use on a daily basis throughout the United States (Hamner & White, 2005).

The primary goal of the systems-based design of the unit load portion of the product supply chain is to reduce supply chain operation costs. According to White (2005), a more systematical

supply chain design process can improve the efficiency of storage and shipping space utilization by 6 to 13 percent. The systems-based design could also reduce global wood consumption for pallet manufacture by an average of 6.7 percent annually and reduce the mass of U.S. packaging by 3.2 million tons annually. This would, in turn, reduce packaging cost and fuel consumption (White et al, 2006).

Component-based design is the traditional method of unit load design. All components of the unit load are developed separately, at different locations, by individual designers charged with reducing their own product cost. Since redesign of one component will influence the performance of other components within the unit loads, the ultimate consequences of the component-based design include product damage, waste of natural resources, high packaging cost, and occupational injuries. White et al (2006) note that 25 percent of all occupational workplace injuries occur during material handling processes, with over half of those related to packaging failure. In 2000, 566 fatalities and 155,000 serious injuries occurred during unit load warehousing and shipping. Packaging failure results in falling boxes and containers which can cause serious human injuries or death in warehouses.

Systems-based unit load design is developed based on understanding how the three components of a unit load supply chain physically and mechanically interact during transit, storage, and distribution. According to White et al (2006), unit load component interactions considered in the systems-based design include:

- Vibration and unit load resonance during distribution
- Load bridging and unit load deformation
- Equipment spans and unit load deflections
- Interfacial friction and load stability
- Compression stress redistribution and product protection
- Vertical stabilization versus horizontal stability

The systems-based design requires supply chain component designers to work together to optimize component costs, reduce waste, improve work place safety, and protect the environment. The systems-based design might have limitations on time and place to get all designers together. In the United States, 12 to 15 percent of the annual operational expense of logistics system can be eliminated using systems-based design instead of component-based design. Furthermore, by means of systems-based design total annual packaging costs can be reduced by 8 to 18 percent (White, 2007).

2.2 Pallet Design

A pallet is a flat and portable structure on which products are efficiently assembled, stored, stacked and transported as a single unit load. More than 450 million new pallets are manufactured annually in the United States, and it is estimated that 1.9 billion pallets are currently in use in the United States (White et al, 2006). Wood has been, and still is, the predominant raw material used in more than 90 percent of all pallets manufactured today. The wooden pallet is a reusable, repairable, and recyclable device for material handling. The relatively high performance and low cost of wood pallets improve the efficiency of material handling.

Because wood is a biological material, its physical and mechanical properties are variable. The mechanical properties are affected by natural characteristics such as density, knots, slope of grain, and moisture content. Wood properties are further complicated by orthotropic characteristics (Bodig & Jayne, 1993). Consequently, the quality of lumber used to make pallets will have a significant effect on handling, storage, and transportation performance. The pallet natural characteristics that occur during manufacturing can further reduce performance when the pallet is actually utilized. As pallet performance has a significant influence in the efficiency of material handling and entire unit load systems, understanding pallet performance is a critical step to improving the performance of the unit load and supply chain logistics system. An improper pallet

design can result in product damage, tipping stacks, and occupational injuries when pallets are handled, shipped, and stored within the supply chain distribution environment. High quality pallets can be designed by carefully managing pallet specifications to accommodate the packaging and materials handling systems.

During a distribution cycle, pallets are subjected to a wide variety of static and dynamic stresses. A reliability-based design procedure, the Pallet Design System (PDS®), was developed through the cooperation of the Pallet and Container Research Laboratory at Virginia Tech, the National Wood Pallet and Container Association (NWPCA), and the U.S Forest Service to insure safer and more reliable pallets. The PDS enables pallet manufactures and users to predict the maximum load capacity, pallet deflection, optimum member dimensions, life expectancy in specific environments, and estimated cost-per-use (Loferski, 1985). To properly use the pallet design system it is necessary to understand the general types of pallet loads and pallet support conditions during use.

To characterize the actual pallet loads and support conditions, Geohring and Wallin (1981) conducted an on-site survey of 234 different loading situations in 88 material handling environments. They classified the support conditions into three groups as illustrated in Figure 2. Results from the survey indicated that 69 percent of pallets were loaded and dead-piled into stacks. 21 percent of pallets were Racked Across the Stringers (RAS) and 10 percent were Racked Across the Deckboards (RAD). To be able to predict structural performance of pallets for these support conditions, suitable models for support mechanisms are necessary. The factors thought to affect pallet response to stresses in use are pallet deck stiffness, joint stiffness, as well as the load and support conditions.

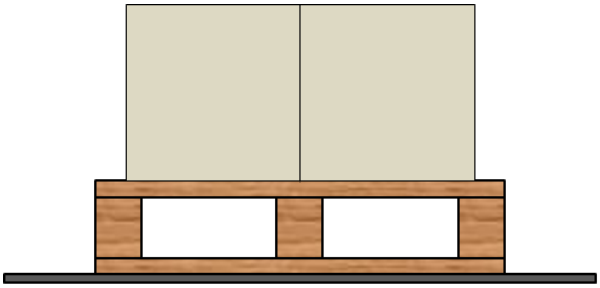

Floor Stacked (69%)

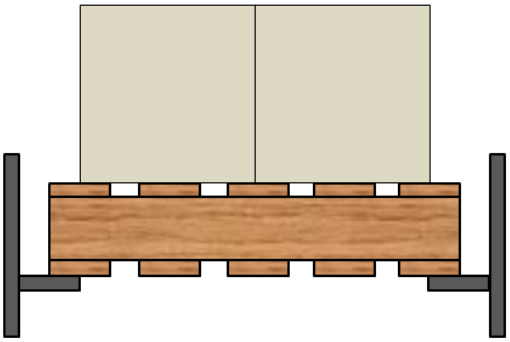

Racked Across Stringers (21%) (RAS)

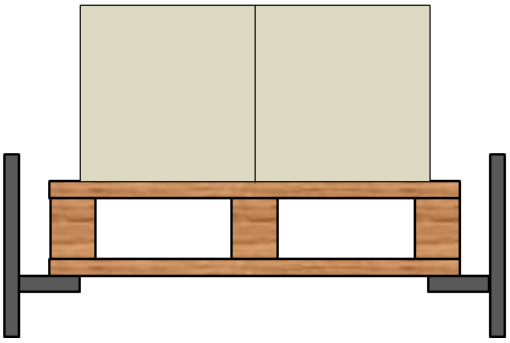

Racked Across Deckboards (10%) (RAD)

Figure 2. General unit load support conditions

2.2.1 Pallet Components in Stack Support Condition

The floor stack mode for pallets is the most commonly used support mode in warehouses. Unit loads are often stored on the floor and stacked on top of one another. In the stack support condition, the top deck of the bottom pallet and the bottom deck of the second pallet are critical structural members. Stringers act as supports for the top deck when the pallet is supported in the floor stack. Some load is transferred to the support directly through the stringers. The remaining load is distributed over the deckboards and is transferred to the stringers as bending reactions (Loferski, 1985). The span between stringers, the number of stringers, and deckboard stiffness are crucial variables affecting load distributions across pallet decks.

Collie (1984) characterized load distributions for pallets used in the stacked support condition. Pallet stiffness, load type, and load configuration had no significant influence on the load redistributions between pallets stacked on one another in the stack support mode. The stack load distributed to the top deckboard of the bottom pallet was dependent on the number of stacked pallets. Further work on the load effects in stacked pallets was carried out by Loferski (1985), who developed analysis methods to compute the load effects, bending stress, and deckboard deflection in the stack support condition. The analysis method was verified by experimentally obtained results and showed good agreement.

To understand the structural behavior of a wood pallet, the material properties of the lumber used to construct the pallet must be known. The stack support condition top and bottom deckboards are assumed as simple or continuous beams and deflection and strength of the decks are independently evaluated. The overall pallet stiffness is dependent on stiffness or modulus of elasticity (MOE) of individual pallet components. Pallet deckboard stiffness, which indicates the ability to safely support loads and to meet serviceability limitations, is one variable that influences the overall pallet performance. Details of the equation for MOE are described in chapter 3. Yoo (2008) studied of the effects of deckboard stiffness on the stress distributions between a pallet deck

and packaging in the stack support condition. Fifteen to twenty-seven percent higher stresses were distributed over a stiffer deckboard when the compression load was applied in the stack condition. The deckboard bending stress level is the crucial design factor when estimating the maximum load-carrying capacity of stacked pallets. An excessively deflected deckboard restricts unit load handling equipment access. The bending stress and deflection of decks of the stacked pallet are the significant factors while the compression perpendicular to grain of the stringers is not considered a design factor (Loferski, 1985).

2.2.2 Pallet Joint stiffness

Typical joints for stringer and block wooden pallets are fastened with nails. When loaded, nailed pallet joints exhibit semi-rigid, nonlinear stiffness with high variability. The stiffness characteristics of the nailed joint have been investigated since the joint stiffness is a critical variable affecting the structural performance of pallets. Wilkinson (1983) conducted an experimental study to establish moment-rotation curves for different numbers of fasteners and characteristics. The study of the moment-rotation relationship for block pallet joints was carried out by Samarasinghe (1987).

Prior to the 1970's the traditional approaches to the analysis and design of nailed joints were based on the simplified assumption that the connection between members was either rigid or pinned. These are simply extreme cases of actual structural behavior of nailed joints. Under either of these two conditions, predicted forces and deflections are inaccurate and lead to either conservative or under-designed joints.

Analog models have been developed to model the nailed joint behavior by representing the joint as a spring element. Zero length spring elements were used to simulate the behavior of the semi-rigid nailed joint of stringer pallets and block pallets in the racked across deckboard (RAD) mode (Loferski, 1985 & Colclough, 1987). The stiffness values of the spring elements can be

determined by rotational stiffness of tested joints. In the stack mode, deckboard-stringer joint models were assumed pinned. However, since these joints were really semi-rigid connections, some moment transfer should occur at the supports. The analysis procedure did not account for the moment transfer response. Loferski (1985) mentioned that this was the reason for the difference between predicted and actual joint stiffness. Samarasinghe (1987) established theoretical and empirical methods for estimating pallet joint behavior based on fastener and wood characteristics.

Several investigators mentioned that the response of a pallet to stable loads is significantly influenced by out-of-plane rotation (rotation modulus) as illustrated in Figure 3 (Loferski, 1985, Colclough, 1987, & Samarasinghe, 1987). The joint rotation modulus represents the degree of fixity of a nailed joint under moment. The rotation modulus is defined as the ratio of the applied moment to the angular rotation (Kyokong, 1979). The rotation modulus can be computed by the slope of the tangent to the linear portion of the moment-rotation curve (Samarasinghe, 1987). Details of equations used in current study are in chapter 3.

2.3 The Effect of Load-Bridging on Pallet Design

Unit loads are classified into three groups based on the stiffness, strength, and form of the products unitized onto pallets: 1. large rigid materials which have great strength to resist crushing and uniform geometry to allow direct construction of a unit load, such as lumber or bricks; 2. irregular shaped strong materials which require secondary packaging (cartons or boxes) to be stacked on a pallet, such as canned goods, grocery items, or electronic equipment; 3. bagged products capable of compressing into a relatively flat surface such as grains, feedstuff, or cement (Tanchoco & Agee, 1980). The load distribution across the pallet decks will be different for each of this situation because of load-bridging.

Load-bridging is a phenomenon which describes the effect of packaging stiffness on the stress distribution applied to the pallet. When the pallet is loaded with stiff packaged products, the

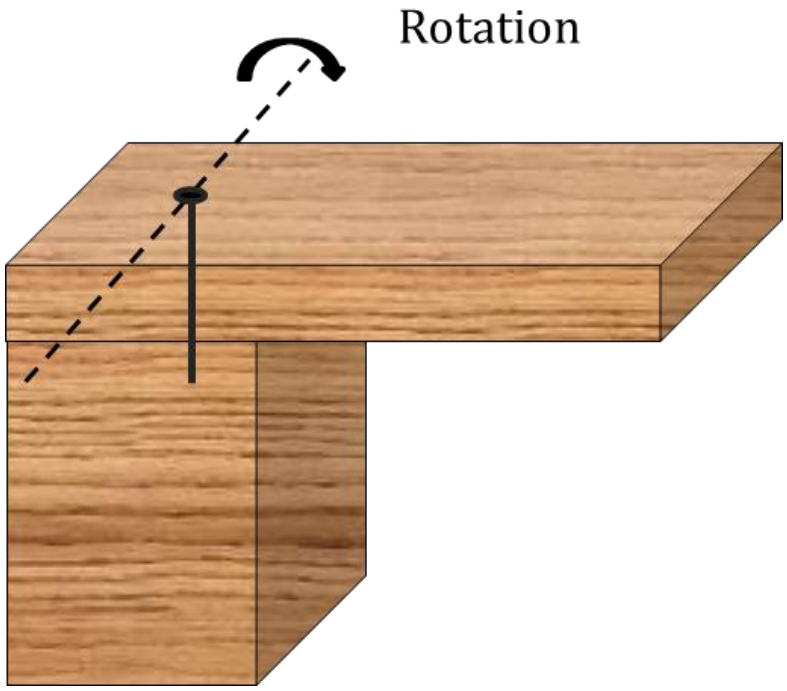

Figure 3. Out-of-plane rotation of a pallet deckboard/stringer connection

deflection of pallet deck causes the load to bridge between the supports where no compressive stresses are over the pallet deck as shown in Figure 4 (Loferski, 1985). The level of load-bridging is a function of the stiffness of packaged products and pallet. The effect of load-bridging on pallet performance will also vary depending on pallet support conditions.

The load-bridging effect of the packaging on a pallet within a unit load has been reported by several investigators. Fagan (1982) studied the load-bridging impact of a unit load on pallet performance under uniform or concentrated loading. Warehouse rack support systems were studied spanning the stringers and deckbaords. An inverse relationship between pallet stiffness and load-bridging was found, but was difficult to quantitatively predict the effect of load-bridging on pallet response. Collie (1984) also investigated the effect of load-bridging on pallet performance. Unit loads supported in racks by a low stiffness pallet exhibited significant load-bridging. However, since it is difficult to estimate the rigidity of the unit load and the pallet stiffness, the bridging effect should be approached carefully. An experimental study conducted by Yoo (2008) showed that stiffer pallet decks resulted in the less decks deflection and more load-bridging under static loads.

2.4 Distribution Packaging

While the consumer and industrial products move through slightly different supply chains, both products are subjected to various static (i.e. bending and compression) and dynamic (i.e. shock and vibration) mechanical stresses. From point and time of origin to point and time of consumption, packaging should be designed to easily and safely move and protect products from any hazard, including external forces, heat and cold, humidity, and corrosion.

Packaging is divided into categories by levels or functions: primary, secondary, and tertiary packaging. For any product, these three levels of packaging may be necessary depending on the intended purpose. Primary packaging is the material that contains and directly contacts the product. Secondary packaging is located outside the primary packaging and contains the primary packaging.

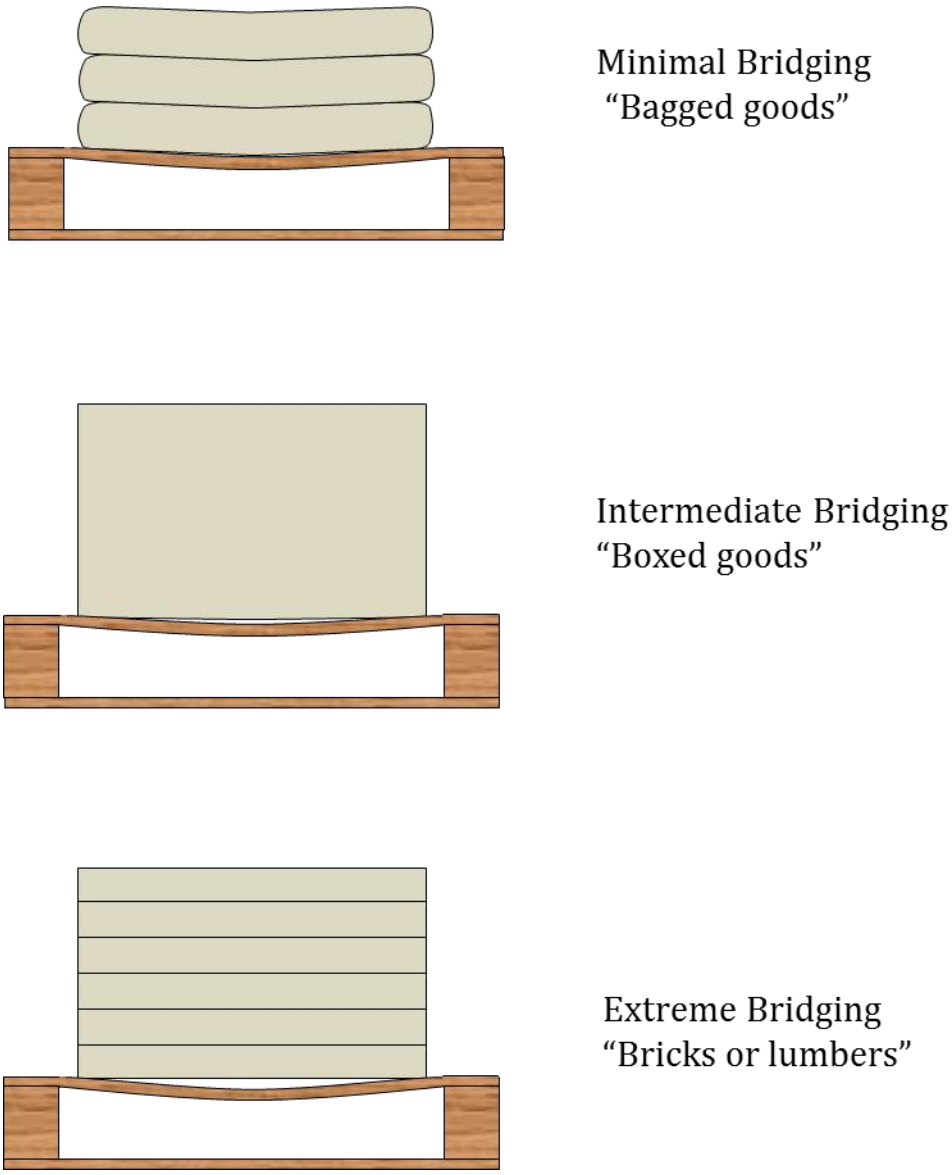

Figure 4. Examples of load-bringing where a pallet is supported in warehouse stack storage

Tertiary packaging enables the product to be handled, stored and transported in an assembled unit. The most typical form of tertiary packaging is corrugated boxes assembled in the unit load form. The styles and forms of packaging stacked on a pallet, and the stacked pattern can affect the performance of the entire unit load as well as the pallet. For example, packaging materials with rigid bottoms like steel drums can transfer more stress to a pallet than more flexible packaging like corrugated boxes (Clarke, 2002). The interlock stacking pattern, rather than the column stacking pattern, reduces the stresses on a pallet (White et al, 2006) while the stacking strength is decreased due to misalignment. To optimize the design of a unit load it is necessary to understand the static mechanical interaction between packaging and the pallet deck.

2.4.1 Corrugated Fiberboard Container

The most widely used material in the manufacture of transport packaging is a corrugated fiberboard. This material consists of one or two flat sheets of paper, called liners, and a corrugated sheet of paper, called the medium as illustrated in Figure 5. This combined structure results in a stronger container. The thickness of corrugated board depends on flute sized and the number of liners. Three commonly used flute sizes applied to the medium are A-, C- and B-flute, listed from the largest to smallest. C-flute single wall board is the most popular flute for packaging materials. It is characterized by a better stacking strength than B-flute and a better printing surface than A-flute. Utilization of these three types of flute depends on the packaged product and level of primary packaging.

The corrugated fiberboard container is the most common type of shipping container being used in a palletized unit loads. Most products are packed into corrugated boxes during handling, storage, and transportation throughout the United States and the World. The most common style of box used for shipping and storage is the Regular Slotted Container (RSC) as shown in Figure 5. Seventeen million tons of corrugated fiberboards are used annually to manufacture RSC, which

accounts for 55 percent of corrugated fiberboard production. All of the flaps are the same length. The two major flaps meet at the center of the box when folded and the minor flaps do not.

The corrugated box is designed to protect products from the hazard of the shipping environment, such as shock, vibration, compression, and moisture. Corrugated boxes that are palletized in a unit load form require enough compression strength to resist the weight of loads stacked above them. Pallet loads are often stacked as many as four or more unit loads high to optimize space utilization during storage. Flute rigidity of corrugated board influences the compression strength of the container. According to TAPPI T 825, the flute rigidity can be measured by applying crushing force perpendicular to the surface of the board referred to as Flat-Crush Testing (FCT). Crushed board, due to a low FCT, can reduce the stiffness and bending strength of a box. Twede and Selke (2005) mentioned that the FCT test is generally used only for single-wall board. A typical FTC for single wall C-flute is 20 psi. Stiffer medium and good flute formation result in a high value of FCT.

2.4.2 Modeling Boxed Products

Attempts have been made to develop models of corrugated container compressive strength by many investigators (Kellicutt and Landt, 1951), (Maltenfort, 1956), (McKee, 1961), (Kawanishi, 1988). Uniform load distributions were assumed; however, little is known about the behavior of a corrugated box containing products stacked on a pallet.

In a typical unit load, the product in the bottom layer of containers rests on a single or overlapped layer of corrugated board which forms the bottom of the box. Weigel (2001) developed the two-dimensional model of the vibrational response of palletized unit loads. Due to the complexity of the modeling process each component of the unit load (product, container, and pallet) was first modeled separately, and then combined to form the unit load model. The model of the product developed by Weigel (2001) consists of two frame elements. One is a vertical frame

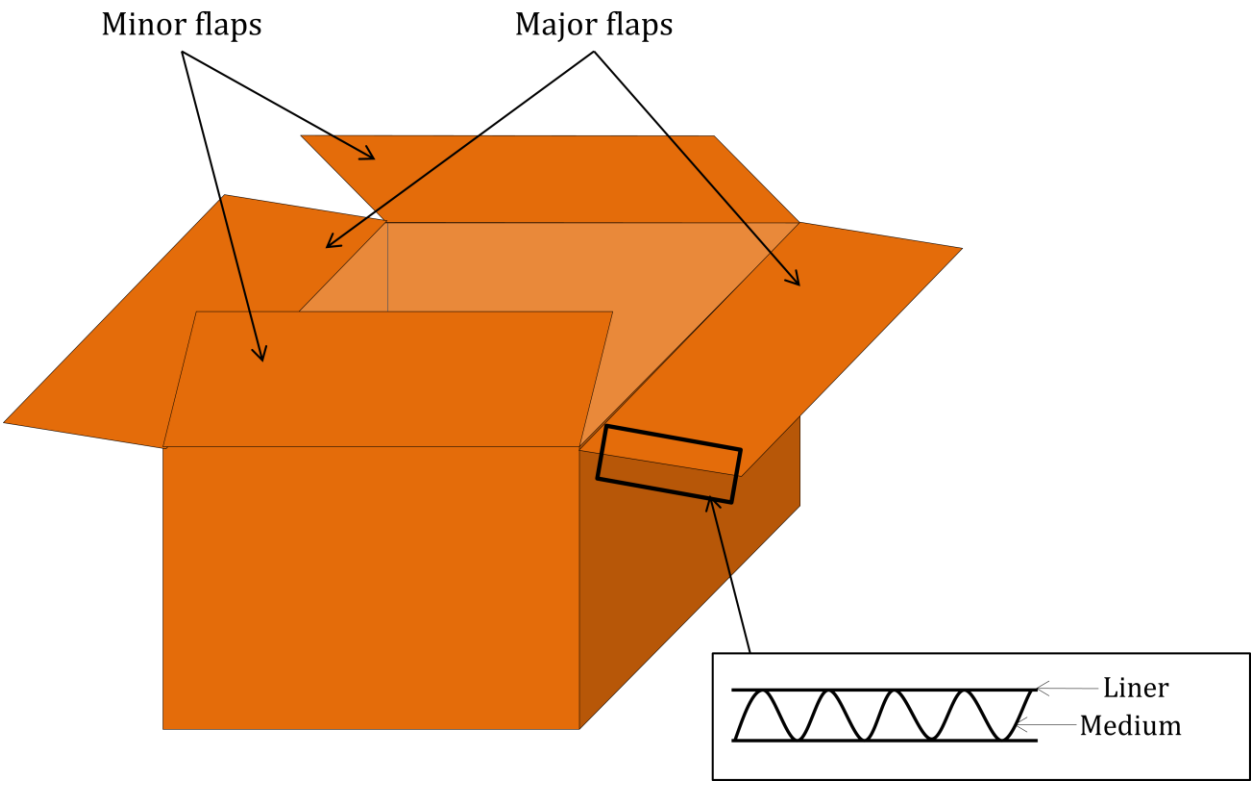

Figure 5. Regular Slotted Container (RSC)

acting as the spring representing the elastic properties of the product and the other is a horizontal element acting as the mass which contains the entire mass of the product, therefore it is rigid. Weigel (2001) also modeled the compression stiffness of the bottom of the corrugated container as a linear spring supporting the product using the spring-mass system analog. In the model, the bottom layer of the container was represented as a vertical frame element (a column) supporting the product model. For modeling corrugated fiberboard which tends to have non-linear elastic characteristics utilizing a frame element with linear elastic properties, it is necessary to determine the flat crush compression stiffness of the corrugated fiberboard at the expected load level (Weigel, 2001). The results of unit load model prediction showed good agreement with actual performance of the unit load.

2.5 Euler-Bernoulli Beam Theory

Euler-Bernoulli beam theory is a fundamental theory of elasticity used as the primary method for structural analysis of beam elements. Calculation of the load-carrying capacity and deflection of beams can be validated by the theory. This beam theory is used in the case for small deflection of a vertically loaded beam only and does not take the shear deflection into account. This theory includes the relationship between the deflection of the beam (y) and the applied load (q) as follows (Gere, 2004):

$$EI\frac{d^4y}{dx^4} = q(x)$$

Note that E is the modulus of elasticity and I is the moment of inertia. The vertical displacement $y(x)$ describes the deflection y of a beam at any point x and is related to the slope θ as follows:

$$\frac{dy}{dx} = \theta(x)$$

Also the relationship between bending moment *M(x)* and curvature $\frac{d^2y}{dx^2}$ is:

$$EI\frac{d^2y}{dx^2} = -M(x) \quad [1]$$

The shear force *Q* is obtained by differentiating the following equation with respect to *x* as follows:

$$EI\frac{d^3y}{dx^3} = -\frac{dM}{dx} = -Q(x) \quad [2]$$

2.5.1 Beams on an Elastic Foundation

The analysis of bending of beams on an elastic foundation is developed on the assumption that the reaction forces of the foundation are proportional at every point to the deflection of the beam at that point. This model presented for the elastic foundation was introduced by Winkler (Hetenyi, 1946). The Winkler foundation model assumed the foundation as a set of closely spaced, independent, and linearly elastic springs without taking the shear resistance of the foundation into account. One of drawbacks of the Winkler model is a discontinuous displacement between the loaded and unloaded foundation surface. To overcome this drawback Hetenyi (1946) modeled the interaction between independent springs by incorporating a two-dimensional elastic beam.

Figure 6 presents the bending of a straight beam supported along its entire length by an elastic medium, caused by a vertical force *P* acting in the principal plane of the symmetrical cross section. The action of the vertical force produces the intensity of distributed reaction force *ky* at a point where the deflection is *y* in the supporting elastic medium. The assumption *p = ky* implies that the supporting medium is elastic following Hooke's law. In the formula, *k* denotes modulus of the foundation (lbs./in.^{2}) which includes the effect of the width of the beam. As shown in Figure 6, an infinitesimal element of distance *dx* is taken from the unloaded parts of the beam. The shear force, *Q*, acting upward to the left of the cross-section and the corresponding bending moment, *M*, acting

clockwise from the left are considered positive. Applying equilibrium of the element in Figure 6, the summation of the vertical forces becomes

$$Q - (Q + dQ) + ky\,dx = 0$$

Hence

$$\frac{dQ}{dx} = ky$$

Using the equation [2]

$$\frac{dQ}{dx} = \frac{d^2M}{dx^2} = ky$$

Using the equation [1]

$$EI\frac{d^4y}{dx^4} = -\frac{d^2M}{dx^2} = -ky$$

Hence

$$EI\frac{d^4y}{dx^4} = -ky \qquad [3]$$

Assuming $y = e^{mx}$

$$EI\frac{d^4y}{dx^4} = EIm^4e^{mx} \qquad [4]$$

Substituting [4] in the equation [3] gives

$$EIm^4e^{mx} = -ke^{mx}$$

$$m^4e^{mx} + \frac{k}{EI}e^{mx} = 0$$

$$m^4 = -\frac{k}{EI}$$

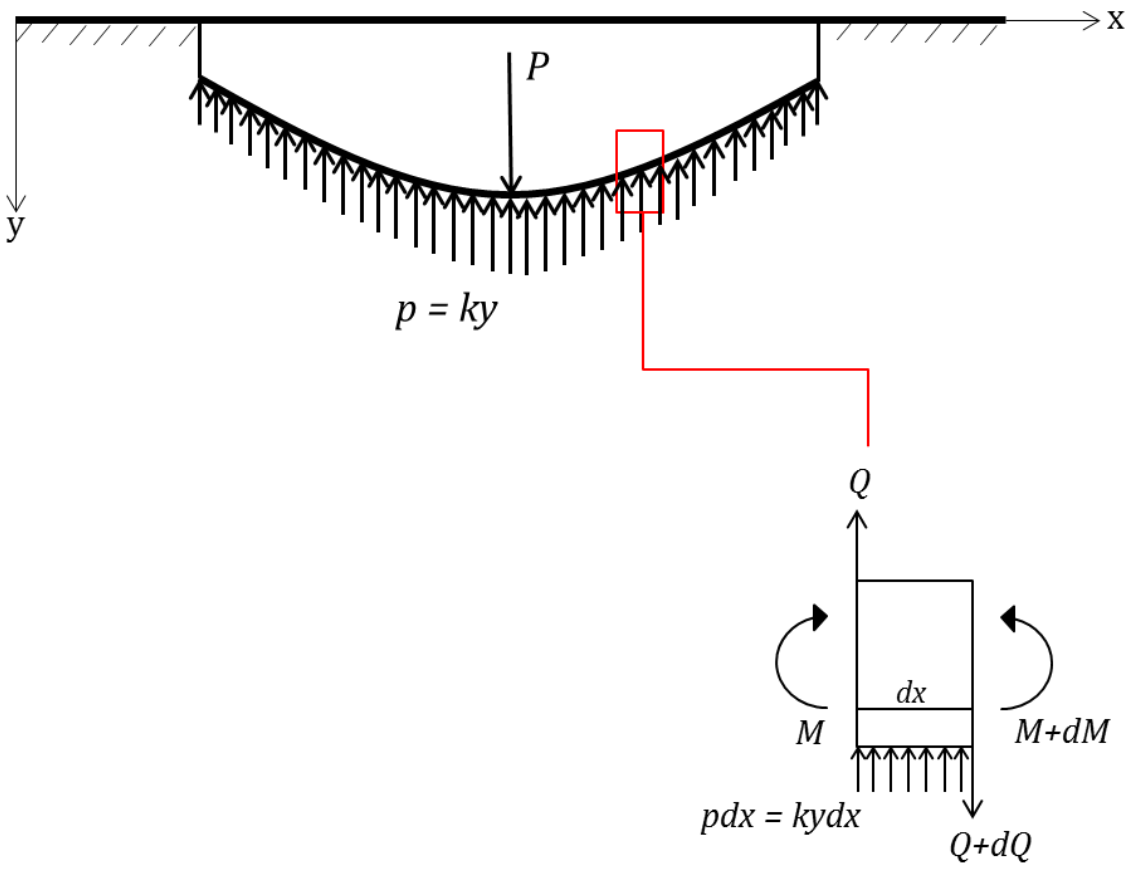

Figure 6. Schematic representation of a deformed beam on an elastic foundation

which has the roots

$$m_1 = -m_3 = \sqrt[4]{\frac{k}{4EI}}(1+i) = \lambda(1+i)$$

$$m_2 = -m_4 = \sqrt[4]{\frac{k}{4EI}}(-1+i) = \lambda(-1+i)$$

where λ includes the elasticity of the supporting medium(k *lbs./in.*^{3}) and the flexural rigidity (EI *lbs./in.*^{2}) thus, called the characteristic of the system and its unit is length^{-1}.

$$\lambda = \sqrt[4]{\frac{k}{4EI}} \qquad [5]$$

The general solution of equation [3] takes the following form

$$y = A_1 e^{m_1 x} + A_2 e^{m_2 x} + A_3 e^{m_3 x} + A_4 e^{m_4 x} \qquad [6]$$

Using

$$e^{i\lambda x} = \cos\lambda x + i\, sin\lambda x$$
$$e^{-i\lambda x} = \cos\lambda x - i\, sin\lambda x$$

and introducing the new constants C_1, C_2, C_3, and C_4, where

$$C_1 = (A_1 + A_4) \qquad C_2 = i(A_1 - A_4)$$
$$C_3 = (A_2 + A_3) \qquad C_4 = i(A_2 - A_3)$$

The equation [6] can be written in a more convenient form as follows

$$y = e^{\lambda x}(C_1 \cos\lambda x + C_2 \sin\lambda x) + e^{-\lambda x}(C_3 \cos\lambda x + C_4 \sin\lambda x) \qquad [7a]$$

Subsequently,

$$\frac{1}{\lambda}\frac{dy}{dx} = \frac{1}{\lambda}\theta = e^{\lambda x}[C_1(\cos\lambda x - \sin\lambda x) + C_2(\cos\lambda x + \sin\lambda x)] \\ -e^{-\lambda x}[C_3(\cos\lambda x + \sin\lambda x) - C_4(\cos\lambda x - \sin\lambda x)] \quad [7b]$$

$$\frac{1}{2\lambda^2}\frac{d^2y}{dx^2} = \frac{1}{2\lambda^2}M = -e^{\lambda x}(C_1\sin\lambda x - C_2\cos\lambda x) + e^{-\lambda x}(C_3\sin\lambda x - C_4\cos\lambda x) \quad [7c]$$

$$\frac{1}{2\lambda^3}\frac{d^3y}{dx^3} = \frac{1}{2\lambda^3}Q = -e^{\lambda x}[C_1(\cos\lambda x + \sin\lambda x) - C_2(\cos\lambda x - \sin\lambda x)] \\ +e^{-\lambda x}[C_3(\cos\lambda x - \sin\lambda x) + C_4(\cos\lambda x + \sin\lambda x)] \quad [7d]$$

2.5.2 General Solution of the Beam Deflection on an Elastic Foundation

The general equations for slope θ of the deflection line, bending moment M, and shear force Q are obtained from [7b-d]. The conditions at the left end of the beam can be obtained by taking x=0 in the equations [7a-d] as follows

$$[y]_{x=0} = y_0 = C_1 + C_2$$

$$\left[\frac{dy}{dx}\right]_{x=0} = \theta_0 = \lambda(C_1 + C_2 - C_3 + C_4)$$

$$\left[-EI\frac{d^2y}{dx^2}\right]_{x=0} = M_0 = 2\lambda^2 EI(-C_2 + C_4)$$

$$\left[-EI\frac{d^3y}{dx^3}\right]_{x=0} = Q_0 = 2\lambda^3 EI(C_1 - C_2 - C_3 - C_4)$$

The constants C's can be determined by the following equations

$$C_1 = \frac{1}{2}y_0 + \frac{1}{4\lambda}\theta_0 + \frac{1}{8\lambda^3 EI}Q_0$$

$$C_2 = \frac{1}{4\lambda}\theta_0 - \frac{1}{4\lambda^2 EI}M_0 - \frac{1}{8\lambda^3 EI}Q_0$$

$$C_3 = \frac{1}{2}y_0 - \frac{1}{4\lambda}\theta_0 - \frac{1}{8\lambda^3 EI}Q_0$$

$$C_4 = \frac{1}{4\lambda}\theta_0 + \frac{1}{4\lambda^2 EI}M_0 - \frac{1}{8\lambda^3 EI}Q_0$$

Substituting these C's in the equation [7a] and putting $\frac{1}{2}\left(e^{\lambda x} + e^{-\lambda x}\right) = Cosh\,\lambda x$ and $\frac{1}{2}\left(e^{\lambda x} - e^{-\lambda x}\right) = Sinh\,\lambda x$, the general solution of the deflection line take the form as

$$y_x = y_0 F_1(\lambda x) + \frac{1}{\lambda}\theta_0 F_2(\lambda x) - \frac{1}{\lambda^2 EI}M_0 F_3(\lambda x) - \frac{1}{\lambda^3 EI}Q_0 F_4(\lambda x) \qquad [8]$$

where

$$F_1(\lambda x) = Cosh\,\lambda x \cos\lambda x$$

$$F_2(\lambda x) = \frac{1}{2}(Cosh\,\lambda x\ sin\,\lambda x + Sinh\,\lambda x \cos\lambda x)$$

$$F_3(\lambda x) = \frac{1}{2}Sinh\,\lambda x \sin\lambda x$$

$$F_4(\lambda x) = \frac{1}{4}(Cosh\,\lambda x\ sin\,\lambda x - Sinh\,\lambda x \cos\lambda x)$$

2.6 Summary

In Chapter 2, systems-based design of unit loads was discussed. The characteristics of each unit load component, including pallet components under the stack support condition and the pallet joint stiffness, were identified. The effect of load-bridging on pallet design was also discussed. Investigation of modeling boxed products related to distribution packaging and corrugated containers in the previous study was described. This chapter also examined the fundamental concept of beams on an elastic foundation theory and general solution of beam deflection on the elastic foundation which was used for this research.

CHAPTER 3

3.0 Experimental Procedures for Determining Input Property Values

The objective of this chapter is to determine input property values for use in modeling pallet deck deflections and compressive stress distributions using the beam on an elastic foundation theory. A schematic drawing of a simplified unit load model is presented in Figure 7. If the unit load model is turned upside down, the top pallet deck is assumed to be a straight short beam partially supported along its length by packaging, which is represented by an elastic supporting medium.

In the unit load form, the pallet deck deflection and compressive stress distribution at the pallet deck/packaging interface can be influenced by many factors such as pallet design, packaging properties, unit load support conditions, package stacking patterns, and so on. The scope of this study is limited to the following three variables:

- Pallet deck stiffness (Modulus of Elasticity)
- Joint rotation modulus
- Packaging stiffness

Values for the three design variables were determined experimentally. The pallet deck component stiffness can be determined in terms of modulus of elasticity (MOE), moment of inertia (I), and length (L) of the deck. The modulus of elasticity of the pallet deck component was measured by a third point bending test. To determine the stiffness of nailed pallet joints, joint rotation modulus was measured. Lastly, the packaging compression stiffness for a box containing bottles, a box containing flour sacks, and an empty box was measured. The test procedure for each of the three input properties will be described in the following sections.

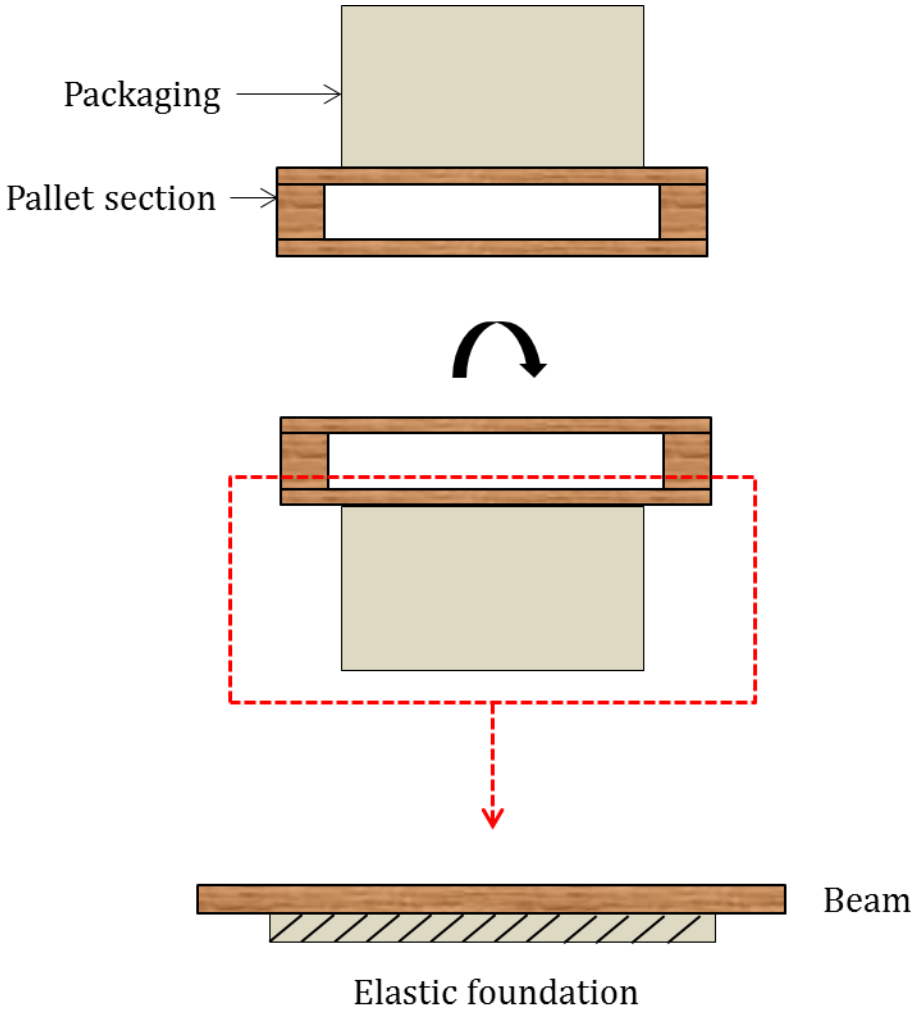

Figure 7. Schematic drawings of a simplified unit load form

3.1 Modulus of Elasticity (MOE)

The modulus of elasticity (MOE, or *E*) of each pallet deck component was measured using a third point bending test and is described in the following section.

3.1.1 Materials and Equipment

Table 1 contains descriptions of all materials and equipment used for the MOE determination. Southern yellow pine was used to construct all test specimens. A 20-inch long deck was used to assemble the pallet sections and a 16-inch long deck was used to construct the test joints for rotation modulus determination. Two different deck thicknesses, 3/4- inch and 3/8-inch, were used for each length of the deck. All deck components were tested using the Material Test System (MTS) servohydraulic machine with a 1000-pound load cell. To record deflection measurements a 0.5 inch Linear Variable Differential Transducer (LVDT) was used.

3.1.2 Test Procedures

Test procedures for measuring MOE are described in this section. Figure 8 shows the third point bending test conducted in accordance with ASTM D-4761-96, Standard Test Methods for Mechanical Properties of Lumber and Wood-Based Structural Material. Figure 9 is a schematic drawing showing details of the bending test set up. Each specimen was tested using a center point load. Prior to testing, the length, width and depth of each deckboard were measured using the digital caliper to the nearest 0.001 inch. Each deckboard was placed on the reaction supports. The load was applied at the center of the samples using a load head of curvature radius 1.875 inches. Each deckboard used to make the pallet section was tested twice using a 16-inch support span. Each deck component used for the test joint was also tested twice using a 14-inch support span. The average of the two test data was used as the input value for modeling. The deckboard deflection was measured using a 0.5-inch Schaevitz LVDT affixed to a yoke in the center of the spans. Three

Table 1. Materials and equipment for MOE test

	Pallet Section	**Nailed Test Joint**
Wood Species	Southern Yellow Pine	Southern Yellow Pine
Deckboard Dimension	20 inches long, 3.5 inches wide	16 inches long, 3.5 inches wide
Deckboard Thickness	3/4 inch, 3/8 inch	3/4 inch, 3/8 inch
Number of Decks	18 decks for each thickness	5 decks for each thickness
Test Machine	MTS 10 GL Electrical-mechanical with a 1000-pound interface load cell model # 27-00112	
LVDT	One, 0.5 inch Schaevitz LVDT Model 050HR-DC (working distance ± 0.5 in, sensitivity 0.001-inch)	

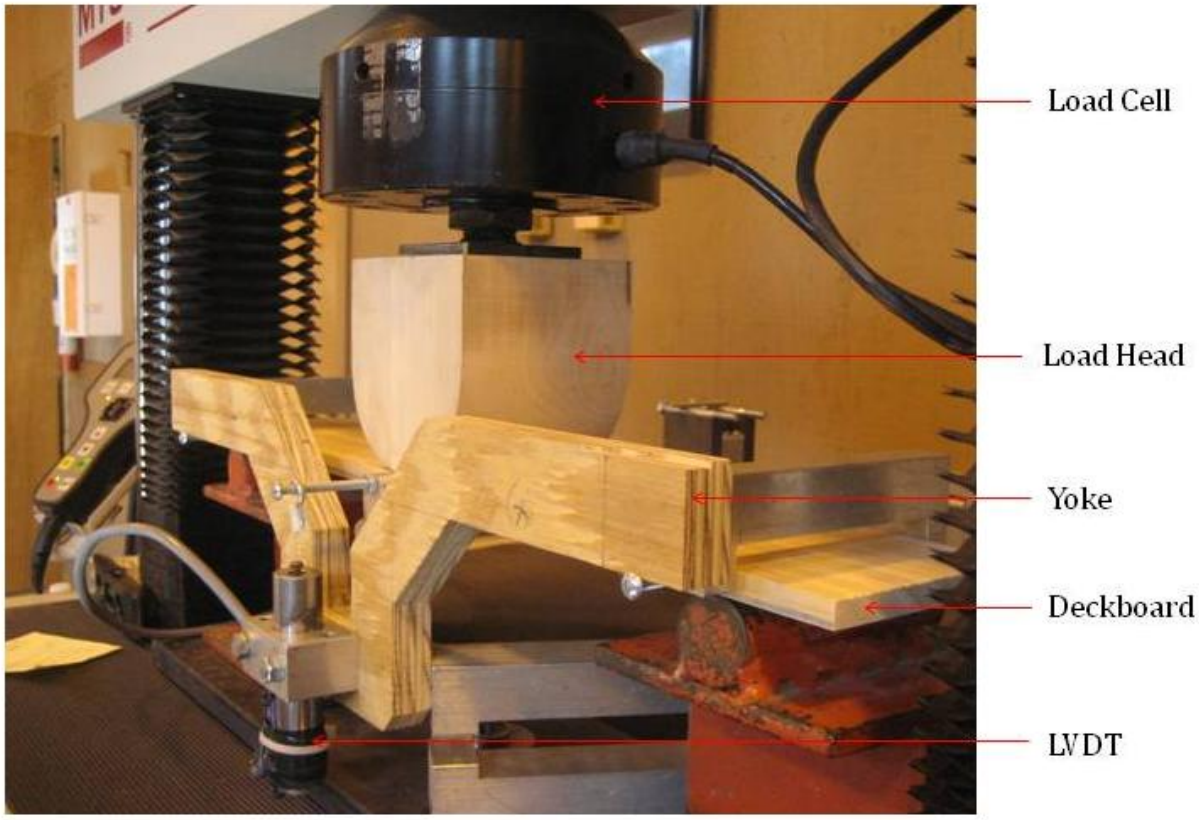

Figure 8. Photograph of the pallet deckboard bending test

screw clamps were used to hang the yoke from the specimen. For the 20-inch long deck, two of the three screw clamps were positioned 2 inches away from each end and the other was at the center of the span. For 16-inch deckboards, two clamps at the ends were placed one inch away from each end to test. All screw clamps were located over the neutral axis of the deckboard depth.

A 300-pound compression load was applied to all 3/4-inch deckboards utilized in both pallet sections and test joints. A 60-pound load was applied to 3/8-inch deckboards used for the pallet sections and a 55-pound load was applied to 3/8-inch deckboards employed for the test joints. The cross head speed of 0.1 in. /min. was used to apply the loads to all deckboards. A MTS electronic data acquisition system controlled the applied load and recorded the corresponding center deflection. The linear portion of the load-deflection curve was taken for calculating MOEs.

3.1.3 Results and Discussion

MOE was computed using the following equation:

$$\text{MOE} = \frac{Pl^3}{48\Delta I}$$

where

P= load (lbs.)

l= span (in.)

Δ= deflection (in.)

I (moment of inertia) (in.^{4}) = $bd^3/12$

where b= deckboard width and d=deckboard depth or thickness

The calculated MOE values of deckboards for both pallet sections and test joints are shown in Table 2. The average MOE is similar for 3/4-inch and 3/8-inch deckboards for pallet sections. However, the average MOE of decks used for joint rotation test was 22% higher than pallet section deck components since the span of the joint rotation deck component was shorter than pallet section deck component. The MOE values of the pallet deckboards were inputs used for pallet deck deflection and stress distribution models. The MOE values for the test joints were applied to

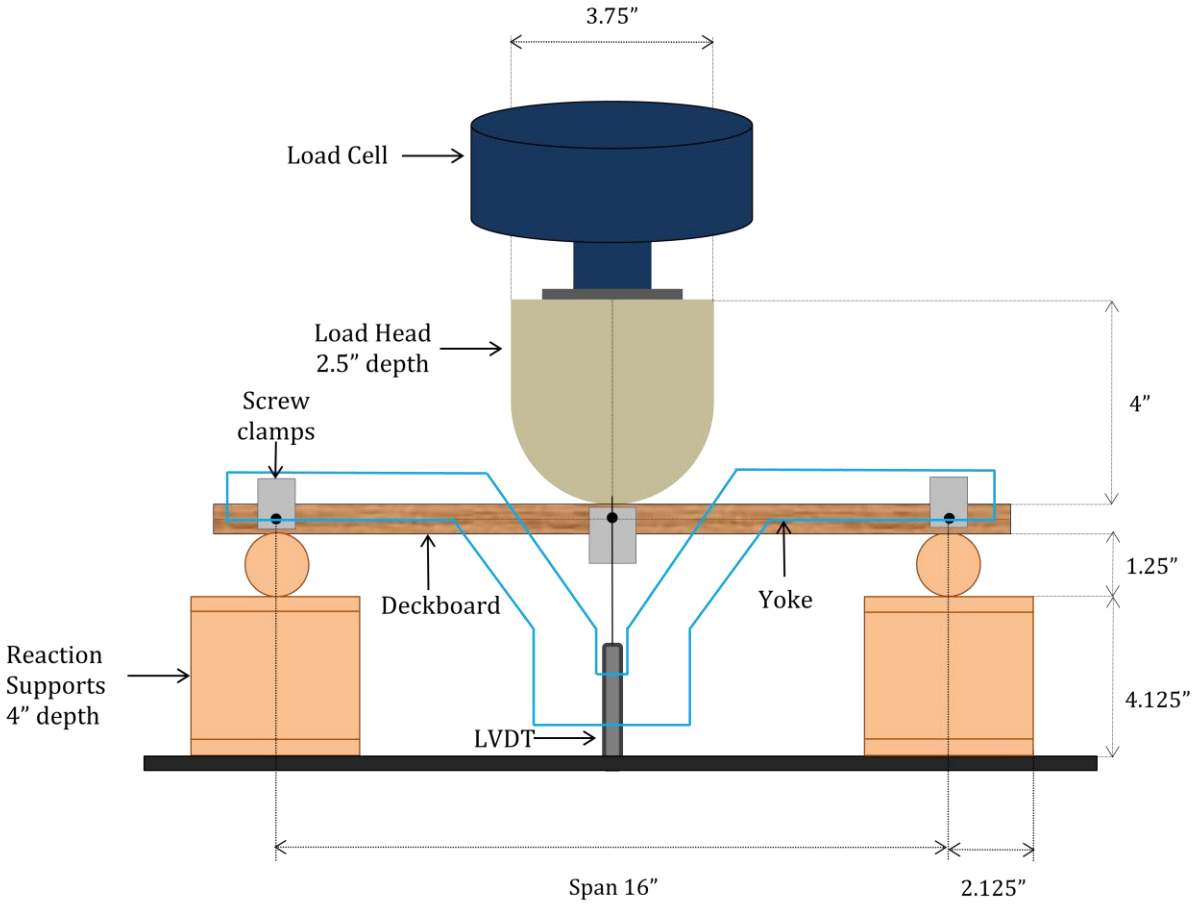

Figure 9. A schematic diagram of the deckboard bending test set up

Table 2. MOE values for deckboards used in assembling pallet sections and test joints (unit: lbs./in.^{2})

Specimen thickness	3/4"		3/8"	
Test specimen	Specimen number	MOE (psi)	Specimen number	MOE (psi)
Pallet section (20")	A-1	1340000	B-1	1081000
	A-2	1236000	B-2	1077000
	A-3	1246000	B-3	1082000
	A-4	1118000	B-4	1023000
	A-5	1178000	B-5	1626000
	A-6	730700	B-6	1408000
	A-7	854500	B-7	716800
	A-8	1238000	B-8	822800
	A-9	1173000	B-9	1131000
	Avg.	1124000	Avg.	1108000
	COV (%)	18	COV (%)	25
Joint Rotation (16")	C-1	1301000	D-1	1587000
	C-2	1404000	D-2	1269000
	C-3	1417000	D-3	1223000
	Avg.	1374000	Avg.	1360000
	COV (%)	4	COV (%)	12

calculate the joint rotation modulus for nailed joints, which is described in section 3.2.

3.2 Joint Rotation Modulus

Three different end conditions of the pallet section, a free end, a nailed joint, and a fixed end, were modeled to investigate the effect of joint stiffness on pallet deck deflections and compressive stress distributions. Due to non-measurable joint stiffness for the free end and fixed end, only the nailed joint was constructed and tested as an input value for the models to determine out-of-plane rotation (Figure 3) or joint rotation modulus (*RM*). Joint rotation modulus is a parameter that indicates the degree of fixity of the nailed joint during out-of-plane rotation. The rotation modulus is defined as the ratio of the applied moment to the angular rotation (Kyokong, 1979). The rotation modulus can be computed by the slope of the tangent to the linear portion of the moment-rotation curve obtained from tested joints (Samarasinghe, 1987).

3.2.1 Materials and Equipment

Materials and equipment used for joint rotation testing are described in Table 3. Five deckboard components, each 6.5-inch long, were made for each deck thickness from three 16- inch long tested deckboards (see Table 2). Each test joint consisted of one deck component and one stringer segment. The same stringer was used to construct all test joints. In order to eliminate the variability of nail penetration depths and to not affect the joint rotation modulus, two different lengths of nails were used to assemble the test joints of the two different deck thicknesses.

3.2.2 Test Procedures

Ten joint rotation test specimens were constructed using tested decks and stringer components. The test joint specimens were assembled by driving two nails with a hand held hammer. Holes were pre-drilled into the nail locations using a 0.095 inch diameter drill bit (80% of the nail wire diameter) to eliminate the probability of splitting the wood. The location of two nails

Table 3. Materials and equipment for joint rotation tests

	Deck board	**Stringer**
Wood Species	Southern Yellow Pine	Southern Yellow Pine
Dimension	6.5 inches long, 3.5 inches wide	3.5 inches long, 1.5 inches wide, 3.5 inches high
Thickness	3/4 inch, 3/8 inch	
Quantity	5 decks for each thickness	10 stringers
Nail types	Helically threaded 2 inches long 0.119 inch wire diameter for 3/8 inch deck Annularly threaded 2.25 inches long 0.122 inch wire diameter for 3/4 inch deck	
Test Machine	810 MTS Servo-hydraulic with 1000 pounds interface load cell model # 1210A-1K-B	
LVDT	Two, 2 inches Schaevitz LVDT Model 200HR-DC (working distance ± 2 in, sensitivity 0.001-inch)	

is illustrated in Figure 10. All nails were driven until the head was flush with the top deck surface. A 2-inch LVDT was attached to the bottom surface of the deckboard. Another LVDT was located on the top surface of the deckboard for vertical deflection measurements as shown in Figure 12. For the LVDT 1, a straight line was drawn one inch away from the edge across the width of each deckboard's bottom surface and the LVDT 1 was attached at the center of the line using a metal I-hook. The other one was the spring loaded LVDT 2 and it was placed on the center of two driven nails to measure the vertical movement of the deckboard above the stringers. The joint rotation samples were fixed to the MTS table by bolting two L-brackets, and then rigidly clamped using C-clamps. A dial gauge was used to measure the amount of the rotational movement of each specimen during testing. Load was continuously applied by the MTS with a 1000-pound interfaced load cell at a rate of 0.1 in. /min. to the specimen until the load stopped increasing. These tests were repeated for all the test specimens. Load and deflection were simultaneously recorded.

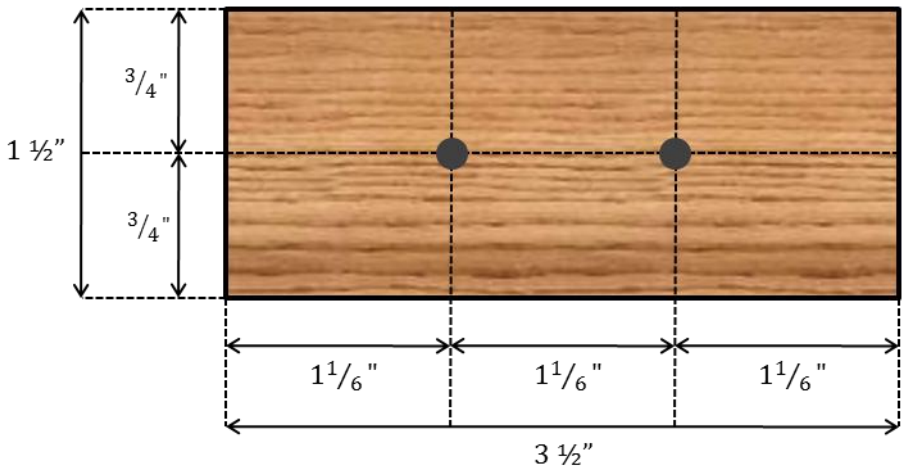

Figure 10. The top view of the nail location in the deckboard/stringer joints

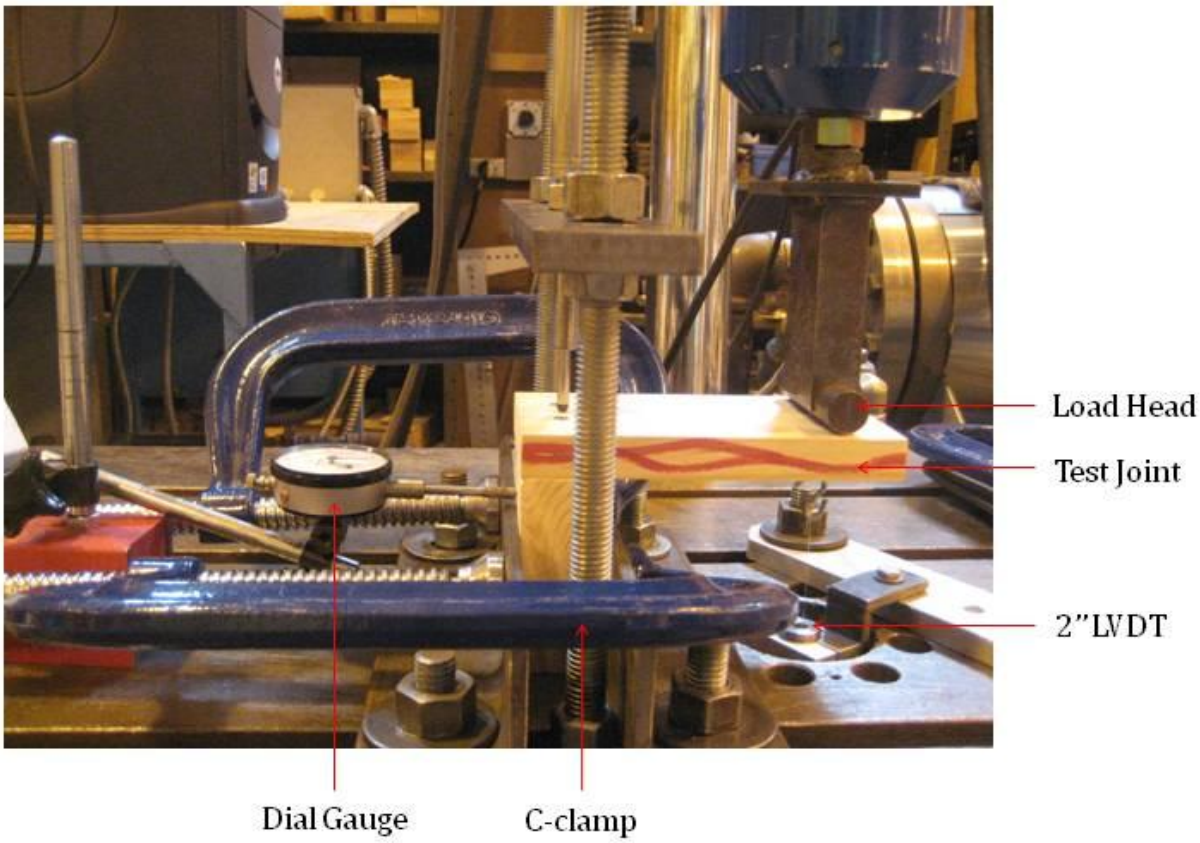

Figure 11. Photograph showing the joint rotation test set up

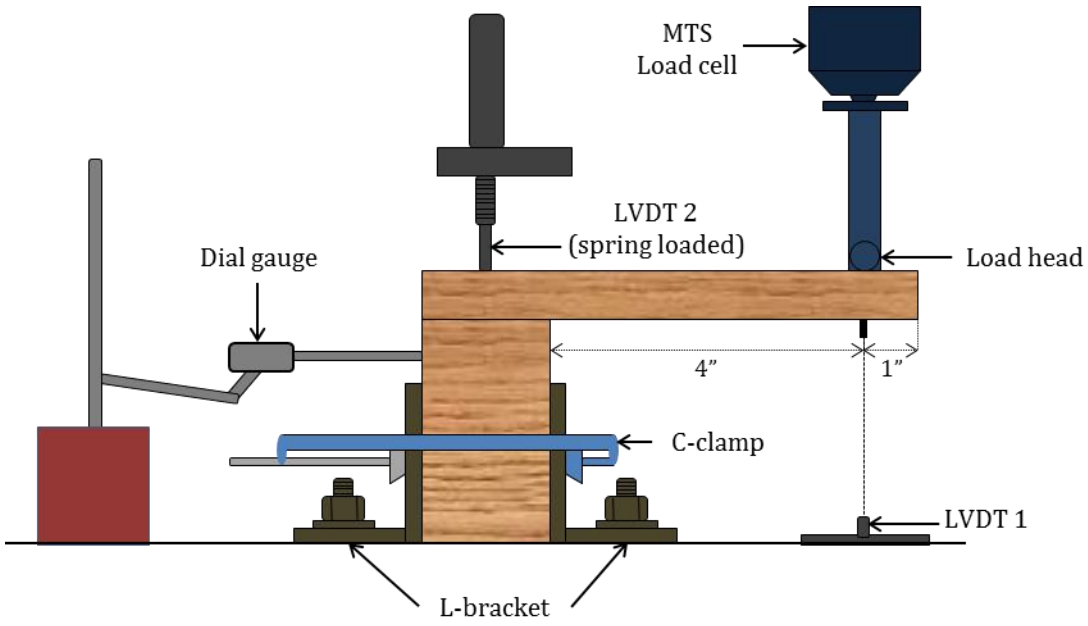

Figure 12. A schematic drawing of joint rotation test set up

3.2.3 Results and Discussion

The result of each test was analyzed by generating the load-deflection curve after all joint rotation tests were complete. Figure 13 shows an example load-deflection curve obtained from 3/8-inch deck joint rotation test.

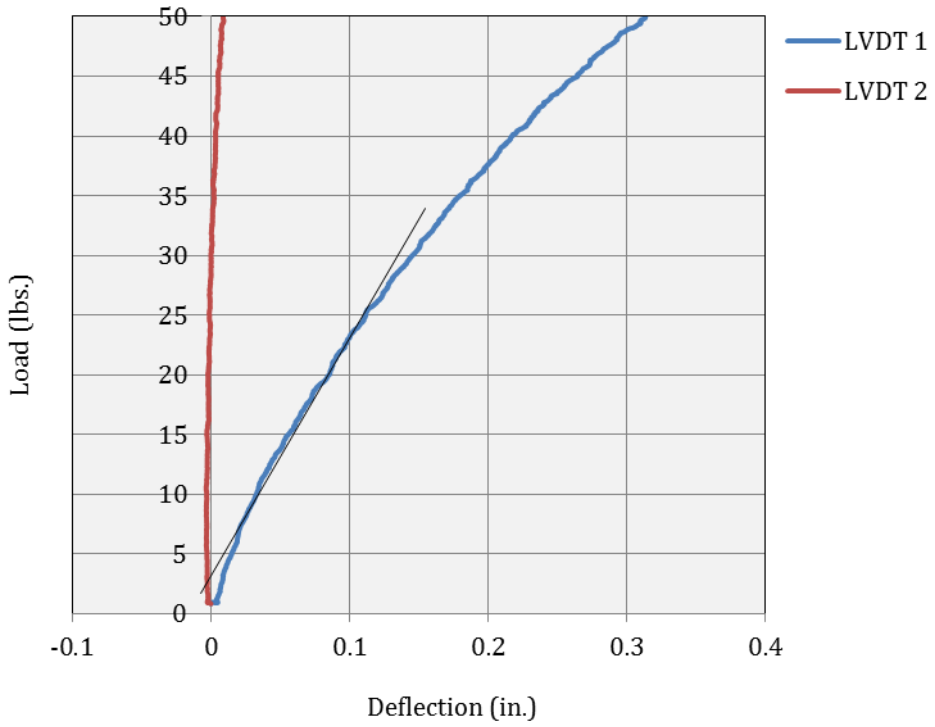

Figure 13. Graph showing load-deflection curve for 3/8-inch deck joint rotation specimen

To determine the joint rotation modulus, pure rotation of the deckboard, excluding deckboard bending and shear displacement of the deckboard must be obtained. Deflections due to the bending and shear are computed using the following equations (Samarasinghe, 1987)

$$\Delta_{bend} = PL\left(\frac{BL}{6EI} + \frac{L^2}{3EI}\right)$$

$$\Delta_{shear} = PL\left(\frac{12L}{5GbdB} + \frac{6}{5Gbd}\right)$$

where

Δ_{bend} = deflection due to bending (in.)

Δ_{shear} = deflection due to shear (in.)

P = load on the joint (lbs.)

L = lever arm (in.)

B = width of the stringer or block (in.)

E = modulus of elasticity (lbs. /in.)

$I = bd^3/12$ = moment of inertia of the deckboard (in.^{4})

b,d = width and depth of the deckboard (in.)

$G = E/16$ = shear modulus of the deckboard (lbs. /in.)

Modulus of elasticity (E) value of each deck used to assemble the test joint was measured and is in Table 2. The equation used to determine deflection due to assumed rigid-body rotation, or Δ_{nail} (Samarasinghe, 1987) is given by

$$\Delta_{total} = \Delta_{nail} + \Delta_{bend} + \Delta_{shear}$$

where

Δ_{total} = total deck board deflection (in.) measured by LVDT 1

Δ_{bend} and Δ_{shear} = obtained from previous equations

Δ_{nail} = deflection due to assumed rigid-body rotation (in.)

As shown in Figure 12, the two LVDTs were separately used to measure Δ_{total}. However, the deflection measured by the spring loaded LVDT over the joint was not included in Δ_{total} due to the negligible deflections recorded. After Δ_{nail} was determined from the above equation, the following equation was used to calculate the rotation modulus of each specimen (Samarasinghe, 1987):

$$RM = \frac{PL^2}{\Delta_{nail}}$$

where

RM = rotation modulus (in-lbs. /radian)

P = load on the joint (lbs.)

Δ_{nail} = deflection due to the assumed rigid-body rotation (in.)

The following is the sample joint rotation modulus calculation for 3/8-inch deck joint rotation test:

$$\Delta_{bend} = 10 * 4 * \left(\frac{1.5 * 4}{6 * 1587483 * 0.015} + \frac{4^2}{3 * 1587483 * 0.015}\right) = 0.011 \text{ in.}$$

$$\Delta_{shear} = 10 * 4 * \left(\frac{12 * 4}{5 * 99218 * 3.501 * 0.369 * 1.5} + \frac{6}{5 * 99218 * 3.501 * 0.369}\right) = 0.002 \text{ in.}$$

$$0.053 = \Delta_{nail} + 0.011 + 0.002$$

$$\Delta_{nail} = 0.039 \text{ in.}$$

$$RM = \frac{10 * 4^2}{0.039} = 4086.9 \text{ in.} - \text{lbs./radian}$$

The results of the rotation test are Table 4. The average rotation modulus is similar for both the 3/4- inch and 3/8-inch deck thickness deckboard. The average of five rotation moduli for each deck thickness was the input value used in order to model the pallet deck deflections and stress distributions for the nailed joint pallet section. Previous studies that investigated the joint rotation modulus also showed large Coefficient of Variation (COV) (%) in the results. The COVs of joint rotation modulus were respectively 41.3% and 29.5% in Samarasinghe's (1987) and White's (2008) works. It is apparent that joint rotation modulus has large variation.

Table 4. The results of Joint Rotation Modulus tests (unit: in-lbs. /radian)

Thickness	Replications	*RM*	Mean	COV (%)
$^{3}/_{4}$"	C-1-1	8675	6494	39
	C-2-1	3826		
	C-2-2	5292		
	C-3-1	5022		
	C-3-2	9653		
$^{3}/_{8}$"	D-1-1	4087	5921	57
	D-2-1	4324		
	D-2-2	11845		
	D-3-1	5496		
	D-3-2	3854		

3.3 Packaging Stiffness

As shown in Figure 7 in section 3.0, the packaging is assumed to be the elastic supporting medium consisting of a series of independent linear spring elements whose stiffness can be represented by a spring constant, also called the "modulus of foundation". It is assumed that at small deformation packaging stiffness is elastic, and therefore can be characterized by its elasticity property *k*. The range of the packaging stiffness varies from flexible to stiff; however, no values have been given this range. The stiffness value of each packaging used in this study is established by the load-deflection curve obtained from the packaging compression test.

3.3.1 Materials and Equipment

Materials and equipment used for the packaging compression test are summarized in Table 5. Three packaging stiffness levels were represented using three different packaging including an empty box, a box containing flour sacks, and a box filled with plastic bottles as shown in Figure 14. All the boxes were made of single-wall C-flute corrugated board with grade of 69-26C-69. The dimensions of all boxes were 15.5-inch long by 7.75-inch wide by 10-inch height. The empty box was employed to investigate the effect of headspace (gap) between the top of the products and the flaps of a corrugated box on the pallet deck deflection and stress distribution models. To represent relatively flexible packages, a corrugated box containing sixteen flour sacks was made in order to determine the stiffness value. The corrugated box containing eighteen plastic bottles was used to represent rigid packaging. No headspace was used in the boxes containing flour sacks or plastic bottles. The modulus of foundation *k* was also assumed to vary along the length of the beam. To determine the variation in stiffness along the box, compression tests were conducted with a small load applicator and repeated along the length of the box as shown in the Figure 15. The load applicator used, was a 2 in. x 2 in. x 12 in. load bar capable of applying a load across the full width of the box. Symmetry was used to measure the stiffness values along the full length of the box. The

Table 5. Materials and equipment for packaging stiffness testing

	Plastic bottles	**Box**	**Flour sacks**
External Dimension (in.) (L x W x D)	3.875"(diameter) x 10" (Height)	15.5 x 7.75 x 10	3.75 x 2.5 x 7.7
Quantity per box	18	-	16
Gross Weight (lbs.)[1]	16.6	0.7	32
Number of boxes tested	6	6	6
Load applicator	2" x 2" x 12" bar made of wood		
Test machine	826.75 MTS servo-hydraulic with 5000 pounds interface load cell model # 661.20E-01		
LVDT	Two, 2 inches Schaevitz LVDT Model 200HR-DC (working distance ± 2 in, sensitivity 0.001-inch)		

Note:

[1] Gross weight of each box filled with each product

Figure 14. A photograph of boxes containing flour sacks and bottles

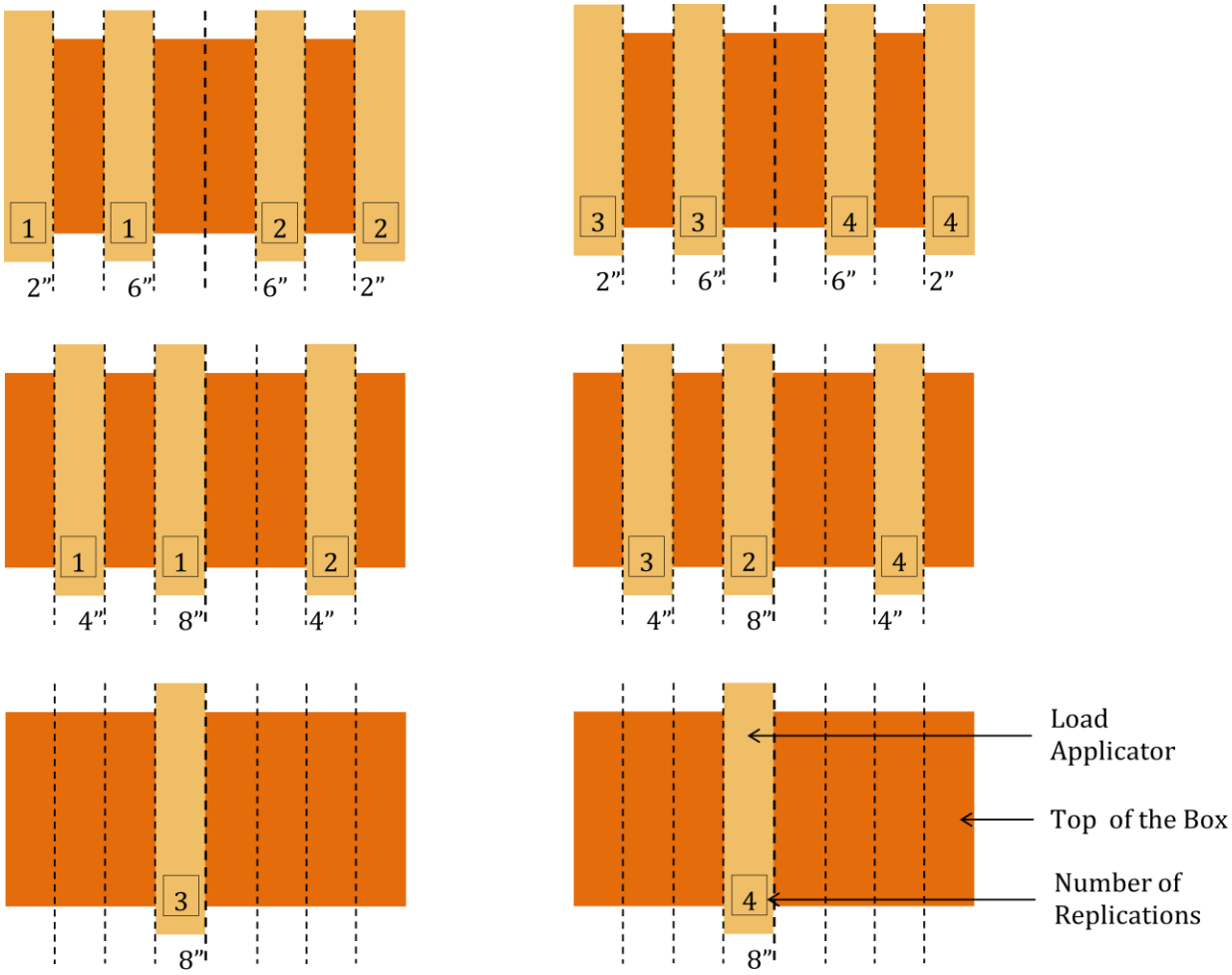

Figure 15. The number of packaging stiffness tests at each location on a box (top view)

length of the box was 15.5 inches, therefore the stiffness was only measured at the box location of 2-, 4-, 6- and 8-inches. Figure 15 illustrates a top view of six boxes of one packaging system which was used to measure four replications at each location. Six boxes of each packaging were necessary to avoid the influence of the test at one location on an adjacent location.

3.3.2 Test Procedures

Two small holes were pre-drilled into the center of each side surface of the load bar. Two screws were driven into each hole to attach a two-inch LVDT for deflection measurement. Each box specimen was placed on a flat rigid surface and the load bar was located on the top of the box. When one side of the box was loaded by the load bar at the edge of the box, the other side of the box edge was loaded by a dead weight of 10 pounds so that rotation of the box could be prevented during testing. A load was continuously applied at a rate of 0.1 in. /min. to the specimen until crush damage was observed on the box. With the load cell at the center of the load bar, a compression load was applied along the length of the box as shown in Figure 16. Load and deflection was automatically recorded by a data acquisition system.

3.3.3 Results and Discussion

An example load-deflection curve for the stiffness of a plastic-bottle-filled box, measured at the 2-inch mark, is shown in Figure 17 and 18. Deflections measured at positions using LVDT 1 and LVDT 2 (Figure 16) are plotted in Figure 17. The slope of the resulting linear elastic portion of the load-deflection curve is the stiffness value of the packaging. Figure 18 shows the re-plotted linear portion taken from the load-deflection curve. A trend line was added to each linear portion of the two load- deflection curves to determine the slope. The two slopes were similar and the average of the two slopes was used as the stiffness value at the measured location.

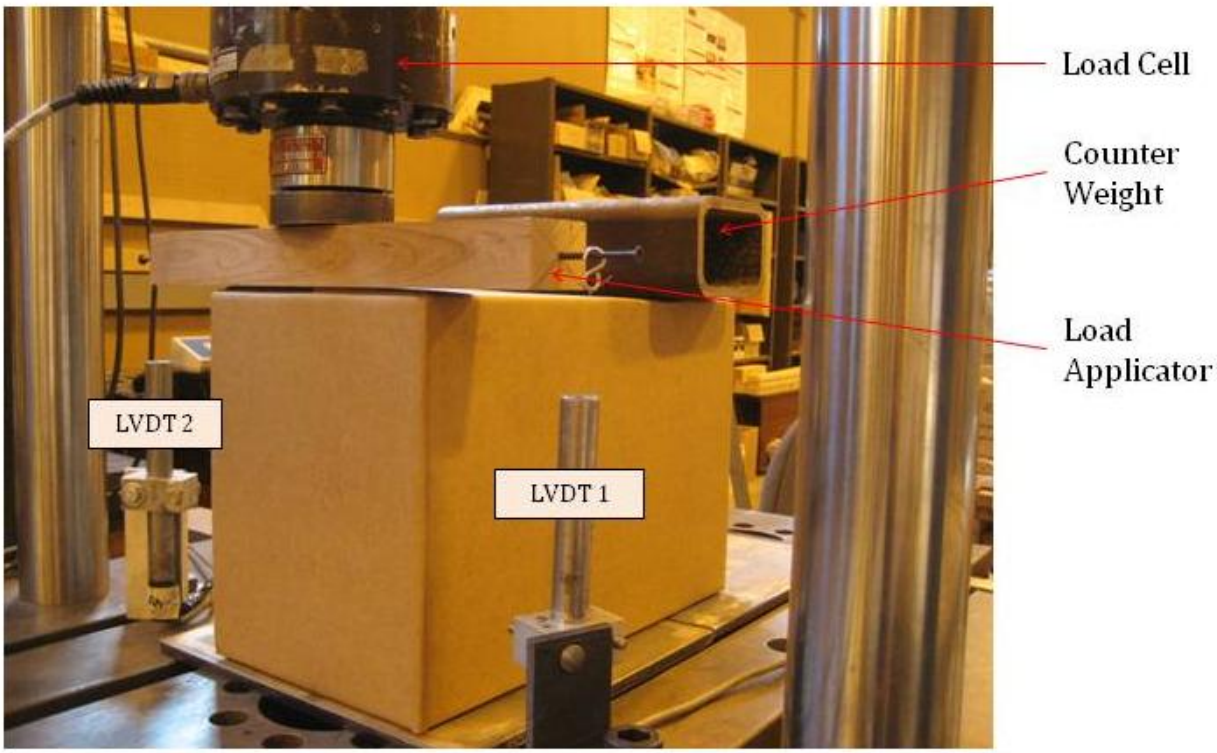

Figure 16. Test set up for measuring packaging stiffness

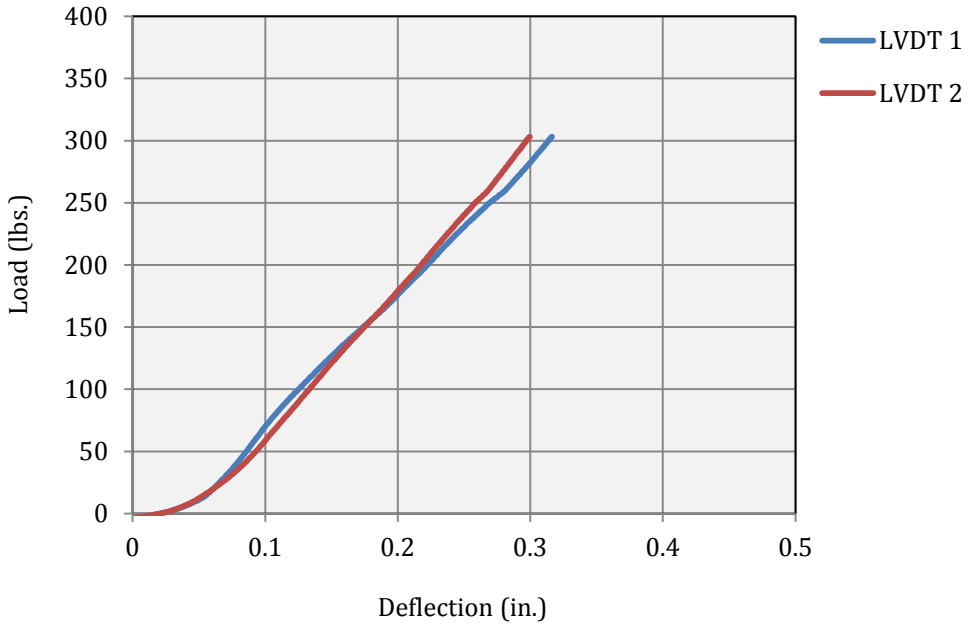

Figure 17. Load-deflection curve for a box containing bottles at 2"

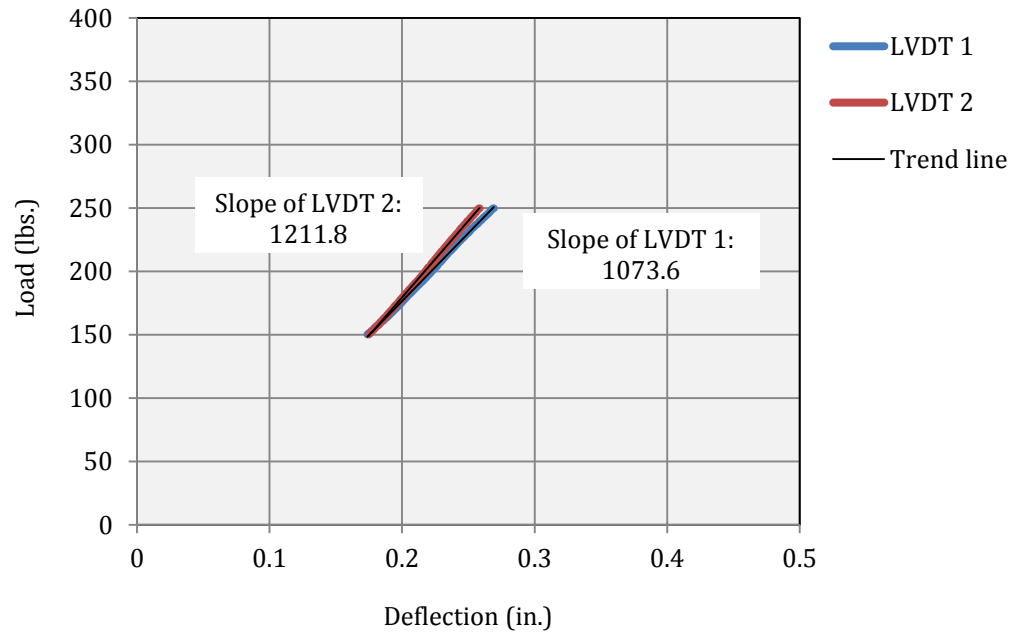

Figure 18. Linear portion from the load-deflection curve (Figure 15) used to determine stiffness

The average stiffness values for all three types of packaging at the four locations are shown in Table 6. The stiffness values measured 8 inches from the end for boxes with bottles and empty boxes were much greater than the other locations. The reason for the difference in stiffness between 8 inches and other locations is the minor flaps effect of the corrugated box. As described in Figure 5, the minor flaps do not meet at the center, whereas the major flaps do. At the box location between 6 inches and 8 inches, only one layer of two major flaps was directly in contact with the bottles while at other locations the bottles were touched by two layers (a minor flap and a major flap) on the top when loaded. Due to the no headspace and cushioning material characteristic of the corrugated board, fewer layers of the flaps at the center caused greater stiffness. However, there was no minor flaps effect on the stiffness of the box with flour sacks. One reason for this might be that the stiffness of flour sacks is similar to the minor flaps' material property. However, the similarity needs to be validated.

For each packaging, the average of the stiffness values measured at four locations was the input value used for modeling. The results from Table 6 show that the box containing flour sacks was the most flexible and the box with bottles was stiffer than the others.

3.4 Summary of Model Input Property Values

This section includes the summary of the input property values required in order to develop the pallet deck deflection and pressure distribution models based on the beam on an elastic foundation theory. It was necessary to conduct experimental studies to determine the values of the three model input: 1) modulus of elasticity (E) of the pallet deckboard assumed as a beam, 2) joint rotation modulus (RM) representing the joint stiffness for the nailed joint pallet section, and 3) the stiffness of the packaging (k) assumed as an elastic foundation. Table 7 is the summary of three input property values used.

Table 6. The results of the packaging stiffness testing (unit: lbs. /in.)

Bottle		Location 2"			Location 4"			Location 6"			Location 8"			**Average 1344.87**
		LVDT 1	LVDT 2	Avg.	LVDT 1	LVDT 2	Avg.	LVDT 1	LVDT 2	Avg.	LVDT 1	LVDT 2	Avg.	
Replication	1	1156.00	1354.00	1255.00	1109.10	1229.40	1169.25	1229.20	1078.10	1153.65	1350.40	1609.70	1480.05	
	2	1073.60	1211.80	1142.70	1337.10	1448.40	1392.75	1012.10	1139.90	1076.00	1924.70	2093.10	2008.90	
	3	1207.80	1390.50	1299.15	1134.90	1294.90	1214.90	1569.20	1262.60	1415.90	1386.80	1330.50	1358.65	COV (%) 15
	4	1163.50	1336.60	1250.05	1317.70	1426.70	1372.20	1207.20	1257.00	1232.10	1781.60	1611.70	1696.65	
Avg.				1236.73			1287.28			1219.41[1]			1636[2]	
Flour		Location 2"			Location 4"			Location 6"			Location 8"			**Average 618.44**
		LVDT 1	LVDT 2	Avg.	LVDT 1	LVDT 2	Avg.	LVDT 1	LVDT 2	Avg.	LVDT 1	LVDT 2	Avg.	
Replication	1	569.83	561.75	565.79	595.66	592.99	594.33	615.18	627.50	621.34	507.93	480.40	494.17	
	2	664.74	732.04	698.39	627.58	657.59	642.59	567.86	561.31	564.59	800.19	703.04	751.62	
	3	371.96	376.55	374.26	693.95	698.13	696.04	708.66	459.33	584.00	747.85	684.61	716.23	COV (%) 9
	4	498.22	521.01	509.62	686.81	499.36	593.09	796.47	773.10	784.79	715.32	693.21	704.27	
Avg.				537.01			631.51			638.68			666.57	
Empty		Location 2"			Location 4"			Location 6"			Location 8"			**Average 853.84**
		LVDT 1	LVDT 2	Avg.	LVDT 1	LVDT 2	Avg.	LVDT 1	LVDT 2	Avg.	LVDT 1	LVDT 2	Avg.	
Replication	1	780.12	886.89	833.51	737.20	652.36	694.78	500.34	689.08	594.71	1382.10	1260.10	1321.10	
	2	587.19	617.72	602.46	822.01	709.70	765.86	960.67	888.91	924.79	643.80	658.91	651.36	
	3	539.56	617.16	578.36	727.90	744.94	736.42	802.86	1057.20	930.03	1068.80	1047.40	1058.10	COV (%) 18
	4	881.05	973.34	927.20	736.75	821.58	779.17	986.28	1096.50	1041.39	1218.80	1225.70	1222.25	
Avg.				735.38			744.06			872.73			1063.20	

Note: Sensitivity study of packaging stiffness was conducted using two values, [1] and [2]. The percent difference of predicted Compressive Stress Intensity Factors between two packaging stiffness values was less than 6%. Details of sensitivity studies are discussed in Chapter 5.

Table 7. Summary of three model input property values

MOE (lbs./in.^{2})				Rotation Modulus (in.-lbs./radian)		Packaging stiffness (lbs. /in.)		
3/4"		3/8"		3/4"	3/8"	Bottled box	Empty box	Flour sacks
A-1	1340000	B-1	1081000	6494	5921	1345	854	618
A-2	1236000	B-2	1077000					
A-3	1246000	B-3	1082000					
A-4	1118000	B-4	1023000					
A-5	1178000	B-5	1626000					
A-6	730700	B-6	1408000					
A-7	854500	B-7	716800					
A-8	1238000	B-8	822800					
A-9	1173000	B-9	1131000					

CHAPTER 4

4.0 Modeling the Interactions of a Pallet Deck and Packaging

Methodologies used to model the interactions of a pallet deckboard and packaging are discussed in chapter 4. The ultimate goal of this chapter is to develop predictive models of compressive stress distributions at the interface between a pallet deckboard and packaging. Pallet deck deflection models were developed using the theory of beams on an elastic foundation, and the developed models were utilized to model the compressive stress distributions. The general concept and solution of the theory were discussed in section 2.5. This chapter is carried out to achieve the overall goal by following specific objectives:

- To develop pallet deck deflection models using the beam on elastic foundation theory for use in predicting deck deflections imposed by packaging
- To develop models of compressive stress distributions at the interface of a pallet deck and packaging using the developed deck deflection models

4.1 Pallet Deck Deflection Models

Lauer (1991) developed a two-dimensional pallet section model to approximate full size pallet response. The simplified physical model was able to easily control experimental variation and interpret factors influencing the pallet response. The pallet section model representing full size pallets was validated by experimental study and provided acceptable correlations with the testing results. For the current study, simplified two-dimensional pallet section and packaging models, which have been validated in the previous study, were developed to reduce computational time and effort. Figure 19(a) illustrates the two-dimensional simplified unit load model comprised of a box containing products stacked on a pallet section in the stack support condition. The stack support condition is the most commonly used support mode for pallets in warehouses. The pallet section

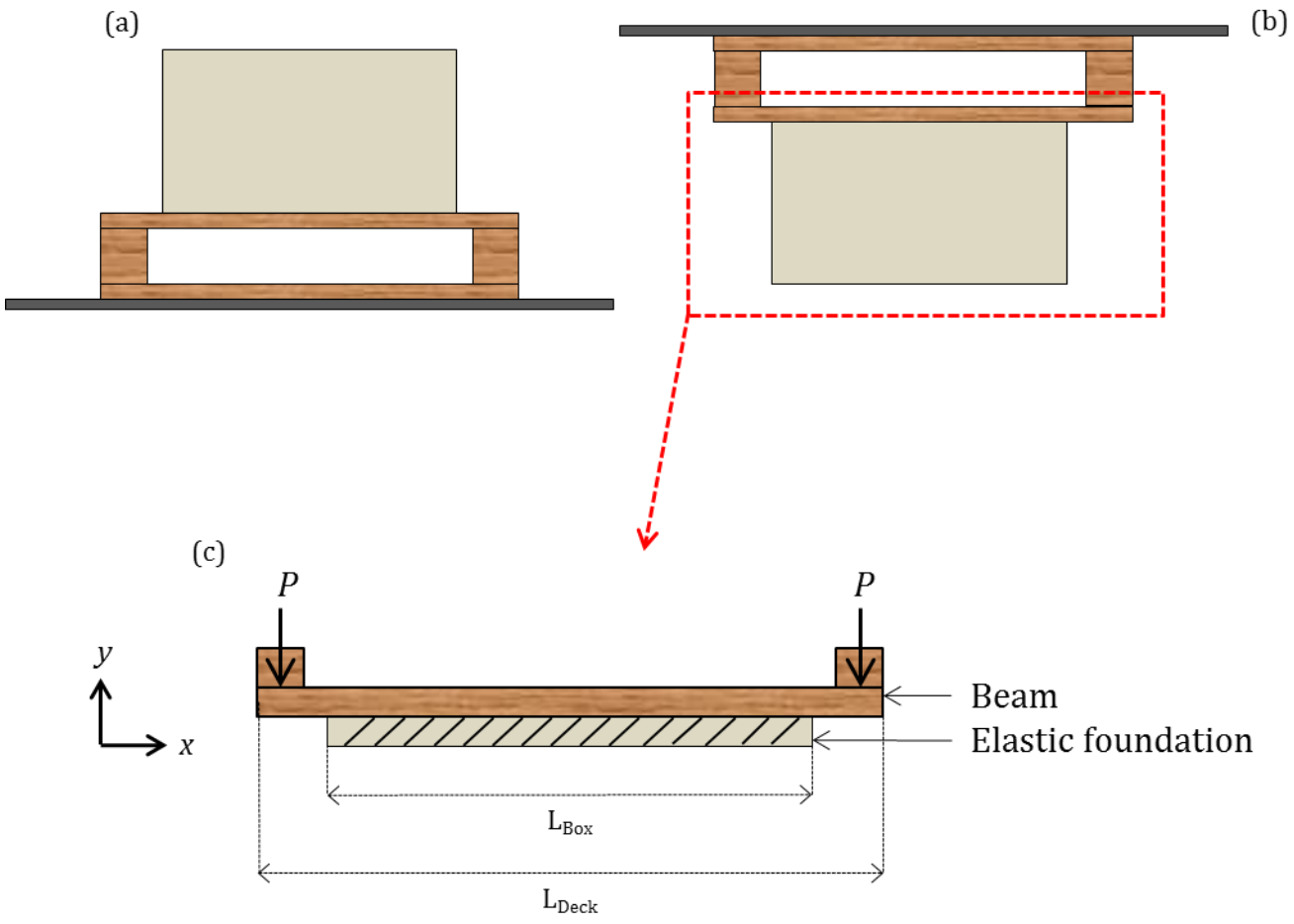

Figure 19. Simplified 2-D unit load model showing schematically that the model physically represents an interaction of the actual packaging on the top of a pallet

model consists of top and bottom deckboards and two stingers. The model of the box containing products is located between two stingers ($L_{Box} < L_{Deck}$) as shown in Figure 19(c). In this case, some load is distributed over the top deckboard and the remaining load is transferred to the stringers as bending reactions. In its simplest form, when assuming that the unit load model is turned upside down (Figure 19(b)), a top pallet deck deflection can be simulated as a one-dimensional beam partially supported by an elastic foundation representing the box containing products. The stingers act primarily as reaction supports in the warehouse stack storage support condition with a unit load sitting on the warehouse floor. For the model turned upside down, therefore, it is assumed that the top deckboard is subjected to two equal concentrated forces, *P,* by two stringers at the ends in the stack support condition (Figure 19(c)). This case can be briefly described as that of a beam with finite length partially supported by an elastic foundation and loaded by two equal concentrated forces, *P*. Euler-Bernoulli beam theory (also known as classical beam theory) and the beam on elastic foundation theory were utilized for unsupported parts and supported parts, respectively, in order to develop pallet deck deflection models which enable the prediction of deck deflection, *y,* at any point, *x*. General solutions for those two theories were discussed in section 2.5.

In this study, the following three different end conditions were separately modeled to investigate the effect of joint stiffness on the pallet deck deflection and compressive stress distribution models: 1) free ends 2) semi-rigid joints and 3) fixed ends. The reaction at each deckboard end in the stack support condition, when the corresponding pallet section is loaded by the packaging, is modeled as described in Figure 20. In the free ends model, the end was assumed to be free to translate but not to rotate. The nailed joint was modeled using rotational spring element representing a semi-rigid joint. The spring constant of the rotational spring was the rotation modulus that was obtained from test results (see Table 7). The fixed end condition assumed that top and bottom decks were perfectly affixed to the stringers. As shown in Figure 20, the top deckboard pivots around the inner edge of the two stringers for all three end conditions in the stack

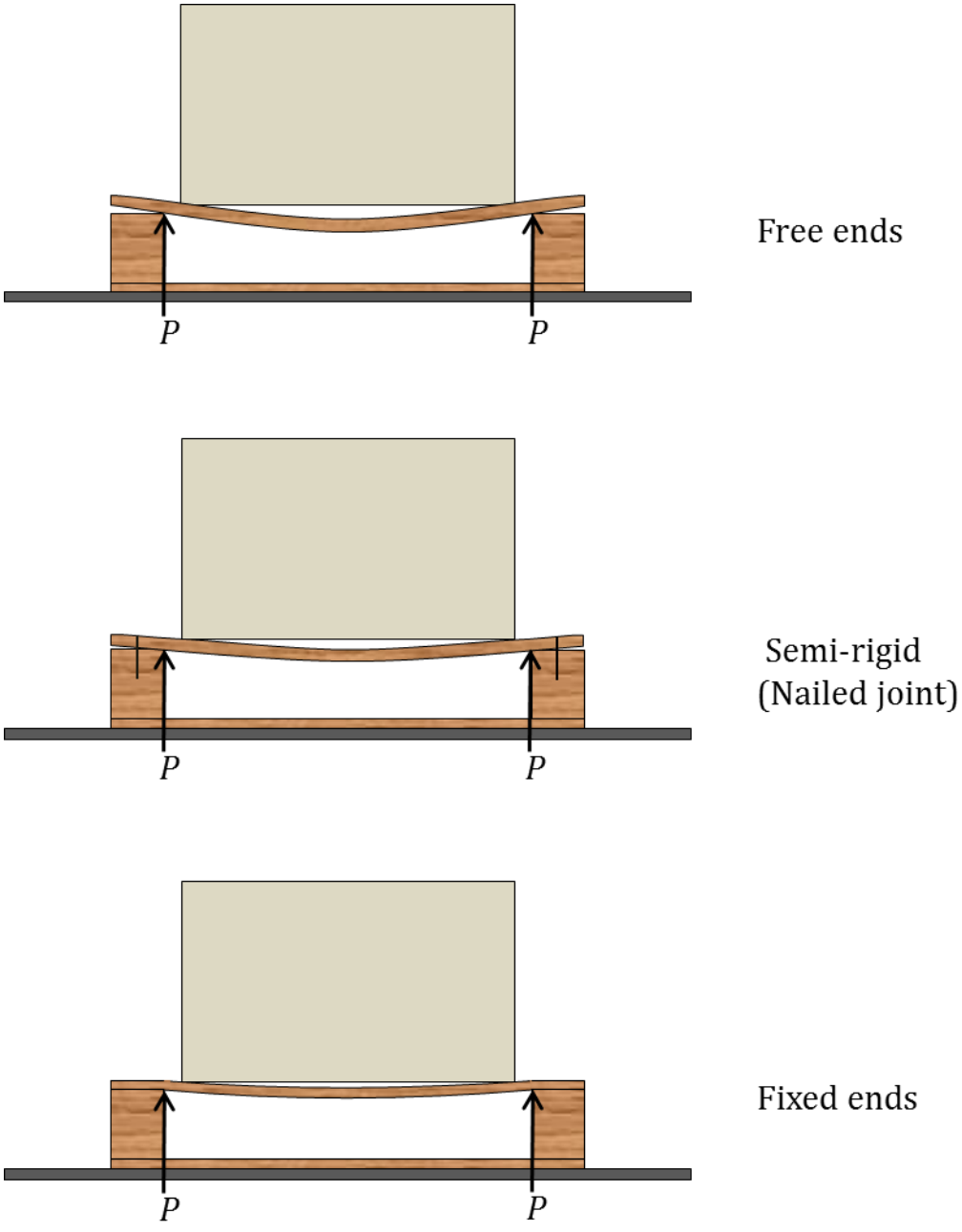

Figure 20. Schematic drawings showing pallet section response for each end condition modeled

support condition. For each case, therefore, each of two equal concentrated forces, *P,* was applied to each of two pivot points. Details of each model of the three conditions are further discussed in the following sections.

4.1.1 Free End Models

Figure 21(a) illustrates the free end model of a top pallet deck partially supported by packaging. Both ends of the model were assumed to be free to translate but not to rotate. The model is simply represented by a beam of finite length with free ends partially supported by an elastic foundation as shown in Figure 21(b). In the model, a concentrated force was applied to the top deck at the inner edge of each stringer, where the pivot point was located. Only a segment between the inner edges of the two stingers of the pallet section was isolated with the ends of this segment labeled A and D (Figure 21(c)). The elastic foundation supporting the beam extended from $x = 0$ to $x = L_2$, therefore the length of the elastic foundation was L_2. The unsupported beam also started at $x = 0$ and extended to $x = -L_1$ at the left end of the beam. Due to symmetry about the center line, the unsupported part from $x = L_2$ to the right end of the beam, was not considered in the model. However, if the supported part from x = 0 and extends to the right end of the beam, that portion must be considered in the beam deflection model.

All reaction forces and moments exerted by the support and end conditions are shown in Figure 21(d) for the free body diagram of the beam with free ends. The sign convention of the free body diagram defined clockwise moment, *M,* and the shearing force, *Q,* acting upward on the left of the elemental section as positive directions as described in Figure 6. As an extension of this convention, the upward-acting loading, *P,* and upward deflection, *y,* were regarded as positive quantities, throughout the whole modeling process in this study. In Figure 21(d), two points A and D are free to translate, therefore there are no shear forces and moment reactions assumed at those points. The forces that corresponded to the deflection were the shear force (*P*) and bending

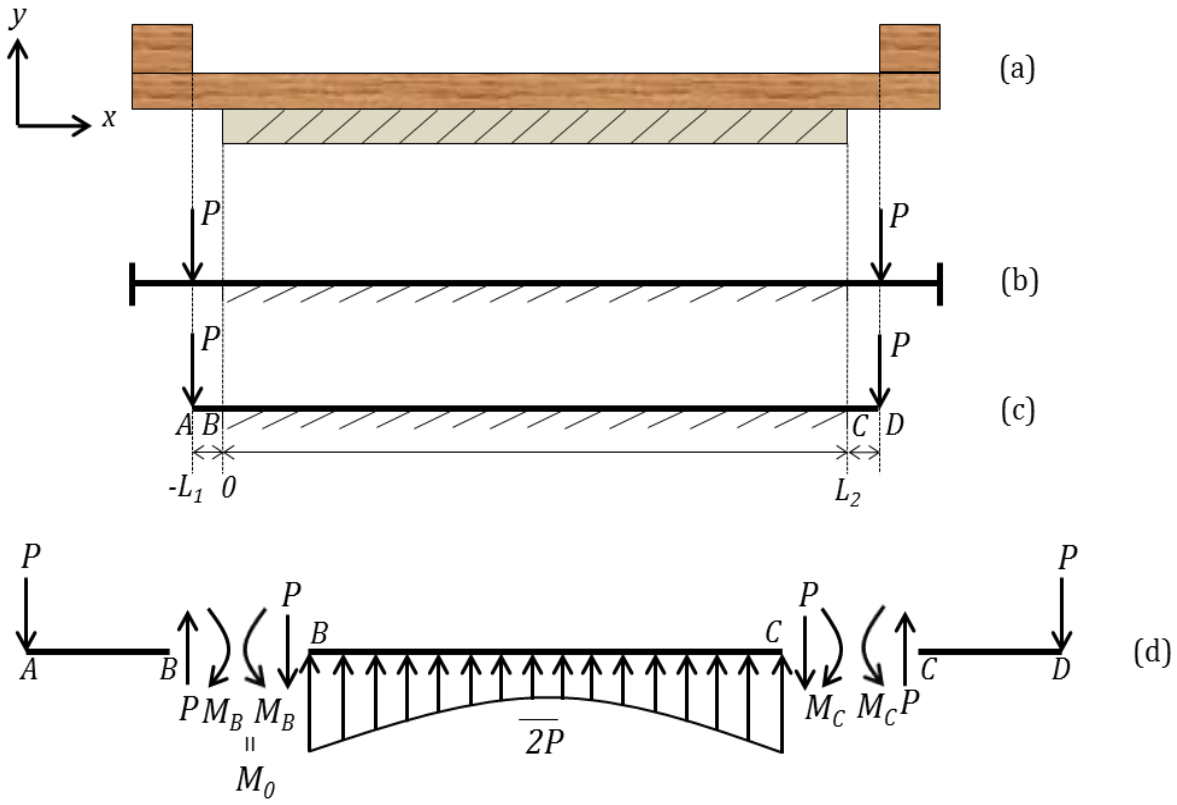

Note: $\overline{2P}$ indicates the sum of the all reaction forces

Figure 21. 1-D beam model with free ends

moment (M) at B and C and the reaction forces at the portion B-C.

4.1.1.1 Modeling Procedures for a Beam with Free Ends

Considering the A-B portion, the interval $-L_1 \le x_1 \le 0$, of the beam in Figure 21(d), the bending moment, M, is given by

$$M(x_1) = P(x_1 + L_1) \quad [9]$$

Since $EI\frac{d^2y}{dx^2} = M(x)$ from equation [1] in section 2.5, equation [9] is written as

$$EI\frac{d^2y}{dx_1{}^2} = P(x_1 + L_1) \quad [10]$$

Since $\frac{dy}{dx} = \theta(x)$, integrating equation [10] with respect to x_1 gives

$$EI\frac{dy}{dx_1} = EI\ \theta(x_1) = \frac{P}{2}(x_1 + L_1)^2 + C_1$$

To obtain C_1, apply the boundary condition, at $x=-L_1$, $\theta=0$ yields $C_1=0$, thus the slope $\theta(x_1)$ is

$$\theta(x_1) = \frac{1}{EI}\left(\frac{P}{2}(x_1 + L_1)^2\right) \quad [11]$$

The deflection $y(x_1)$ is given by integrating equation [11] with respect to x_1 as

$$EI\ y(x_1) = \frac{P}{6}(x_1 + L_1)^3 + C_2$$

$$y(x_1) = \frac{1}{EI}\left(\frac{P}{6}(x_1 + L_1)^3 + C_2\right) \quad [12]$$

The unknown C_2 must be obtained to determine the beam deflection y for any given x_1 on the interval $-L_1 \le x_1 \le 0$.

Considering the B-C portion of the interval $0 \le x_2 \le L_2$ of the beam in Figure 21(d), the deflection, y, as a function of, x_2, can be obtained by the following equation, which represents the

general solution of the beam deflection on an elastic foundation.

$$y(x_2) = y_0F_1(\lambda x_2) + \frac{1}{\lambda}\theta_0F_2(\lambda x_2) - \frac{1}{\lambda^2 EI}M_0F_3(\lambda x_2) - \frac{1}{\lambda^3 EI}Q_0F_4(\lambda x_2) \quad [13]$$

By taking consecutive derivatives of equation [13] and applying

$$\frac{dF_1}{dx_2} = -4\lambda F_4 \qquad \frac{dF_2}{dx_2} = \lambda F_1 \qquad \frac{dF_3}{dx_2} = \lambda F_2 \qquad \frac{dF_4}{dx_2} = \lambda F_3$$

the slope $\theta(x_2)$, moment $M(x_2)$, shear force $Q(x_2)$ can be expressed as

$$\theta(x_2) = \theta_0F_1(\lambda x_2) - \frac{1}{\lambda EI}M_0F_2(\lambda x_2) - \frac{1}{\lambda^2 EI}Q_0F_3(\lambda x_2) - 4\lambda y_0F_4(\lambda x_2) \quad [14]$$

$$M(x_2) = M_0F_1(\lambda x_2) + \frac{1}{\lambda}Q_0F_2(\lambda x_2) + \frac{k}{\lambda^2}y_0F_3(\lambda x_2) + \frac{k}{\lambda^3}\theta_0F_4(\lambda x_2) \quad [15]$$

$$Q(x_2) = Q_0F_1(\lambda x_2) + \frac{k}{\lambda}y_0F_2(\lambda x_2) + \frac{k}{\lambda^2}\theta_0F_3(\lambda x_2) - 4\lambda M_0F_4(\lambda x_2) \quad [16]$$

where

$y_0 =$ deflection $y\ at\ x = 0$

$\theta_0 =$ slope $\theta\ at\ x = 0$

$M_0 =$ bending moment $M\ at\ x = 0$

$Q_0 =$ shear force $Q\ at\ x = 0$

$F_1(\lambda x_2) = Cosh\ \lambda x_2 \cos \lambda x_2$

$F_2(\lambda x_2) = \frac{1}{2}(Cosh\ \lambda x_2\ sin\ \lambda x_2 + Sinh\ \lambda x_2 \cos \lambda x_2)$

$F_1(\lambda x_2) = \frac{1}{2}Sinh\ \lambda x_2 \sin \lambda x_2$

$F_2(\lambda x_2) = \frac{1}{4}(Cosh\ \lambda x_2\ sin\ \lambda x_2 - Sinh\lambda x_2 \cos \lambda x_2)$

$$\lambda = \sqrt[4]{\frac{k}{4EI}}$$

where

k = modulus of foundation

EI = modulus of elasticity*moment of inertia

Five unknowns (C_2, y_0, θ_0, M_0, Q_0), from equation [12] and [13], were computed using the following five boundary conditions. Applying the boundary conditions yields the following equations

(a) at $x_2 = 0$; $Q_0 = P$

$$Q_0 = P \tag{17}$$

(b) at $x_1 = 0$ and $x_2 = 0$; $M(x_1) = M(x_2) = M_0$

using equation [9]

$$M(x_1) = P(x_1 + L_1)$$

$$M_0 = PL_1 \tag{18}$$

(c)at $x_1 = 0$ and $x_2 = 0$; $y(x_1) = y(x_2) = y_0$

using equation [12]

$$y(x_1) = \frac{1}{EI}\left(\frac{P}{6}(x_1 + L_1)^3 + C_2\right)$$

$$y_0 = \frac{1}{EI}\left(\frac{P}{6}{L_1}^3 + C_2\right)$$

$$y_0 - \frac{1}{EI}C_2 = \frac{P{L_1}^3}{6EI} \tag{19}$$

(d)at $x_2 = L_2$; $M = M_0$

using equation [15]

$$M(L_2) = M_0 = M_0F_1(\lambda x_2) + \frac{1}{\lambda}Q_0F_2(\lambda x_2) + \frac{k}{\lambda^2}y_0F_3(\lambda x_2) + \frac{k}{\lambda^3}\theta_0F_4(\lambda x_2)$$

$$0 = (F_1(\lambda x_2) - 1)M_0 + \frac{1}{\lambda}Q_0F_2(\lambda x_2) + \frac{k}{\lambda^2}y_0F_3(\lambda x_2) + \frac{k}{\lambda^3}\theta_0F_4(\lambda x_2) \tag{20}$$

substituting for $Q_0 = P$ and $M_0 = PL_1$ from equations [17] and [18] in equation [20] gives

$$\frac{k}{\lambda^2} y_0 F_3(\lambda x_2) + \frac{k}{\lambda^3} \theta_0 F_4(\lambda x_2) = -(F_1(\lambda x_2) - 1) PL_1 - \frac{P}{\lambda} F_2(\lambda x_2) \quad [21]$$

(e) at $x_2 = L_2$; $Q = -P$

using equation [16]

$$Q(x_2) = -P = Q_0 F_1(\lambda x_2) + \frac{k}{\lambda} y_0 F_2(\lambda x_2) + \frac{k}{\lambda^2} \theta_0 F_3(\lambda x_2) - 4\lambda M_0 F_4(\lambda x_2) \quad [22]$$

$Q_0 = P$ and $M_0 = PL_1$ from equations [17] and [18] are substituted into equation [22]

$$-P - PF_1(\lambda x_2) + 4\lambda F_4(\lambda x_2) PL_1 = +\frac{k}{\lambda} y_0 F_2(\lambda x_2) + \frac{k}{\lambda^2} \theta_0 F_3(\lambda x_2) \quad [23]$$

To obtain the remaining three unknowns $y_0, C_2,$ and θ_0, equations [19], [21], and [23] are represented in a matrix form as follows:

$$\begin{bmatrix} 1 & -\frac{1}{EI} & 0 \\ \frac{kF_3(\lambda x_2)}{\lambda^2} & 0 & \frac{kF_4(\lambda x_2)}{\lambda^3} \\ \frac{kF_2(\lambda x_2)}{\lambda} & 0 & \frac{kF_3(\lambda x_2)}{\lambda^2} \end{bmatrix} \begin{bmatrix} y_0 \\ C_2 \\ \theta_0 \end{bmatrix} = \begin{bmatrix} \frac{PL_1{}^3}{6EI} \\ -(F_1(\lambda x_2) - 1) PL_1 - \frac{P}{\lambda} F_2(\lambda x_2) \\ -P - PF_1(\lambda x_2) + 4\lambda F_4(\lambda x_2) PL_1 \end{bmatrix}$$

solving for $y_0, C_2,$ and θ_0 by

$$\begin{bmatrix} y_0 \\ C_2 \\ \theta_0 \end{bmatrix} = \begin{bmatrix} 1 & -\frac{1}{EI} & 0 \\ \frac{kF_3(\lambda x_2)}{\lambda^2} & 0 & \frac{kF_4(\lambda x_2)}{\lambda^3} \\ \frac{kF_2(\lambda x_2)}{\lambda} & 0 & \frac{kF_3(\lambda x_2)}{\lambda^2} \end{bmatrix}^{-1} \begin{bmatrix} \frac{PL_1{}^3}{6EI} \\ -(F_1(\lambda x_2) - 1) PL_1 - \frac{P}{\lambda} F_2(\lambda x_2) \\ -P - PF_1(\lambda x_2) + 4\lambda F_4(\lambda x_2) PL_1 \end{bmatrix}$$

$$y_0 = (F_4 * \lambda * (P + F_1 * P - 4 * F_4 * L1 * P * \lambda))/(k * (F_3^2 - F_2 * F_4)) - (F_3 * \lambda^2 * (L1 * P * (F_1 - 1) + (F_2 * P)/\lambda))/(k * (F_3^2 - F_2 * F_4))$$

$$C_2 = (EI * F_4 * \lambda * (P + F_1 * P - 4 * F_4 * L1 * P * \lambda))/(k * (F_3^2 - F_2 * F_4)) - (EI * F_3 * \lambda^2 * (L1 * P * (F_1 - 1) + (F_2 * P)/\lambda))/(k * (F_3^2 - F_2 * F_4)) - (L1^3 * P)/6$$

$$\theta_0 = (F_2 * \lambda^3 * (L1 * P * (F_1 - 1) + (F_2 * P)/\lambda))/(k * (F_3^2 - F_2 * F_4)) - (F_3 * \lambda^2 * (P + F_1 * P - 4 * F_4 * L1 * P * \lambda))/(k * (F_3^2 - F_2 * F_4))$$

Once the three unknowns were determined by solving the above matrix form, they were applied to equation [12] and [13] to obtain deflection $y(x_1)$ and deflection $y(x_2)$. All input values used for modeling the predicted free ends beam deflections are tabulated in Table 8. Each force *P* was determined by sum of 175 pounds (applied compression load on the top of the box, 350 pounds, divided by 2) and the weight of each packaging shown in Table 5.

Table 8. Input values used for modeling the free ends beam deflections

		Bottle	**Empty**	**Flour**
P (lbs.)		183	175	190
k (lbs./in.)		1345	854	615
L_1 (in.)		0.5		
L_2 (in.)		16		
EI (lbs.in.^{2})		**E**	**I**	**EI**
	1	854500	0.1051	89810
3/4"	2	1238000	0.1253	155100
	3	1173000	0.1255	147200
	1	716800	0.0147	10540
3/8"	2	822800	0.0153	12590
	3	1131000	0.0145	16400

4.1.1.2 Results and Discussion for Free End Deflection Models

Data obtained from modeling were analyzed by the following process presented in Figure 22. By computing the matrix form and all equations derived in the previous section, the initial deflection curve of the top pallet deck partially supported by packaging (x = 0 to 16-inch) was obtained as shown in Figure 22. The initial deflection curve plots of deflection *y* in inches for any given location *x* in inches from *x* = -0.5 to 16 were generated. It was initially assumed the unit load model was turned upside down (see Figure 19(b)) and the y-axis of the initial deflection curve was reversed to predict the original deflected shape of the top deck (see Figure 19(a)). Since the reference was at x = -0.5-inch, the deflection value at the location *x* is -0.5-inch (pivot point) was subtracted from all points of deflection. The same process was used for deflections of all three different end conditions.

Figure 23, 24, and 25 are graphs showing predictive models of the free end pallet deck (beam) deflections by the box containing bottles, the empty box, and the box containing flour sacks, respectively. Each figure contains six different color plots of deflection models to show the effect of pallet deck stiffness on the pallet deck deflection for the free end connection. The effects of pallet deck stiffness and packaging stiffness property on the free end deck deflection models are discussed in this section. As shown in each legend in Figure 22, 23 and 24, each color represents different *EI* (modulus of elasticity (*E*) X moment of inertia (*I*)) of which the first three *EI*s and the last three *EI*s indicate the pallet deck with 3/4-inch and 3/8-inch thickness, respectively. It is hypothesized that the thicker pallet deckboard components increase the stiffness of the pallet section. The thinner pallet decks (3/8-inch) resulted in more deflections than the thicker decks (3/4-inch) by all of three different packaging stiffness values (three *k* values) used for free ends models. The deflection *y* was plotted against the location of the deckboard at every 0.1-inch and 0.4-inch on the intervals $-0.5 \leq x \leq 0$ and $0 \leq x \leq 16$, respectively.

Assuming free ends, the maximum predicted deflections of the 3/4-inch deckboard, supporting the empty box and the box containing flour sacks, were 20% and 50% greater respectively than the predicted maximum deflection by bottles in a box. The 3/8-inch deckboard predicted deflection increased by 36% and 91% supporting an empty box and flours in a box, respectively compared to the box containing bottles. The lower stiffness 3/8-inch deckboard deflected 88%, 113%, and 140% more than the 3/4-inch deckboard when supporting the bottles, empty box, and flour sacks respectively. The 3/4-inch deckboard were about 50% stiffer than the 3/8-inch deckboard. The model predicted significant sensitivity of deck deflection to changes in deck stiffness and packaging stiffness for free end condition.

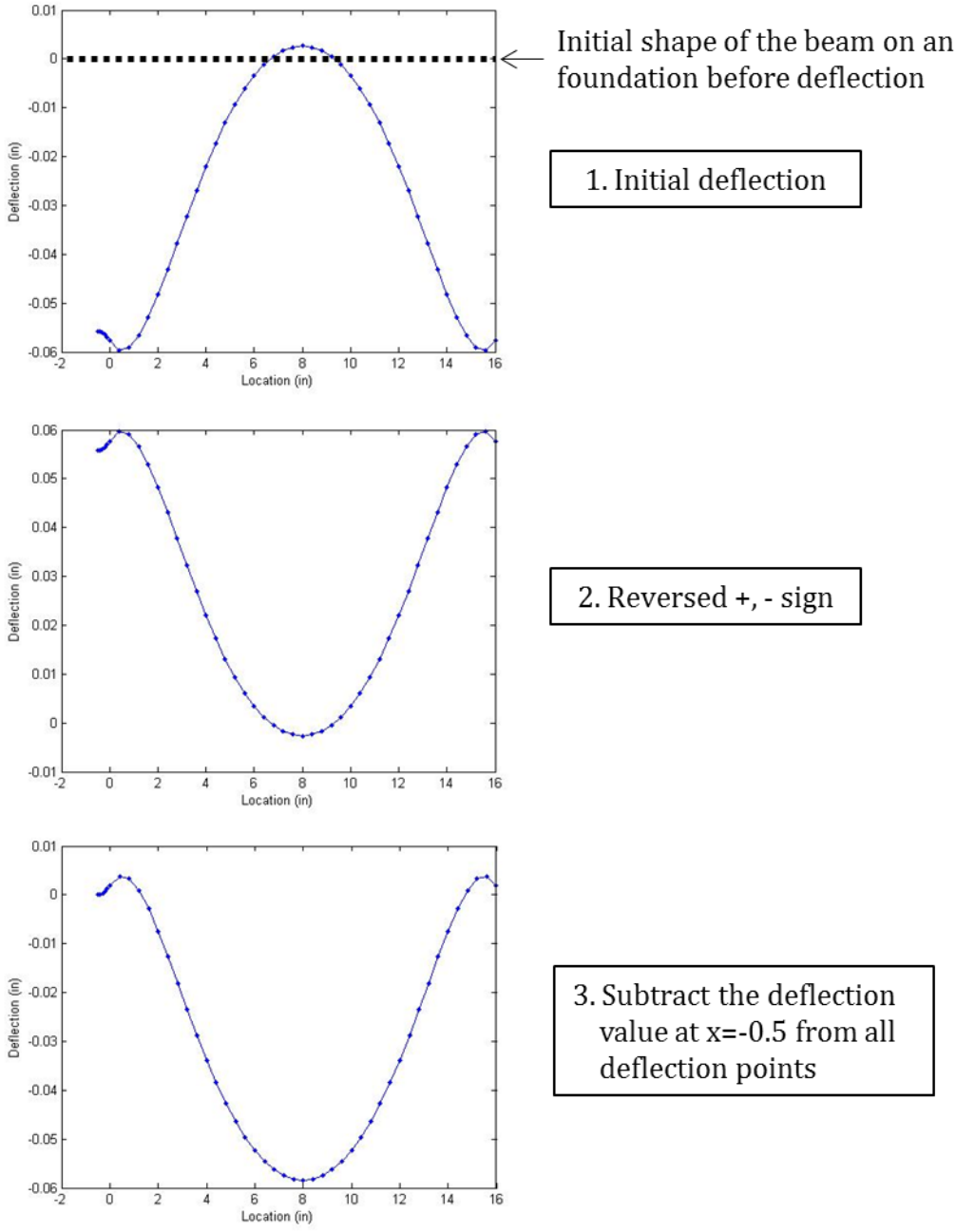

Figure 22. Schematic diagrams showing the deck deflection data inversion and normalization process

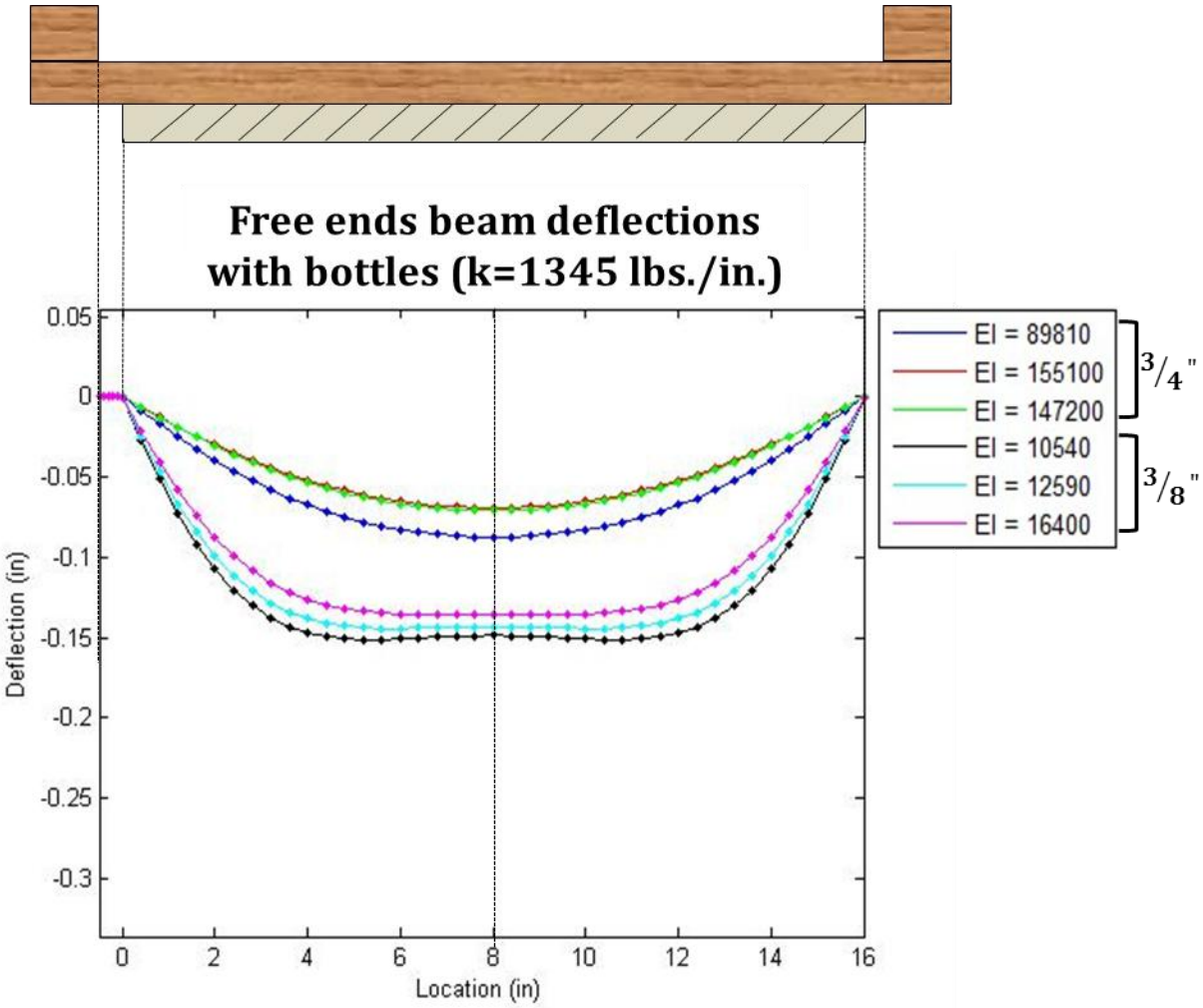

Figure 23. Free end model prediction of beam deflection loaded by a box containing plastic bottles for two deckboard thicknesses

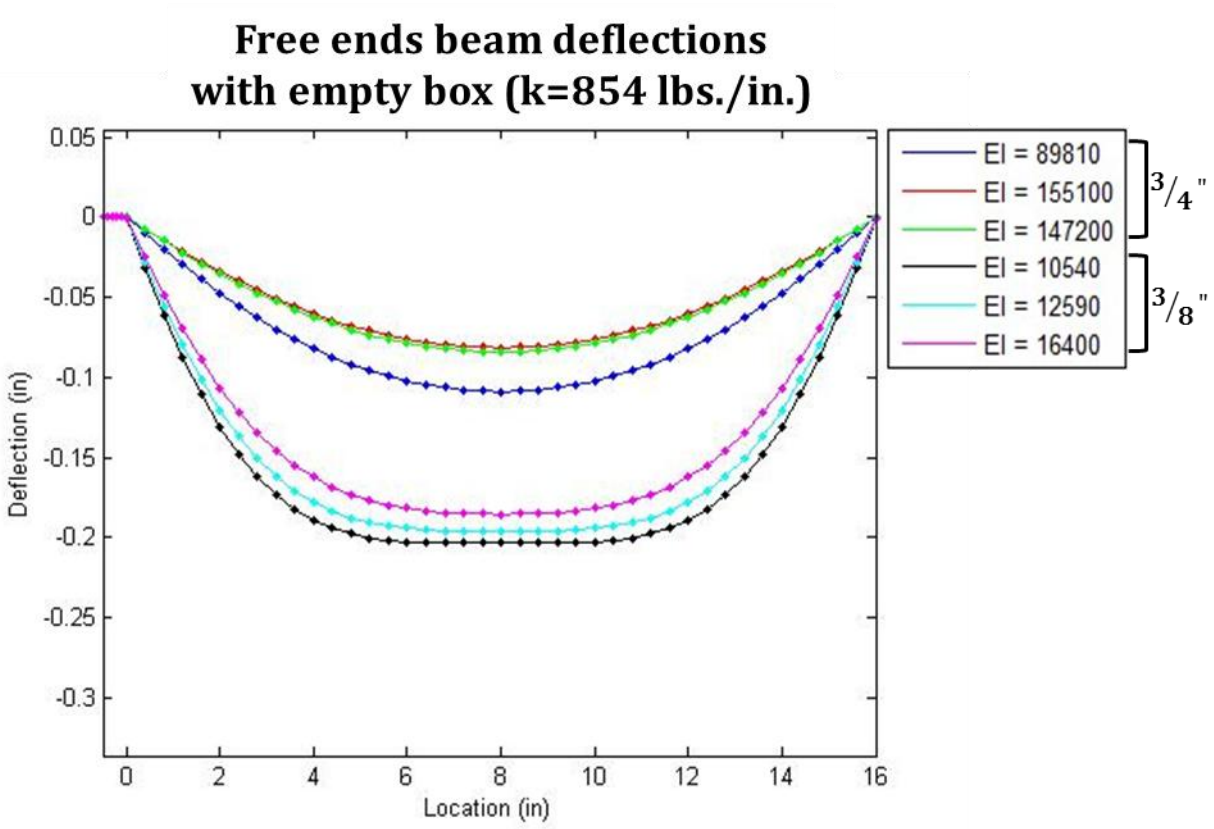

Figure 24. Free end model prediction of beam deflection loaded by an empty box for two deckboard thicknesses

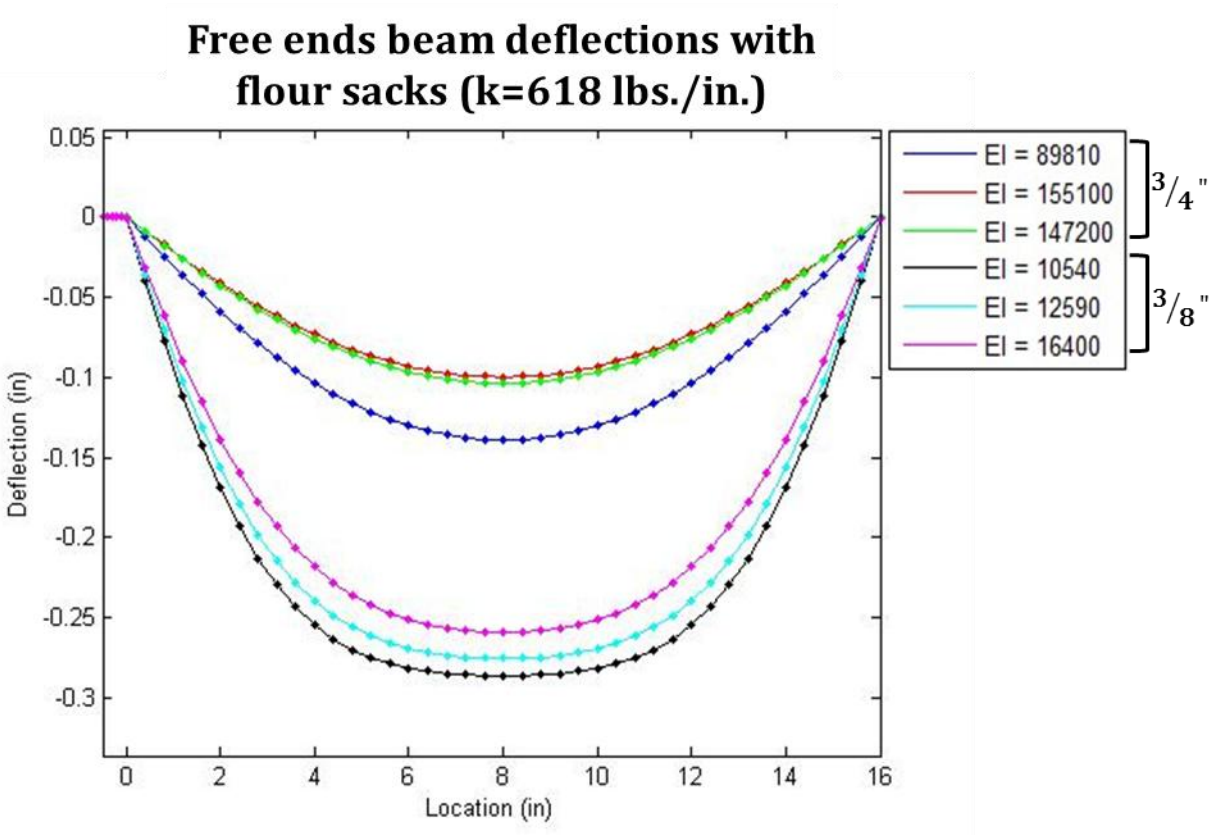

Figure 25. Free end model prediction of beam deflection loaded by a box containing flour sacks for two deckboard thicknesses

4.1.2 Semi-Rigid Joint Models

The nailed joints were modeled as semi-rigid connections including a certain degree of relative rotational stiffness. The zero-length rotational springs were used to model the semi-rigid connections as shown in Figure 26(b). The rotational spring represents a support that provides some rotational restraint but does not provide any translational restraint (Chen, 1997). The spring stiffness can be determined by the ratio of units of moment to unit rotation. The spring constant for rotational stiffness was experimentally determined using the joint rotation test setup shown in Figure 12. The spring constant obtained from joint rotation testing is called the rotation modulus. The testing procedures for the rotation modulus were described in section 3.2 and the results were shown in Table 4.

Due to the semi-rigid connection, shear forces and moment reactions exist at the both ends of the beam. The scope of this research was limited to model only the segment between the inner edges of the two stringers of the pallet section as in the free end model. The location of the applied concentrated forces *P* for semi-rigid models was the same as in the free end models. The moment at point A (M_A) was defined in terms of the force exerted by nails (F_N) and the distance between the nail location and the inner edge of the stringer (d). Therefore the moment was defined as $M_A = F_N \times d$ as shown in Figure 26(b). Figure 27 shows a schematic drawing showing the calculation for F_N. The F_N can be computed by the following equation:

$$\mathrm{RM} = \frac{M}{\theta} = \frac{F_N d^2}{\Delta}$$

$$\mathrm{M} = F_N * d$$

$$\theta = \Delta/d \quad (\text{for small } \theta, \tan\theta = \theta)$$

$$F_N = \frac{RM\,\Delta}{d^2}$$

where

RM= Rotation Modulus (in.-lbs./radian)

M= moment (in.-lbs.)

θ = rotation (radian)

F_N = force exerted by nails (lbs.)

d = distance between the nail location and the inner edge of the stringer (in.)

Δ = vertical displacement of the neutral axis of the depth of the deck at the nail location (in.)

The deflection (Δ) in Table 9 is the average of 18 replications experimentally measured from testing. The testing procedure will be further described in chapter 5. The deflection data are tabulated in Table 1 of Appendix A. The measured deflection was assumed to be not affected by deck stiffness, packaging stiffness and nail type. M_A value used for predicting the semi-rigid joint beam deflection is tabulated in Table 9. The average of M_A for 3/4-inch and 3/8-inch deckboards was used in the semi-rigid model.

Table 9. Moment (M_A) value used for semi-rigid joints model

	RM (in.-lbs. /radian)	**Deflection (Δ) (in.)**	**d (in.)**	**F_N ($RM*\Delta/d^2$) (lbs.)**	**M_A (F_N*d) (in.-lbs.)**	**Avg. M_A**
3/4"	6494	-0.003	0.75	-34.63	25.97	24.83
3/8"	5921	-0.003	0.75	-31.58	23.69	

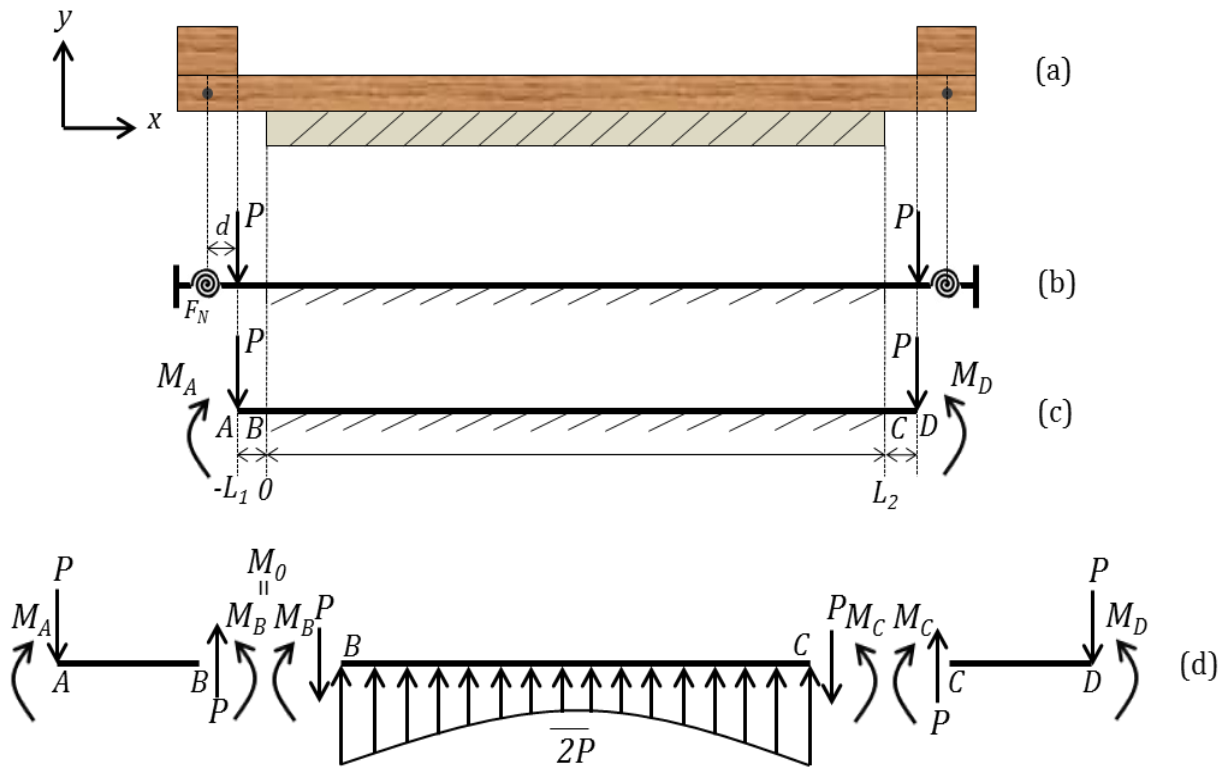

Note: $\overline{2P}$ indicates the sum of the all reaction forces

Figure 26. 1-D beam model with semi-rigid joints

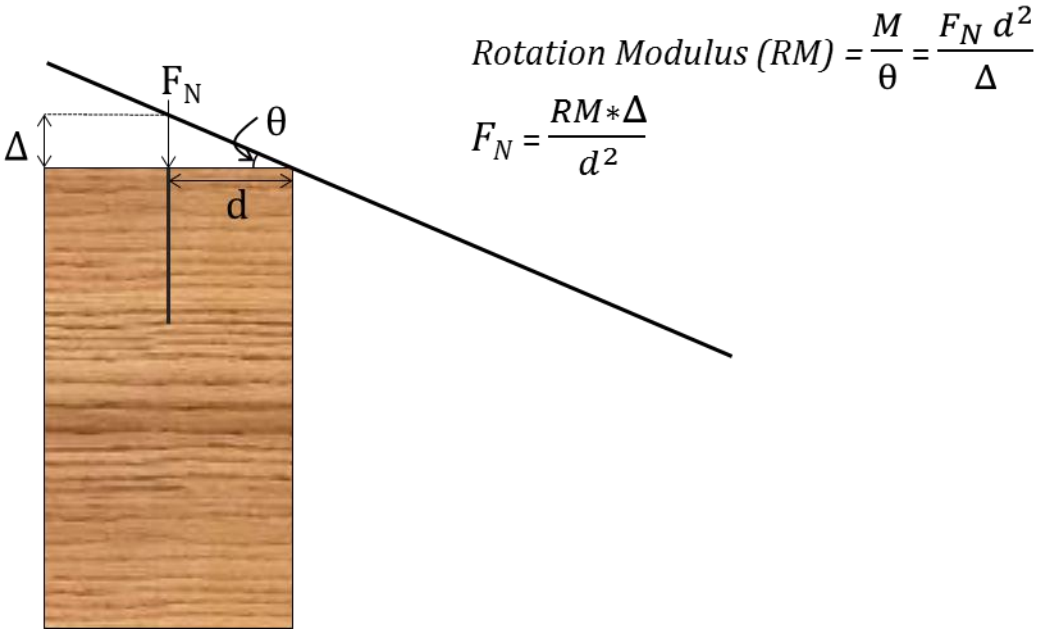

Figure 27. A schematic drawing showing the calculation for F_N

4.1.2.1 Modeling Procedures for a Beam with Semi-Rigid Joints

Considering the A-B portion, the interval $-L_1 \le x_1 \le 0$, of the beam in Figure 26(d) the bending moment M is given by

$$M(x_1) = M_A - P(x_1 + L_1) \qquad [24]$$

Since $EI\frac{d^2y}{dx^2} = M(x)$ from the equation [1] in section 2.5, equation [24] is written as

$$EI\frac{d^2y}{dx_1{}^2} = M_A - P(x_1 + L_1) \qquad [25]$$

Since $\frac{dy}{dx} = \theta(x)$, integrating equation [25] with respect to x_1 gives

$$EI\frac{dy}{dx_1} = EI\,\theta(x_1) = M_A x_1 - \frac{P}{2}(x_1 + L_1)^2 + C_1$$

To obtain C_1, apply the boundary condition, at $x=-L_1$, $\theta=0$ yields $C_1=0$, thus the slope $\theta(x_1)$ is

$$\theta(x_1) = \frac{1}{EI}\left(M_A x_1 - \frac{P}{2}(x_1 + L_1)^2 + M_A L_1\right) \qquad [26]$$

The deflection $y(x_1)$ is given by integrating the equation [26] with respect to x_1 as

$$EI\,y(x_1) = \frac{M_A}{2}x_1{}^2 - \frac{P}{6}(x_1 + L_1)^3 + M_A L_1 x_1 + C_2$$

$$y(x_1) = \frac{1}{EI}\left(-\frac{P}{6}(x_1 + L_1)^3 + \frac{M_A}{2}x_1{}^2 + M_A L_1 x_1 + C_2\right) \qquad [27]$$

The unknown C_2 must be obtained to determine the beam deflection y at any point x_1 on the interval $-L_1 \le x_1 \le 0$.

Considering the B-C portion of the interval $0 \le x_2 \le L_2$ of the beam presented in Figure 26(d) the deflection y as a function of x_2 can be obtained by equation [13].

Five unknowns (C_2, y_0, θ_0, M_0, Q_0), from equation [27] and [13], were evaluated using the following five boundary conditions. Applying the boundary conditions gives the following equations

(a) at $x_2 = 0$; $Q_0 = P$

$$Q_0 = P \tag{28}$$

(b) at $x_1 = 0$ and $x_2 = 0$; $M(x_1) = M(x_2) = M_0$

using the equation [24]

$$M(x_1) = M_A - P(x_1 + L_1)$$
$$M_0 = M_A - PL_1 \tag{29}$$

(c) at $x_1 = 0$ and $x_2 = 0$; $y(x_1) = y(x_2) = y_0$

using the equation [27]

$$y(x_1) = \frac{1}{EI}\left(-\frac{P}{6}(x_1 + L_1)^3 + \frac{M_A}{2}{x_1}^2 + M_A L_1 x_1 + C_2\right)$$
$$y_0 = \frac{1}{EI}\left(-\frac{P}{6}{L_1}^3 + C_2\right)$$
$$y_0 - \frac{1}{EI}C_2 = -\frac{P{L_1}^3}{6EI} \tag{30}$$

(d) at $x_2 = L_2$; $M = M_0$

using equation [15]

$$M(L_2) = M_0 = M_0 F_1(\lambda x_2) + \frac{1}{\lambda}Q_0 F_2(\lambda x_2) + \frac{k}{\lambda^2}y_0 F_3(\lambda x_2) + \frac{k}{\lambda^3}\theta_0 F_4(\lambda x_2)$$
$$0 = (F_1(\lambda x_2) - 1)M_0 + \frac{1}{\lambda}Q_0 F_2(\lambda x_2) + \frac{k}{\lambda^2}y_0 F_3(\lambda x_2) + \frac{k}{\lambda^3}\theta_0 F_4(\lambda x_2) \tag{31}$$

substituting for equations [28] and [29] in equation [31] yields

$$\frac{k}{\lambda^2}y_0 F_3(\lambda x_2) + \frac{k}{\lambda^3}\theta_0 F_4(\lambda x_2) = -(F_1(\lambda x_2) - 1)(M_A - PL_1) - \frac{P}{\lambda}F_2(\lambda x_2) \tag{32}$$

(e) at $x_2 = L_2$; $Q = -P$

$$Q(x_2) = -P = Q_0F_1(\lambda x_2) + \frac{k}{\lambda}y_0F_2(\lambda x_2) + \frac{k}{\lambda^2}\theta_0F_3(\lambda x_2) - 4\lambda M_0F_4(\lambda x_2) \quad [33]$$

substituting for equations [28] and [29] in equation [33] gives

$$\frac{k}{\lambda}y_0F_2(\lambda x_2) + \frac{k}{\lambda^2}\theta_0F_3(\lambda x_2) = -P - PF_1(\lambda x_2) + 4\lambda F_4(\lambda x_2)(M_A - PL_1) \quad [34]$$

To determine the three unknowns $y_0, C_2,$ and θ_0, equations [30], [32], and [34] can be written in a matrix form as

$$\begin{bmatrix} 1 & -\frac{1}{EI} & 0 \\ \frac{kF_3(\lambda x_2)}{\lambda^2} & 0 & \frac{kF_4(\lambda x_2)}{\lambda^3} \\ \frac{kF_2(\lambda x_2)}{\lambda} & 0 & \frac{kF_3(\lambda x_2)}{\lambda^2} \end{bmatrix} \begin{bmatrix} y_0 \\ C_2 \\ \theta_0 \end{bmatrix} = \begin{bmatrix} -\frac{PL_1{}^3}{6EI} \\ -(F_1(\lambda x_2) - 1)(M_A - PL_1) - \frac{P}{\lambda}F_2(\lambda x_2) \\ -P - PF_1(\lambda x_2) + 4\lambda F_4(\lambda x_2)(M_A - PL_1) \end{bmatrix}$$

Computing $y_0, C_2,$ and θ_0 by

$$\begin{bmatrix} y_0 \\ C_2 \\ \theta_0 \end{bmatrix} = \begin{bmatrix} 1 & -\frac{1}{EI} & 0 \\ \frac{kF_3(\lambda x_2)}{\lambda^2} & 0 & \frac{kF_4(\lambda x_2)}{\lambda^3} \\ \frac{kF_2(\lambda x_2)}{\lambda} & 0 & \frac{kF_3(\lambda x_2)}{\lambda^2} \end{bmatrix}^{-1} \begin{bmatrix} -\frac{PL_1{}^3}{6EI} \\ -(F_1(\lambda x_2) - 1)(M_A - PL_1) - \frac{P}{\lambda}F_2(\lambda x_2) \\ -P - PF_1(\lambda x_2) + 4\lambda F_4(\lambda x_2)(M_A - PL_1) \end{bmatrix}$$

$y_0 = (F_4 * \lambda * (P + F_4 * P - 4 * F_4 * \lambda * (M_A - L1 * P)))/(k * (F_3^2 - F_2 * F_4)) - (F_3 * \lambda^2 * ((F_1 - 1) * (M_A - L1 * P) + (F_2 * P)/\lambda))/(k * (F_3^2 - F_2 * F_4))$

$C_2 = (L1^3 * P)/6 - (EI * F_3 * \lambda^2 * ((F_1 - 1) * (M_A - L1 * P) + (F_2 * P)/\lambda))/(k * (F_3^2 - F_2 * F_4)) + (EI * F_4 * \lambda * (P + F_1 * P - 4 * F_4 * \lambda * (M_A - L1 * P)))/(k * (F_3^2 - F_2 * F_4))$

$$\theta_0 = (F_2 * \lambda^3 * ((F_1 - 1) * (M_A - L1 * P) + (F_2 * P)/\lambda))/(k * (F_3^2 - F_2 * F_4)) - (F_3 * \lambda^2 * (P + F_1 * P - 4 * F_4 * \lambda * (M_A - L1 * P)))/(k * (F_3^2 - F_2 * F_4))$$

The three unknowns determined by solving the above matrix form, were applied to equation [27] and [13] to determine deflection $y(x_1)$ and deflection $y(x_2)$. All input values used for modeling the deflections are in Table 10.

Table 10. Input values used for model prediction of the semi-rigid joint beam deflection

		Bottle	**Empty**	**Flour**
P (lbs.)		183	175	190
k (lbs./in.)		1345	854	618
L_1 (in.)		0.5		
L_2 (in.)		16		
EI (lbs.in.^{2})		**E**	**I**	**EI**
	1	1118000	0.1251	139900
3/4"	2	1178000	0.1249	147100
	3	730700	0.1236	90310
	1	1023000	0.0150	15350
3/8"	2	1626000	0.0145	23580
	3	1408000	0.0146	20560

4.1.2.2 Results and Discussion for Semi-Rigid Joint Models

Figure 28, 29, and 30 present the plots of predicted semi-rigid joint beam deflection models supporting bottles contained a box, an empty box, and a box containing flour sacks, respectively. Each figure has six different plots including three replications for each deck thickness. The maximum predicted deflection of 3/8-inch deckboard supporting bottles in a box was, on average, 62% greater than 3/4-inch deckboard. The lower stiffness 3/8-inch deckboard deflected 85%, and 108% more than the 3/4-inch deckboard when supporting empty box and flour sacks respectively. When comparing the semi-rigid joint deflection models of three different packaging stiffness properties, lower stiffness packaging results in greater effect of the pallet deck stiffness on the maximum predicted deflection. The 3/8-inch pallet deck showed greater influence of the packaging stiffness on the maximum predicted deflection than the 3/4-inch pallet deck for the semi-rigid joint pallet. Stiffer packaging has less effect of the pallet deck stiffness on the resulted maximum predicted deflections.

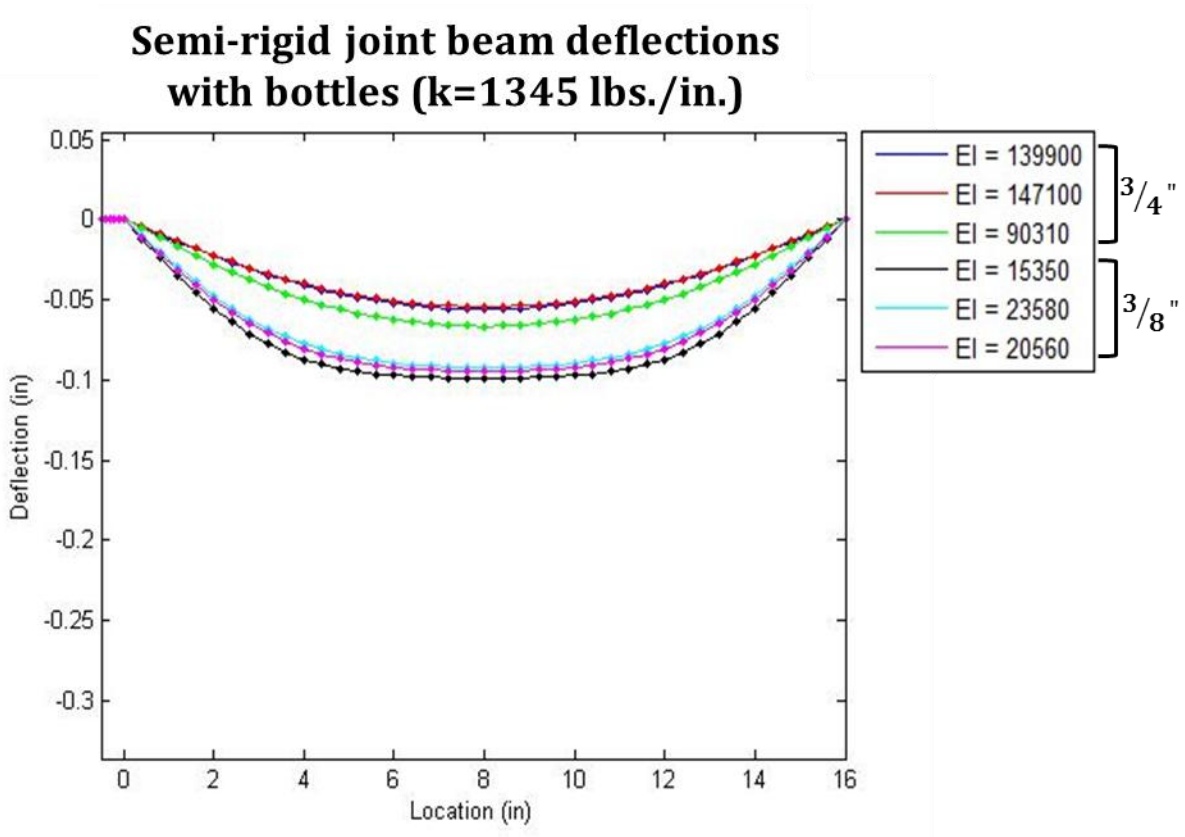

Figure 28. Semi-rigid joint model prediction of beam deflection loaded by a box containing plastic bottles for two deckboard thicknesses

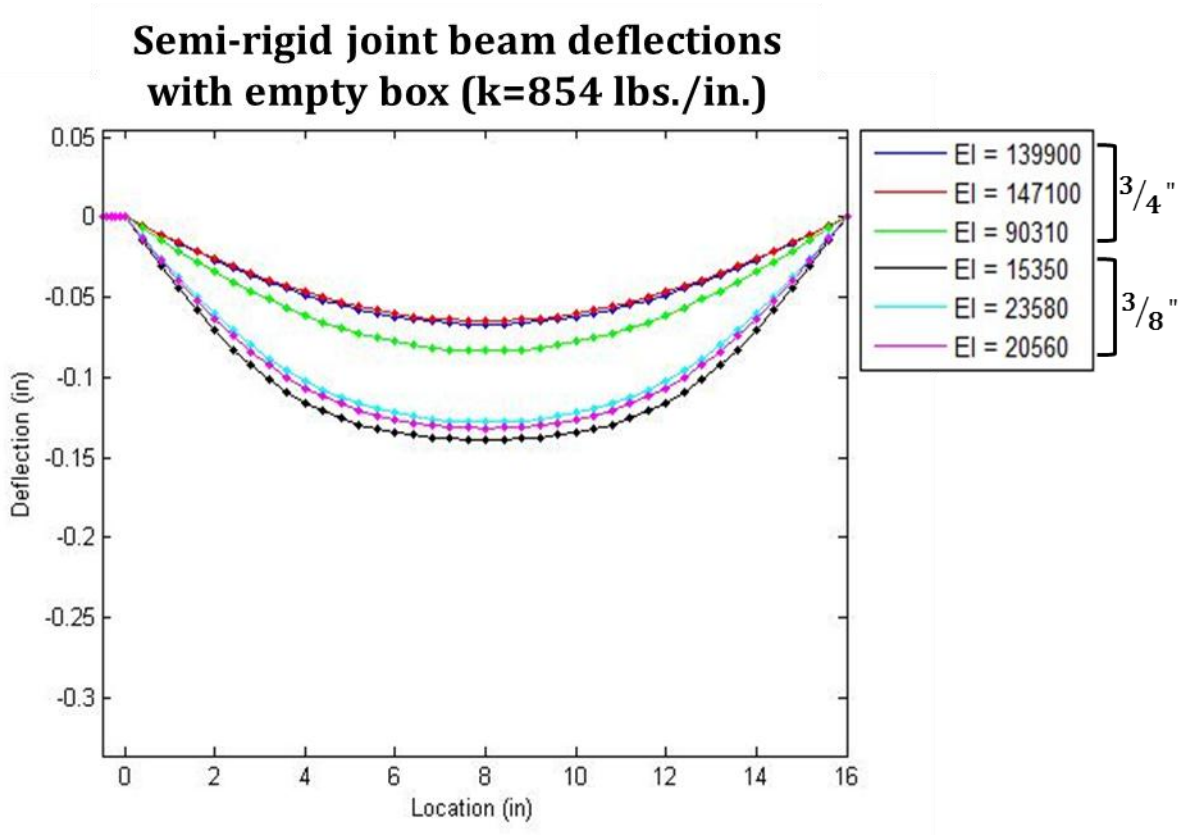

Figure 29. Semi-rigid joint model prediction of beam deflection loaded by an empty box for two deckboard thicknesses

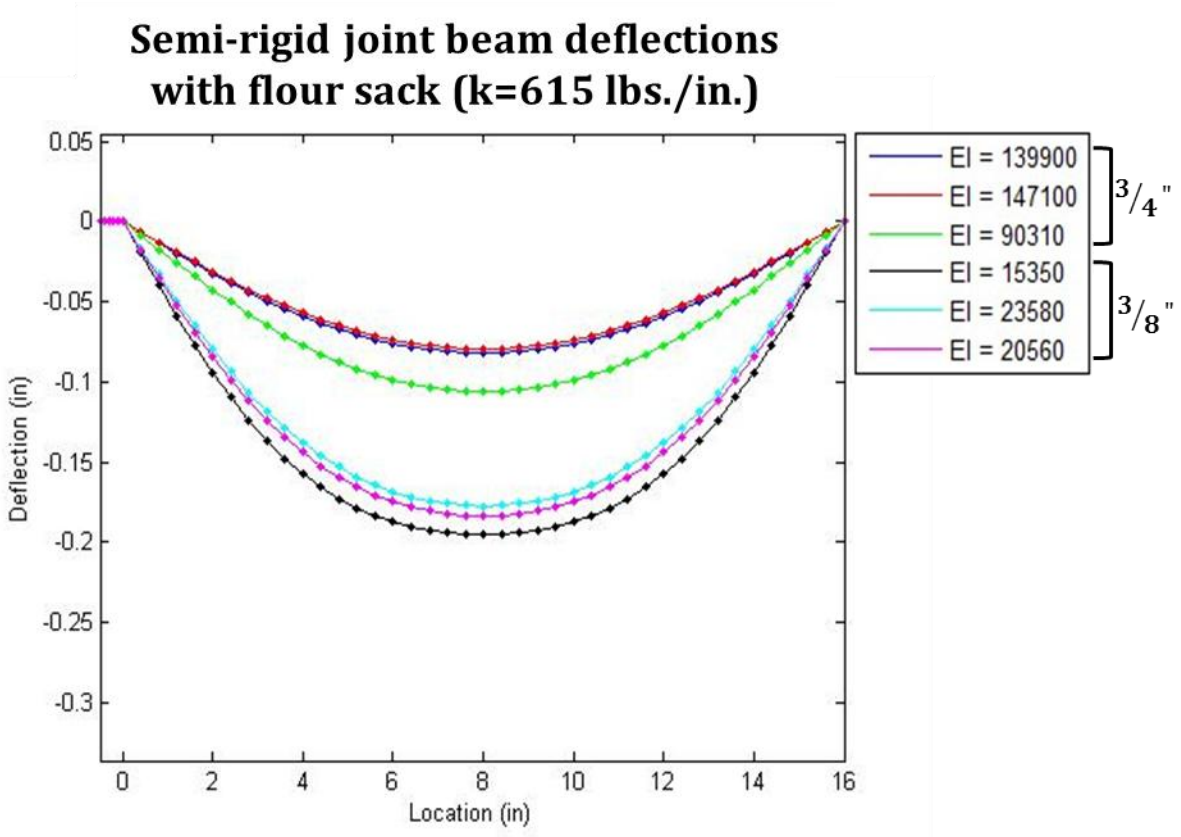

Figure 30. Semi-rigid joint model prediction of beam deflection loaded by a box containing flour sacks for two deckboard thicknesses

4.1.3 Fixed End Models

For the simulated fixed end condition, it was assumed that the stringers are affixed to the pallet deck at the deckboard ends, therefore the stringer portions contacting the deck were assumed to be fixed supports. Two equal concentrated forces, *P,* were applied at the same pivot locations as in the free end and semi-rigid joint conditions as shown in Figure 31(b). The beam with fixed ends, point *A* and *B*, can neither translate nor rotate under the action of applied loads. Consequently, the shear force and moment reactions exist at the both fixed ends. The free body diagram in Figure 31(d) presents all moments and reaction forces generated by applying loads to the beam on an elastic foundation. As in the cases of free end model and semi-rigid joint model, the portion C-D was not considered in the model due to symmetry.

4.1.3.1 Modeling Procedures for a Beam with Fixed Ends

Considering the A-B portion, the interval $-L_1 \leq x_1 \leq 0$, of the beam in Figure 31(d) the bending moment *M* is given by

$$M(x_1) = M_A - P(x_1 + L_1) \quad [35]$$

Since $EI\frac{d^2y}{dx^2} = M(x)$ from equation [1] in section 2.5, equation [35] is expressed as

$$EI\frac{d^2y}{dx_1^{\,2}} = M_A - P(x_1 + L_1) \quad [36]$$

Since$\frac{dy}{dx} = \theta(x)$, integrating equation [36] with respect to x_1 gives

$$EI\frac{dy}{dx_1} = EI\,\theta(x_1) = M_A x_1 - \frac{P}{2}(x_1 + L_1)^2 + C_1$$

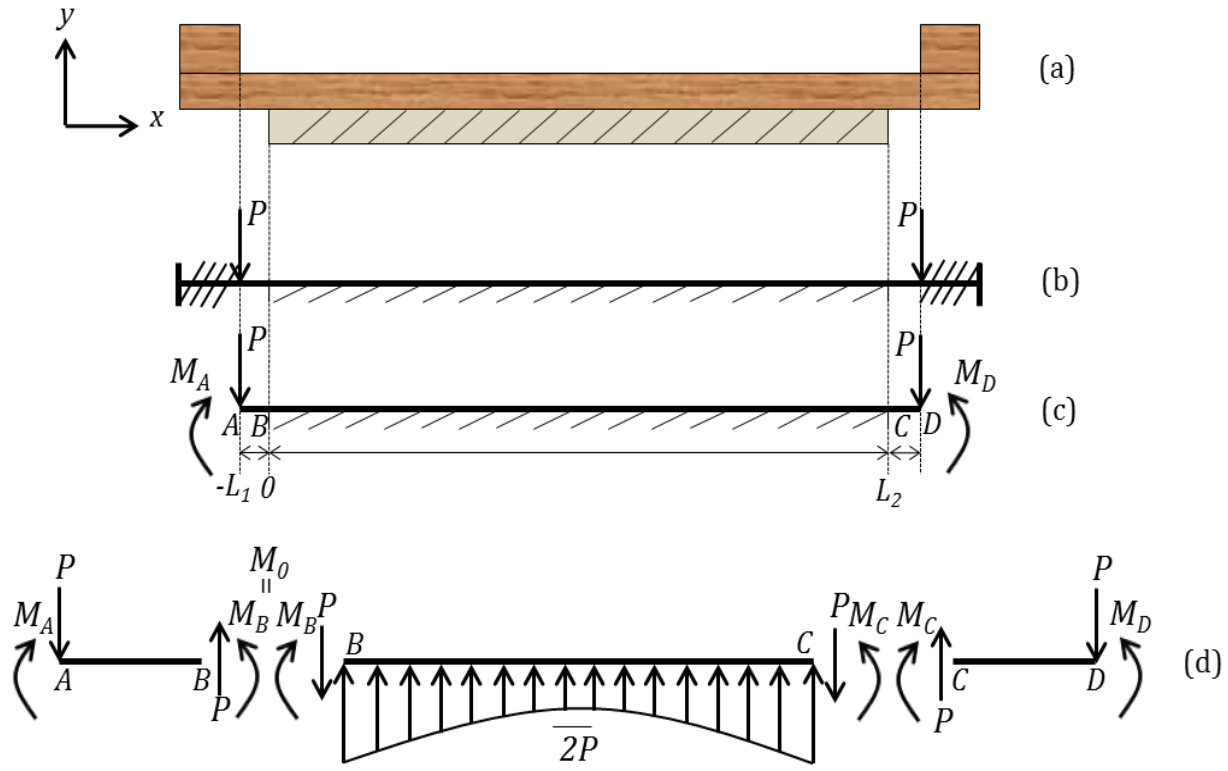

Note: $\overline{2P}$ indicates the sum of the all reaction forces

Figure 31. 1-D beam model with fixed ends

The slope $\theta\ (x_1)$ is obtained by using the boundary condition: at $x=-L_1$, $\theta=0$, thus $C_1=M_AL_1$

$$\theta(x_1) = \frac{1}{EI}\left(M_A x_1 - \frac{P}{2}(x_1 + L_1)^2 + M_A L_1\right) \quad [37]$$

The deflection y(x_1) is given by integrating the equation [37] with respect to x_1 as

$$EI\ y(x_1) = \frac{M_A}{2}{x_1}^2 - \frac{P}{6}(x_1 + L_1)^3 + M_A L_1 x_1 + C_2$$

$$y(x_1) = \frac{1}{EI}\left(-\frac{P}{6}(x_1 + L_1)^3 + \frac{M_A}{2}{x_1}^2 + M_A L_1 x_1 + C_2\right) \quad [38]$$

The two unknowns M_A and C_2 must be obtained to determine the beam deflection y for any given x_1 on the interval $-L_1 \le x_1 \le 0$.

Considering the B-C portion of the interval $0 \le x_2 \le L_2$ of the beam presented in Figure 31(d) the deflection y as a function of x_2 can be obtained by equation [13], which represents the general solution of the beam deflection on an elastic foundation.

Six unknowns ($M_A, C_2, y_0, \theta_0, M_0, Q_0$), from the equation [38] and [13], were determined using the following six boundary conditions. Applying the boundary conditions gives the following equations

(a) at $x_2 = 0$; $Q_0 = P$

$$Q_0 = P \quad [39]$$

(b) at $x_1 = 0$ and $x_2 = 0$; $M(x_1) = M(x_2) = M_0$

using equation [35]

$$M(x_1) = M_A - P(x_1 + L_1)$$

$$M_0 - M_A = -PL_1 \quad [40]$$

(c) at $x_1 = 0$ and $x_2 = 0$; $y(x_1) = y(x_2) = y_0$

using equation [38]

$$y(x_1) = \frac{1}{EI}\left(-\frac{P}{6}(x_1 + L_1)^3 + \frac{M_A}{2}{x_1}^2 + M_A L_1 x_1 + C_2\right)$$

$$y_0 = \frac{1}{EI}\left(-\frac{P}{6}{L_1}^3 + C_2\right)$$

$$y_0 - \frac{1}{EI}C_2 = -\frac{P{L_1}^3}{6EI} \qquad [41]$$

(d) at $x_2 = L_2$; $M = M_0$

using equation [15]

$$M(L_2) = M_0 = M_0 F_1(\lambda x_2) + \frac{1}{\lambda}Q_0 F_2(\lambda x_2) + \frac{k}{\lambda^2}y_0 F_3(\lambda x_2) + \frac{k}{\lambda^3}\theta_0 F_4(\lambda x_2)$$

$$0 = (F_1(\lambda x_2) - 1)M_0 + \frac{1}{\lambda}Q_0 F_2(\lambda x_2) + \frac{k}{\lambda^2}y_0 F_3(\lambda x_2) + \frac{k}{\lambda^3}\theta_0 F_4(\lambda x_2) \qquad [42]$$

substituting for Q_0 from equations [39] in equation [42]

$$\frac{k}{\lambda^2}y_0 F_3(\lambda x_2) + (F_1(\lambda x_2) - 1)M_0 + \frac{k}{\lambda^3}\theta_0 F_4(\lambda x_2) = -\frac{P}{\lambda}F_2(\lambda x_2) \qquad [43]$$

(e) at $x_2 = L_2$; $Q = -P$

$$Q(x_2) = -P = Q_0 F_1(\lambda x_2) + \frac{k}{\lambda}y_0 F_2(\lambda x_2) + \frac{k}{\lambda^2}\theta_0 F_3(\lambda x_2) - 4\lambda M_0 F_4(\lambda x_2) \qquad [44]$$

substituting for equations [39] in equation [44] yields

$$\frac{k}{\lambda}y_0 F_2(\lambda x_2) - 4\lambda F_4(\lambda x_2)M_0 + \frac{k}{\lambda^2}\theta_0 F_3(\lambda x_2) = -P - PF_1(\lambda x_2) \qquad [45]$$

(f) at $x_1 = 0$ and $x_2 = 0$; $\theta(x_1) = \theta(x_2) = \theta_0$

using equation [37]

$$\theta(x_1) = \frac{1}{EI}\left(M_A x_1 - \frac{P}{2}(x_1 + L_1)^2 + M_A L_1\right)$$

$$\theta_0 = \frac{1}{EI}\left(-\frac{P}{2}{L_1}^2 + M_A L_1\right)$$

$$\theta_0 - \frac{L_1}{EI}M_A = -\frac{P{L_1}^2}{2EI} \qquad [46]$$

To obtain the five unknowns $y_0, C_2, M_0,\ \theta_0$ and M_A , equations [40], [41], [43], [45] and [46] can be written in a matrix form as

$$\begin{bmatrix} 0 & 0 & 1 & 0 & -1 \\ 1 & -\frac{1}{EI} & 0 & 0 & 0 \\ \frac{kF_3(\lambda x_2)}{\lambda^2} & 0 & F_1(\lambda x_2) - 1 & \frac{kF_4(\lambda x_2)}{\lambda^3} & 0 \\ \frac{kF_2(\lambda x_2)}{\lambda} & 0 & -4\lambda F_4(\lambda x_2) & \frac{kF_3(\lambda x_2)}{\lambda^2} & 0 \\ 0 & 0 & 0 & 1 & -\frac{L_1}{EI} \end{bmatrix} \begin{bmatrix} y_0 \\ C_2 \\ M_0 \\ \theta_0 \\ M_A \end{bmatrix} = \begin{bmatrix} -PL_1 \\ -\frac{P{L_1}^3}{6EI} \\ -\frac{P}{\lambda}F_2(\lambda x_2) \\ -P - PF_1(\lambda x_2) \\ -\frac{P{L_1}^2}{2EI} \end{bmatrix}$$

solving for $y_0, C_2, M_0,\ \theta_0$ and M_A by

$$\begin{bmatrix} y_0 \\ C_2 \\ M_0 \\ \theta_0 \\ M_A \end{bmatrix} = \begin{bmatrix} 0 & 0 & 1 & 0 & -1 \\ 1 & -\frac{1}{EI} & 0 & 0 & 0 \\ \frac{kF_3(\lambda x_2)}{\lambda^2} & 0 & F_1(\lambda x_2) - 1 & \frac{kF_4(\lambda x_2)}{\lambda^3} & 0 \\ \frac{kF_2(\lambda x_2)}{\lambda} & 0 & -4\lambda F_4(\lambda x_2) & \frac{kF_3(\lambda x_2)}{\lambda^2} & 0 \\ 0 & 0 & 0 & 1 & -\frac{L_1}{EI} \end{bmatrix}^{-1} \begin{bmatrix} -PL_1 \\ -\frac{P{L_1}^3}{6EI} \\ -\frac{P}{\lambda}F_2(\lambda x_2) \\ -P - PF_1(\lambda x_2) \\ -\frac{P{L_1}^2}{2EI} \end{bmatrix}$$

$$y_0 = -(k * ((P * \lambda * (2 * F_4 * L1 + 4 * F_4^2 * L1^2 * \lambda + 2 * F_1 * F_4 * L1))/2 - (F_3 * P * \lambda * (L1^2 * \lambda + 2 * F_2 * L1 - F_1 * L1^2 * \lambda))/2) + (P * \lambda * (2 * EI * F_1^2 * \lambda^3 - 2 * EI * \lambda^3 + 8 * EI * F_2 * F_4 * \lambda^3))/2)/(k * (F_2 * F_4 * L1 * k - F_3^2 * L1 * k - EI * F_2 * \lambda^3 + EI * F_1 * F_2 * \lambda^3 + 4 * EI * F_3 * F_4 * \lambda^3))$$

$$C_2 = (L1^3 * P)/6 - (P * EI^2 * F_1^2 * \lambda^4 + 4 * F_2 * P * EI^2 * F_4 * \lambda^4 - P * EI\text{^}2 * \lambda^4 + P * k * EI * F_1 * F_4 * L1 * \lambda + (F_3 * P * k * EI * F_1 * L1^2 * \lambda^2)/2 + 2 * P * k * EI * F_4^2 * L1^2 * \lambda^2 + P * k * EI * F_4 * L1 * \lambda - (F_3 * P * k * EI * L1^2 * \lambda^2)/2 - F_2 * F_3 * P * k * EI * L1 * \lambda)/(F_2 * F_4 * L1 * k^2 - F_3^2 * L1 * k^2 - EI * F_2 * k * \lambda^3 + EI * F_1 * F_2 * k * \lambda^3 + 4 * EI * F_3 * F_4 * k * \lambda^3)$$

$$M_0 = ((P * (-2 * EI * F_2^2 + 2 * EI * F_3 + 2 * EI * F_1 * F_3) * \lambda^2)/2 + (P * (F_3^2 * L1^2 * k - F_2 * F_4 * L1^2 * k))/2)/(F_2 * F_4 * L1 * k - F_3^2 * L1 * k - EI * F_2 * \lambda^3 + EI * F_1 * F_2 * \lambda^3 + 4 * EI * F_3 * F_4 * \lambda^3)$$

$$\theta_0 = -((L1 * P * \lambda^2 * (2 * F_2^2 + F_2 * L1 * \lambda - F_1 * F_2 * L1 * \lambda))/2 - (F_3 * L1 * P * \lambda^2 * (2 * F_1 + 4 * F_4 * L1 * \lambda + 2))/2)/(F_2 * F_4 * L1 * k - F_3^2 * L1 * k - EI * F_2 * \lambda^3 + EI * F_1 * F_2 * \lambda^3 + 4 * EI * F_3 * F_4 * \lambda^3)$$

$$M_A = (P * (2 * EI * F_3 * \lambda^2 - F_3^2 * L1^2 * k - 2 * EI * F_2^2 * \lambda^2 + F_2 * F_4 * L1^2 * k - 2 * EI * F_2 * L1 * \lambda^3 + 2 * EI * F_1 * F_3 * \lambda^2 + 2 * EI * F_1 * F_2 * L1 * \lambda^3 + 8 * EI * F_3 * F_4 * L1 * \lambda^3))/(2 * (F_2 * F_4 * L1 * k - F_3^2 * L1 * k - EI * F_2 * \lambda^3 + EI * F_1 * F_2 * \lambda^3 + 4 * EI * F_3 * F_4 * \lambda^3))$$

The five unknowns were determined by solving the above matrix form, then applied to equation [38] and [13] to get deflection $y(x_1)$ and deflection $y(x_2)$. All input values used for modeling the deflections are in Table 11.

Table 11. Input values used for model prediction the fixed ends beam deflection

		Bottle	Empty	Flour
P (lbs.)		183	175	190
k (lbs./in.)		1345	854	618
L_1 (in.)		0.5		
L_2 (in.)		16		
EI (lbs.in.^{2})		**E**	**I**	**EI**
	1	1340000	0.1249	167400
3/4"	2	1236000	0.1256	155200
	3	1246000	0.1257	156600
	1	1081000	0.0144	15570
3/8"	2	1077000	0.0144	15510
	3	1082000	0.0145	15690

4.1.3.2 Results and Discussion for Fixed End Models

Figure 32, 33, and 34 are graphs showing the models of the fixed end pallet deck predicted deflections, of 3/4-inch and 3/8-inch deck thickness, resulted from three different stiffness packaging. There is little difference in predicted deflections of 3/4-inch deckboard between packaging stiffness levels. The ranges of predicted deflection from the lowest to highest stiffness packaging were 19% and 78% for the 3/4-inch and 3/8-inch respectively. The maximum deflections of 3/8-inch deckboard were respectively 216%, 302%, and 373% greater than the deflection of 3/4-inch deckboard supporting the bottles, empty box, and flour sacks. Therefore, from the developed model it was predicted that the 3/8-inch deck has more effect of the packaging stiffness on the maximum predicted deflection than 3/4-inch deck.

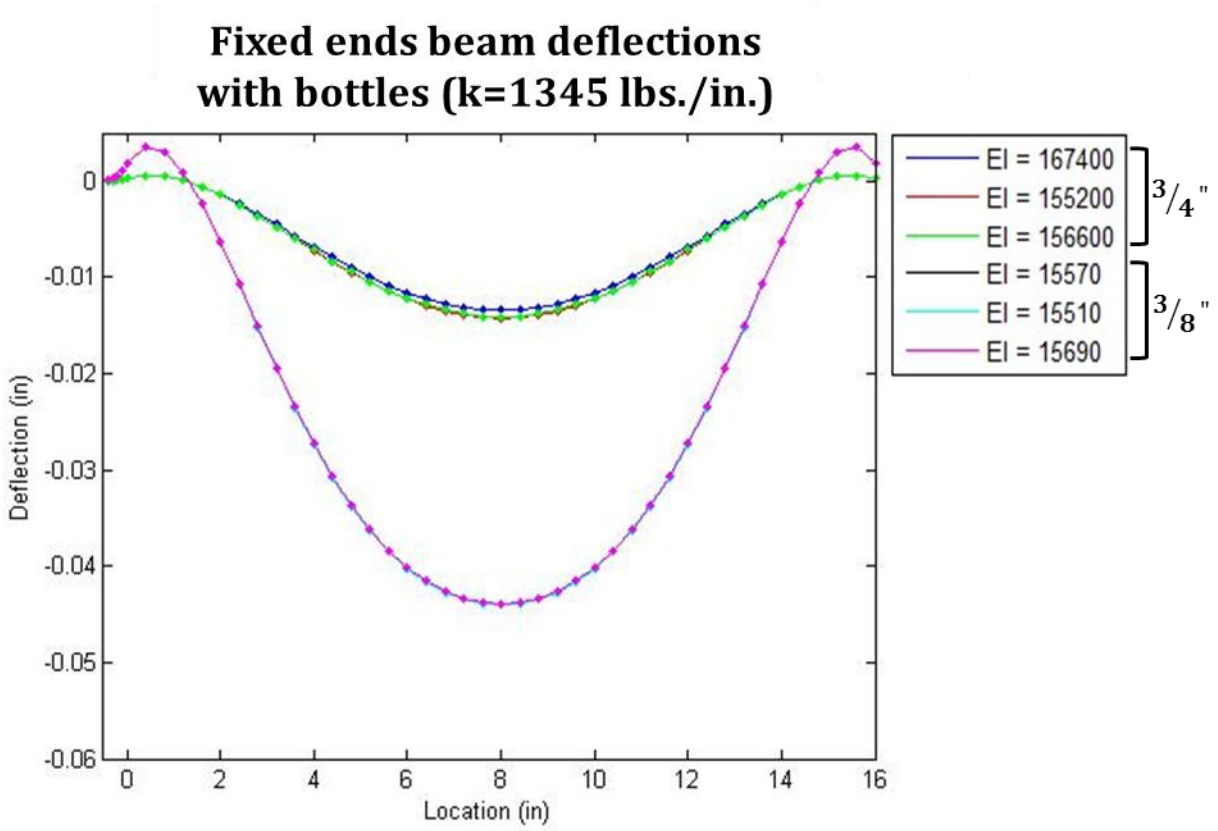

Figure 32. Fixed end model prediction of beam deflection loaded by a box containing plastic bottles for two deckboard thicknesses

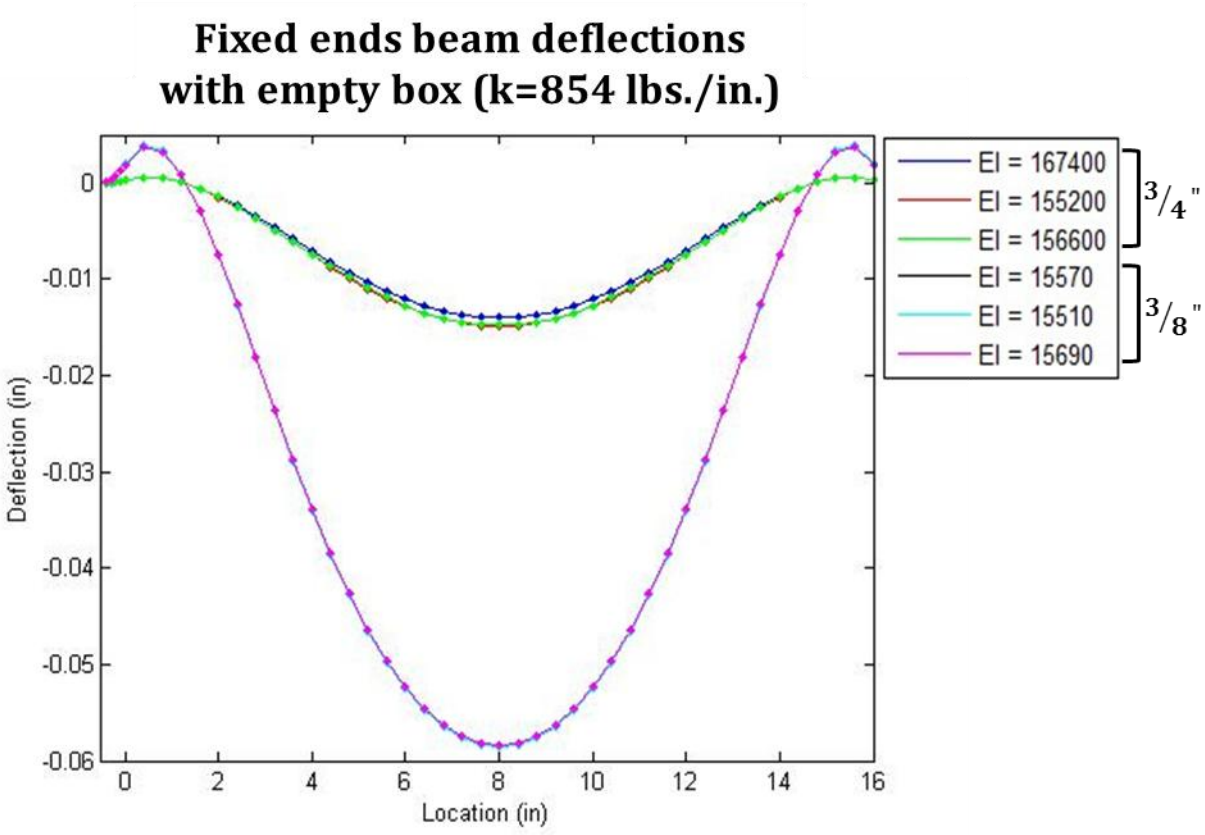

Figure 33. Fixed end model prediction of beam deflection loaded by an empty box for two deckboard thicknesses

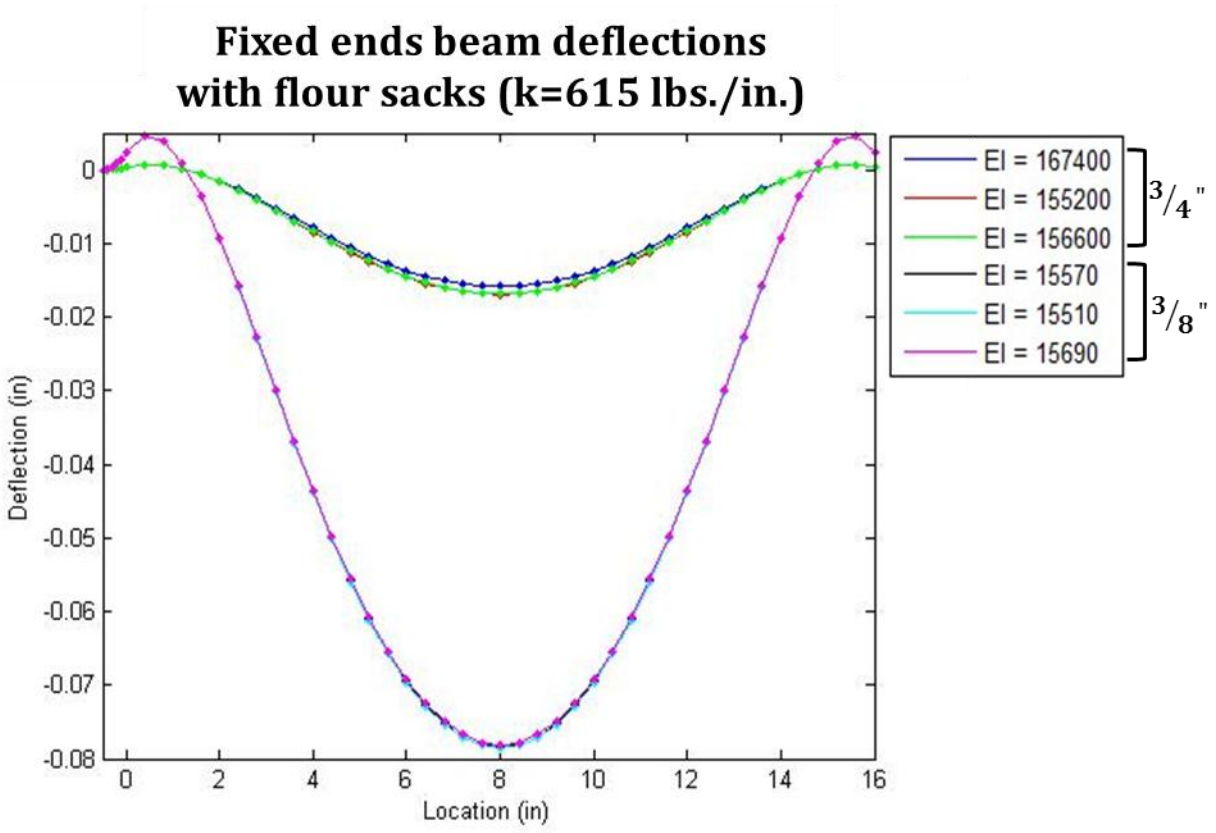

Figure 34. Fixed end model prediction of beam deflection loaded by a box containing flour sacks for two deckboard thicknesses

4.1.4 The Effect of Joint Fixity on the Predicted Pallet Deck Deflection

Figure 35 presents a graph showing the effect of joint fixity on the maximum predicted deck deflection of pallet deck assembled with three end conditions, free ends, semi-rigid joints, and fixed ends. Each plot represents the averaged maximum predicted deflection of three replications of each deck thickness and packaging combination for each end condition. The absolute value was taken from each deflection value in order to determine the maximum predicted deflection since the sign convention defined the downward deflection as a negative quantity. The maximum predicted deflections were the greatest for the free end condition and the lowest for the fixed end condition. The maximum predicted deflections of 3/4-inch were respectively 427% and 507% greater for semi-rigid joint condition and free end condition, than the fixed end condition. The maximum predicted deflections of 3/8-inch were respectively 91% and 236% greater for semi-rigid joint condition and free end condition than the fixed end condition. The maximum predicted deflection of 3/4-inch deckboard was significantly more sensitive to changes in joint stiffness than 3/8-inch deckboard. The greater maximum deckboard deflections were predicted by lower joint stiffness, lower pallet stiffness, and lower packaging stiffness. The more deflected pallet deck can cause greater stress concentrations around pallet stringer segments. The pallet deck stiffness did not significantly influence the predicted maximum deflection of the deckboard supporting the bottles for the semi-rigid joint condition.

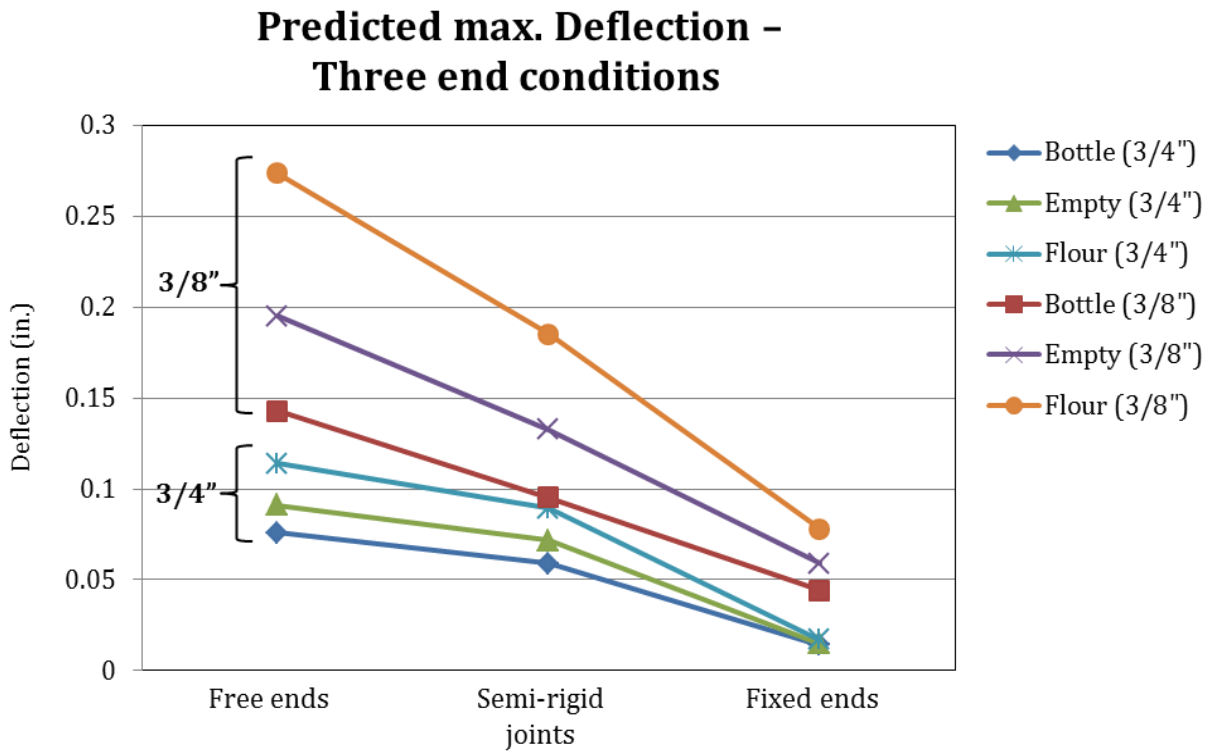

Figure 35. The effects of joint fixity on the predicted maximum deck deflection of the three different end condition pallet decks

4.2 Compressive Stress Distribution Models

Compressive stress distribution models at the interface between the pallet deckboard and packaging were obtained using the developed deck deflection models. The determination of pressure distribution (compressive stress distribution) along the pallet deck is illustrated in Figure 36. The y-axis of the initial deflection curve was reversed to predict the original deflection shape of the top deck. Deflections were normalized to zero since the package elastic foundation representing the bottom surface of packaging was assumed not touching the deckboard beam deflection below the zero point due to the deflection of the bottom of the packaging. This assumption was made to predict the effect of load-bridging on compressive stress (pressure) distribution models as presented in Figure 37. Due to the load-bridging effect no stresses or pressures were observed in the portion of the deckboard where the deflection *y* values were below zero. The portion of zero-pressure deckboard referring to load-bridging area was defined by 0.4-inch times the number of zero-pressure points times the width of deckboard (3.5-inch). The compressive stress (pressure) value at each point *x* was calculated by the following equation

$$P(x) = ky(x)/3.5$$

where

P(x) = Pressure per unit area at any point *x*, or Intensity of reaction force at any point *x*
k = Stiffness of packaging
y(x) =Deflection at any point *x*
3.5 = the width of the beam (deckboard) in inches

Figure 6 presents the bending of the beam (deckboard) supported along its entire length by an elastic medium caused by a vertical force *P* acting in the principal plane of the symmetrical cross section. The action of vertical force produces the intensity of the distributed reaction force *ky* at a point where the deflection is *y* in the supporting elastic medium. The reaction force *ky* was divided by the width (3.5-inch) of the pallet deckboard representing the beam width to obtain the intensity

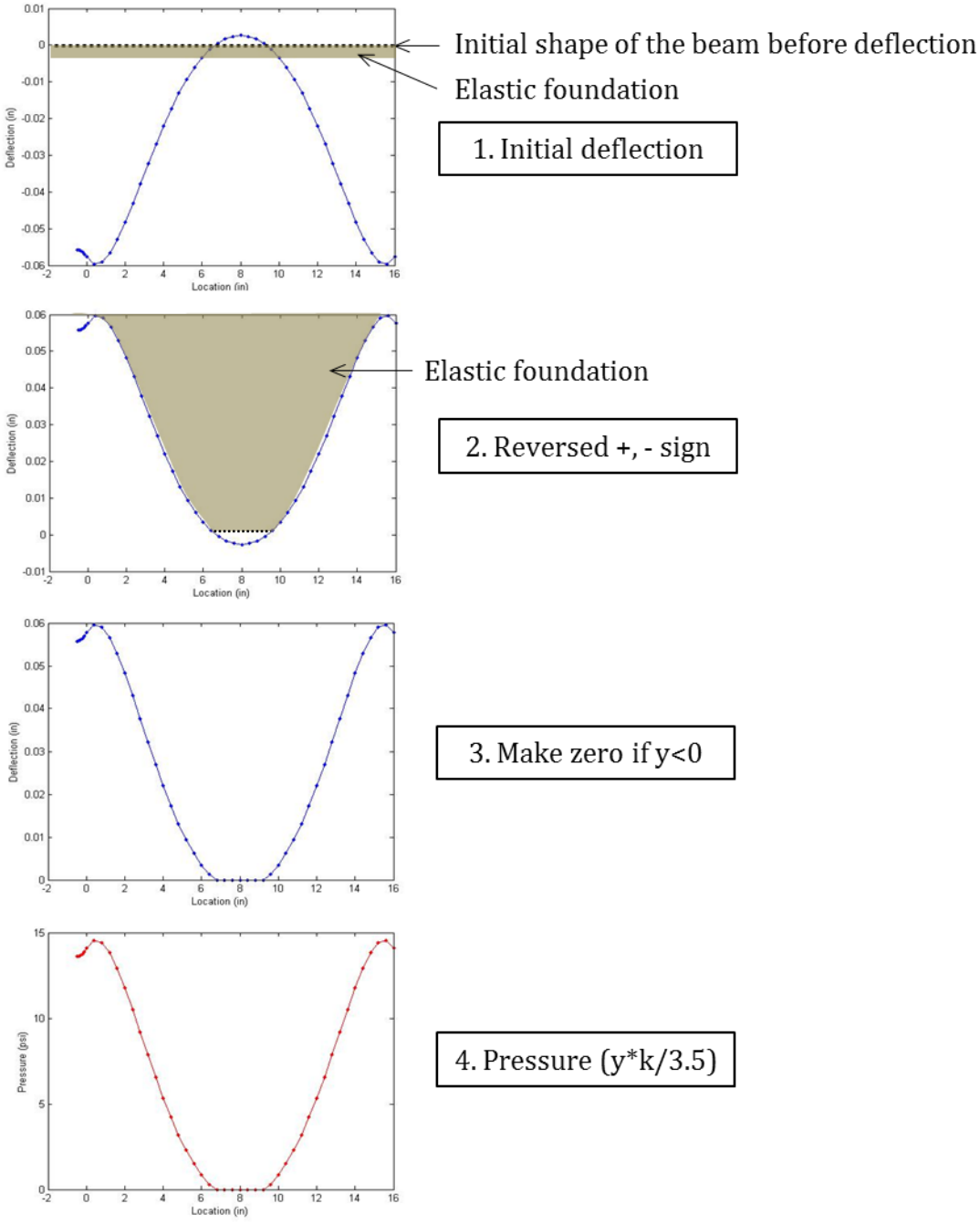

Figure 36. Schematic diagrams illustrating the calculation of pressure on the elastic foundation (packaging) along the beam length (deckboard)

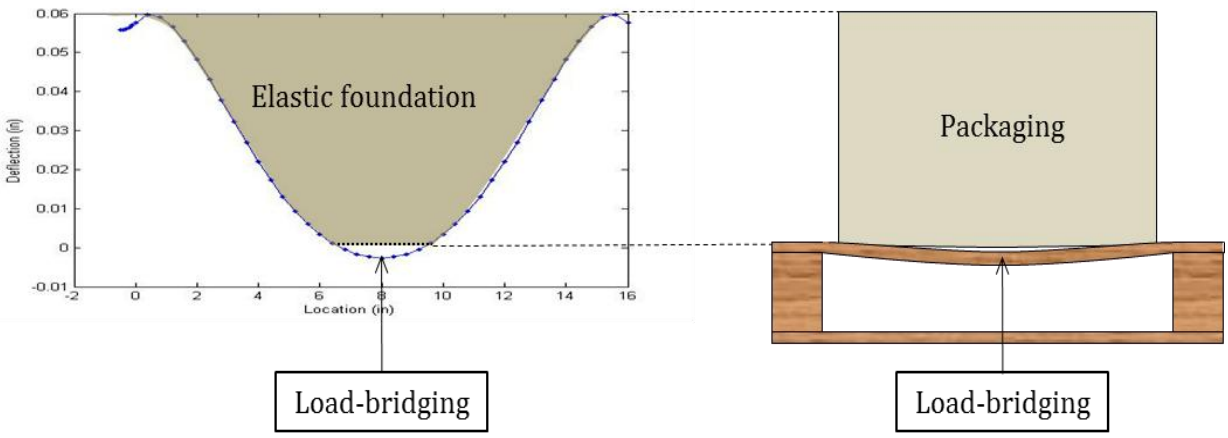

Figure 37. A schematic diagram illustrating the effect of Load-bridging and showing the region of zero deflection of the elastic foundation (packaging)

of distributed reaction force per unit area.

4.2.1 Free End Models

Figure 38, 39, and 40 show the predictive compressive stress distribution at the interface between the top deck of free end pallet sections and the three different packages. Each stress distribution model was developed using the process described in Figure 36. The results of the model prediction of compressive stress distribution showed that the stresses were not uniformly distributed across a pallet deck. The predictive models showed that greatest compressive stresses (pressures) were concentrated at the ends of the deckoard. The maximum stresses predicted over the free end 3/8-inch pallet deckboard supporting the bottles, empty box, and flour sacks were respectively 94%, 103%, and 123% higher than 3/4-inch deck. The less stiff the pallet deck the more the load-bridging. The applied stress was calculated by sum of the applied force to the model and the weight of the packaging divided by the area of two contacts, packaging and pallet deckboard. The applied stresses of three packaging systems were tabulated in Table 12. The same applied stresses were used for semi-rigid joint and fixed end conditions.

Table 12. Applied stresses

	Applied Force (lbs.)	**Weight of Pkg (lbs.)**	**Contact Area (in^2)**	**Applied Stress ($lbs./in^2$)**
Bottles	350	16.6	56	6.5
Empty box	350	0.7	56	6.25
Flour sacks	350	32	56	6.82

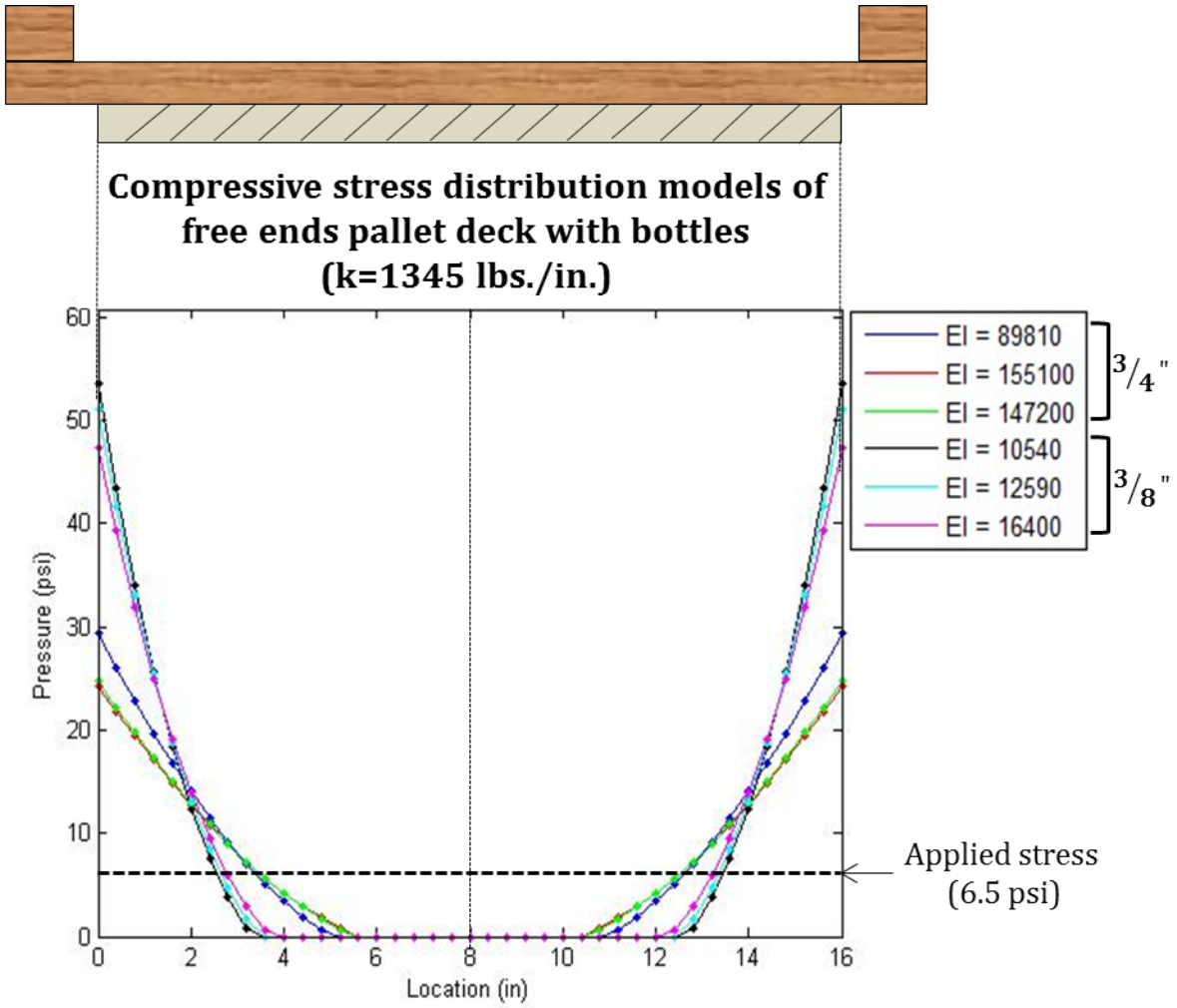

Figure 38. Free end model prediction of compressive stress distribution by a box containing plastic bottles for two deckboard thicknesses

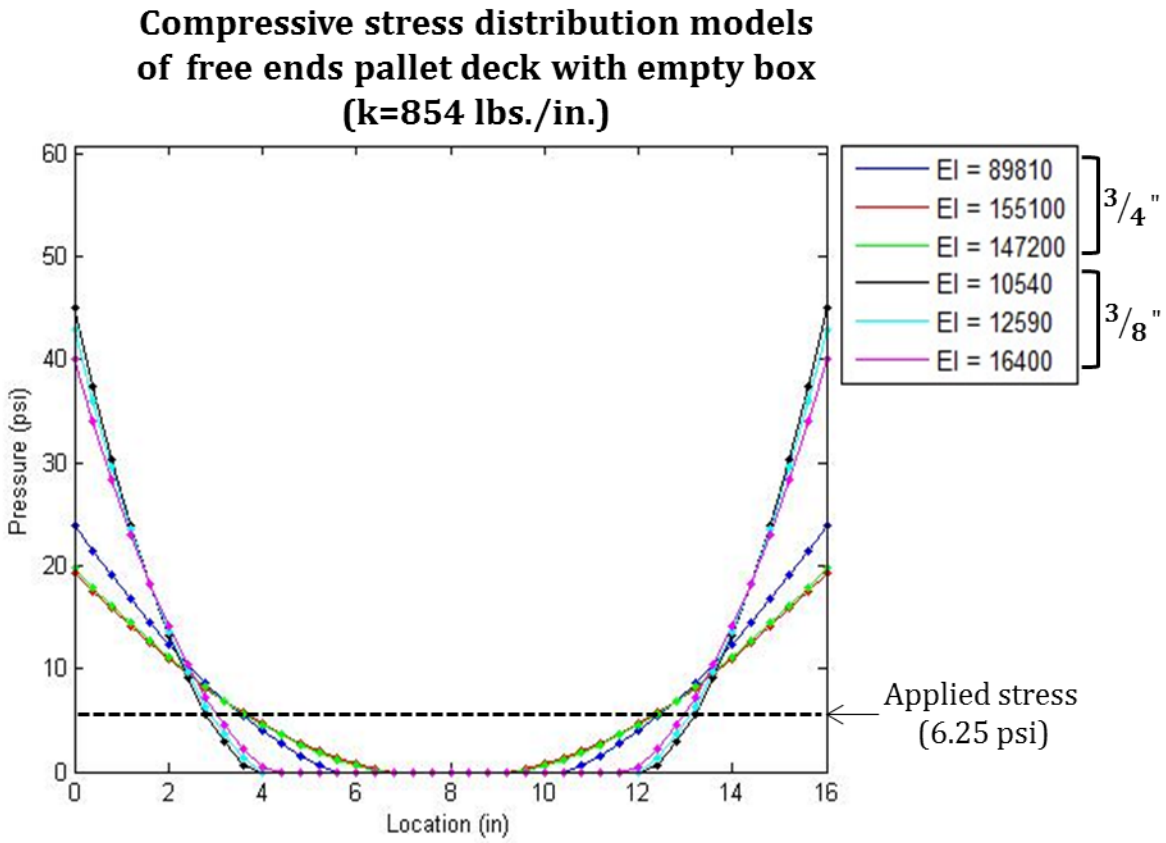

Figure 39. Free end model prediction of compressive stress distribution by an empty box for two deckboard thicknesses

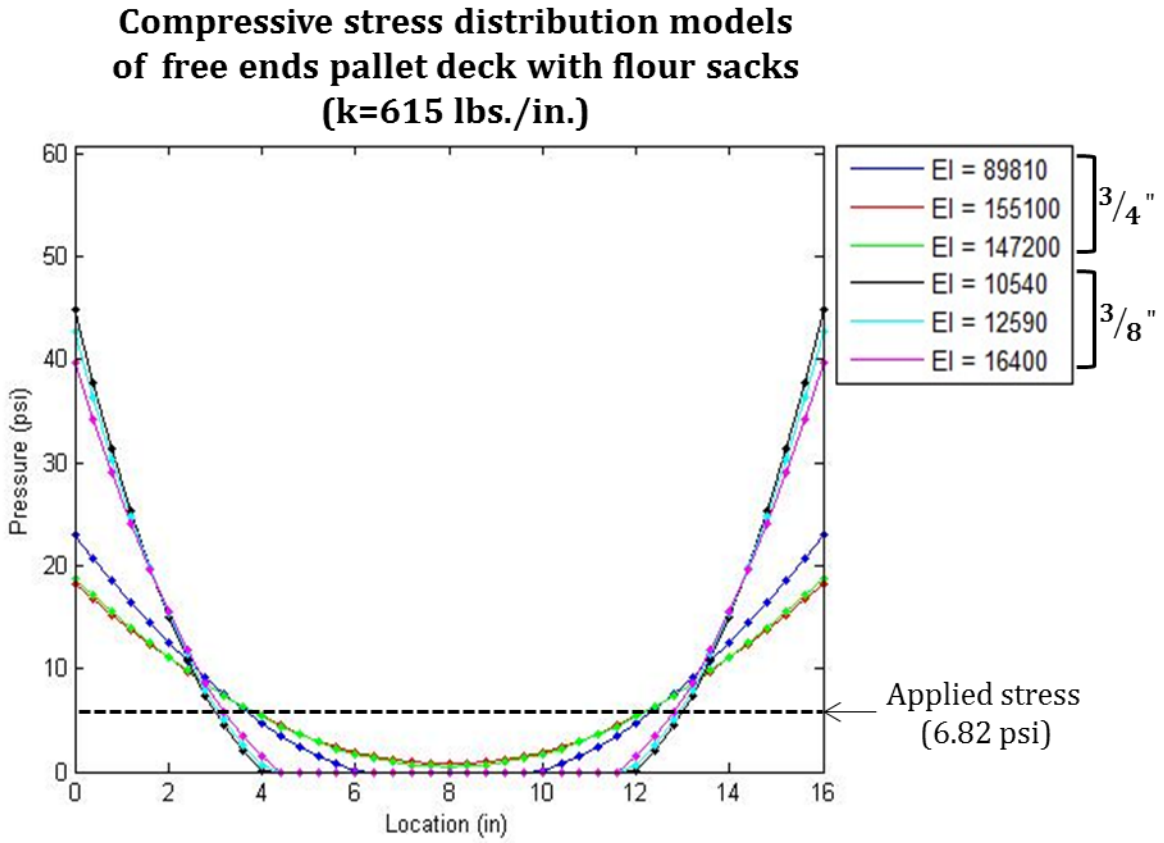

Figure 40. Free end model prediction of compressive stress distribution by a box containing flour sacks for two deckboard thicknesses

4.2.2 Semi-Rigid Joint Models

The semi-rigid joint connection including a certain degree of relative rotational stiffness was used to model the nailed joint. The rotational stiffness of nailed joint for 3/4-inch and 3/8-inch pallet deck was experimentally determined and used to develop the predictive models of compressive stress distributions.

The predicted compressive stress distribution showed that the stresses were not uniformly distributed across a pallet deck. The predictive models also showed that greatest compressive stresses (pressures) were concentrated at the ends of the deckoard. Figure 41 shows the semi-rigid joint models of compressive stress distribution at the interface between two different pallet deck stiffness represented by 3/4-inch and 3/8-inch thickness with a box containing plastic bottles. The predicted maximum stress of the 3/8-inch decks was 55% higher than 3/4-inch decks. The predicted maximum stresses distributed across the 3/4-inch and 3/8-inch deckboards were respectively 230% and 411% higher than the applied stress by the bottles. Figure 42 shows compressive stress distribution models of semi-rigid joint pallet deckboard supporting the empty box. The predicted maximum stresses distributed across the 3/8-inch thick deckboard supporting the empty box were 65% higher than the 3/4-inch thick deckboard. The predicted maximum stresses distributed across the 3/4-inch and 3/8-inch deckboards were respectively 182% and 364% greater than the applied stress by the empty box. Figure 43 presents that the maximum stresses distributed over the 3/8-inch deckboard supporting flour sacks in a box is approximately 73% greater than the 3/4-inch deck. The 3/4-inch and 3/8-inch deckboards loaded by the flour sacks in a box resulted in respectively 149% and 329% higher predicted maximum stresses than the applied stress. The compressive stress distribution of the semi-rigid joint were significantly affected by pallet stiffness and packaging stiffness. The stiffer the pallet decks the lower the predicted maximum stress. The greater the packaging stiffness the greater the predicted maximum stress.

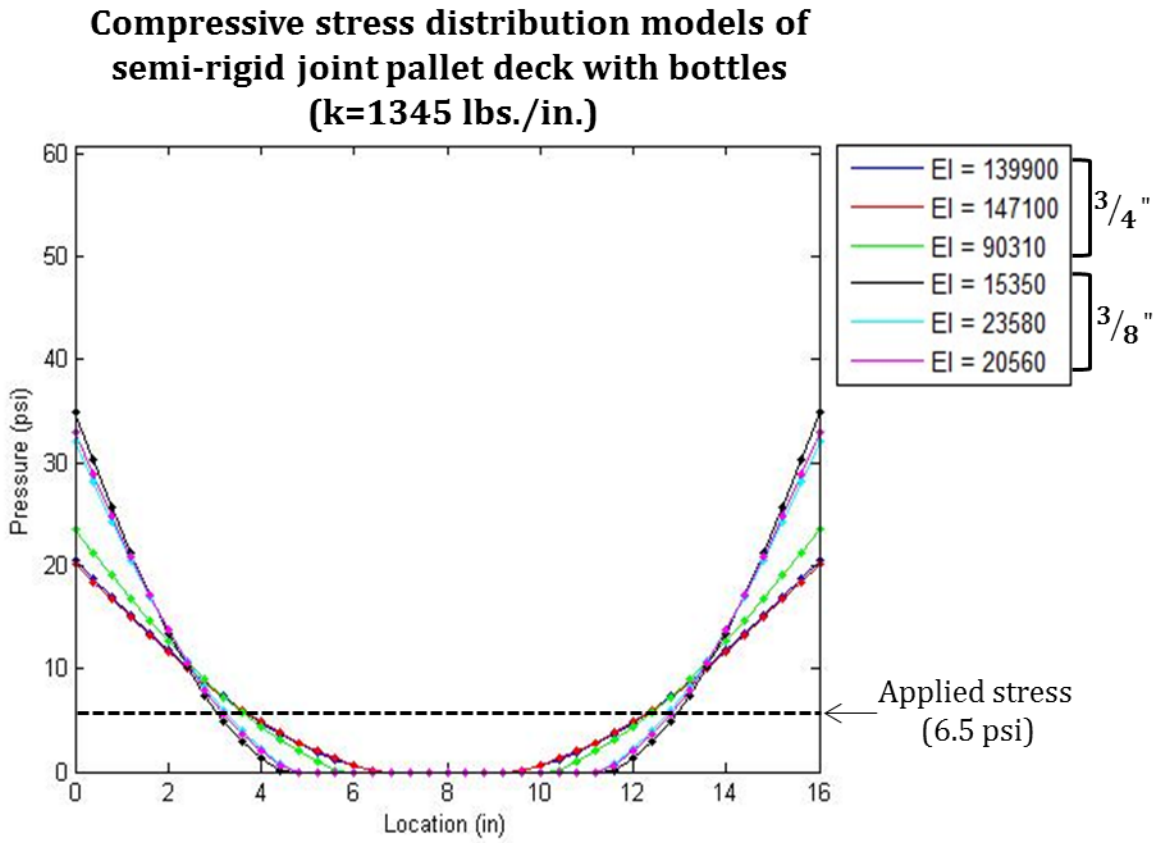

Figure 41. Semi-rigid joint model prediction of compressive stress distribution by a box containing plastic bottles for two deckboard thicknesses

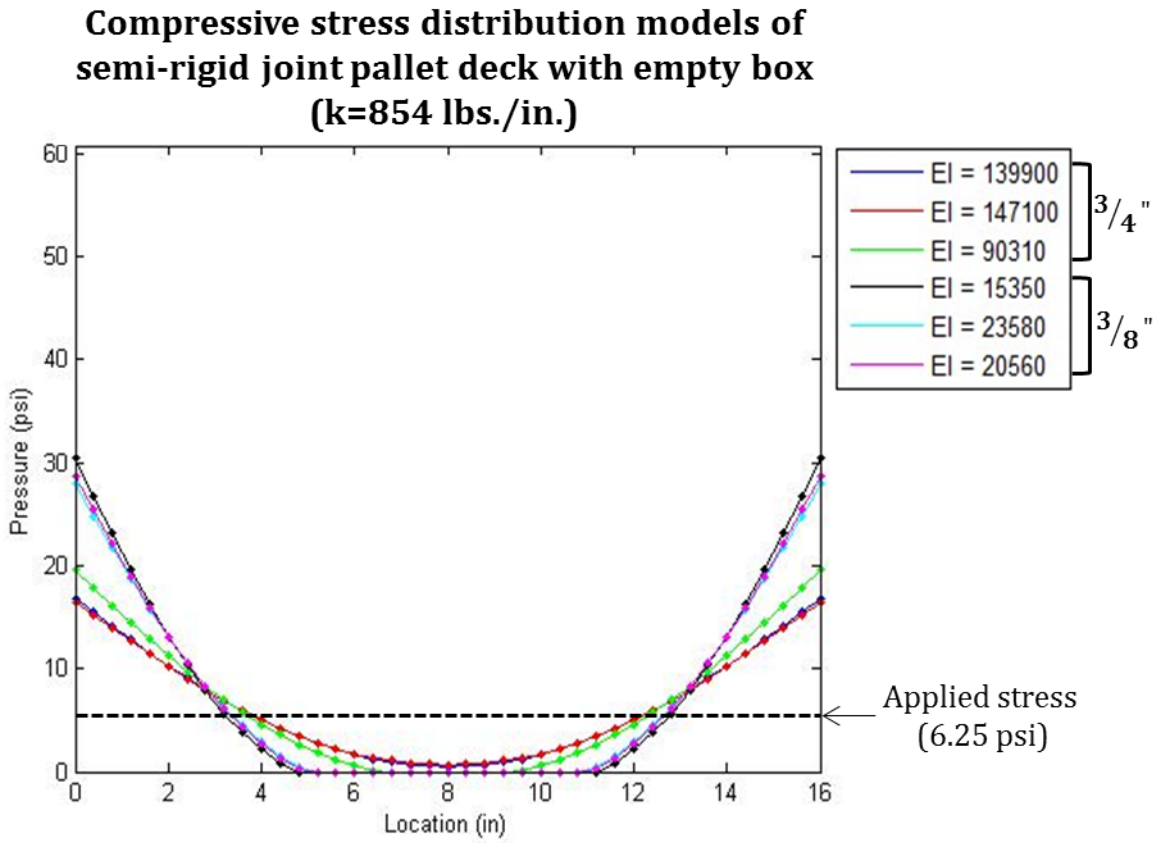

Figure 42. Semi-rigid joint model prediction of compressive stress distribution by an empty box for two deckboard thicknesses

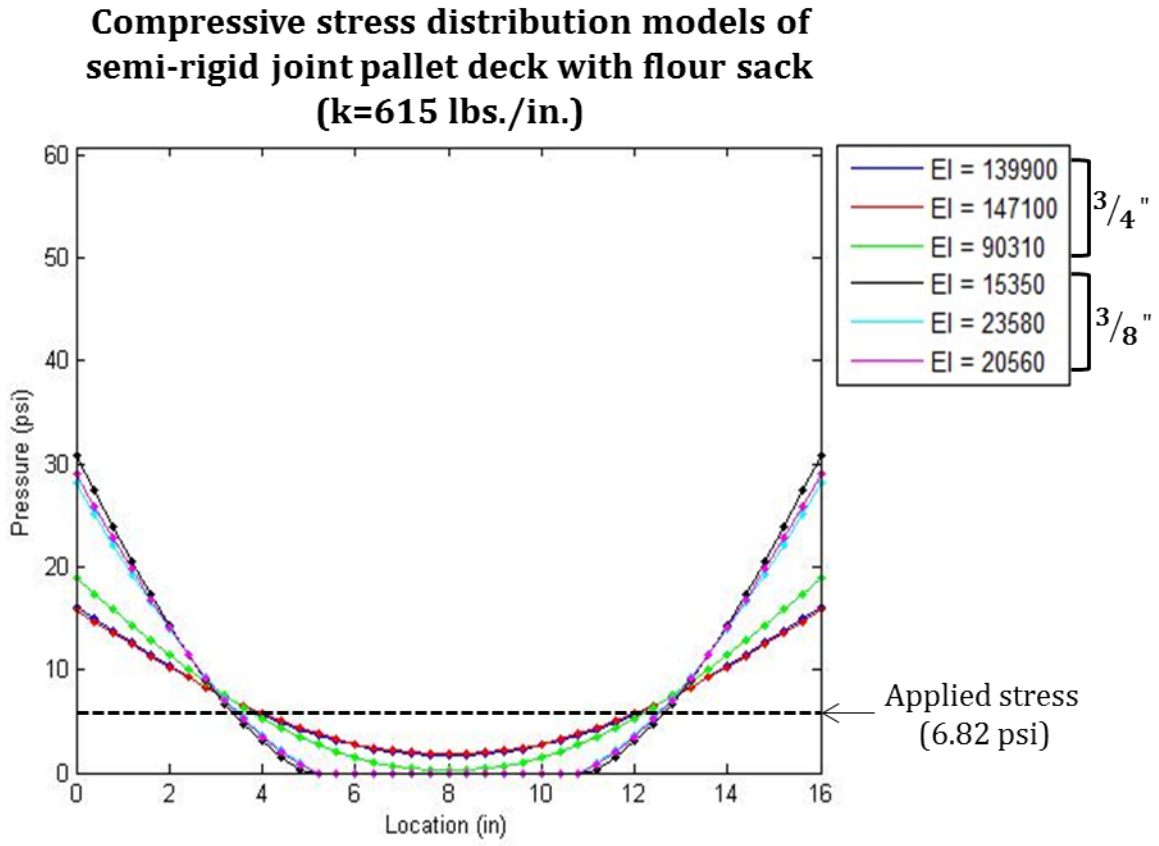

Figure 43. Semi-rigid joint model prediction of compressive stress distribution by a box containing flour sacks for two deckboard thicknesses

4.2.3 Fixed End Models

Figure 44, 45, and 46 show the predictive compressive stress distribution models of fixed end pallet deckboard supporting three different types of packages. The model prediction of compressive stress distribution resulted that the stresses were not uniformly distributed across a pallet deck. The predictive models showed that greatest compressive stresses (pressures) were concentrated at the ends of the deckoard. The maximum stresses predicted over the free end 3/8-inch pallet deckboard supporting the bottles, empty box, and flour sacks were respectively 70%, 71%, and 68% higher than the 3/4-inch deck.

The predicted maximum stresses distributed across the 3/4-inch and 3/8-inch deckboards were respectively 40% and 139% higher than the applied stress by the bottles. The predicted maximum compressive stresses distributed over the 3/4-inch and 3/8-inch deckboard supporting the empty box were respectively 27% and 118% greater than the applied load. The 3/4-inch and 3/8-inch deckboards loaded by the flour sacks in a box resulted in respectively 40% and 139% higher predicted maximum stresses than the applied stress. The models showed no load-bridging over the 3/4-inch deckboard supporting three different packages and the 3/8-inch deckboard supporting flour sacks in a box as shown in Figure 46.

4.2.4 The Effect of Joint Fixity on the Predicted Maximum Stress

Figure 47 presents a graph showing the effect of joint fixity on the predicted maximum stress over pallet decks assembled with three end conditions, free ends, semi-rigid joints, and fixed ends. Each plot represents the averaged predicted maximum stress of three replications of each deck thickness and packaging combination for each end condition. The greater the joint fixity the less the predicted maximum stress. The predicted maximum stresses were similar for flour sacks and empty boxes for all three end conditions.

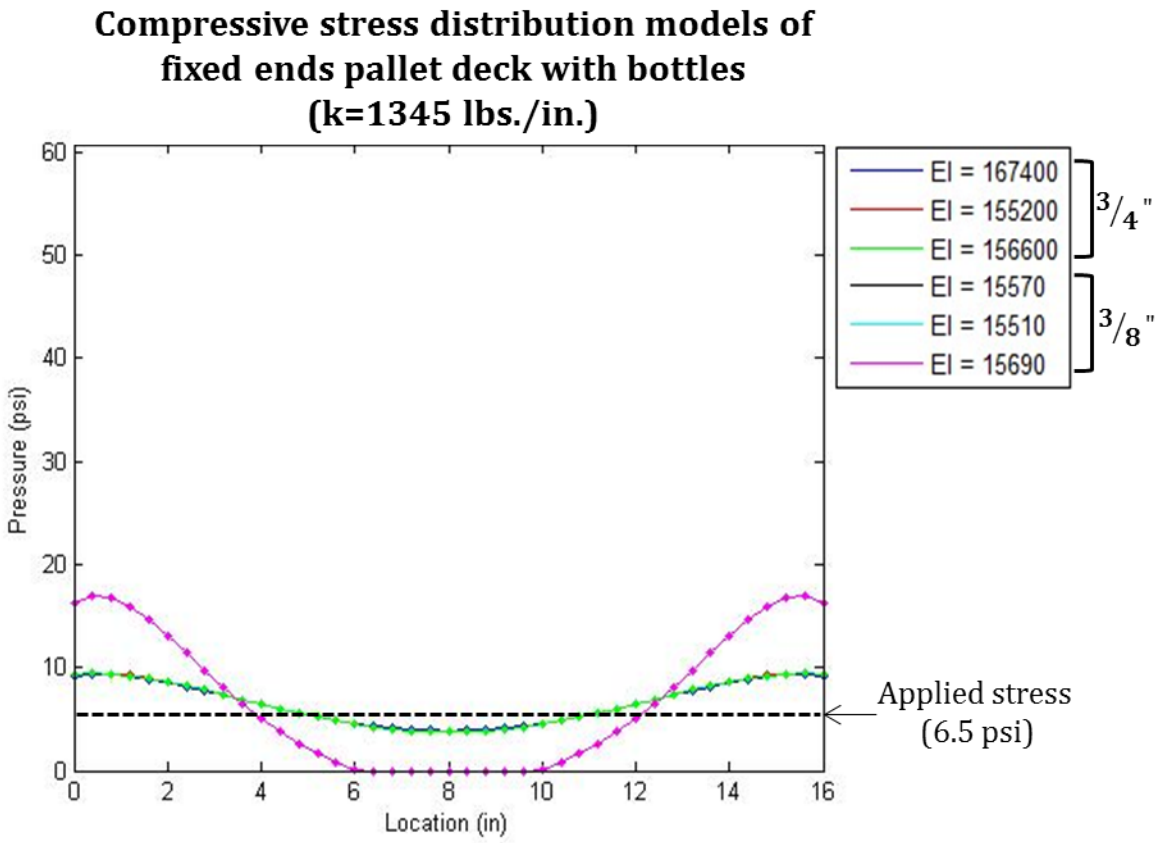

Figure 44. Fixed end model prediction of compressive stress distribution by a box containing plastic bottles for two deckboard thicknesses

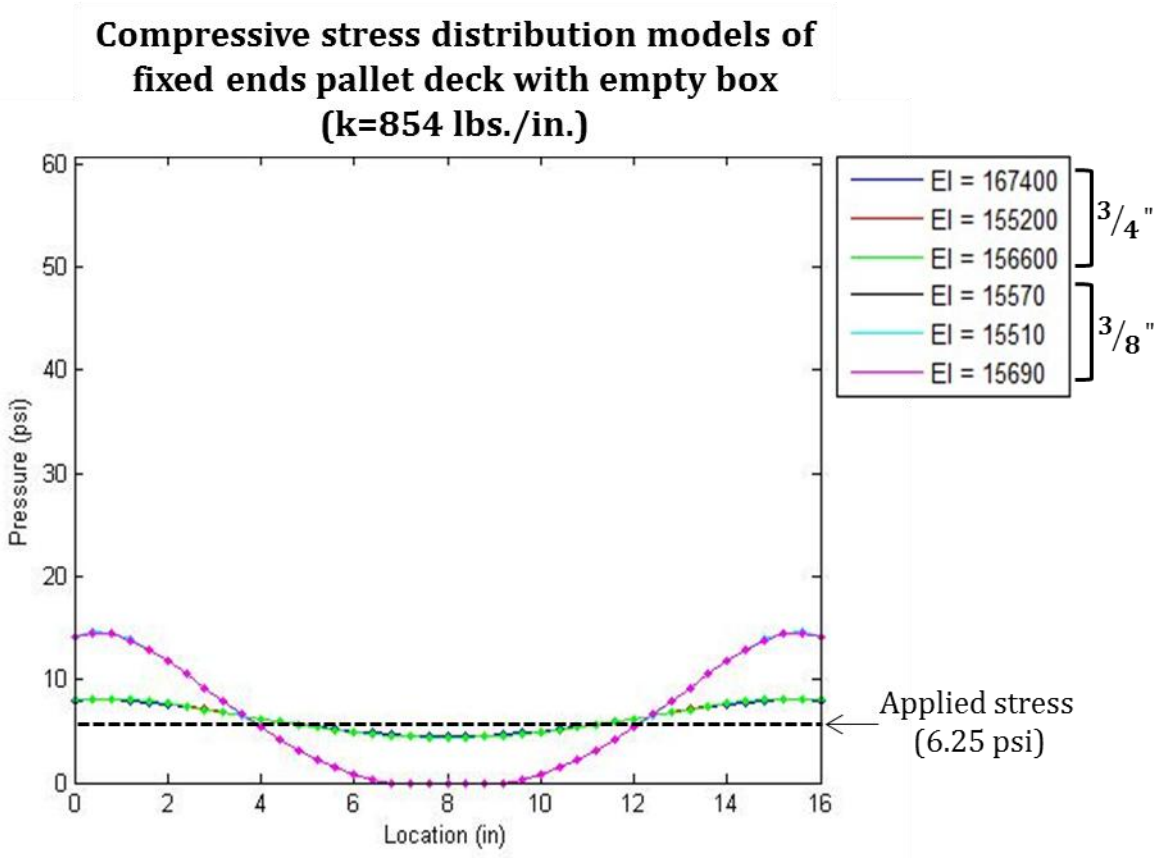

Figure 45. Fixed end model prediction of compressive stress distribution by an empty box for two deckboard thicknesses

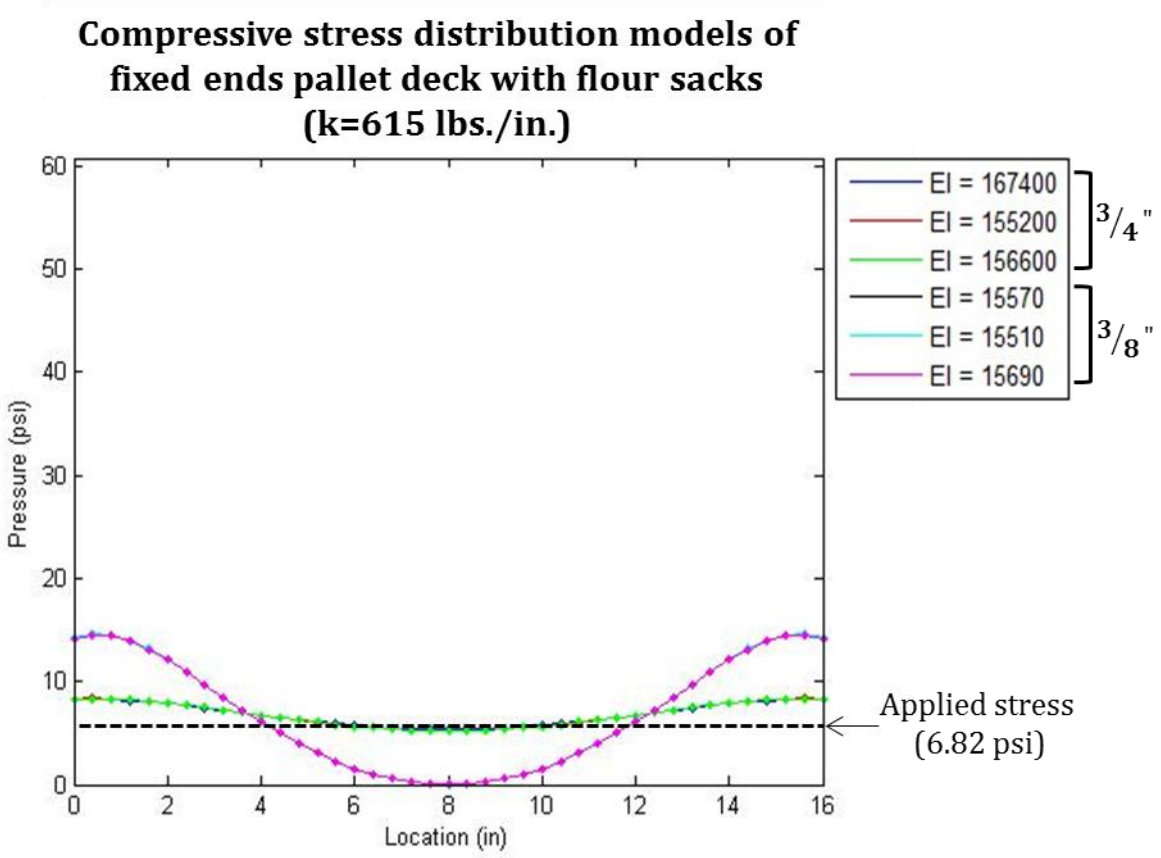

Figure 46. Fixed end model prediction of compressive stress distribution by a box containing flour sacks for two deckboard thicknesses

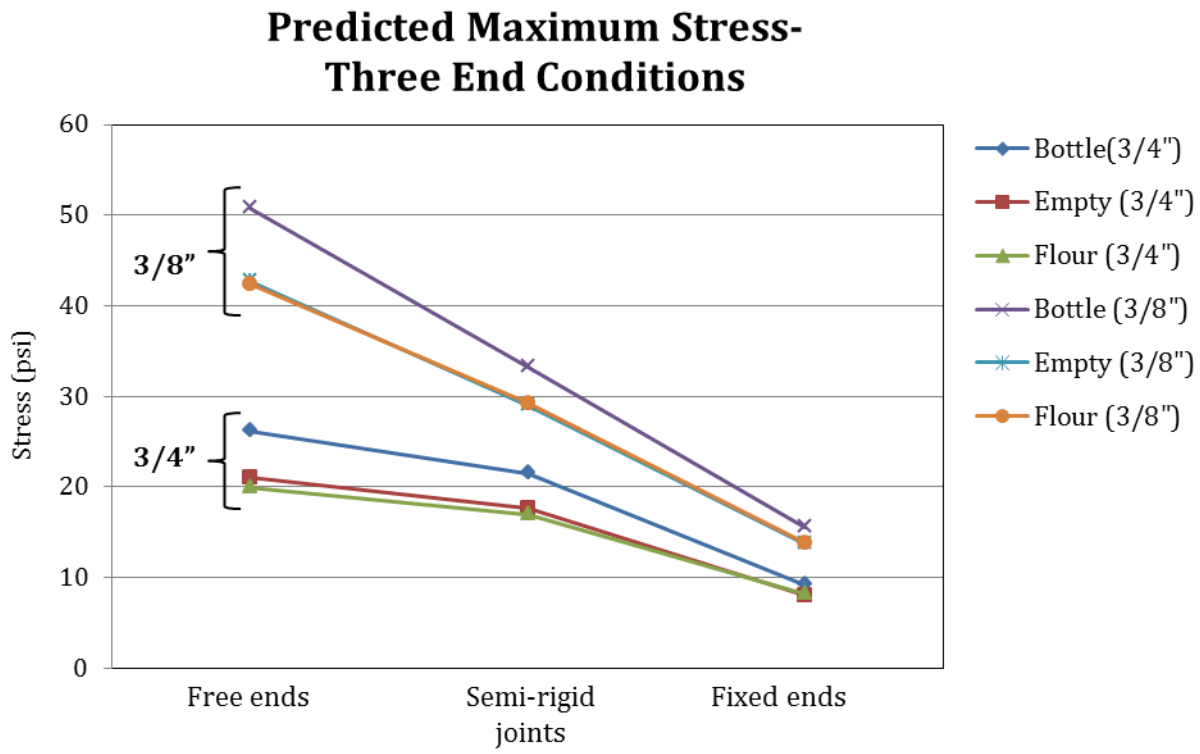

Figure 47. The effects of joint fixity on the predicted maximum deck deflection of the three different end condition pallet decks

4.2.5 Effective Bearing Area

The predictive compressive stress distribution models showed that the effect of pallet deck and packaging stiffness on the load-bridging. Effective bearing area can refer to the area of contact between two objects. Therefore, it represents region where the compressive stresses are more than zero psi at the interface between the top pallet deck and the bottom of the packaging. Figure 48 illustrates the computation of effective bearing area at the interface between the top pallet deck and the bottom surface of packaging using the predicted load-bridging area from the stress distribution models. The effective bearing area was calculated by subtracting the load-bridging area from the maximum effective bearing area. Figure 49 shows the comparison of effective bearing areas depending on different pallet deck stiffness and packaging stiffness. The stiffer the pallet deck and pallet joint the greater the effective bearing area. The lower stiffness packaging resulted in the greater effective bearing area with all three packages. The predicted effective bearing area was more influenced by pallet deck stiffness than the packaging stiffness. The predicted effective bearing area (%) is tabulated in Table 13.

Table 13. Predicted effective bearing area (%)

	Free ends		**Semi-rigid**		**Fixed ends**	
	3/4"	3/8"	3/4"	3/8"	3/4"	3/8"
Bottles	68	47	82	60	100	80
Empty	81	52	95	63	100	85
Flour	93	55	100	65	100	100

4.2.6 Discussion

Compressive stresses were not uniformly distributed across pallet deck and stresses were but concentrated around inner stringers as shown in all predicted models. All predictive compressive stress distributions were influenced by pallet deck stiffness, packaging stiffness, and joint fixity. Comparing the effective bearing areas among three different end conditions, stiffer

joints resulted in greater effective bearing area, or lower load-bridging, with all three packages. Less stiff pallet decks supporting stiffer packaging resulted in more load-bridging. The models also predicted that stiffer joint, stiffer deck and flexible packaging reduced the maximum compressive stress levels.

Table 14 shows the Compressive Stress Intensity Factor (SIF) of each model determined by the ratio of the maximum pressure (Figure 38 through 46) to the applied pressure (Table 12). Figure 50 is a graph showing the comparison of SIFs for three different end conditions, three different packages, and two different pallet deck thicknesses. SIF was reduced for stiffer joints, stiffer pallet decks and more flexible packages. These factors are useful to packaging designers to calculate the maximum compressive stresses on packaging which occur during warehouse storage. Figure 51 shows an example calculation of the maximum compressive stress at the interface between the pallet and packaging. If stresses were uniformly distributed, the compression strength of the product or package must be at least 5.87 psi. However, because the pallet deckboards deflect, one must design a flexible package (example: 3/4- and 3/8-inch deck semi-rigid supporting flour sacks in a box) has to resist the compressive stresses of 2.487 x 5.87= 14.6 psi, or 4.294 x 5.87= 25.2 psi plus a safety factor depending pallet deck stiffness.

The previous study conducted by Yoo (2008) constructed three-stringer pallet section using nailed joint and the pallet deck material Plexiglas. Three different density foams were used to simulate different packaging stiffness in the previous study. The previous study conducted compression test on flour sacks stacked on the pallet section to predict the real packaging performance. The test result showed that the compressive stress distribution of the flour sacks over the pallet deck was similar to the results of the 4pcf foam stress distribution. Compressive Stress Intensity Factors of the 4pcf foam was 2.6 for 3/4-inch deckboards. The SIF of 4pcf foam in the previous study is similar to the SIF of flour (2.48) in the current study.

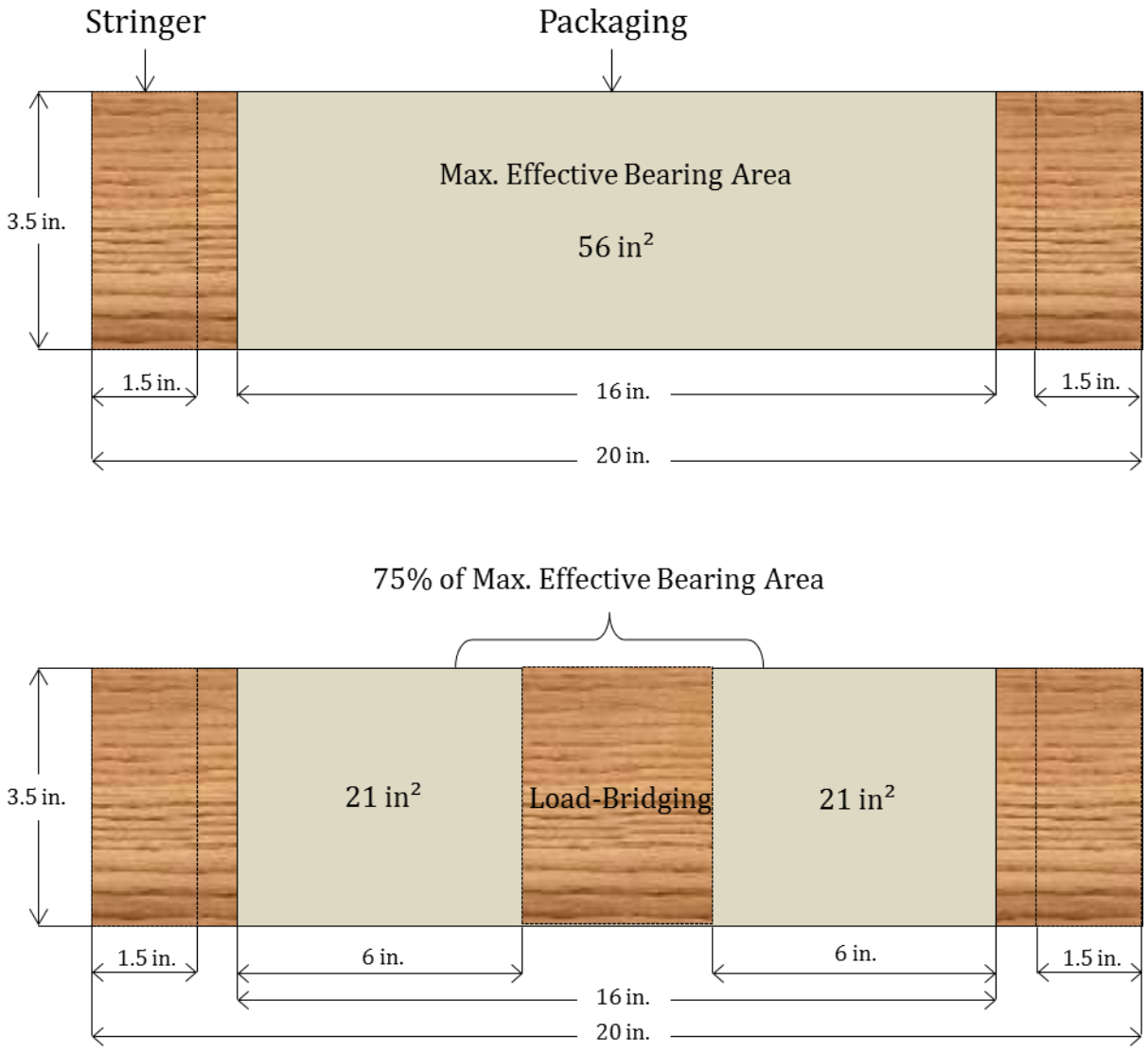

Figure 48. A schematic drawing showing an example of calculation of the effective bearing area and load-bridging

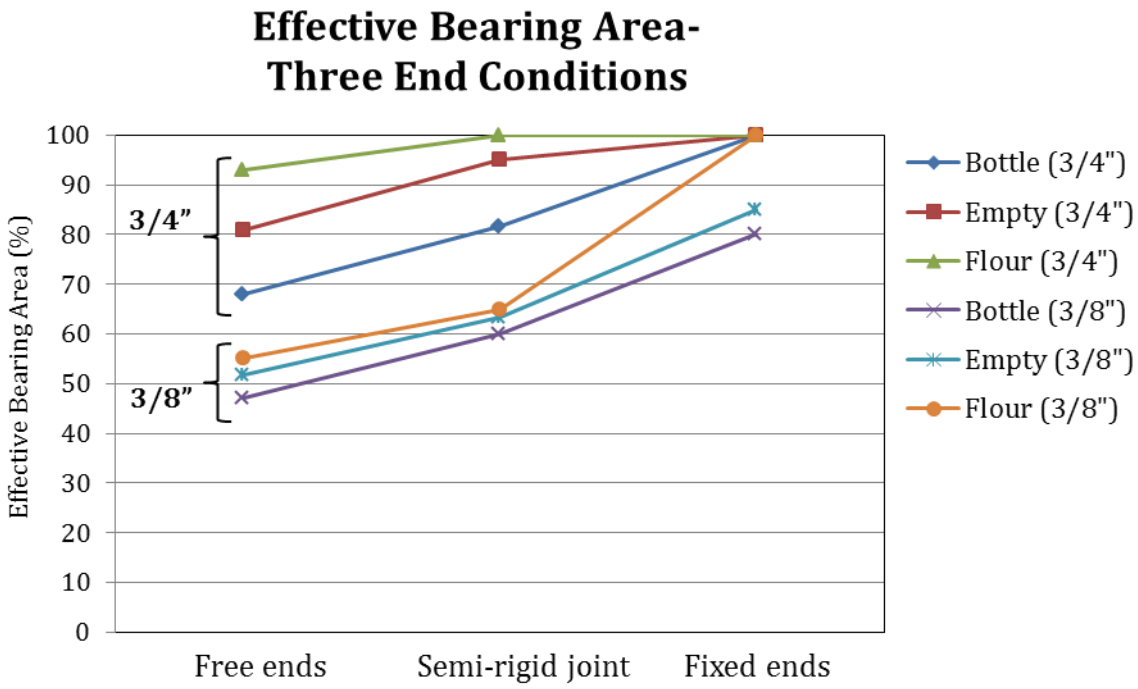

Figure 49. The effect of the pallet deck stiffness, packaging stiffness, and joint stiffness on the effective bearing area

Table 14. Compressive Stress Intensity Factors (SIF)

	Free ends		**Semi-rigid**		**Fixed ends**	
	3/4"	3/8"	3/4"	3/8"	3/4"	3/8"
Bottles	4.019	7.814	3.293	5.113	1.407	2.394
Empty	3.361	6.837	2.817	4.643	1.275	2.180
Flour	2.926	6.226	2.487	4.294	1.201	2.020

Note: Stress Intensity Factor = $\frac{Maximum\ Pressure}{Applied\ Pressure}$

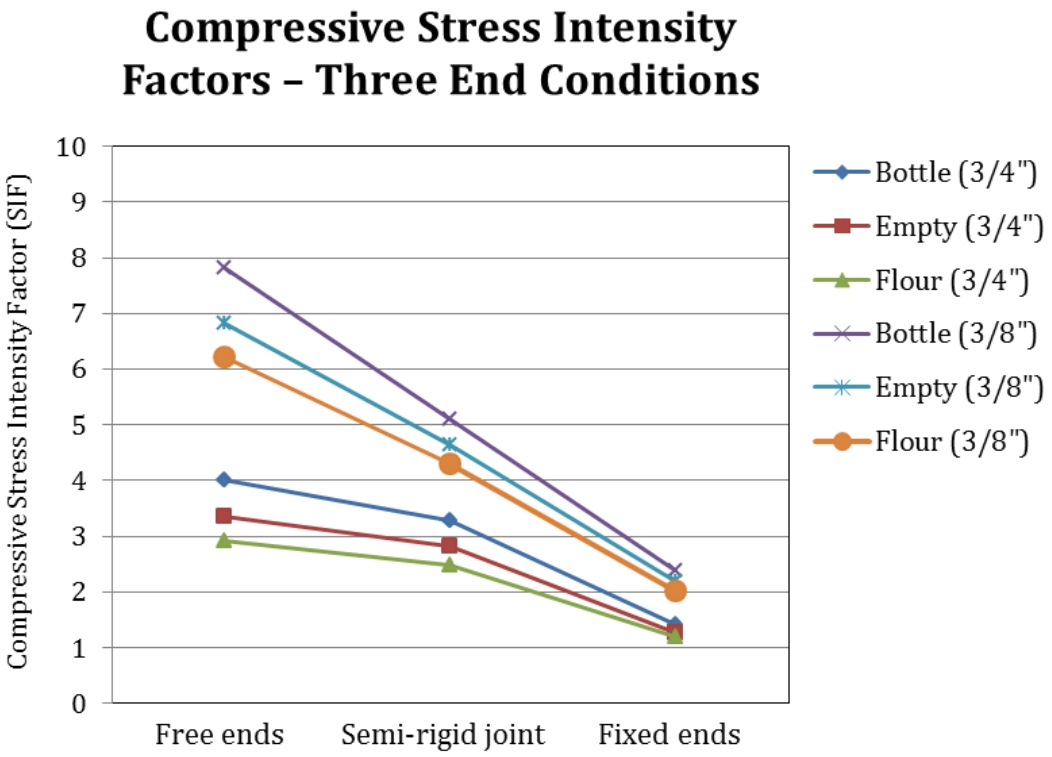

Figure 50. Compressive Stress Intensity Factors for three different end conditions

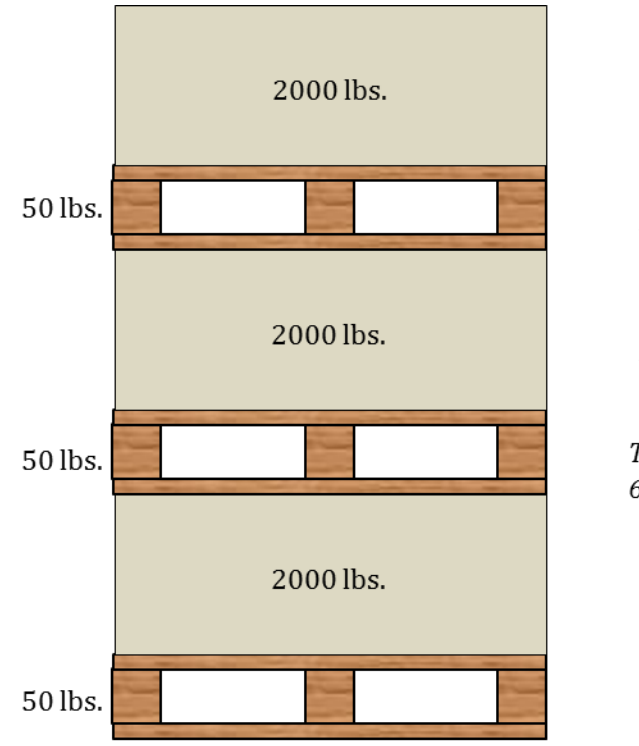

Weight of each SKU: 2000 lbs.
x The number of SKUs: 3
Total weight of SKUs: 6000 lbs.

Weight of each pallet: 50 lbs.
x The number of pallets on bottom pallet: 2
Total weight of pallets: 100 lbs.

Total loads on the top deck of the bottom pallet : 6000 lbs. + 100 lbs. = 6100 lbs.

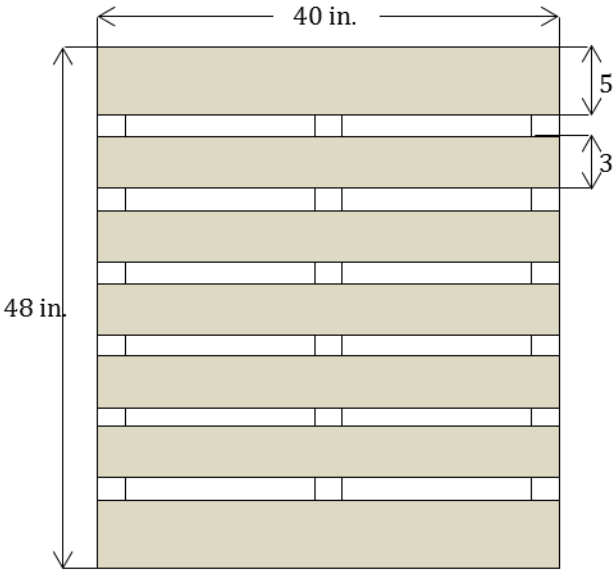

Top deck bearing area (in.^{2}):
(5.5 x 40 x 2) + (3.5 x 40 x 5) = 1040 in.^{2}

Applied stress (lbs./ in^2, psi):
6100 lbs. / 1040 in.^{2} = 5.87 psi

5.87 (applied stress) x Compressive Stress Intensity Factor = predicted maximum compressive stress

Ex) 5.87 psi x 2.487 (SIF of 3/4-inch deck semi-rigid supporting flours) = 14.6 psi
5.87 psi x 4.294 (SIF of 3/8-inch deck semi-rigid supporting flours) = 25.2 psi

Figure 51. Example calculation of the maximum compressive stress at the pallet/packaging interface using compressive stress intensity factors

CHAPTER 5

5.0 Validation of Compressive Stress Distribution Models

Chapter 5 discusses the validation of compressive stress distribution models developed in chapter 4. The developed models are to validate by comparison to experimental data. This chapter contains descriptions of all materials and equipment used. Test procedures and experimental results are also discussed. The objective of this chapter is:

- To quantify compressive stress distributions at the interface between a pallet deck and packaging for use in validating developed predictive compressive stress distribution models

5.1 Materials and Equipment

This section describes all materials used to construct pallet sections and packaging and the equipment used in deckboard deflection and pressure distribution measurements. Three different pallet sections were constructed using three different end conditions: free ends, semi-rigid joints, and fixed ends.

5.1.1 Pallet Section

This section contains descriptions of all materials used to construct pallet section test specimens as follows:

- Wood species: Southern Yellow Pine
- Component dimensions
  - Deckboards
    - 20-inch long, 3.5-inch wide, 3/4 inches thick
    - 20-inch long, 3.5-inch wide, 3/8 inches thick
  - Stringers: 3.5-inch long, 1.5-inch wide, 3.5-inch high

- Number of components

			Free Ends	Semi-rigid Joints	Fixed Ends	Total
Number of pallet sections			6	6	6	18
Number of Components	Deckboard	3/4"	6	6	6	18
		3/8"	6	6	6	18
	Stringer		12	12	12	36

- Pallet section fastening

Free Ends	Semi-rigid Joints	Fixed Ends
Finishing nail[1]	Helical nail[2] Annular nail[3]	Epoxy Adhesive

Note:

[1] 2-inch long 0.094-inch wire diameter

[2] Helically threaded 2-inch long 0.119-inch wire diameter for 3/8 inch deck

[3] Annularly threaded 2.25-inch long 0.122-inch wire diameter for 3/4 inch deck

5.1.2 Packaging

Materials used for three different packaging stiffness levels include:

- Empty Box
  - Regular Slotted Container (RSC) (Single-wall C-flute 69-26C-69)
  - External Dimension (L x W x H) (in.): 15.5 x 7.75 x 10
  - Weight (lbs.): 0.7
- Flour sack
  - External Dimension (L x W x H) (in.): 3.75 x 2.5 x 7.7
  - Weight (lbs.): 2 lbs. per one flour sack
  - Filled weight (lbs.): 32 lbs.

- Polyethylene Terephthalate (PET) Plastic beer bottle
  - External Dimension (Diameter x H) (in.): 3.875 x 10
  - Weight (lbs.): 0.92 per one bottle
  - Filled weight (lbs.): 16.6 lbs.
- Number of specimens

	Box	Flour sack	Plastic Bottle
Quantity per box	-	16	18
# of boxes tested	36	36	36

5.1.3 Equipment

Equipment used to test specimens includes:

- Pressure measurement system (sensor specifications are described in Figure 49)
  - Two pressure film sensors (I-Scan®) for two different pressure ranges:
    - I-Scan® Model # 5315, 0 to 5 psi
    - I-Scan® Model # 5315, 0 to 30 psi
  - Sensitivity range
    - 5 psi: 0.3-5 psi
    - 30 psi: 3-30 psi
  - Data acquisition hardware
    - Scanning electronics (*Evolution*® Handle)
    - Personal Computer (PC)
  - I-Scan® pressure and force measurement analysis software
- Linear Variable Differential Transducer (LVDT)
  - Two, 0.5 inch Schaevitz LVDT Model 050HR-DC (working distance ± 0.5 in.)
  - Two, 1 inch Schaevitz LVDT Model 100HR-DC (working distance ± 1 in.)
  - Two, 2 inch Schaevitz LVDT Model 200HR-DC (working distance ± 2 in.)
- Test machine

- 826.75 MTS servo-hydraulic with 5000 pounds interface load cell model # 661.20E-01

- Load applicator
  - 16.25-inch long, 9-inch wide, 0.6-inch thickness plywood

Pressure distribution at the interface between a pallet deck and packaging was quantified using the pressure measurement system, which includes a thin, flexible and reusable film sensor, data acquisition hardware (scanning electronics and PC), and analysis software. The system displays and records dynamic and static interface pressure distribution data directly to the PC. Figure 52 shows a photograph of the film sensor used and its specifications. The scanning electronics rapidly scan and record pressure data from 2016 of independent sensing elements, or sensels as described in Figure 52, contained within the sensor (Tekscan, Inc, 2007). Two different sensor ranges (0 to 5 psi and 0 to 30 psi), were used to measure various pressure ranges from 0.3 to 30 psi between two contact surfaces (top of pallet deck and bottom of packaging). The linearity range of those two sensors, indicating the degree of sensitivity consistency of the sensor, was less than ± 3%. The sensitivity of the sensor represents how much the sensor's output changes when the applied pressure changes. The resolution of the sensors which indicates sensor spacing or sensel density was 6.3 per square inch.

5.2 Experimental Procedures

This section contains descriptions of all test specimens (pallet sections and packaging) preparations and experimental design. Test procedures are described in this section as well.

5.2.1 Pallet Section Assembly

All pallet sections used were assembled with one top, one bottom deckboard, and two stringer segments. Eighteen pallet sections (six pallet sections of each of the three end conditions)

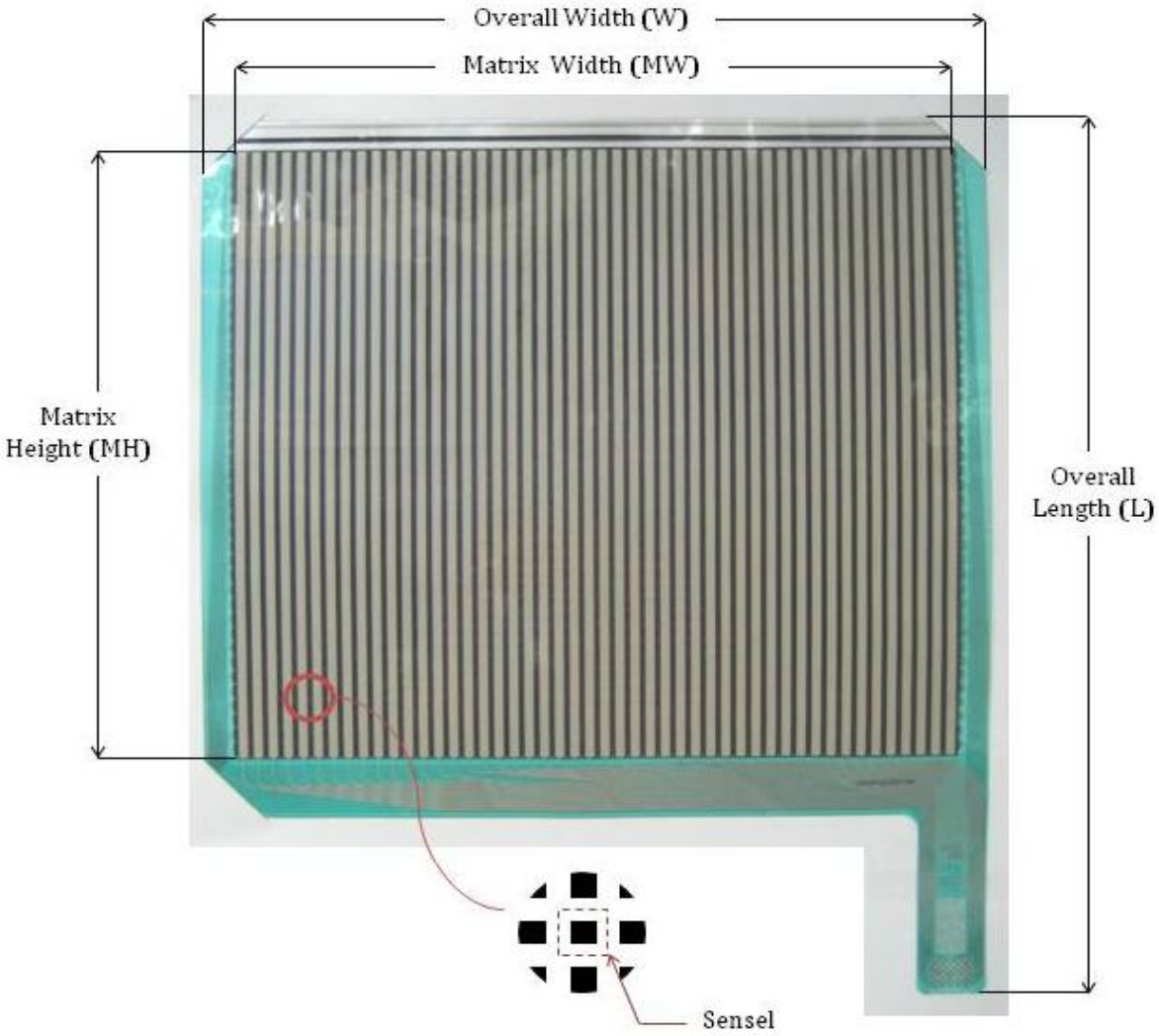

Model Number	Pressure Range	Overall Length (L) in.	Overall Width (W) in.	Matrix Width (MW) in.	Matrix Height (MH) in.	Column Qty.	Row Qty.	Total No. of Sensels
5315	0-5 psi 0-30 psi	24.50	20.86	19.20	16.80	48	42	2016

Figure 52. Pressure sensor specifications

were constructed from the tested deckboard components (the test to measure MOE was discussed in section 3.1). Six pallet sections of each end condition were constructed from three of 3/4-inch and three of 3/8-inch deck thickness. Each pallet section with free ends used one finishing nail, 2-inch long and 0.094-inch wire diameter, to link the deckboards and stringers. A straight line was drawn across the width of the top and bottom deck surfaces of each pallet section 0.75-inch from each end. A hole was drilled 2.25-inch into the center of the line using a 0.139-inch diameter drill bit (147% of the nail wire diameter). The depth of drilled hole was the same as the length of the nail so that the finishing nail head was flush with top surface of each deckboard section. Semi-rigid joint pallet section assembly used the same nailing assembly and nail type as the joint rotation test specimen (section 3.2). Fixed ends pallet section was constructed using epoxy adhesive to affix the deckboards and stringers. The test specimens were rigidly clamped using C-clamps to ensure the components were fully fixed each other and remained untested for 24 hours after gluing assembly was complete. The constructed pallet sections using three different end conditions are shown in Figure 53.

The experimental design is described in the block diagram presented in Figure 54. Nondestructive testing was conducted on each pallet section with three different packaging. Each test combination included three replications.

5.2.2 Packaging Preparation

The three different packages, 1) empty boxes, 2) boxes containing plastic bottles and 3) flour sacks, were the same types used for packaging stiffness testing (section 3.3). One hundred and eight corrugated boxes were constructed using the same board grade, size, and shape as that used in the stiffness testing. Details and specifications of the product contained in boxes were described in section 3.3.1 and 5.1.2.

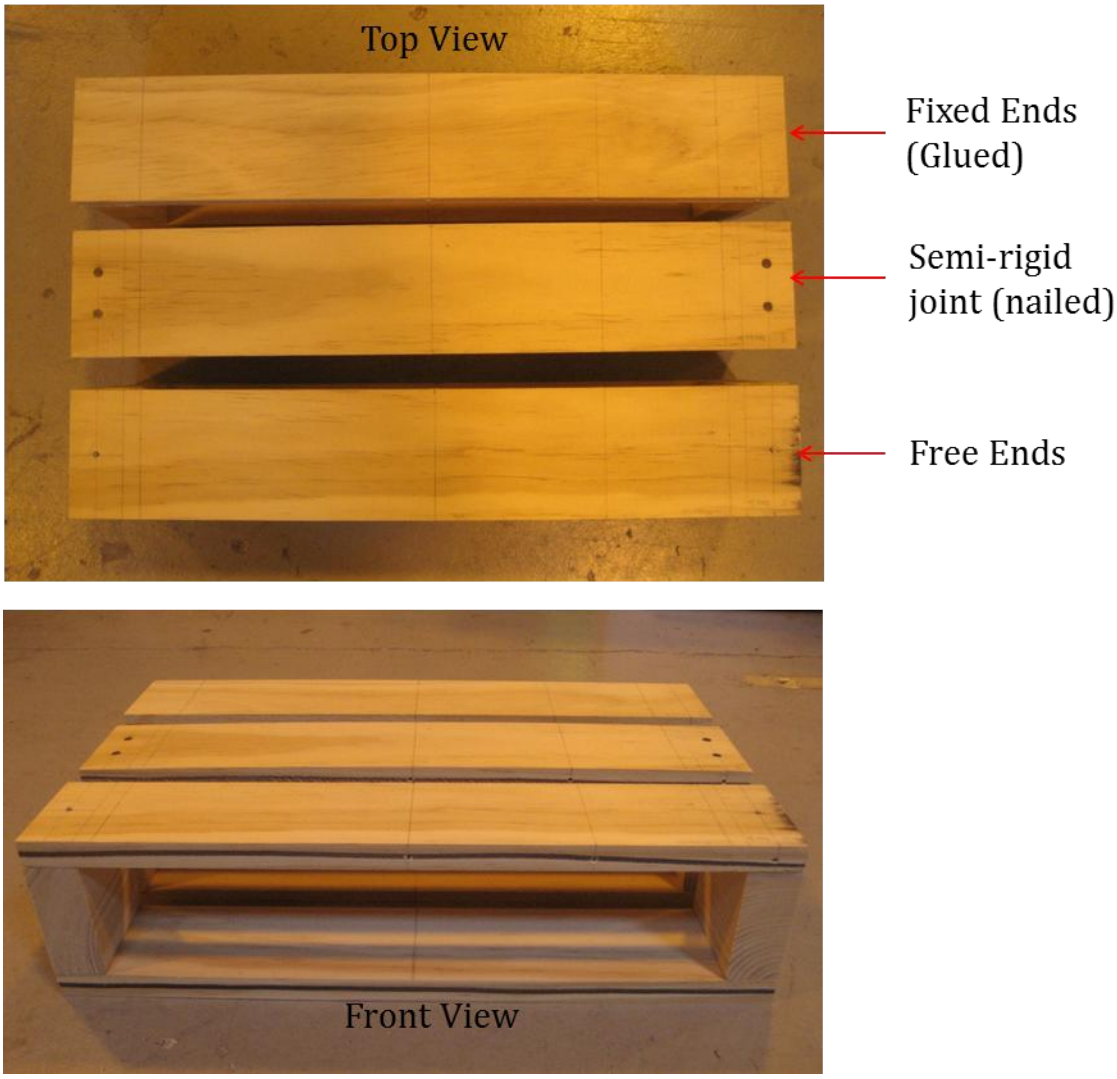

Figure 53. Pallet section specimens constructed with three different end conditions

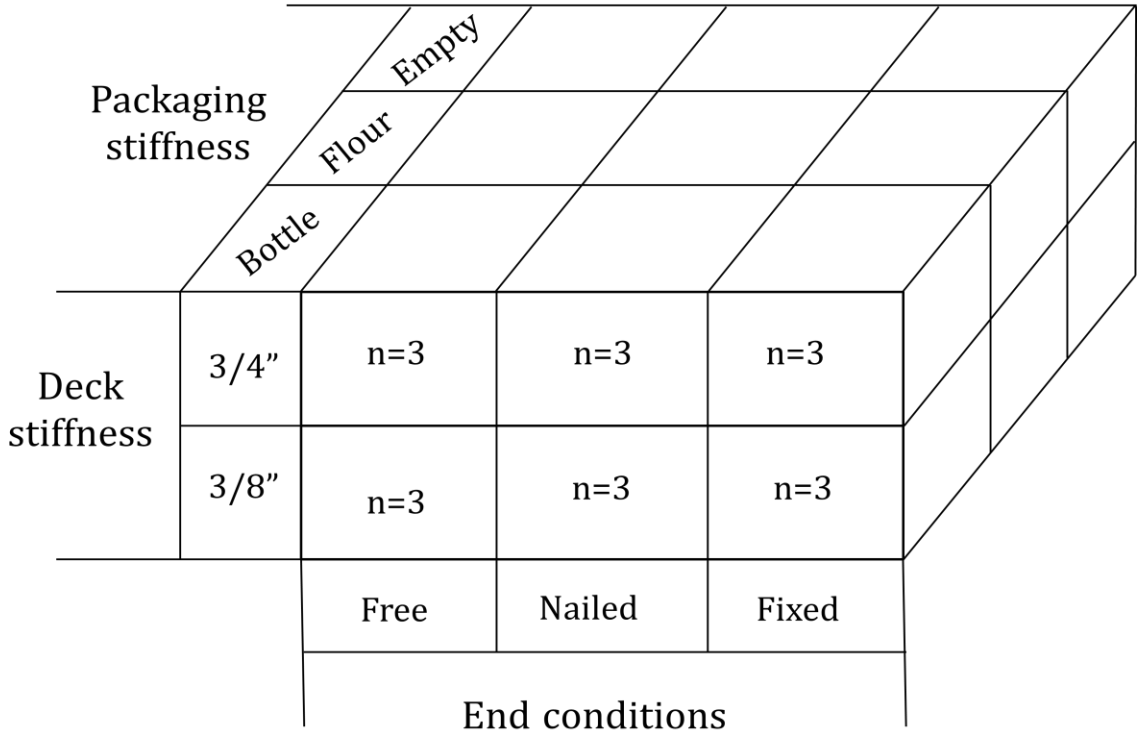

Figure 54. Experimental design

5.2.3 Pressure Sensor Calibration

Prior to testing, it was necessary to calibrate the two pressure sensors. The digital output is converted to an actual engineering unit, such as PSI or g/cm^2 by calibration (I-Scan User Manual, 2004). Two different sensors, 5 psi and 30 psi, were used to measure two different pressure ranges during testing, therefore the two sensors were separately calibrated using different levels of loading. This pressure measurement system enables users to perform two different types of calibration: linear and 2-point power law. For the current study, the 2-point power law calibration, which is suitable if measurement loads vary considerably during testing, was performed. Two different calibration loads, 30 pounds and 1100 pounds, approximately 20% and 80% of the expected maximum test load, were applied to the sensor using the compression tester squeezer (Lansmont Corporation, 2011). A 16-inch by 16-inch inflatable air bag was placed between the sensor and the top platen of the compression tester to apply the uniform load to the sensor over the entire area. The two calibration loads applied were 280-/900-pound and 300-/1100-pound for 5 psi and 30 psi sensor, respectively. The software automatically calculates and displays saturation pressure during calibration. The saturation pressures, which are the point at which the sensor output no longer varies with applied pressure, were 4.422 psi and 24.094 psi for 5 psi and 30 psi sensor, respectively.

5.2.4 Test Procedures

Six small holes were pre-drilled, and then six screws were driven into each of the six holes to attach six LVDTs (two, 2-inch, two, 1-inch, and two, 0.5-inch) for deflection measurement. The locations of the three LVDTs (one of each LVDT length) are illustrated in a schematic diagram of test setup in Figure 56. The other three LVDTs were located symmetrically. Because symmetry about the span center line, where the 2-inch LVDT was attached, was assumed, only half of the pallet section needs to be considered to measure the pallet deck deflection by which the complexity

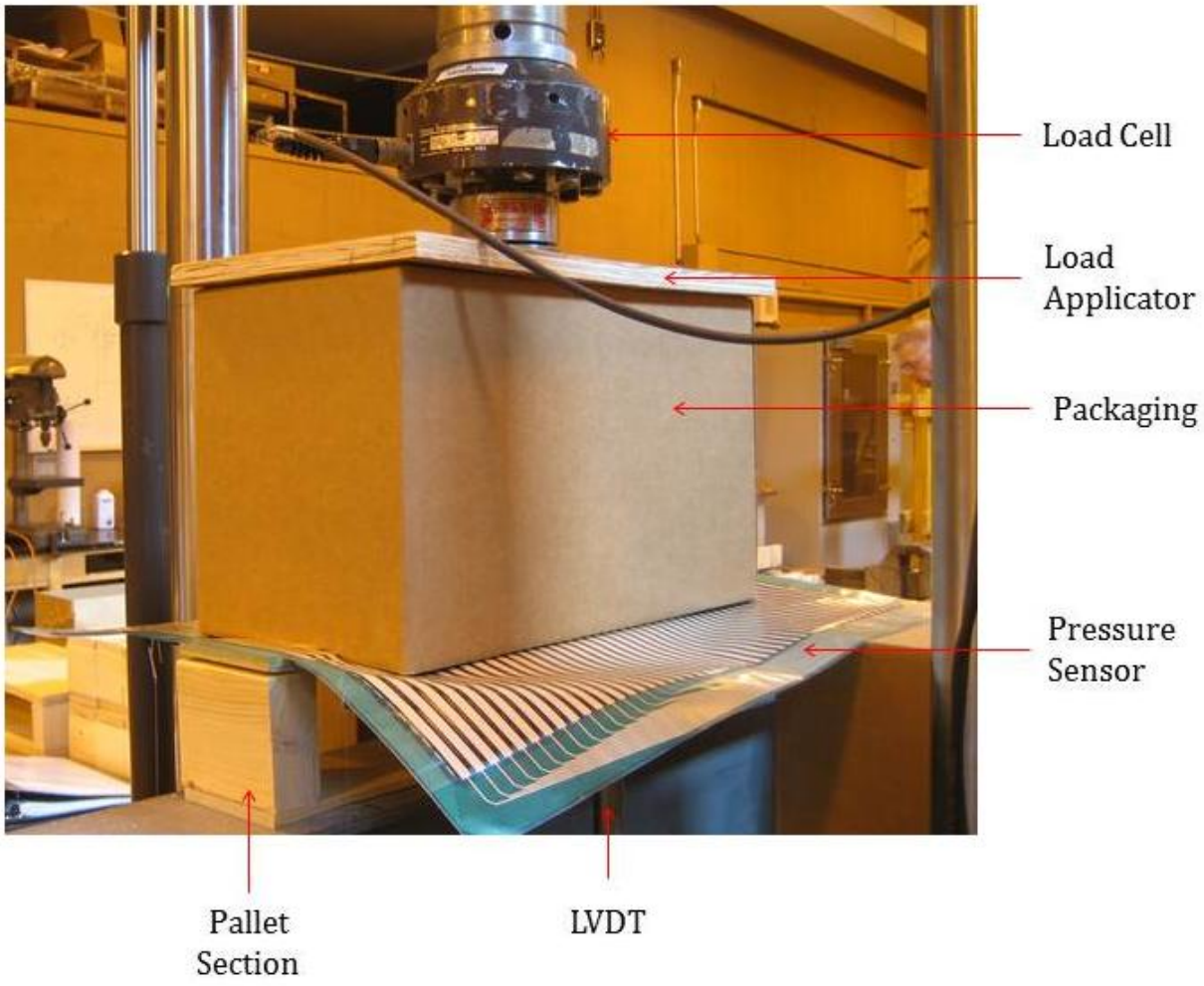

Figure 55. Test setup for pressure distributions

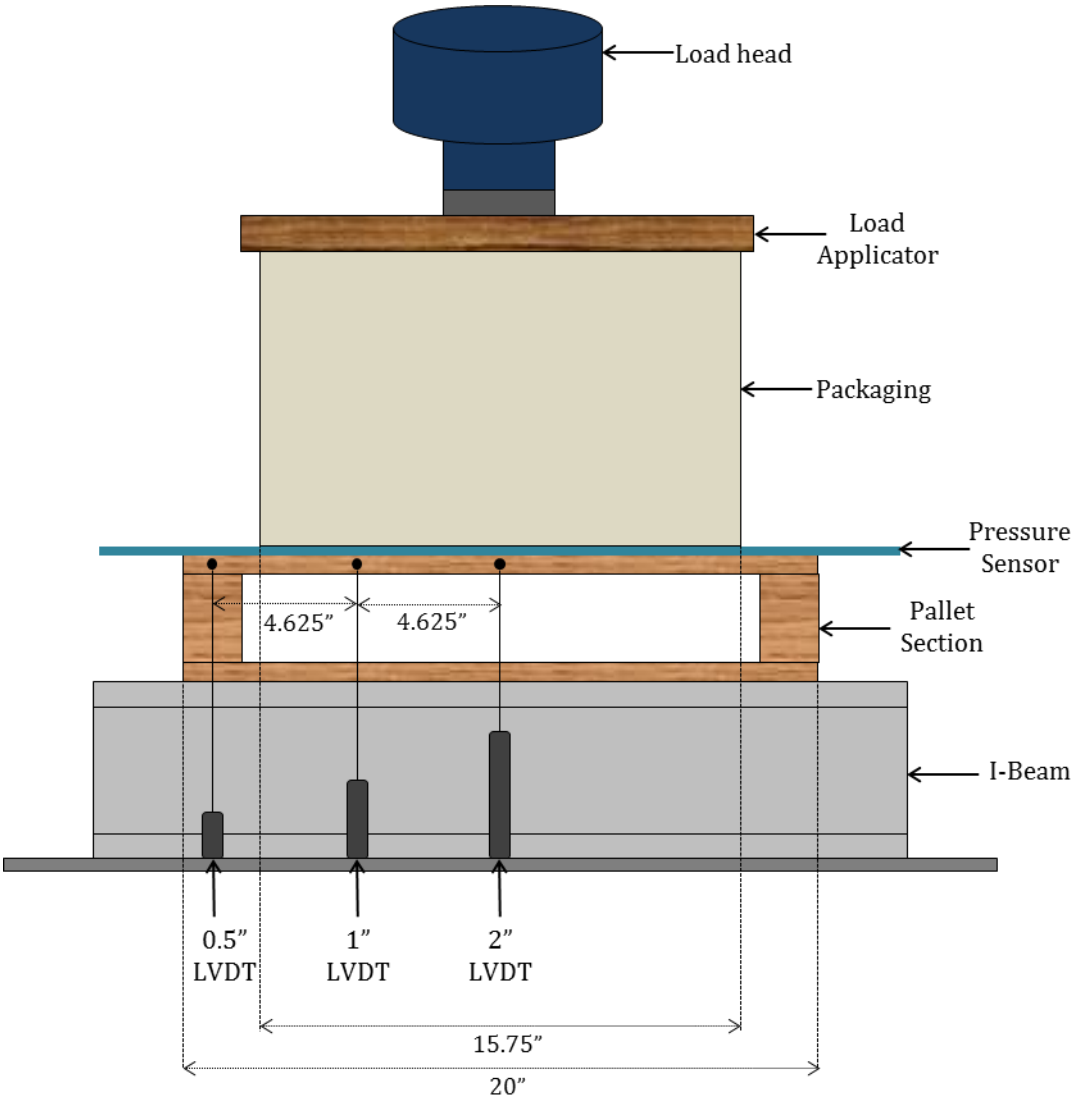

Figure 56. A schematic drawing of test set up for pressure distribution measurement

of the analysis could be reduced.

The pallet section was placed on the I-beam and six LVDTs were attached to the pallet section. The pressure sensor was placed on the top of the pallet section to cover the entire surface of the top deckboard. The corners of the sensor were set flat on the horizontal plane in order to avoid false pressure readings caused by bending of the sensor. The sensor was connected to the scanning electronics called *Evolution*® Handle which gathers data from the sensor, and then processes and sends this data to the computer. Prior to testing, the 'Measurement units' dialog box had to be checked to ensure the units were set as inches for units of length, pounds for force, and PSI for pressure. The sensor model was selected in order that the system displayed correct data and the correct calibration file for the sensor was loaded. Then, the box containing products was located on the center of the pallet section and the load applicator was placed and covered the top surface of the packaging. 350 pound loads was applied to the specimen using 826.75 MTS servo-hydraulic with 5000 pounds interface load cell at a rate of 0.1 in. /min. When the loads reached 350 pounds, the sensor pressure measurement was captured by clicking the snapshot icon on the Toolbar of the I-Scan system and the test was stopped at the same time. The MTS system controlled the applied load and recorded the corresponding pallet deck deflections at six locations of LVDTs. The test was stopped on empty box specimens at 280 pound loads because the load stopped increasing and crush damage was observed. These test procedures were repeated for the other pressure range measurement sensor with new boxes containing the same products stacked on the same pallet section. After placing the other sensor, the correct calibration file for the sensor was loaded.

5.3 Pressure Data Analysis

Figure 57 shows the images of pressure distributions captured, at the interface between a box containing plastic bottles and the top deck of the fixed ends pallet section, using the 5 psi and 30 psi sensors when the applied load reached 350 pounds. The captured image displays the

recording in two-dimensional form with the color of each sensel location representing the pressure sensed at that point on the sensor. Pressure data was analyzed in a spreadsheet by copying the captured pressure image and saving to the Microsoft Excel as a text file of the actual pressure values. Examples of the captured pressure images and the corresponding actual values of the pressure data are shown in Figure 57. Each colored sensel represents the pressure measured between the packaging and pallet section. The entire area of sensed pressure shows the contact between top surface of the pallet section and the bottom surface of the box. The value shown in each cell in the table represents the corresponding actual pressure value for each sensel. As seen in Figure 57, the calibrated legend shows the pressure range that corresponds to each of the 13 possible colors. The number shown on each color in the legend is the lowest value in that color range.

Figure 58 shows the pressure data was merged together based on assumed symmetric response. Considering sensitivity ranges and saturation pressures of two different sensors, the reliable data ranges of 5 psi and 30 psi sensors were 0.3 psi to 4.422 psi and 3 psi to 24.094 psi, respectively. All pressures above the maximum value are displayed as red which represents the saturation pressure. In the table, any data out of those reliable ranges were ignored, and then the data sets of two sensor pressure measurements were merged by fitting 5 psi sensor data into 30 psi sensor data set. The data across the width of the sensed area excluding 0 psi was averaged along the length of the box at every 0.4-inch, which is the width of each sensel. The averaged pressures were plotted as a function of the length of the box as shown in an example of the actual plot in Figure 58. The pressure data plotted from 8-inch to 16-inch was merged into the location from 0.4-inch to 8-inch. Because of the symmetry about the center line of the pressure distributions, only the half, from 0.4-inch to 8-inch, was considered. Then, the merged data from 0.4-inch to 8-inch was plotted into 8-inch to 16-inch due to the symmetry used as presented in Figure 58. All pressure data were analyzed using the same process. The pressure distribution plots of all tests are shown in

section 5.4.

5.4 The Pressure Distribution Results

Figure 59, 60, and 61 show images of pressure distribution captured at the interface between the top deck of the pallet section and three types of packages, using the 5 psi and 30 psi sensors. The results showed higher pressures near the ends of the 3/8-inch deckboard than 3/4-inch deckboard. The pressure distributions of the pallet deckboard supporting the empty box had greater load-bridging areas (no pressure areas) than other packages. The pressures distributions measured across the deckboard loaded by the flour sacks in a box showed the lowest load-bridging areas (more pressures sensed across the deckboard). The greater joint fixity and pallet deck stiffness resulted in less load-bridging. The pressures measured across the interface between the deckboard and the bottles showed the minor flaps and major flaps of the bottom of the box (see Figure 5). The images of the bottles showed lower pressures in the center across the length due to the gap between two major flaps. The tabulated raw pressure values of each pressure image are presented in Tables 1 through 10 of Appendix A.

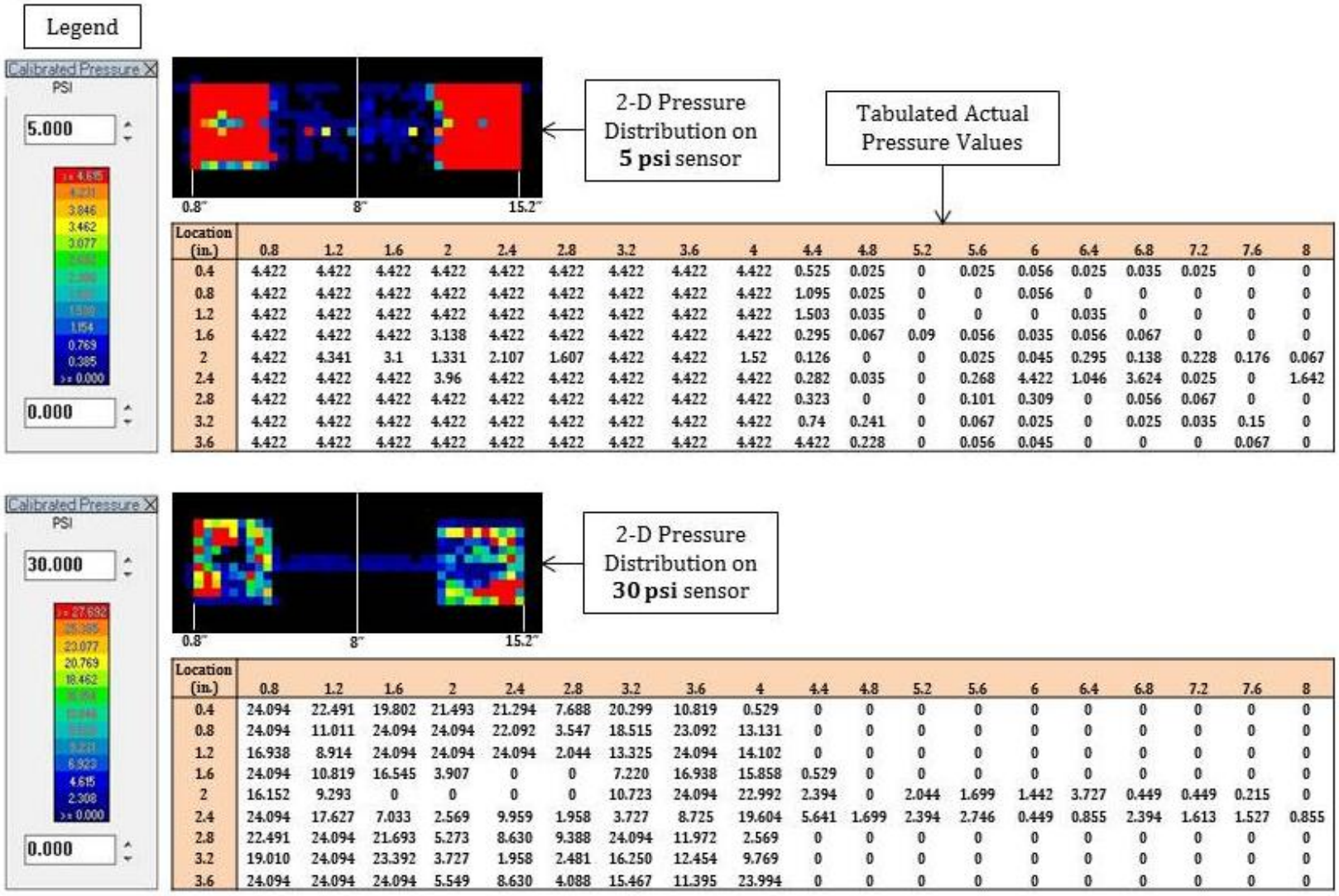

Location (in.)	0.8	1.2	1.6	2	2.4	2.8	3.2	3.6	4	4.4	4.8	5.2	5.6	6	6.4	6.8	7.2	7.6	8
0.4	4.422	4.422	4.422	4.422	4.422	4.422	4.422	4.422	4.422	0.525	0.025	0	0.025	0.056	0.025	0.035	0.025	0	0
0.8	4.422	4.422	4.422	4.422	4.422	4.422	4.422	4.422	4.422	1.095	0.025	0	0	0.056	0	0	0	0	0
1.2	4.422	4.422	4.422	4.422	4.422	4.422	4.422	4.422	4.422	1.503	0.035	0	0	0	0.035	0	0	0	0
1.6	4.422	4.422	4.422	3.138	4.422	4.422	4.422	4.422	4.422	0.295	0.067	0.09	0.056	0.035	0.056	0.067	0	0	0
2	4.422	4.341	3.1	1.331	2.107	1.607	4.422	4.422	1.52	0.126	0	0	0.025	0.045	0.295	0.138	0.228	0.176	0.067
2.4	4.422	4.422	4.422	3.96	4.422	4.422	4.422	4.422	4.422	0.282	0.035	0	0.268	4.422	1.046	3.624	0.025	0	1.642
2.8	4.422	4.422	4.422	4.422	4.422	4.422	4.422	4.422	4.422	0.323	0	0	0.101	0.309	0	0.056	0.067	0	0
3.2	4.422	4.422	4.422	4.422	4.422	4.422	4.422	4.422	4.422	0.74	0.241	0	0.067	0.025	0	0.025	0.035	0.15	0
3.6	4.422	4.422	4.422	4.422	4.422	4.422	4.422	4.422	4.422	4.422	0.228	0	0.056	0.045	0	0	0	0.067	0

Location (in.)	0.8	1.2	1.6	2	2.4	2.8	3.2	3.6	4	4.4	4.8	5.2	5.6	6	6.4	6.8	7.2	7.6	8
0.4	24.094	22.491	19.802	21.493	21.294	7.688	20.299	10.819	0.529	0	0	0	0	0	0	0	0	0	0
0.8	24.094	11.011	24.094	24.094	22.092	3.547	18.515	23.092	13.131	0	0	0	0	0	0	0	0	0	0
1.2	16.938	8.914	24.094	24.094	24.094	2.044	13.325	24.094	14.102	0	0	0	0	0	0	0	0	0	0
1.6	24.094	10.819	16.545	3.907	0	0	7.220	16.938	15.858	0.529	0	0	0	0	0	0	0	0	0
2	16.152	9.293	0	0	0	0	10.723	24.094	22.992	2.394	0	2.044	1.699	1.442	3.727	0.449	0.449	0.215	0
2.4	24.094	17.627	7.033	2.569	9.959	1.958	3.727	8.725	19.604	5.641	1.699	2.394	2.746	0.449	0.855	2.394	1.613	1.527	0.855
2.8	22.491	24.094	21.693	5.273	8.630	9.388	24.094	11.972	2.569	0	0	0	0	0	0	0	0	0	0
3.2	19.010	24.094	23.392	3.727	1.958	2.481	16.250	12.454	9.769	0	0	0	0	0	0	0	0	0	0
3.6	24.094	24.094	24.094	5.549	8.630	4.088	15.467	11.395	23.994	0	0	0	0	0	0	0	0	0	0

Figure 57. An Example of pressure images and actual pressure values of the two different pressure range sensors

Location (in.)	0.8	1.2	1.6	2	2.4	2.8	3.2	3.6	4	4.4	4.8	5.2	5.6	6	6.4	6.8	7.2	7.6	8
0.4	24.094	22.491	19.802	21.493	21.294	7.688	20.299	10.819	0.000	0.525	0	0	0	0	0	0	0	0	0
0.8	24.094	11.011	24.094	24.094	22.092	3.547	18.515	23.092	13.131	1.095	0	0	0	0	0	0	0	0	0
1.2	16.938	8.914	24.094	24.094	24.094	0.000	13.325	24.094	14.102	1.503	0	0	0	0	0	0	0	0	0
1.6	24.094	10.819	16.545	3.907	0	0	7.220	16.938	15.858	0.000	0	0	0	0	0	0	0	0	0.616
2	16.152	9.293	3.1	1.331	2.107	1.607	10.723	24.094	22.992	0.000	0	0	0	0	0	0	0	0	0
2.4	24.094	17.627	7.033	0.000	9.959	0.000	3.727	8.725	19.604	5.641	0	0	0	1.046	3.624	0	0	1.642	0
2.8	22.491	24.094	21.693	5.273	8.630	9.388	24.094	11.972	0.000	0	0	0	0	0	0	0	0	0	0
3.2	19.010	24.094	23.392	3.727	0.000	0.000	16.250	12.454	9.769	0	0	0	0	0	0	0	0	0	0
3.6	24.094	24.094	24.094	5.549	8.630	4.088	15.467	11.395	23.994	0.74	0	0	0	0	0	0	0	0	0
Average	21.67	16.94	18.21	11.18	13.83	5.26	14.4	15.95	17.06	1.9	0	0	0	1.05	3.62	0	0	1.64	0.62

Location (in.)	8.4	8.8	9.2	9.6	10	10.4	10.8	11.2	11.6	12	12.4	12.8	13.2	13.6	14	14.4	14.8	15.2
0.4	0	0	0	0	0	0	0	1.713	0	4.633	3.727	3.100	0	0	0	0	3.100	0
0.8	0	0	0	0	0	0	0.511	1.642	12.164	22.691	21.393	24.094	22.192	24.094	22.791	14.394	20.696	11.298
1.2	0.996	0	0	0	0	0	0	0	6.288	4.451	0	8.536	8.820	6.474	24.094	20.895	24.094	5.181
1.6	0	0	0	0	0	0	0	0	0	0	8.253	0	16.447	11.683	0	9.483	18.120	10.628
2	0	0	0.787	0	0	0	0	0	8.914	12.261	0	12.937	9.769	14.783	12.841	19.604	24.094	11.683
2.4	3.368	0	0.724	3.368	1.095	3.546	0	3.100	5.641	7.970	3.997	0	0	0	0.000	4.088	14.588	13.034
2.8	0.819	0	0	0	0	0	0	0	9.483	3.458	5.826	0	0	0	7.126	11.972	21.593	8.914
3.2	0	0	0	0	0	0	0	0	5.641	17.135	13.810	5.733	8.536	4.542	24.094	24.094	24.094	24.094
3.6	0	0	0	0	0	0	0	0	7.688	22.092	20.696	15.761	24.094	24.094	24.094	24.094	24.094	9.578
Average	1.73	0	0.76	3.37	1.1	3.55	0.51	2.37	8.104	13.51	12.18	14.31	15.57	14.25	19.32	16.97	21.72	12.57

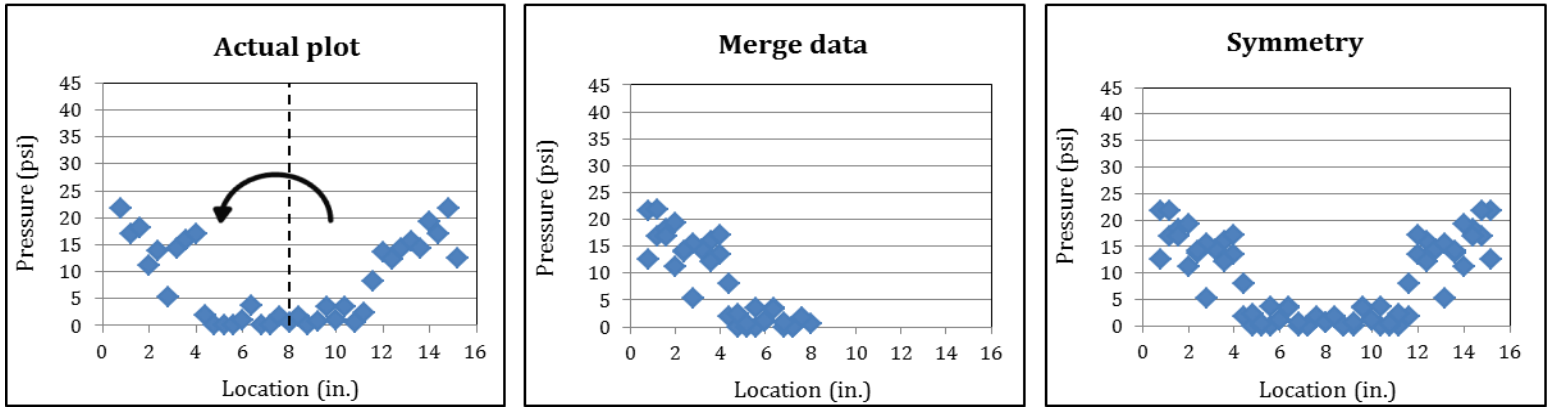

Figure 58. Schematic diagrams showing for pressure data was merged together based on assumed symmetric response

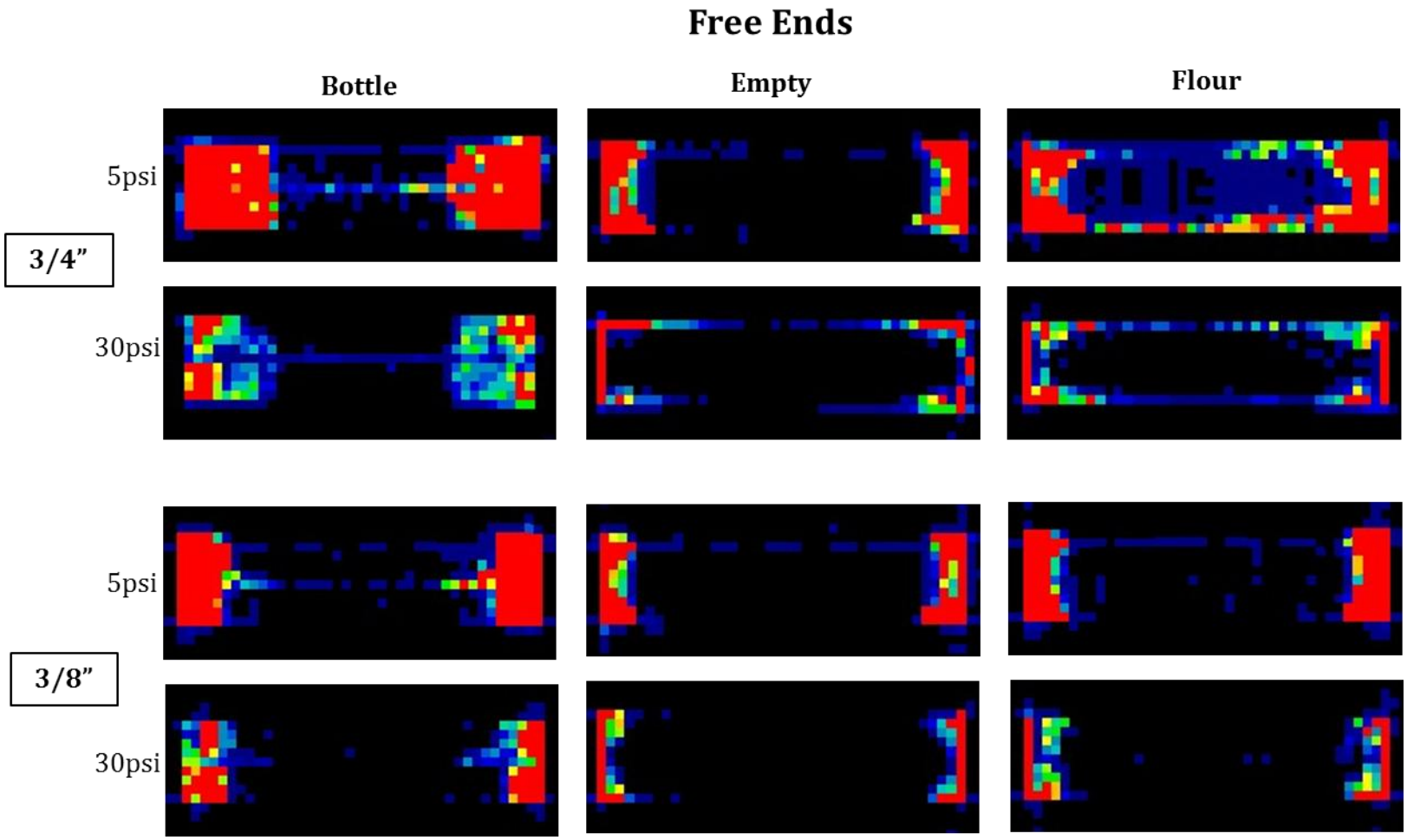

Figure 59. Images of pressure distribution captured at the interface between the top deck of the free ends pallet section and three types of packages, using the 5 psi and 30 psi sensors

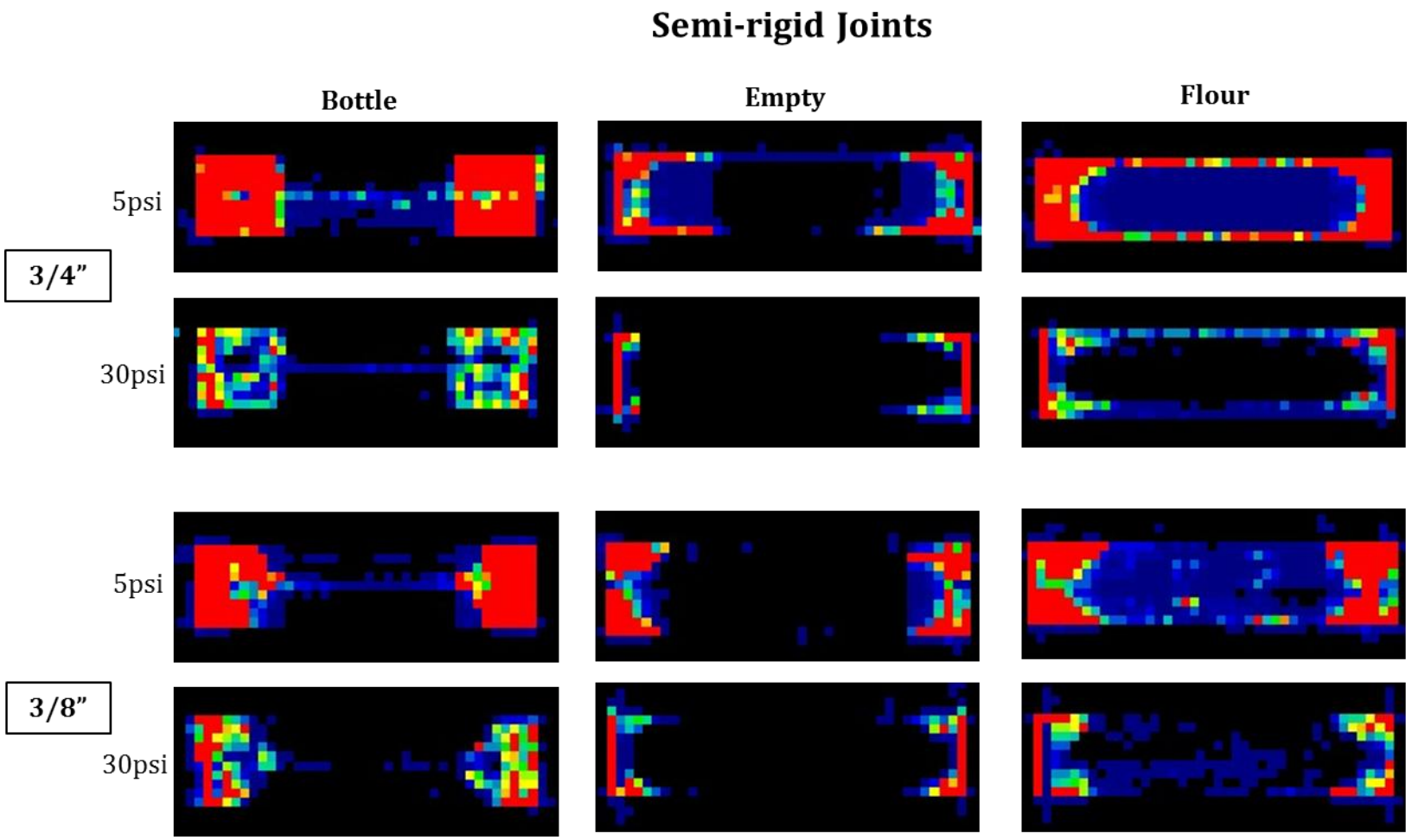

Figure 60. Images of pressure distribution captured at the interface between the top deck of the semi-rigid joints pallet section and three types of packages, using the 5 psi and 30 psi sensors

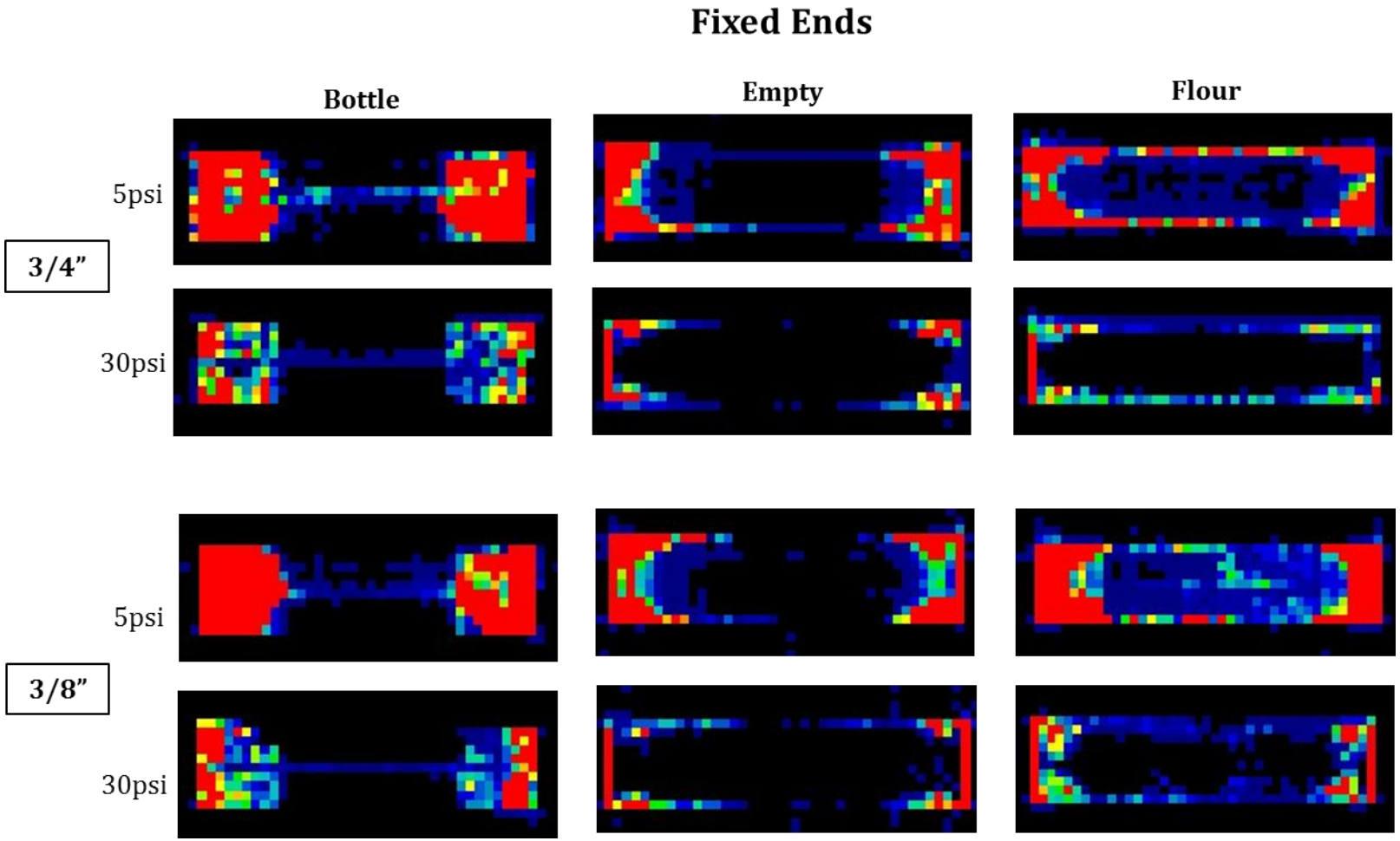

Figure 61. Images of pressure distribution captured at the interface between the top deck of the fixed ends pallet section and three types of packages, using the 5 psi and 30 psi sensors

5.5 Validation of Pallet Deck Deflection Models

The predicted pallet deck deflection was used to predict the compressive stress distributions. Figure 62 shows graphs comparing predicted and measured maximum deflections for three end conditions. The measured maximum deflections of 3/8-inch and 3/4-inch deckboards supporting three different packages in all three end conditions were respectively about 50% and 30% greater than the predicted deflections. The results show that the pallet deck supporting stiffer packaging deflected more than decks supporting the packaging of lower stiffness.

There are two explanations for the difference between predicted and measured maximum deflections. A fundamental assumption of the prediction model is that the compressive stresses were distributed by an elastic foundation all the way across the beam. However, during testing, there was a region where the compressive stresses were zero across the pallet deck due to load-bridging. The lower stiffness pallet deck (3/8-inch) has more load-bridging than the stiffer 3/4-inch deck. Therefore, the difference between predicted and measured maximum deflection was greater for 3/8-inch pallet deck than 3/4-inch deck. The deflection of the package should be measured at the center of the deck span to validate the predicted maximum deflection of the unit load section. The reason for greater predicted deflection of the deck supporting stiffer packaging could be that the plywood load applicator deformed during testing and transferred load to the contents of the box and then to the bottom of the box rather than to the box perimeter as occurs with lower stiffness packaging. This pressure distribution is shown in Figure 59, 60 and 61.

Therefore, future studies should measure the package deflection to validate the predicted pallet deck deflection. The method of load application should be designed to provide a uniformly distributed load.

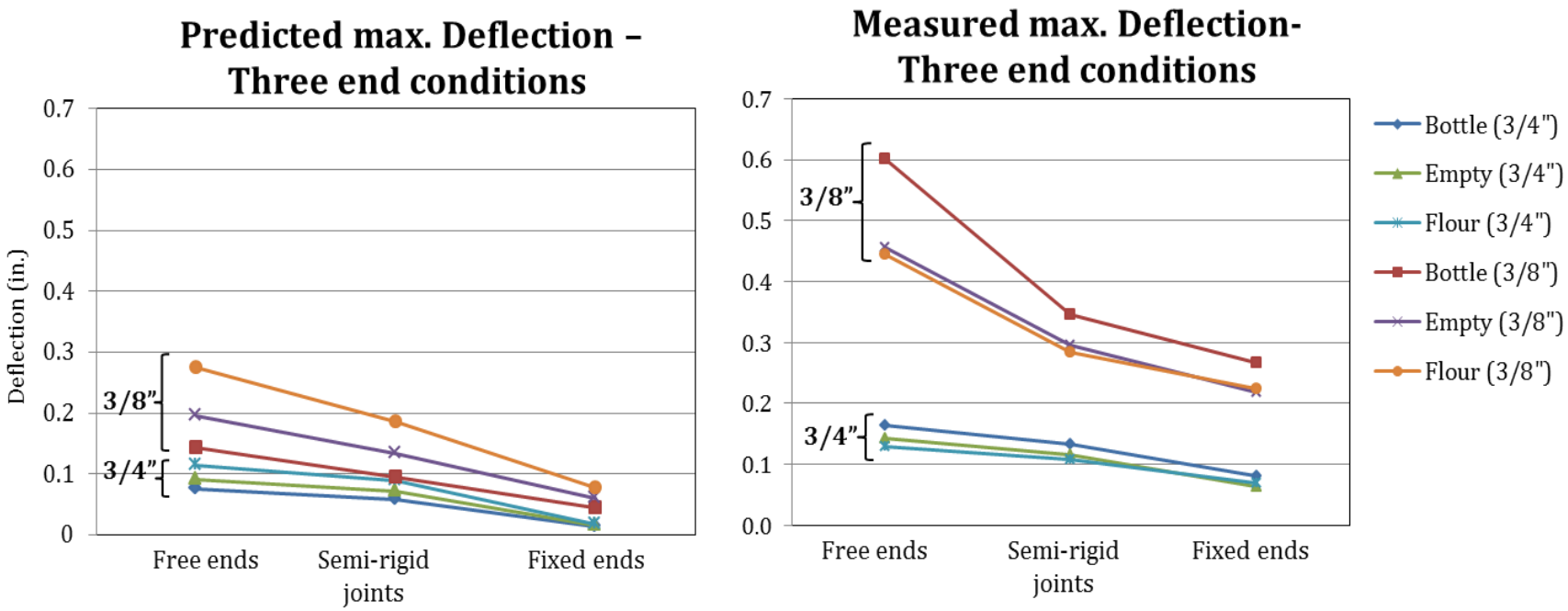

Figure 62. Comparison of predicted and measured maximum deflections for three end conditions

5.6 Validation of Compressive Stress Distribution Models

The predictive compressive stress distribution models developed in section 4.2 were validated by comparing to experimental results. This section includes the comparisons of the predictive models and experimentally measured compressive stress distributions. Each of graphs, shown in the following sections, was selected from three replications. The other compared results are shown in Appendix B.

To represent the uncertainty in a predictive model, 95% confidence bounds were used as part of a graphical presentation of results in a statistical analysis. The graphical measure was chosen for statistical analysis in this research because it is more beneficial to view the entire data set at once while the numerical measure is more focused on the value of one parameter. The confidence bounds are confidence intervals for a predicted response. The width of the interval indicates the degree of certainty of the fit. For example, a wider interval indicates greater certainty. To produce confidence bounds, a second-order polynomial curve fit to the measured data was generated using MATLAB. The MATLAB uses an interval of ±2Δ for the command function, which corresponds to a 95% confidence interval for the measured data. The interval of ±2Δ in the MATLAB represents the following equation:

$$2\Delta = \bar{x} \pm 1.96\frac{\sigma}{\sqrt{n}}$$

where

$\bar{x}$ = sample mean

1.96 = the probability that a normal distribution is between -1.96 and 1.96 to be 95%

σ = standard deviation

n = the number of sample

In the following sections, constructed 95% confidence bounds of the second-order polynomial curves of the measured data are presented with predictive compressive stress distribution models in order to visually evaluate if the models falls within the bounds.

5.6.1 Free Ends

Comparisons of predicted models and measured compressive stress distributions for free end condition with a box containing bottles, an empty box, and a box containing flour sacks are shown in Figures 63, 65, and 67, respectively. The results show that the predicted maximum compressive stresses at the ends (around inner stringers) were higher than measured maximum stresses in 3/8-inch deck for all three packaging cases. The difference between the measured and predicted results is due to the limited pressure range of the pressure sensor used. The maximum pressure the sensor was able to measure was 24.094 psi which is the saturation pressure for 30 psi sensor. Therefore, the Compressive Stress Intensity Factors (SIFs) of the compressive stress (pressure) distribution might be greater than SIFs of the measured results in free ends condition.

Figures 64, 66, and 68 show the validations of compressive stress distribution models using second-order polynomial curves with 95% confidence bounds. The validation results showed that all 3/4-inch deckboard models of three different packaging fell within the 95% bounds. However, compressive stress distributions predicted between 3/8-inch deckboards and three different packaging did not have good agreement with the confidence interval around inner stringers at the ends due to the capacity limitation in the pressure sensor as mentioned above. Validation of other replicate test is shown in Appendix B.

5.6.2 Semi-Rigid Joints

The maximum stresses measured over the free end 3/8-inch pallet deckboard supporting the bottles, empty box, and flour sacks were respectively 4%, 8%, and 19% higher than the 3/4-inch

deck. The measured maximum stresses distributed across the 3/4-inch and 3/8-inch deckboards were respectively 292% and 302% higher than the applied stress by the bottles. The measured maximum compressive stresses over the 3/4-inch and 3/8-inch deckboard supporting the empty box were respectively 170% and 193% greater than the applied load. The 3/4-inch and 3/8-inch deckboards loaded by the flour sacks in a box resulted in respectively 149% and 198% higher measured maximum stresses than the applied stress.

The developed predictive compressive stress distribution models of semi-rigid joints for three different packages were compared with measured tests results as shown in Figure 69, 71, and 73. 95% confidence bounds of second-order polynomial fit to the measured data was constructed in order to statistically validate the predictive models as presented in Figure 70, 72, and 74. The results of the validation by 95% confidence bounds show that the predictive compressive stress distribution models provided good fits to the measured data for all cases in the semi-rigid joint condition. The validation results of the other two replications for each deck thickness with each packaging are shown in Appendix B.

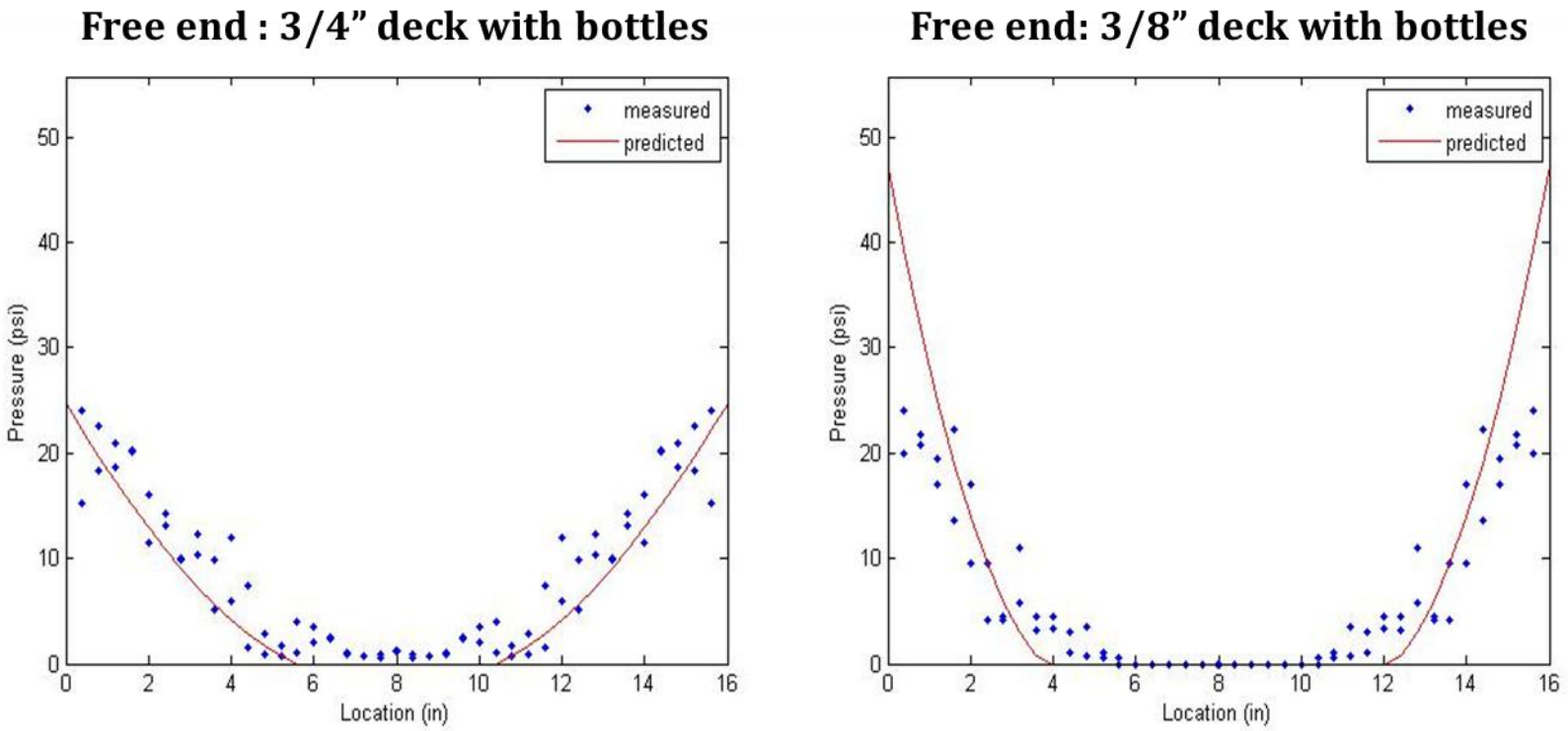

Figure 63. Comparisons of predicted models and measured compressive stress distributions for 3/4-inch and 3/8-inch free end decks with bottles in a box

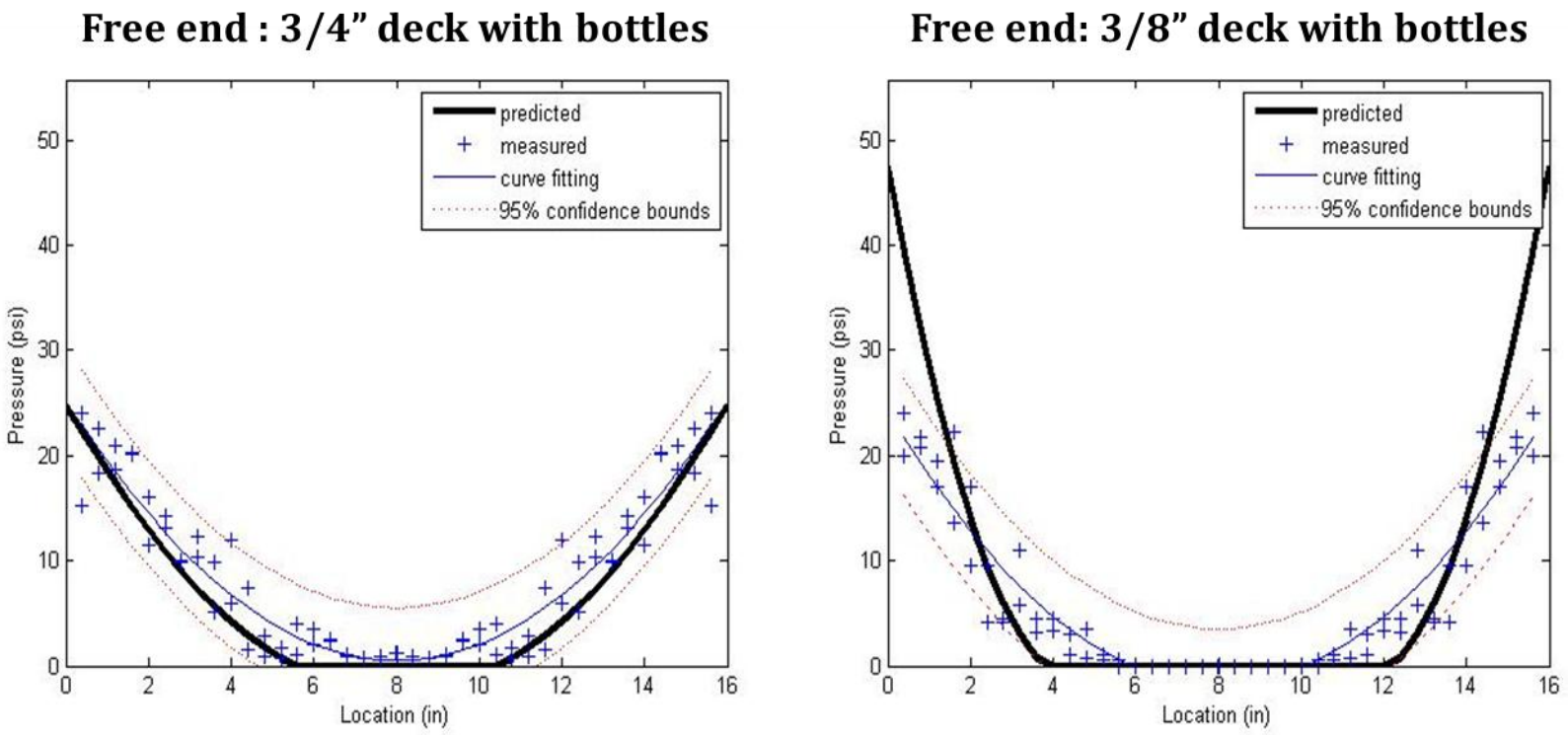

Figure 64. Validation of the predictive compressive stress distribution models for free end with a box containing bottles using second-order polynomial fit with 95% confidence bounds

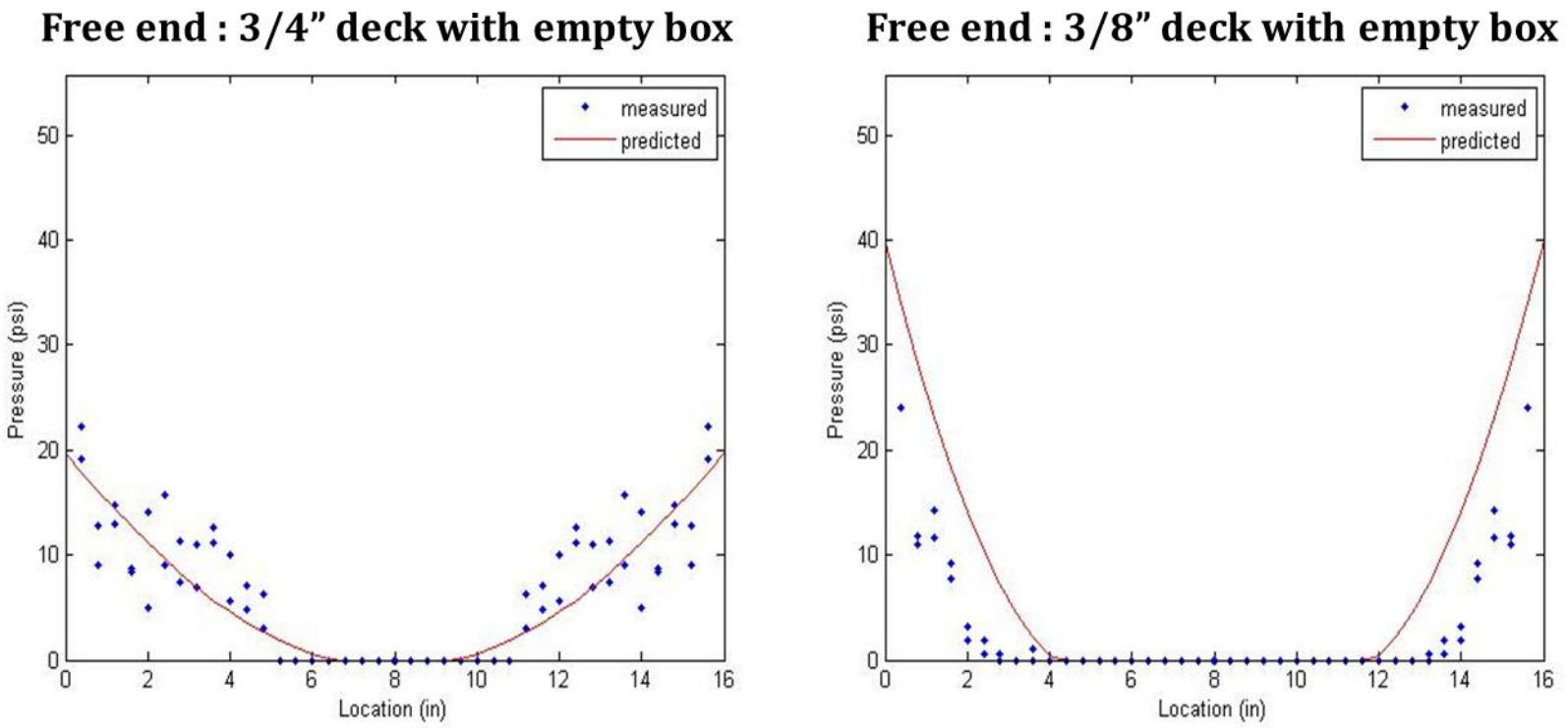

Figure 65. Comparisons of predicted models and measured compressive stress distributions for 3/4-inch and 3/8-inch of free end decks with an empty box

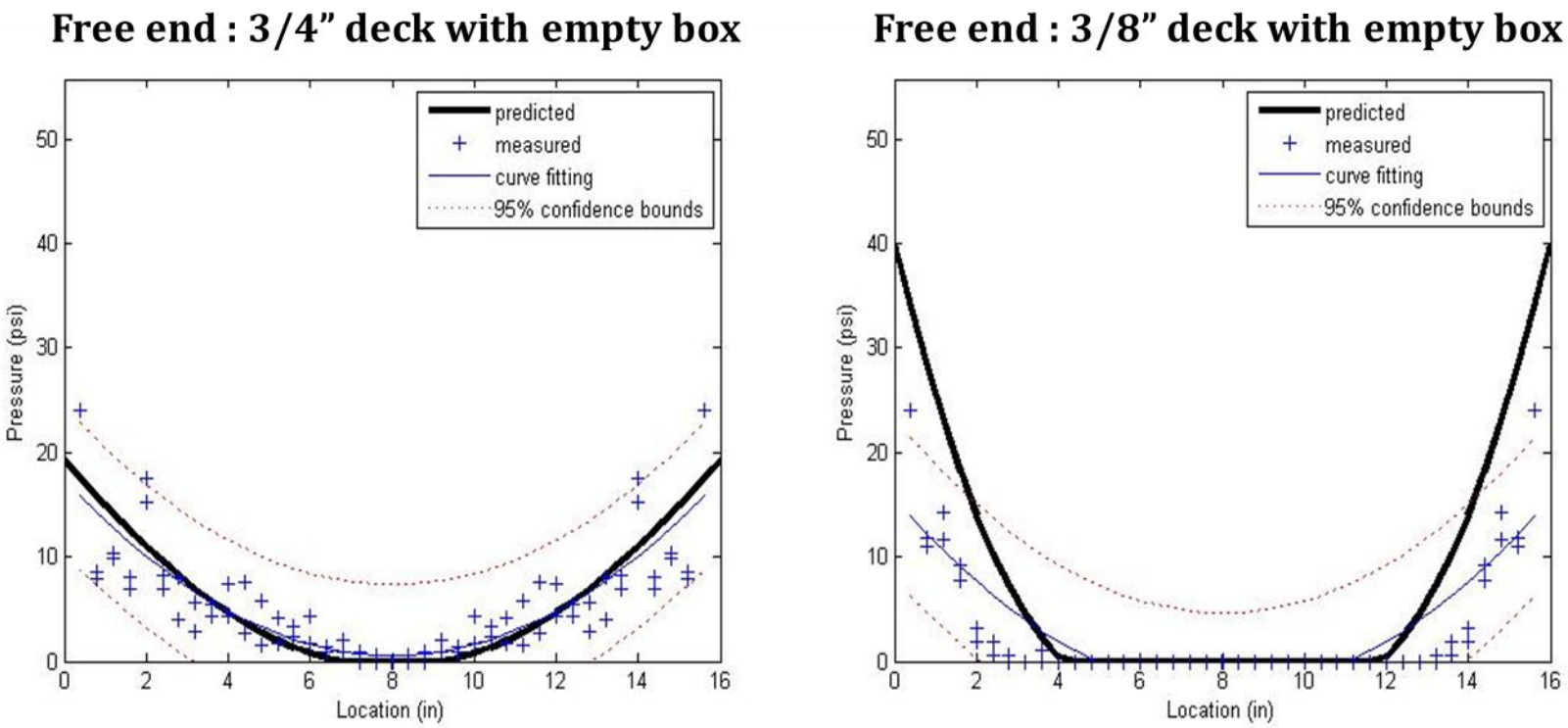

Figure 66. Validation of the predictive compressive stress distribution models for free end with an empty box using second-order polynomial fit with 95% confidence bounds

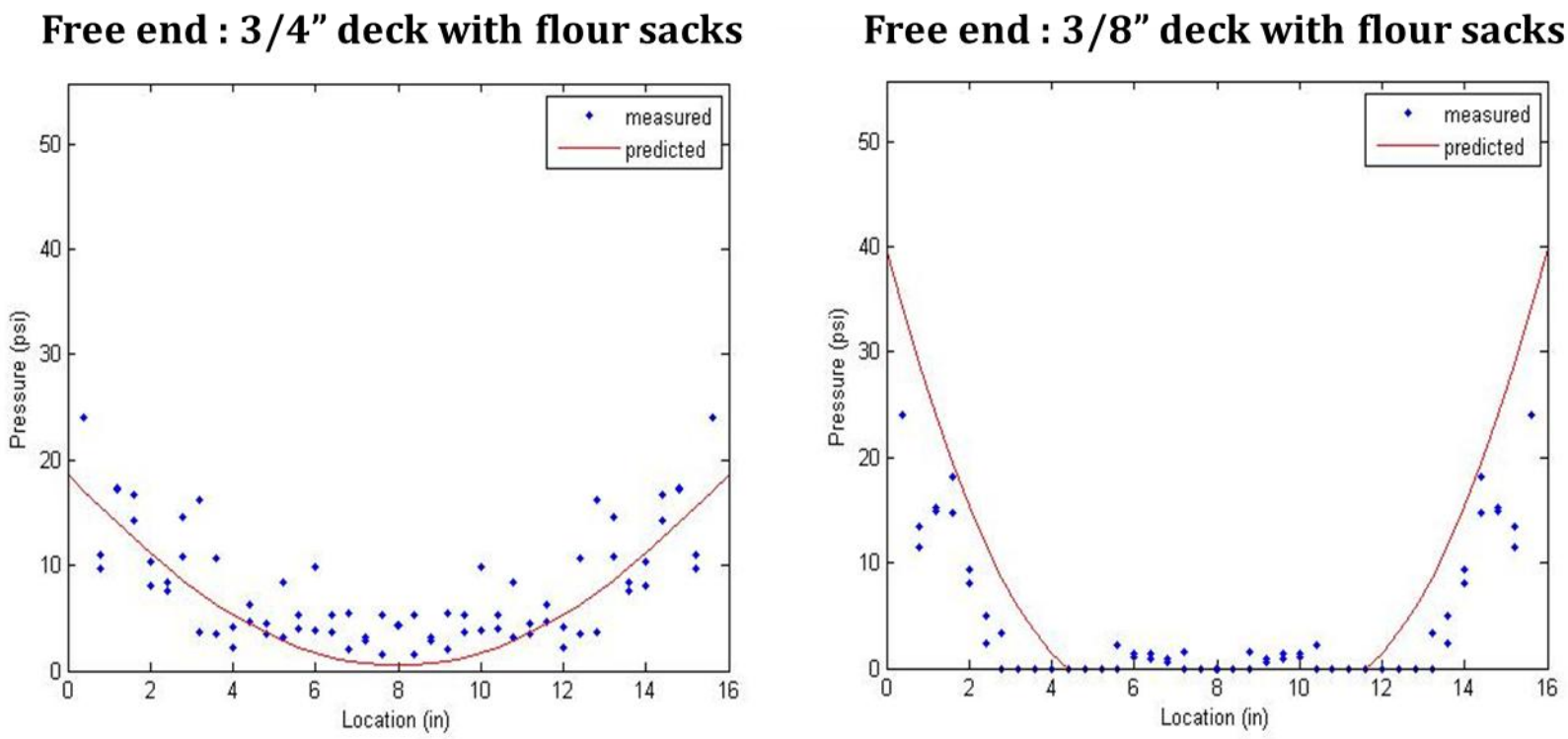

Figure 67. Comparisons of predicted models and measured compressive stress distributions for 3/4-inch and 3/8-inch free end decks with flour sacks in a box

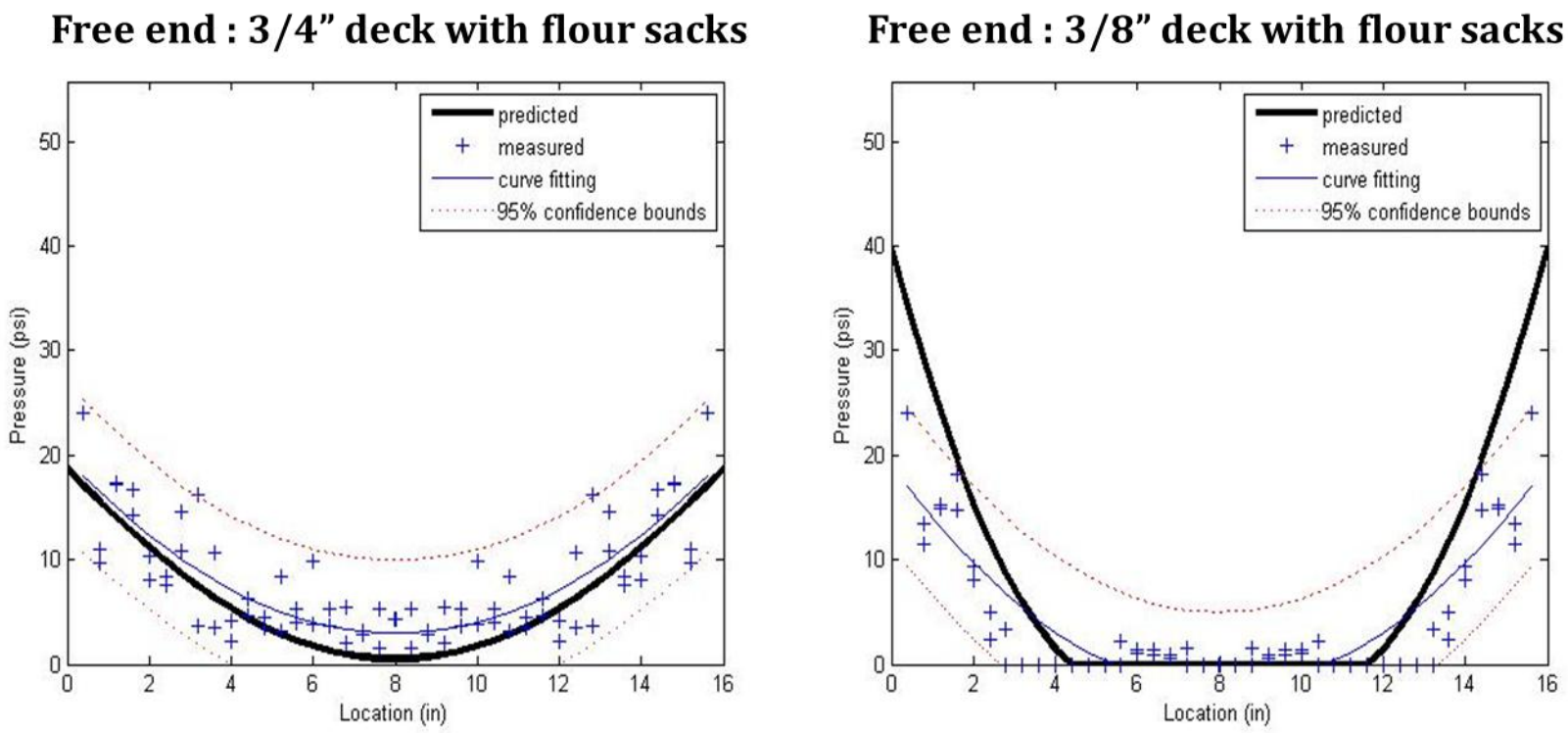

Figure 68. Validation of the predictive compressive stress distribution models for free end with a box containing flour sacks using second-order polynomial fit with 95% confidence bounds

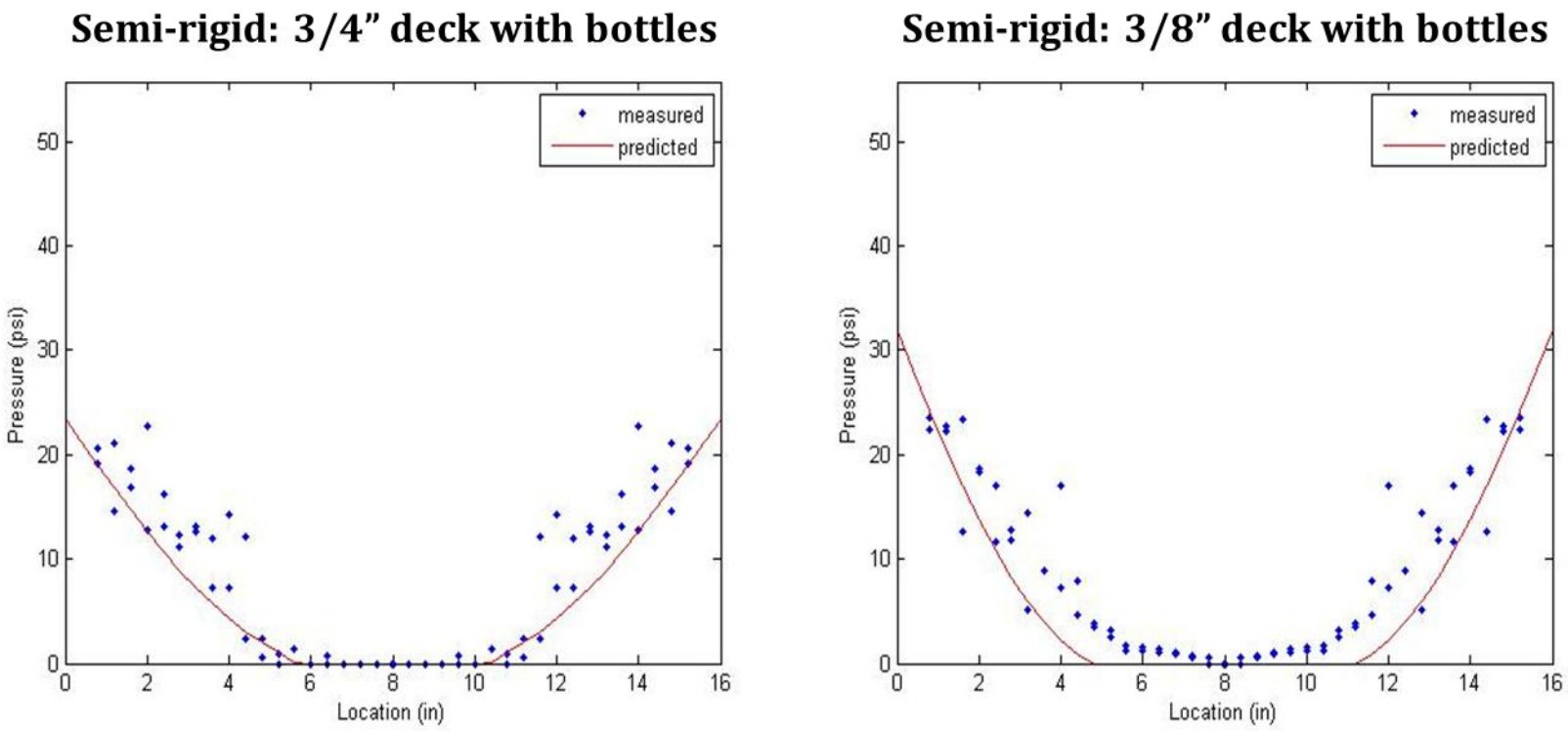

Figure 69. Comparisons of predicted models and measured compressive stress distributions for 3/4-inch and 3/8-inch of semi-rigid joint decks with bottles in a box

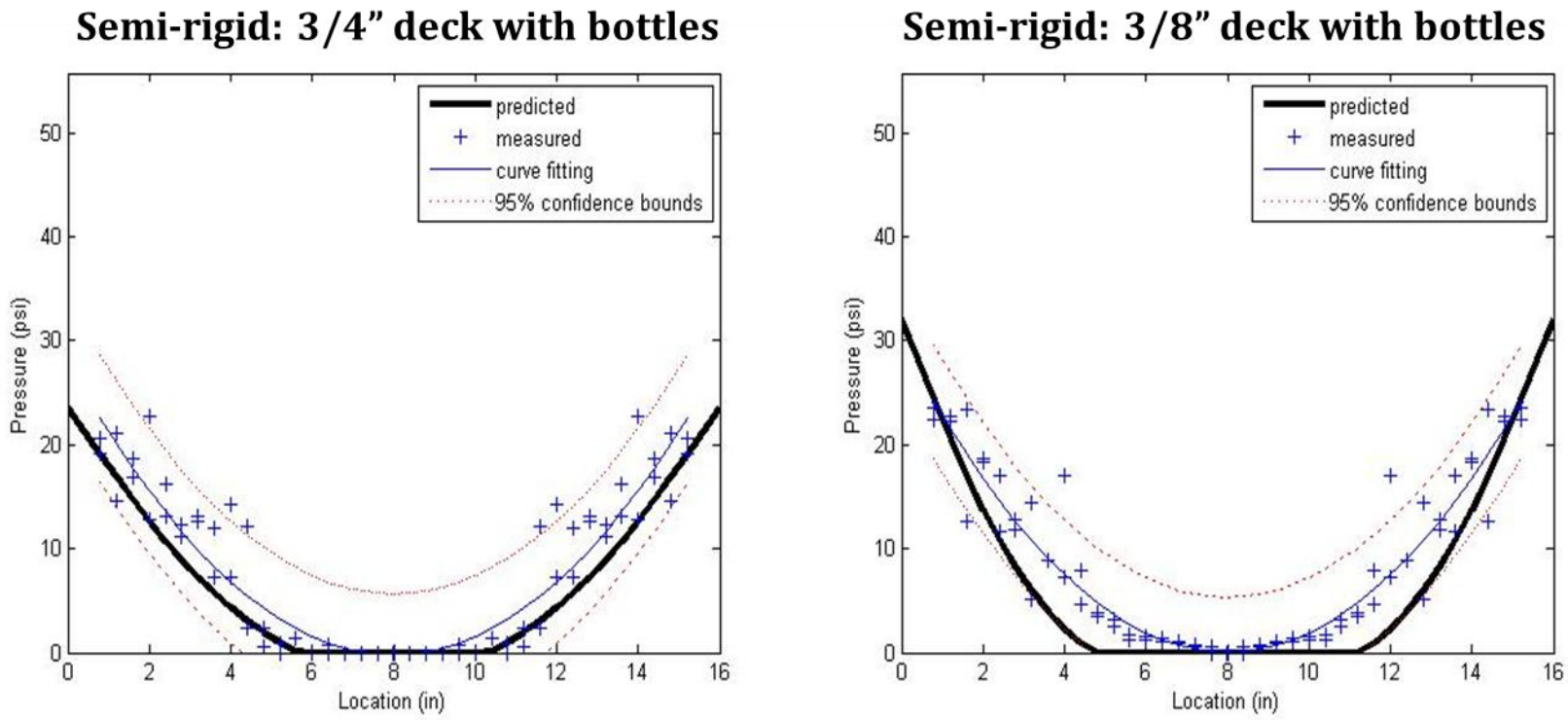

Figure 70. Validation of the predictive compressive stress distribution models for semi-rigid joint with a box containing bottles using second-order polynomial fit with 95% confidence bounds

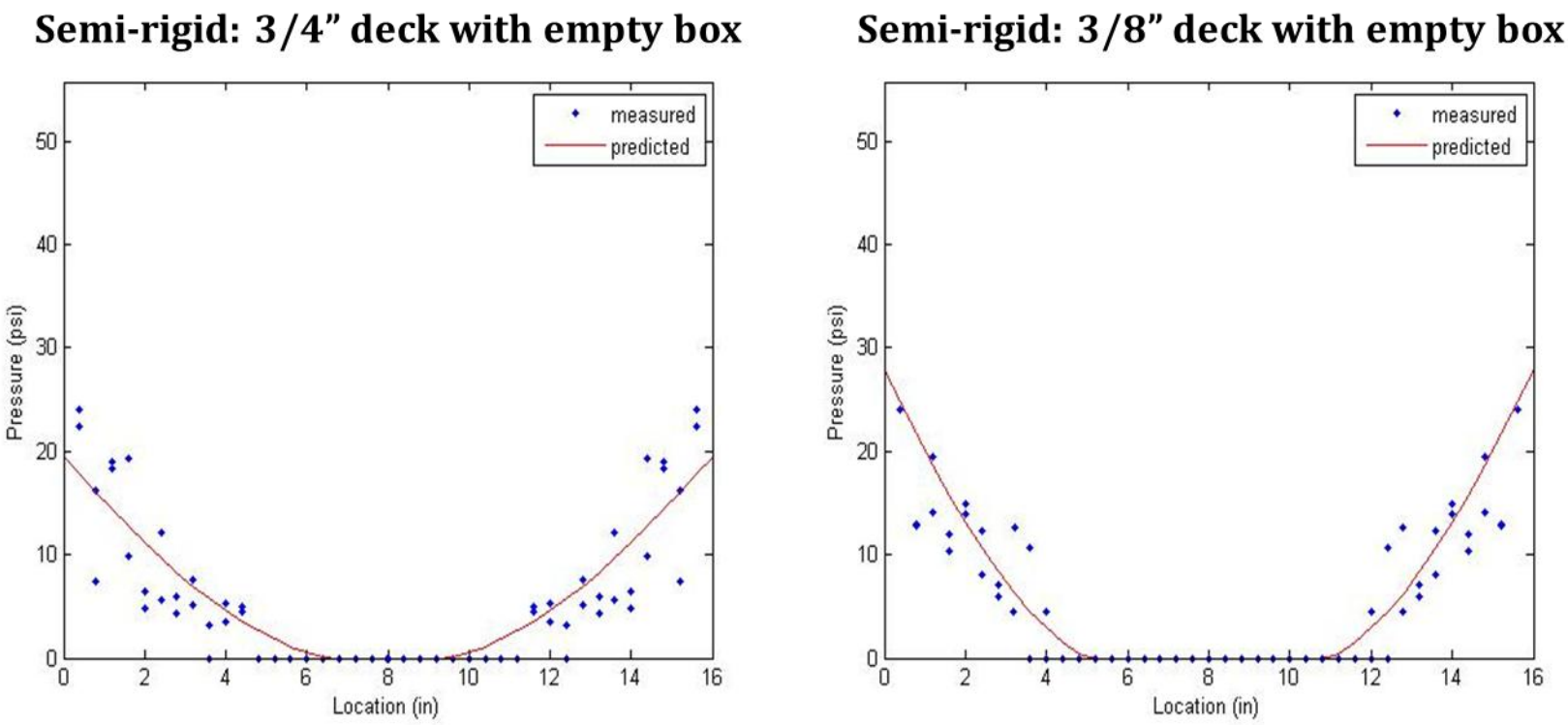

Figure 71. Comparisons of predicted models and measured compressive stress distributions for 3/4-inch and 3/8-inch semi-rigid joint decks with empty boxes

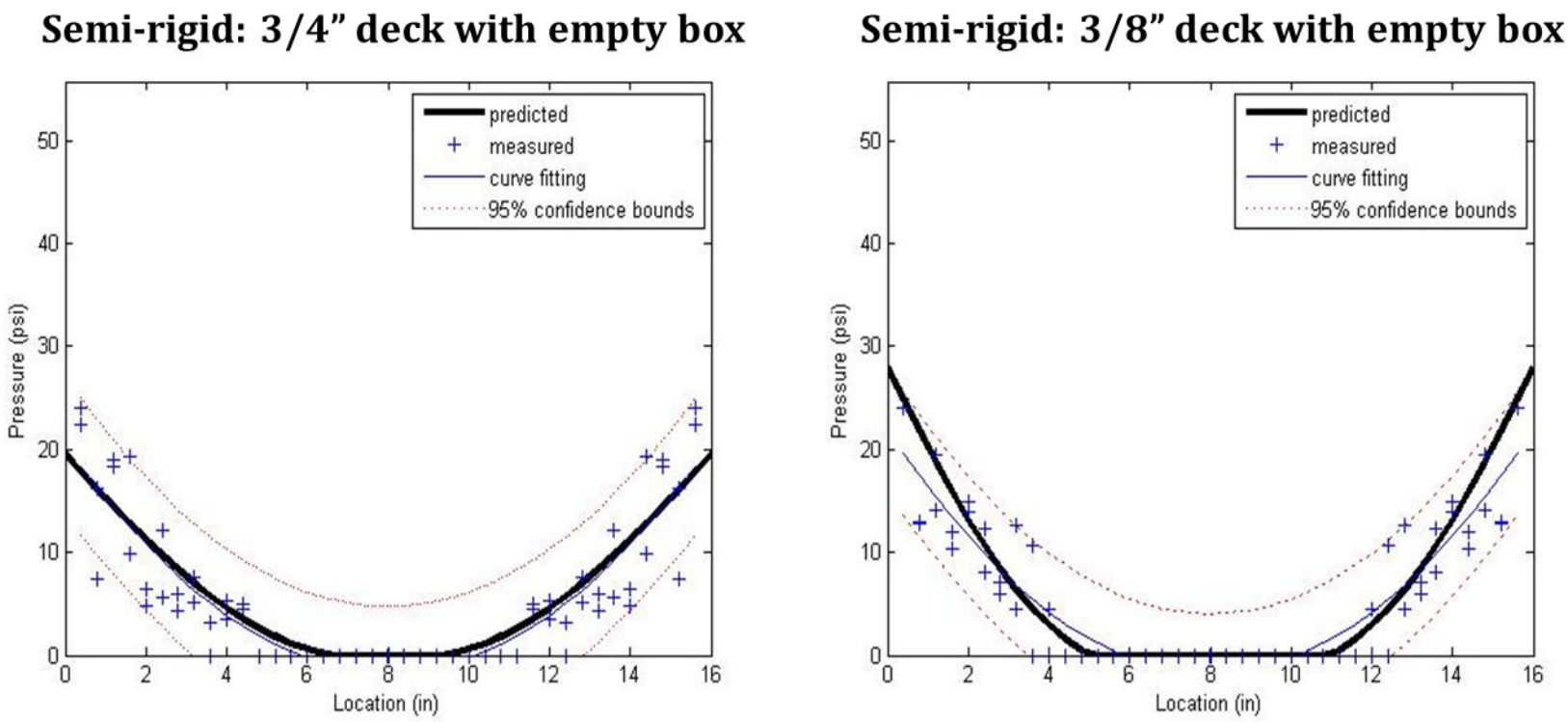

Figure 72. Validation of the predictive compressive stress distribution models for semi-rigid joint with an empty box using second-order polynomial fit with 95% confidence bounds

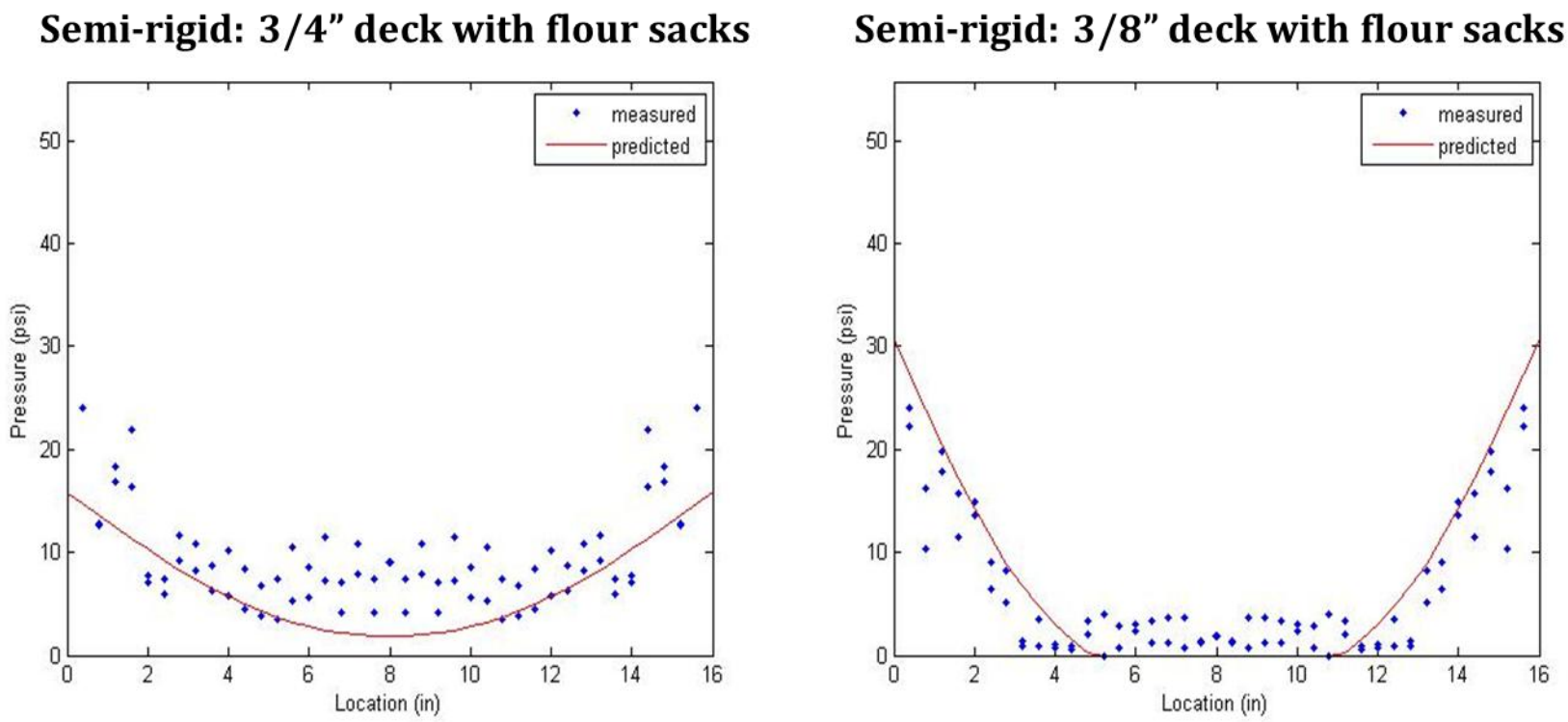

Figure 73. Comparisons of predicted models and measured compressive stress distributions for 3/4-inch and 3/8-inch semi-rigid joint decks with flour sacks in a box

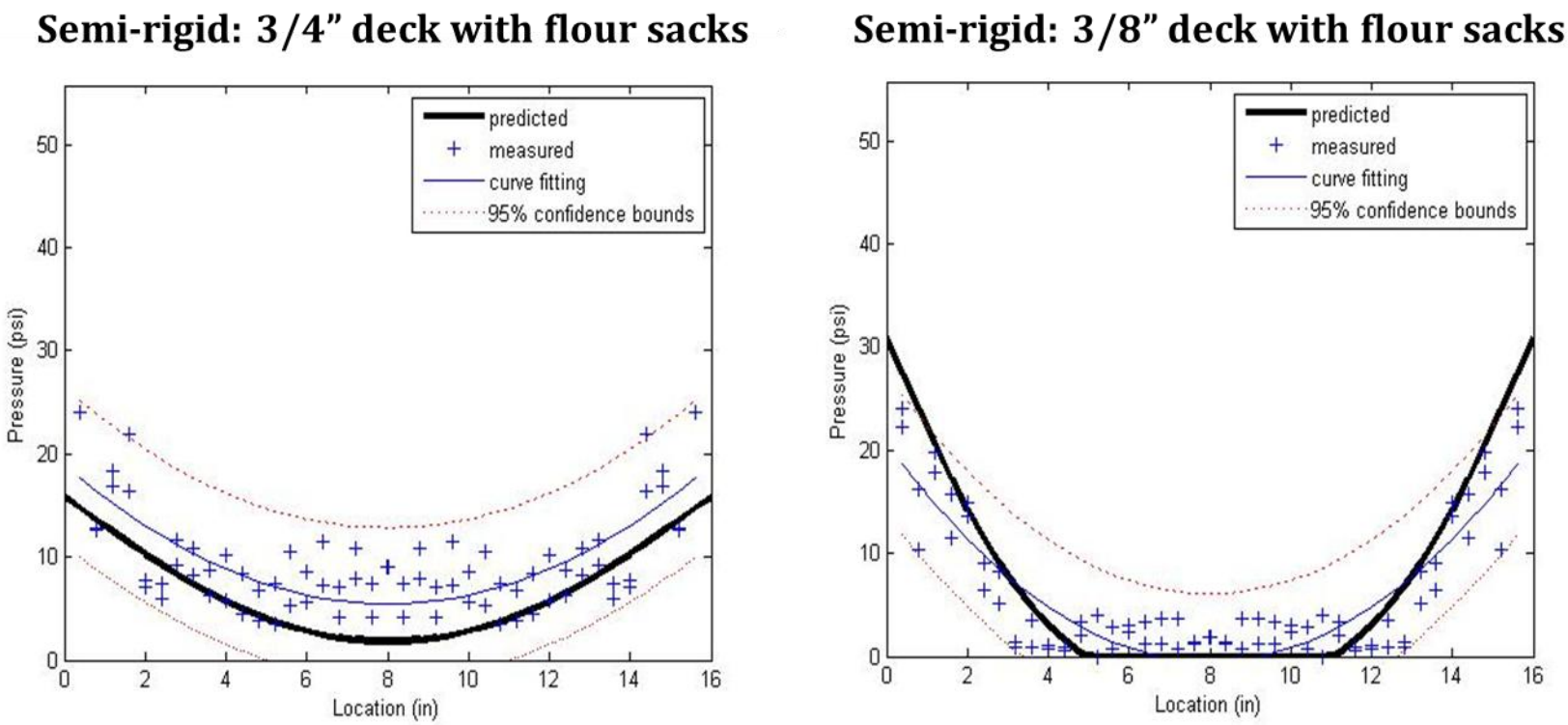

Figure 74. Validation of the predictive compressive stress distribution models for semi-rigid joint with a box containing flour sacks using second-order polynomial fit with 95% confidence bounds

5.6.3 Fixed End

Figure 75, 77, and 79 show that the predicted compressive stress distributions in the fixed end condition compared to the experimentally measured results. The results show that the measured data have greater stresses near the ends of the 3/4-inch deckboard. The difference between predicted and measured results might be due to limitation in construction of the fixed end pallet section test specimen. It was difficult to perfectly affix the deckboard to stringers using Epoxy adhesive for the construction of the fixed end pallet section test specimen. This non-fully fixed ends led greater stresses around the stringers due to the more deflection of the deckboard than fully fixed ends.

Validated predictive compressive stress distribution models for fixed ends using second-order polynomial fit with 95% confidence bounds are presented in Figure 76, 78, and 80. The polynomial fits to the measure compressive stress distributions across 3/4-inch deckboard showed wider confidence bounds indicating greater uncertainty than 3/8-inch deckboard. All of the predictive models of 3/8-inch deckboard fell within 95% bounds. The validations for other replications are included in Appendix B.

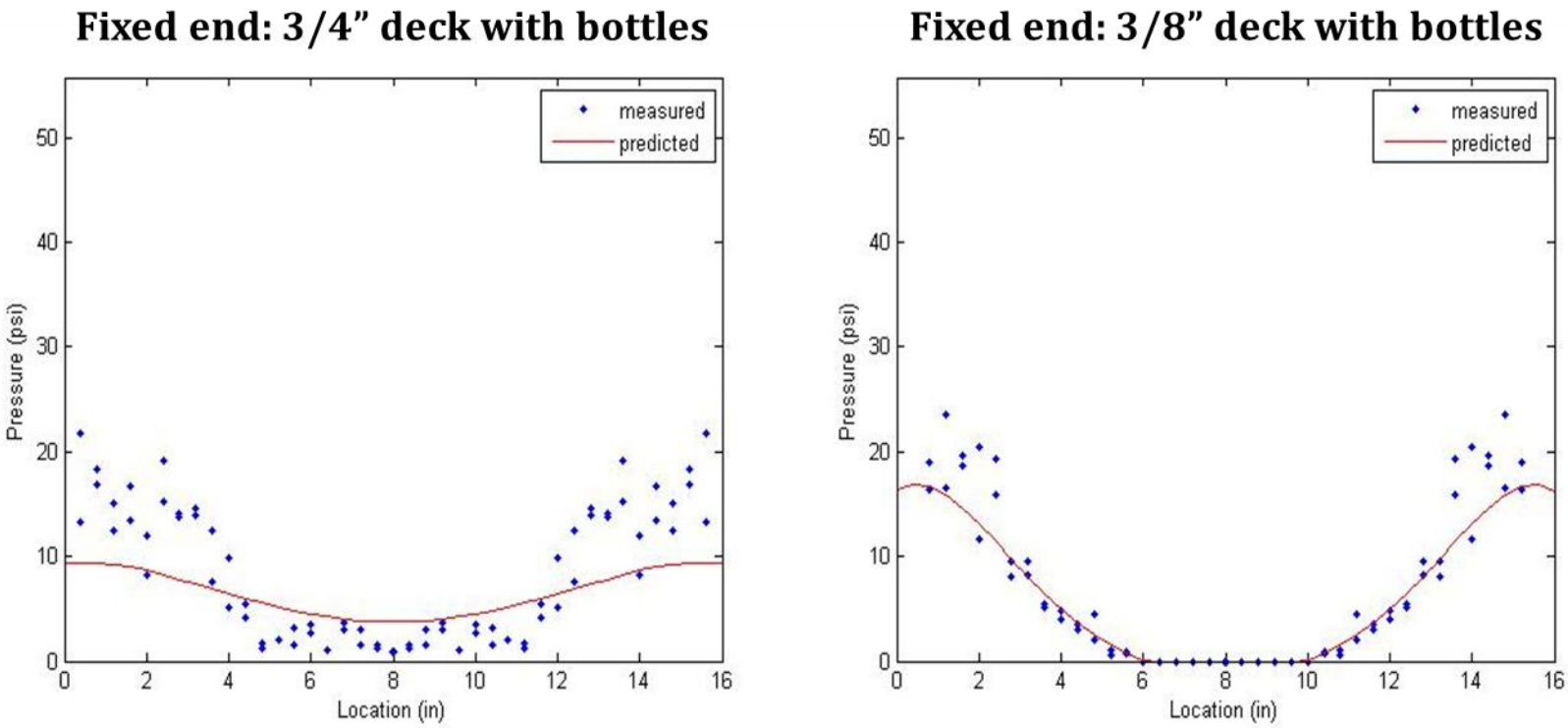

Figure 75. Comparisons of predicted models and measured compressive stress distributions for 3/4-inch and 3/8-inch fixed end decks with bottles in a box

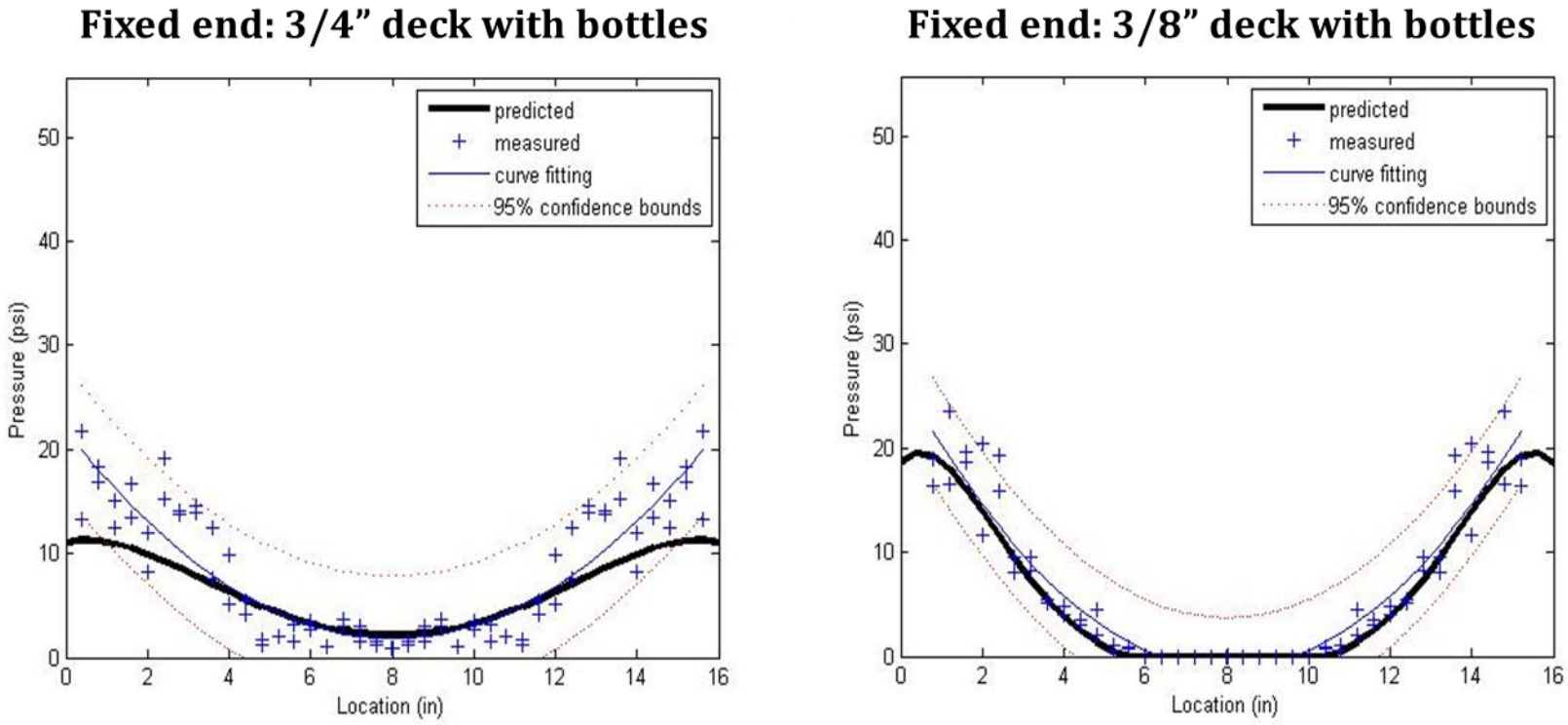

Figure 76. Validation of the predictive compressive stress distribution models for fixed end with a box containing bottles using second-order polynomial fit with 95% confidence bounds

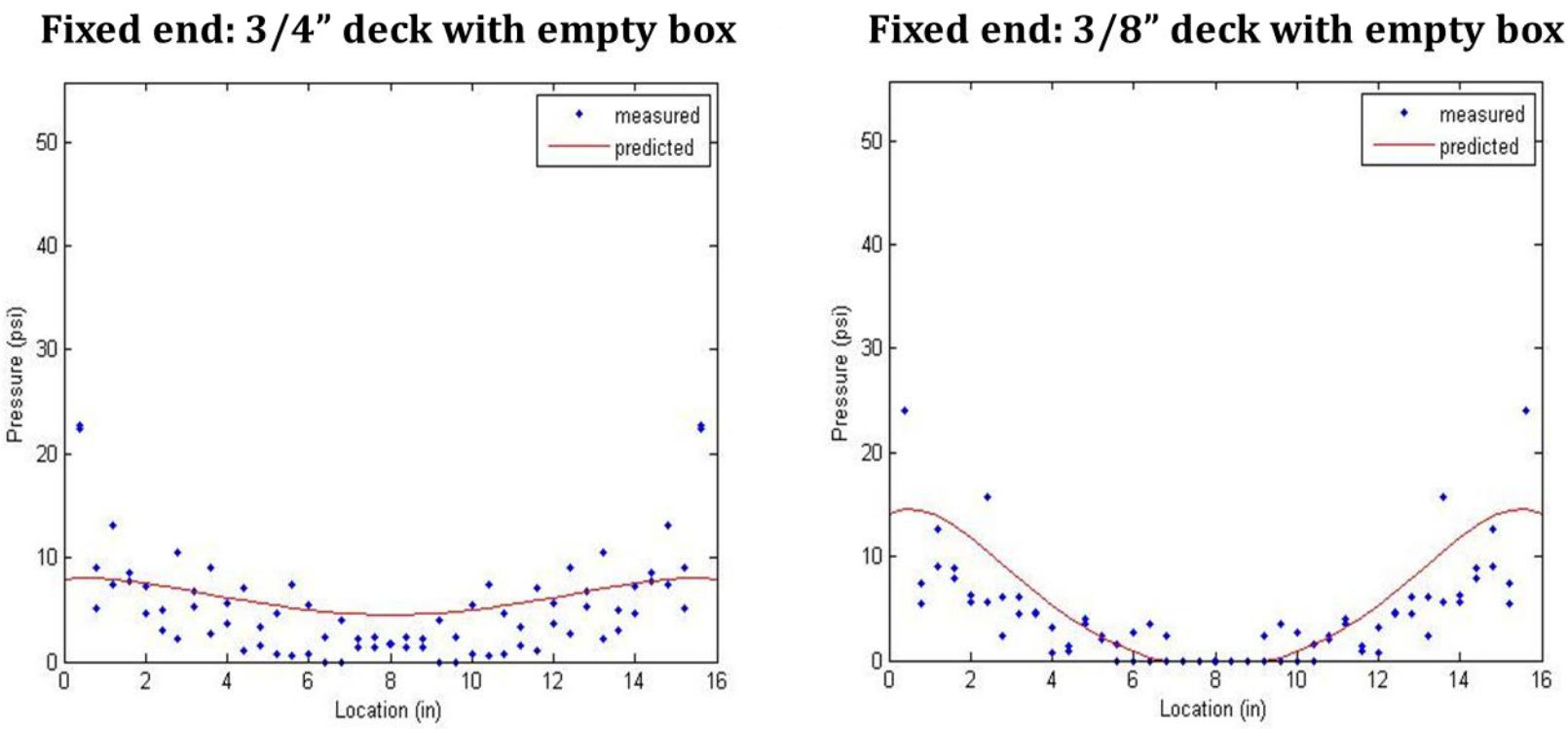

Figure 77. Comparisons of predicted models and measured compressive stress distributions for 3/4-inch and 3/8-inch fixed end decks with an empty box

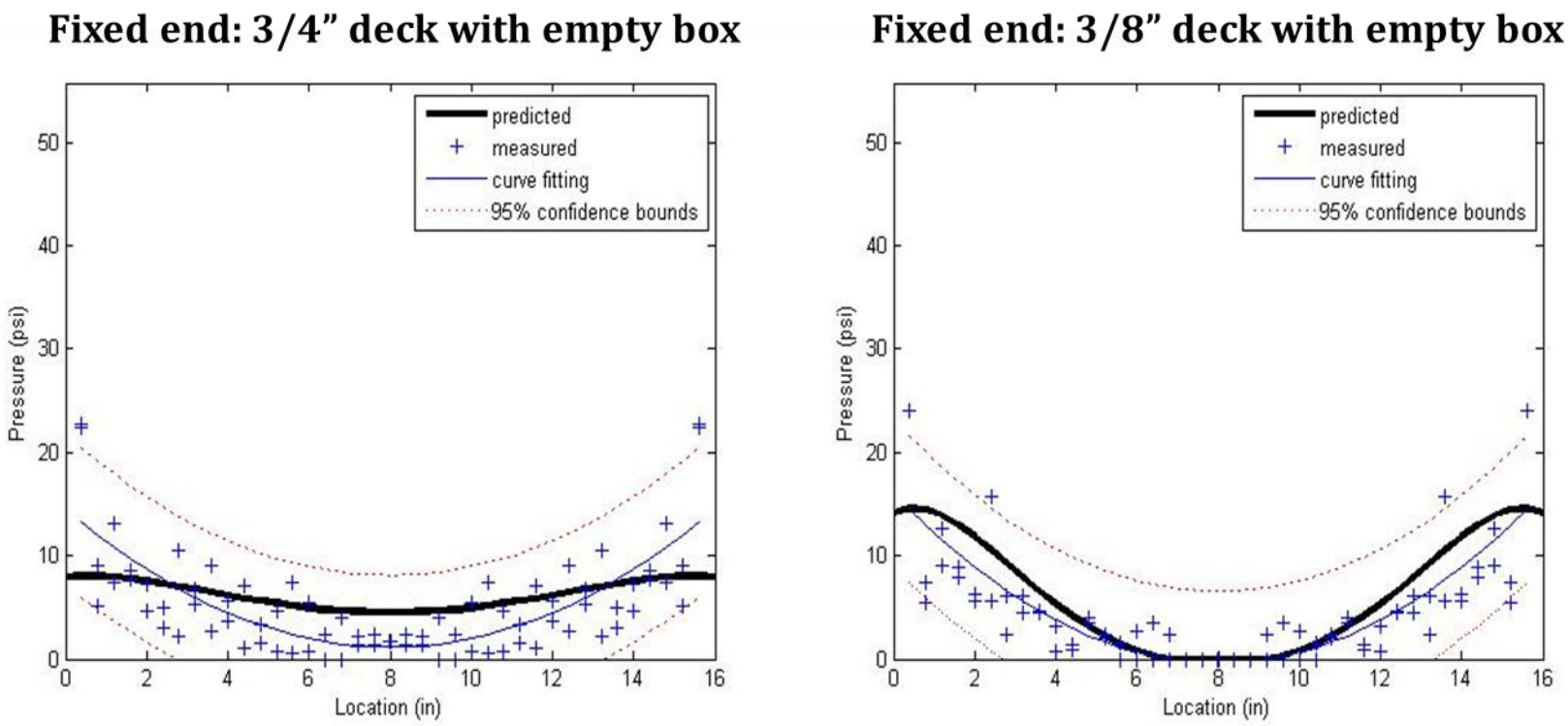

Figure 78. Validation of the predictive compressive stress distribution models for fixed end with an empty box using second-order polynomial fit with 95% confidence bounds

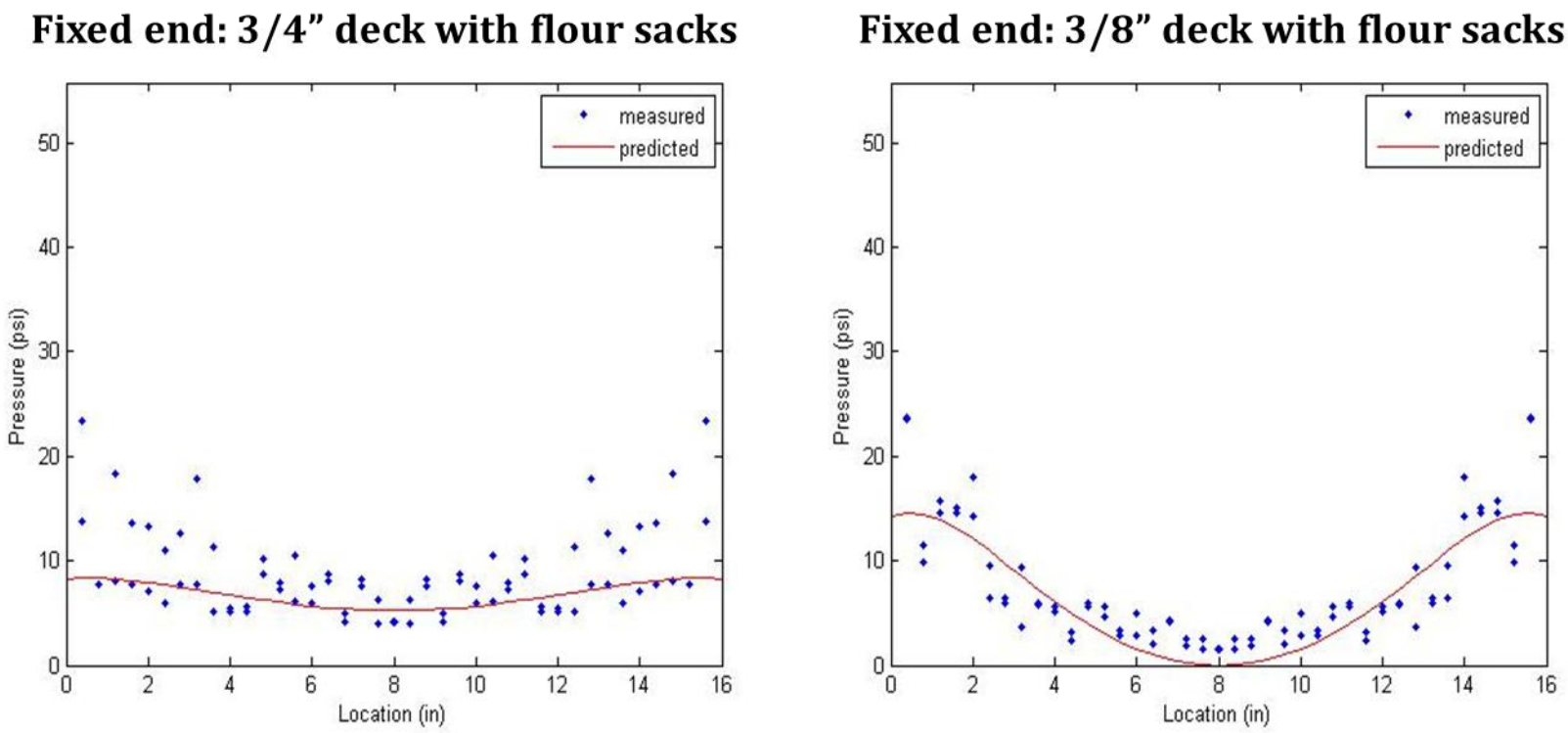

Figure 79. Comparisons of predicted models and measured compressive stress distributions for 3/4-inch and 3/8-inch fixed end decks with flour sacks in a box

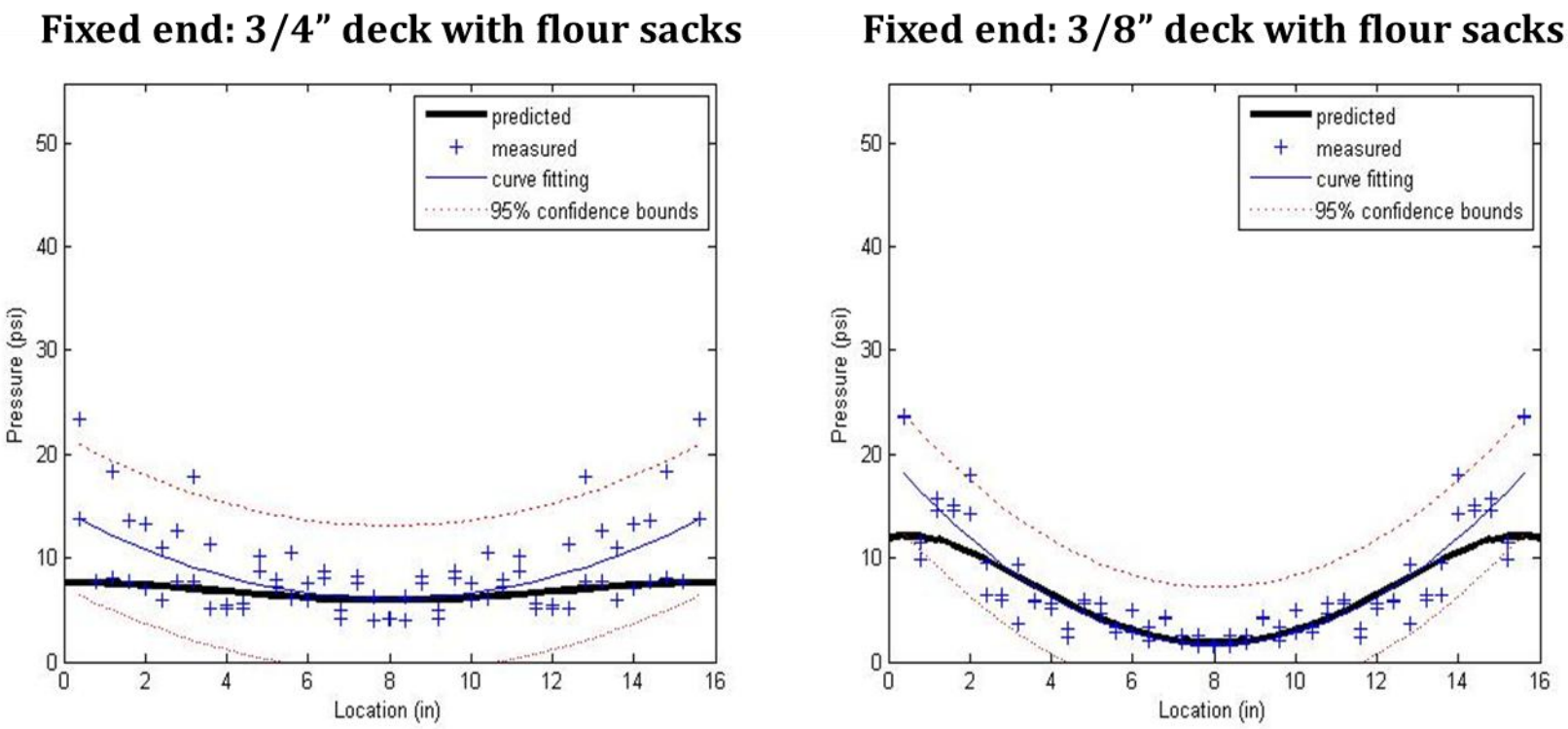

Figure 80. Validation of the predictive compressive stress distribution models for fixed end with a box containing flour sacks using second-order polynomial fit with 95% confidence bounds

5.7 Sensitivity Studies

Sensitivity studies are presented in this section. The sensitivity studies were performed for use in determining which material properties significantly influence the compressive stress distributions at the interface between the pallet deck and packaging. The sensitivity evaluation was approached using various material properties of interest, with all other properties remaining unchanged. Sensitivity of Compressive Stress Intensity Factors (SIF) and bearing areas of the predictive compressive stress distribution models to changing pallet deck stiffness (EI) and packaging stiffness (k) were evaluated. To determine the effect of a given property, the lowest property value was reduced by a factor of 0.5 and the greatest property value was increased by a factor of 2 for both pallet deck stiffness (EI) and packaging stiffness (k). The percentage of changes in SIFs and bearing areas was calculated for each case.

Tables 15 and 16 include the results of the sensitivity of SIFs and bearing areas to changing pallet deck properties. The summarized results of the sensitivity study are shown in Table 17 and 18. The results show effects of pallet deck stiffness and packaging stiffness on SIFs with percentage changes ranging from 2 to 26% (absolute value of change) for all three end conditions. The fixed end condition had the least effect of increased pallet deck stiffness on SIFs for all three package types. The sensitivity of the effective bearing areas to increasing the pallet deck stiffness was not significant in the fixed end condition. The effective bearing areas on free end and semi-rigid joint deckboard supporting were not affected by increasing the pallet deck stiffness. The semi-rigid joint condition showed the lowest percentage changes on both SIFs and bearing areas by the decreased pallet deck stiffness. The sensitivity of SIFs to increasing packaging stiffness was not significant in the 3/8-inch deckboard for semi-rigid joint condition. Reducing packaging stiffness did not have a significant effect on the effective bearing areas of either semi-rigid or fixed end condition. The sensitivity study concluded that changing both pallet deck stiffness and packaging stiffness more significantly influenced the SIFs than bearing areas.

Table 15. Sensitivity of the Compressive Stress Intensity Factors and Bearing areas of predictive models to changes in pallet stiffness

Pallet Stiffness: **2** x greatest actual EI							
		SIF (actual)	SIF (affected)	Change (%)	Bearing Area (actual) (%)	Bearing Area (affected) (%)	Change (%)
Free end	Bottles	3.731	2.815	-25	70	100	30
	Empty box	3.091	2.300	-26	85	100	15
	Flour sacks	2.677	1.997	-25	100	100	0
Semi-rigid	Bottles	3.490	2.674	-23	75	100	25
	Empty box	2.993	2.250	-25	90	100	10
	Flour sacks	2.502	1.901	-24	100	100	0
Fixed end	Bottles	1.393	1.242	-11	100	100	0
	Empty box	1.264	1.143	-10	100	100	0
	Flour sacks	1.193	1.100	-8	100	100	0

Table 16. Sensitivity of the Compressive Stress Intensity Factors and Bearing areas of predictive models to changes in pallet stiffness

Pallet Stiffness: 0.5 x lowest actual EI							
		SIF (actual)	SIF (adjusted)	Change (%)	Bearing Area (actual) (%)	Bearing Area (adjusted) (%)	Change (%)
Free end	Bottles	8.272	10.165	23	45	35	-10
	Empty box	7.222	8.805	22	50	40	-10
	Flour sacks	6.572	7.965	21	55	45	-10
Semi-rigid	Bottles	3.323	3.379	2	70	70	0
	Empty box	4.883	5.604	15	60	55	-5
	Flour sacks	3.468	3.723	7	75	70	-5
Fixed end	Bottles	2.397	3.017	26	80	70	-10
	Empty box	2.182	2.477	14	85	75	-10
	Flour sacks	2.023	2.330	15	100	80	-20

Table 17. Sensitivity of the Compressive Stress Intensity Factors and Bearing areas of predictive models to changes in packaging stiffness

2 x greatest packaging stiffness (Bottle)							
		SIF (actual)	SIF (adjusted)	Change (%)	Bearing Area (actual) (%)	Bearing Area (adjusted) (%)	Change (%)
Free end	3/4"	4.520	5.555	23	65	60	-5
	3/8"	8.272	10.163	23	45	35	-10
Semi-rigid	3/4"	3.293	4.055	23	80	70	-10
	3/8"	3.323	3.380	2	75	70	-5
Fixed end	3/4"	1.393	1.701	22	100	100	0
	3/8"	2.395	3.014	26	100	70	-30

Table 18. Sensitivity of the Compressive Stress Intensity Factors and Bearing areas of predictive models to changes in packaging stiffness

0.5 x lowest packaging stiffness (Flour sacks)							
		SIF (actual)	SIF (adjusted)	Change (%)	Bearing Area (actual) (%)	Bearing Area (adjusted) (%)	Change (%)
Free end	3/4"	3.362	2.514	-25	80	100	20
	3/8"	6.572	5.447	-17	55	57.5	2.5
Semi-rigid	3/4"	2.451	1.876	-23	100	100	0
	3/8"	3.468	3.098	-11	75	80	5
Fixed end	3/4"	1.193	1.108	-7	100	100	0
	3/8"	2.021	1.779	-12	100	100	0

Figure 81 is a graph showing sensitivity of predicted maximum compressive stress to changes in packaging stiffness (k) ranging from 100 lbs./in. to 7000 lbs./in., with pallet deck stiffness (EI) remaining unchanged. Material property values used to determine the EI ranges are tabulated in Table 19. Minimum EI was 9800 lbs.-in.^{2} and maximum EI was 570000 lbs.-in.^{2}. The predicted maximum stress level ranged from 7 psi to 51 psi depending on packaging and pallet deck stiffness. The average of predicted maximum compressive stresses for all package stiffness levels was two and a half times greater for minimum EI than maximum EI across the pallet deck stiffness range evaluated. Within the range of package stiffness from 100 to 500 (lbs./in), the predicted maximum stress sharply increases. The greater the pallet deck stiffness the more sensitive the maximum stress to packaging stiffness. Figure 82 shows sensitivity of predicted maximum compressive stress to changing the EI for two different package stiffness levels, 100 lbs./in. and 7000 lbs./in.. The average of predicted maximum compressive stresses for all pallet deck stiffness levels was three times greater for the maximum packaging stiffness than the minimum packaging stiffness across the package stiffness range evaluated. The predicted maximum compressive stresses were dramatically decreased in the pallet deck EI range from 9800 to 70000 (lbs.-in.$^{2)}$. The less stiff the packaging the more sensitive the maximum stress to pallet deck stiffness.

Table 19. Material property values for EI determination

	b (in.)	d (in.)	I (in.^{4})	E (psi)	EI (lbs.-in.^{2})
Minimum	3.5	0.375	0.015	653000	9800
Maximum	5.5	0.875	0.307	1850000	570000

Note: I (moment of inertia) (in.^{4}) = $bd^3/12$

where b= deckboard width and d=deckboard depth or thickness

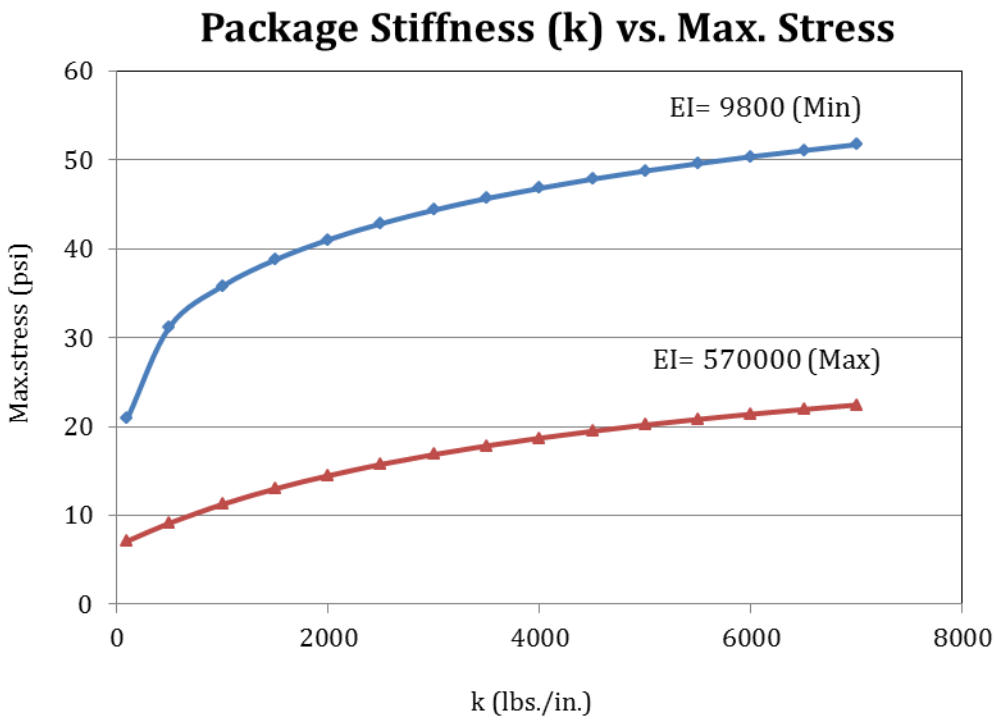

Figure 81. Sensitivity of predicted maximum compressive stress to changes in packaging stiffness

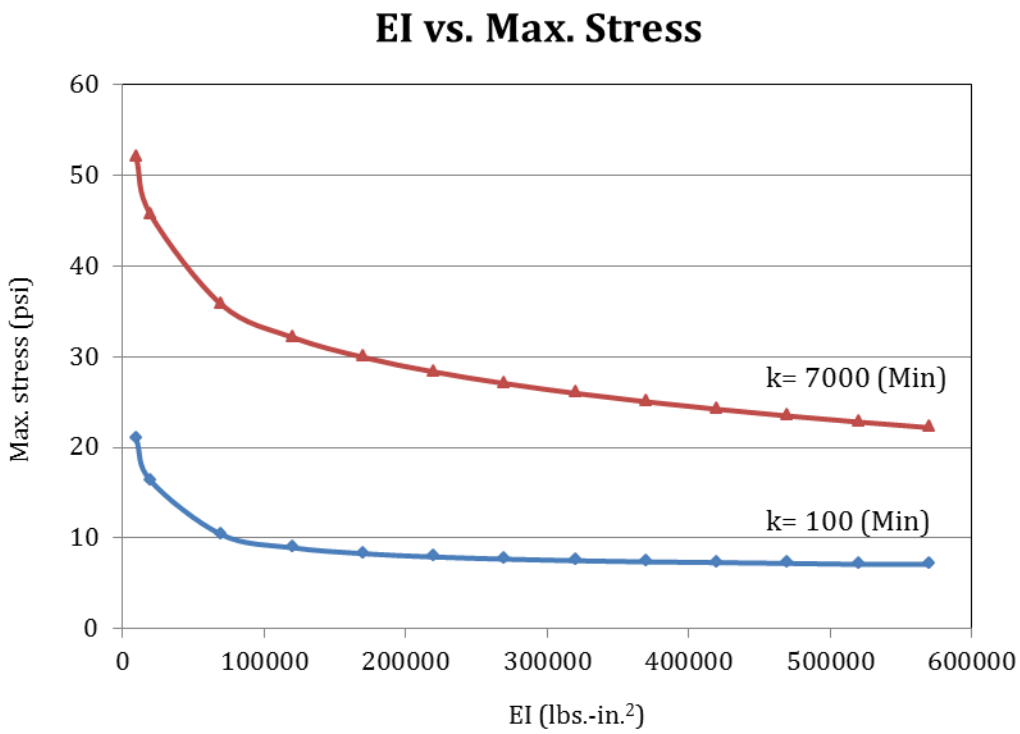

Figure 82. Sensitivity of predicted maximum compressive stress to changes in pallet deck stiffness

CHAPTER 6 Summary, Conclusions and Recommendations for Future Study

6.0 Summary

A theoretical procedure was developed for predicting compressive stress distributions at the interface between a pallet deckboard and packaging. The procedure is based on the principle of a beam on an elastic foundation. The effects of different joint fixity, pallet deck stiffness, and packaging stiffness on the compressive stress distributions were investigated experimentally. The theoretical predictions were compared to the experimental results of compressive stress distributions measured using pressure measurement. The procedure allows pallet and packaging designers to improve the efficiency of components of a unit load.

This research used the principles of the beam on an elastic foundation to predict pallet deck deflections and the resulting compression stresses at a pallet deck/packaging interface. To determine the effect of joint fixity, three different end conditions, 1) free end, 2) semi-rigid joint (nailed joint), and 3) fixed end, were modeled and tested. Two different pallet deck stiffness levels represented by, 3/4-inch and 3/8-inch thickness, were used to simulate the range of pallet deckboard stiffness. The effect of the packaging stiffness (k) levels on the compressive stress distributions was evaluated using three different packages, 1) a box containing plastic bottles (k = 1345 lbs./in.), 2) an empty box (k = 854 lbs./in.), and 3) a box containing flour sacks (k = 615 lbs./in.). Values of three design variables were determined experimentally for use in modeling pallet deck deflections and compressive stress distributions: 1) Modulus of Elasticity (MOE) of pallet deckboard, 2) joint rotation modulus for nailed joints (semi-rigid joint), and 3) vertical packaging compression stiffness.

Compressive Stress Intensity Factors (SIF) based on the ratio of average applied stress and maximum predicted stress were calculated. The effective bearing area at the interface between the top pallet deck and the bottom surface of packaging was calculated using the predicted load-

bridging area from the stress distribution models. Studies were performed to determine the sensitivity of the predictive models' SIFs and bearing areas to changes in pallet deck stiffness and packaging stiffness.

The predictive models of compressive stress distributions were validated by comparison to experimental data. Pressure distribution at the interface between a pallet deck and packaging was quantified using the pressure measurement system including pressure sensors, data acquisition hardware, and analysis software.

6.1 Conclusions

The specific conclusions are summarized as follows:

1. The principle of a beam on an elastic foundation can be used to model stresses at the interface of a package and a pallet and was found to be sensitive to joint fixity, pallet stiffness, and packaging stiffness. The developed prediction models were validated by comparison to experimental results. For statistical analysis, 95% confidence bounds of curves fit to the measured data were produced to determine the degree of uncertainty in predictive models. All predictions fell within the 95% confidence bounds of the experimental data except the 3/8-inch deck with free ends and 3/4-inch deck with fixed ends. The difference between predicted and measured stresses was due to a limitation in pressure sensor range and test specimen construction for the free end model and fixed end model, respectively.

2. The beam on an elastic foundation model of pallet deck deflections indicated that the deck deflection of a 3/4-inch pallet deck was more sensitive to joint fixity than a 3/8-inch deck for all three packaging stiffness levels. Greater joint stiffness resulted in lower predicted pallet deck deflection.

3. Compressive stress distributions are non-uniformly distributed across the interface between pallet deckboards and packaging. Maximum compressive stresses observed near the ends of the deckboard over the stringer were greater than 24 psi while other regions had stresses less than 0.3 psi.

4. Stiffer pallet produces lower maximum predicted and measured compressive stresses on the packaging than lower stiffness pallet.

5. Compressive stresses at the pallet/packaging interface are inversely correlated with deck and joint stiffness. Stiffer pallet deckboard and higher joint stiffness results in lower compressive stresses.

6. A measure of the stress concentration is the Compressive Stress Intensity Factor (SIF), defined as the ratio of the predicted maximum compressive stress to the average applied stress. Less stiff pallets with stiffer packaging resulted in greater SIF for all end condition models. The free end model had greatest SIF among three different end condition models. Stiffer joint, stiffer pallet deck and more flexible packaging resulted in lower compressive stress intensity.

7. Higher joint stiffness and higher pallet deck stiffness results in higher effective bearing area. In contrast, greater packaging stiffness produces lower effective bearing area. For all packages and pallet stiffness tested, the effective bearing area was less than the total bearing area. The effective bearing area was more influenced by pallet deck stiffness than by the packaging stiffness.

6.2 Research Limitations

Limitations of the research include

1. One-dimensional models were developed. More accurate results would be obtained using a two-dimensional model.
2. The length of packaging was shorter than the span between two stringers for models and test specimens.
3. There was a limitation in pressure sensor ranges (0-5 psi and 0-30 psi). Pressure greater than 30 psi should be used.
4. Only 3/4-inch and 3/8-inch thick deckboards were used to construct two-stringer pallet sections at a single span. Other pallet designs should be evaluated.
5. Three packaging stiffness levels with a corrugated box containing plastic bottles and flour sacks and an empty corrugated box were considered to test and develop predictive models. Other packaging should be tested.
6. Only three end conditions (free end, semi-rigid joint and fixed end) were considered.
7. Epoxy glue was used to affix the deckboard to stringers in simulated fixed end condition. There was a difficulty in construction of fully fixed end pallet section test specimen.
8. Floor stack support condition was simulated. Other support conditions should be simulated in future study.

6.3 Recommendations for Future Study

Recommendations for future study include

1. Compressive stress distribution models for three-stringer pallet section should be developed.

2. A wide range of pressure sensor should be used to increase accuracy in measuring stress levels.
3. Full length of packaging to cover the entire pallet deck should be modeled and tested.
4. Three-stringer pallet section should be modeled and tested.
5. Deflection measurement should be improved in future study.
6. Development of a two-dimensional model is recommended.
7. A wide range of packaging stiffness levels should be used to develop models.

REFERENCE

Bodig, J., & Jayne, B. A. (1993). *Mechanics of Wood and Wood Composites (Rev. ed.)*.Malabar, FA: Krieger publishing company. 712 pp.

Chen, W. F. (1997). *Handbook of structural engineering*. Boca Raton, FL: CRC Press. 1768 pp.

Clancy, D. A. (1988). A new package to reduce damage claims. *Transportation & Distribution*, 29 (12), 20.

Clarke, J. W. (2002). Balance your pallet design. *Pallet Enterprise*, 91. Retrieved May 10, 2009, from http://www.palletenterprise.com/articledatabase/articles/page91.pdf

Colclough, R.G. (1987). *The Development and Verification of Analysis Models for Block Type Wooden Pallets*. M.S. Thesis, Virginia Polytechnic Institute and State University, Blacksburg, VA.

Collie, S.T. (1984). *Laboratory Verification of Pallet Design Procedures*. M.S. Thesis, Virginia Polytechnic Institute and State University, Blacksburg, VA.

Fagan, G.B. (1982). *Load-Support Conditions and Computerized Test Apparatus for Wooden Pallets*. M.S. Thesis, Virginia Polytechnic Institute and State University, Blacksburg, VA.

FPInnovation™ (2009). *Pallet Trends 09*. Retrieved October, 2010, from http://www.solutionsforwood.ca/_docs/reports/PalletTrends09.pdf

Gere, J. M. (2004). *Mechanics of materials*. Belmont, CA: Brooks/Cole-Thomson Learning. 940 pp.

Goehring, C.B., & Wallin, W.B. (1981). *A Survey of Loads, Loading Conditions, and Handling Environment Condiitons for Wooden Pallets*. Northeastern Forest Experiment Station, Forestry Sciences Laboratory, Princeton, WV.

Hamner, P., & White, M. S. (2005). How to design around a unit load. *Pallet Enterprise* Retrieved May 10, 2009, from http://www.palletenterprise.com/articledatabase/view.asp?articleID= 1519

Hetényi, M. (1946). *Beams on elastic foundation: Theory with applications in the fields of civil and mechanical engineering*. Ann Arbor: The University of Michigan Press. 255 pp.

Kawanishi, K. (1989). Estimation of the compressive strength of fiberboard boxes and its application to box design using a personal computer. *Packaging Technology and Science*, 2(1), 29-39.

Kellicutt, K. Q., & Landt, E. F. (1951). Basic design data for use of fiberboard in shipping containers. *Fibre Containers*, 36(12), 62, 67-68, 70, 75-76, 80.

Kyokong, B. (1979). *The Development of a Model of the Mechanical Behavior of Wooden Pallets*. Ph. D. Dissertation, Virginia Polytechnic Institute and State University, Blacksburg, VA.

Lauer, I. A. III. (1991). *Studies of wood pallet response to forced vibration*. M. S. thesis, Virginia Polytechnic Institute and State University, Blacksburg, VA.

Liu, D. H. F., & Liptak, B. G. (1999). *Environmental Engineers' Handbook*. Boca Raton, FL: CRC Press LLC. 1431 pp.

Loferski, J.R. (1985). *A Reliability Based Design Procedure for Wood Pallets*. Ph. D. Dissertation, Virginia Polytechnic Institute and State University, Blacksburg, VA.

Maltenfort, G. G. (1956). Compression strength of corrugated containers Parts I-IV. *Fibre Containers*, 43(3, 4, 6, 7).

McKee, R. C., Gander, J. W., & Wachuta, J. R. (1961). Edgewise compression strength of corrugated board. *Paperboard Packaging*, 46(11), 70-76.

Samarasinghe, S. (1987). *Predicting Rotation Modulus for Block Pallet Joints*, M.S. Thesis, Virginia Polytechnic Institute and State University, Blacksburg, VA.

Tanchoco, J.M., & Agee, M.H. (1980), *Unit Load Interfaces*. The Department of Industrial Engineering, Virginia Polytechnic Institute and State University, Blacksburg, VA.

Tekscan, Inc (2004). *I-SCAN® Pressure Measurement System User Manual Version 5.7x*.

Tekscan, Inc (2007). *Sensor Model/Map: 5315*. Retrieved January, 2011, from http://www.tekscan.com/5315-pressure-sensor

Twede, D., & Selke, S. E. M. (2005). *Handbook of paper and wood packaging Technology*. Lancaster, PA: DEStech Publications, Inc. 517 pp.

Weigel, T. G. (2001). *Modeling the dynamic interactions between wood pallets and corrugated containers during resonance*. Ph.D. Dissertation, Virginia Polytechnic Institute and State University, Blacksburg, VA.

White, M. S. (2005). The effect of mechanical interactions between pallets and packaging on packaging costs. *Preshipment testing newsletter* (4), 18, 20, 22.

White, M. S. (2007). Systems based design Retrieved August 28, 2008, from http://www.whiteandcompany.net/systems-based.htm

White, M. S., & Hamner, P. (2005). Pallets move the world: the case for developing system based designs for unit loads. *Forest product journal*, 55(3), 8-16.

White, M. S., Rupert, R. L., & Clarke, J. W. (2006). *Unit load design short course*, The Department of Wood Science and Forest Products, Virginia Polytechnic Institute and State University, Blacksburg, VA.

White, M. S., Rupert, R. L., & Clarke, J. W. (2006). *Basic corrugated packaging and unit load design short course*, The Department of Wood Science and Forest Products Virginia Polytechnic Institute and State University, Blacksburg, VA.

Wilkinson, T. L. (1983). *Rotational Characteristics of Pallet Joints*. U.S.D.A. Forest Service, Forest Products Laboratory.

Yoo, J. (2008). *Quantitative Analysis of the Compressive Stress Distributions across Pallet Decks Supporting Packaging in Simulated Warehouse Storage*. M.S. thesis, Virginia Polytechnic Institute and State University, Blacksburg, VA.

APPENDIX A

Pallet deck deflections measured during unit load section compression testing

Table 1. Pallet deck deflection used to calculate M_A for the semi-rigid joint model

Replications	Deflection (in.)
3/4"_ Bottle_1	-0.011
3/4"_ Bottle_2	-0.023
3/4"_ Bottle_3	-0.008
3/8"_ Bottle_1	0.028
3/8"_ Bottle_2	0.021
3/8"_ Bottle_3	0.014
3/4"_ Empty_1	-0.022
3/4"_ Empty_2	-0.026
3/4"_ Empty_3	-0.021
3/8"_ Empty_1	-0.006
3/8"_ Empty_2	-0.002
3/8"_ Empty_3	-0.005
3/4"_ Flour_1	-0.012
3/4"_ Flour_2	-0.02
3/4"_ Flour_3	-0.011
3/8"_ Flour_1	0.021
3/8"_ Flour_2	0.012
3/8"_ Flour_3	0.007

APPENDIX B

Comparisons of predicted and measured compressive stress distributions

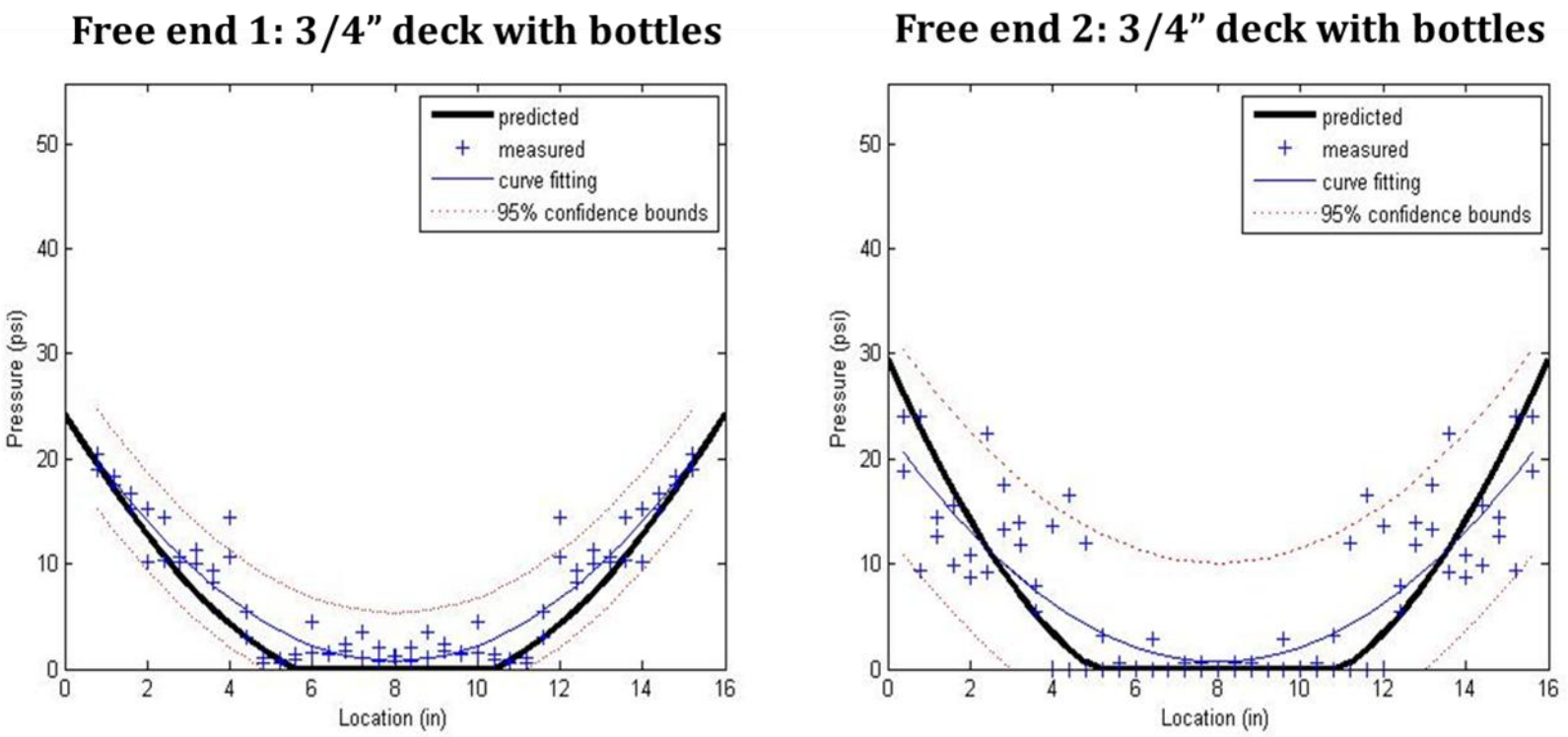

Figure 1.Validation of the predictive compressive stress distribution models for 3/4-inch free end deckboard with a box containing bottles using second-order polynomial fit with 95% confidence bounds

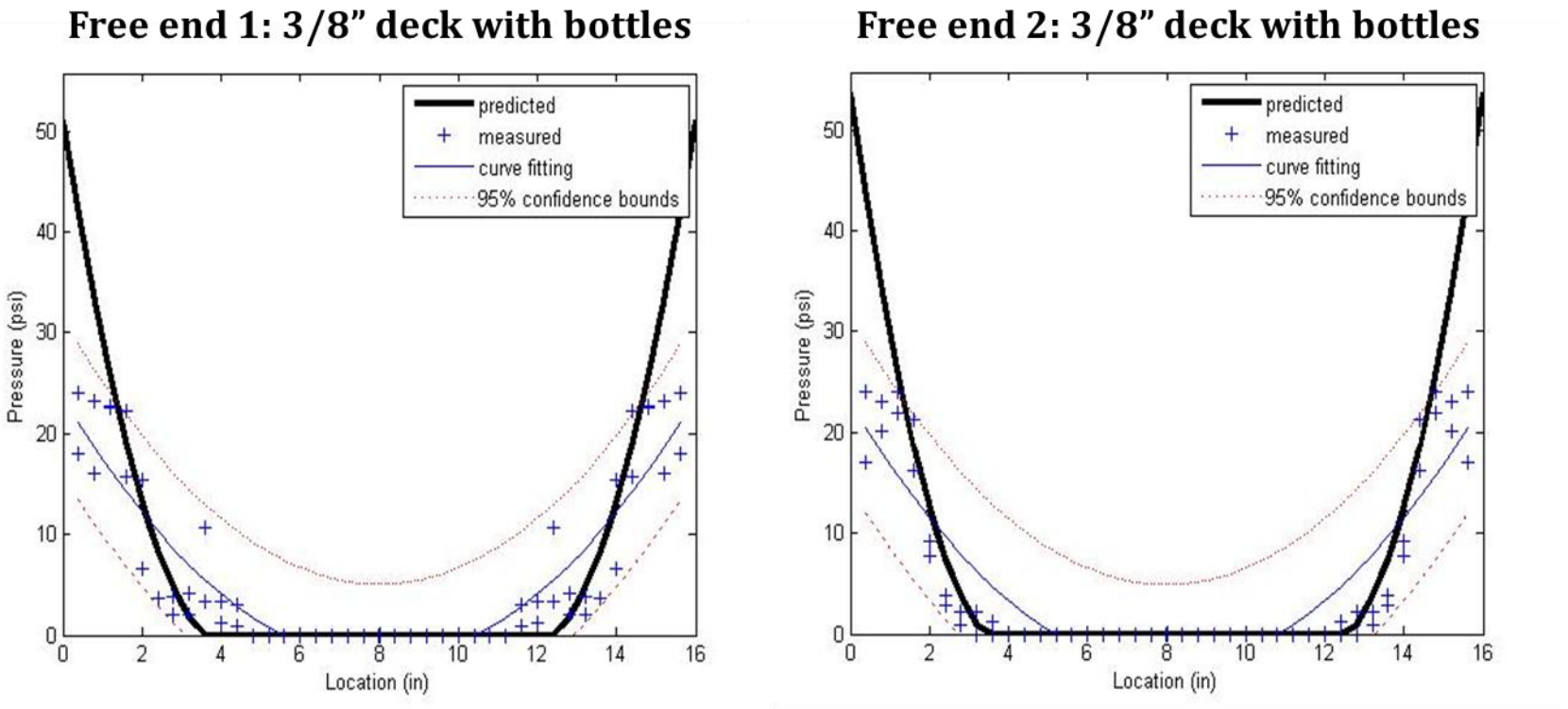

Figure 2. Validation of the predictive compressive stress distribution models for 3/8-inch free end deckboard with a box containing bottles using second-order polynomial fit with 95% confidence bounds

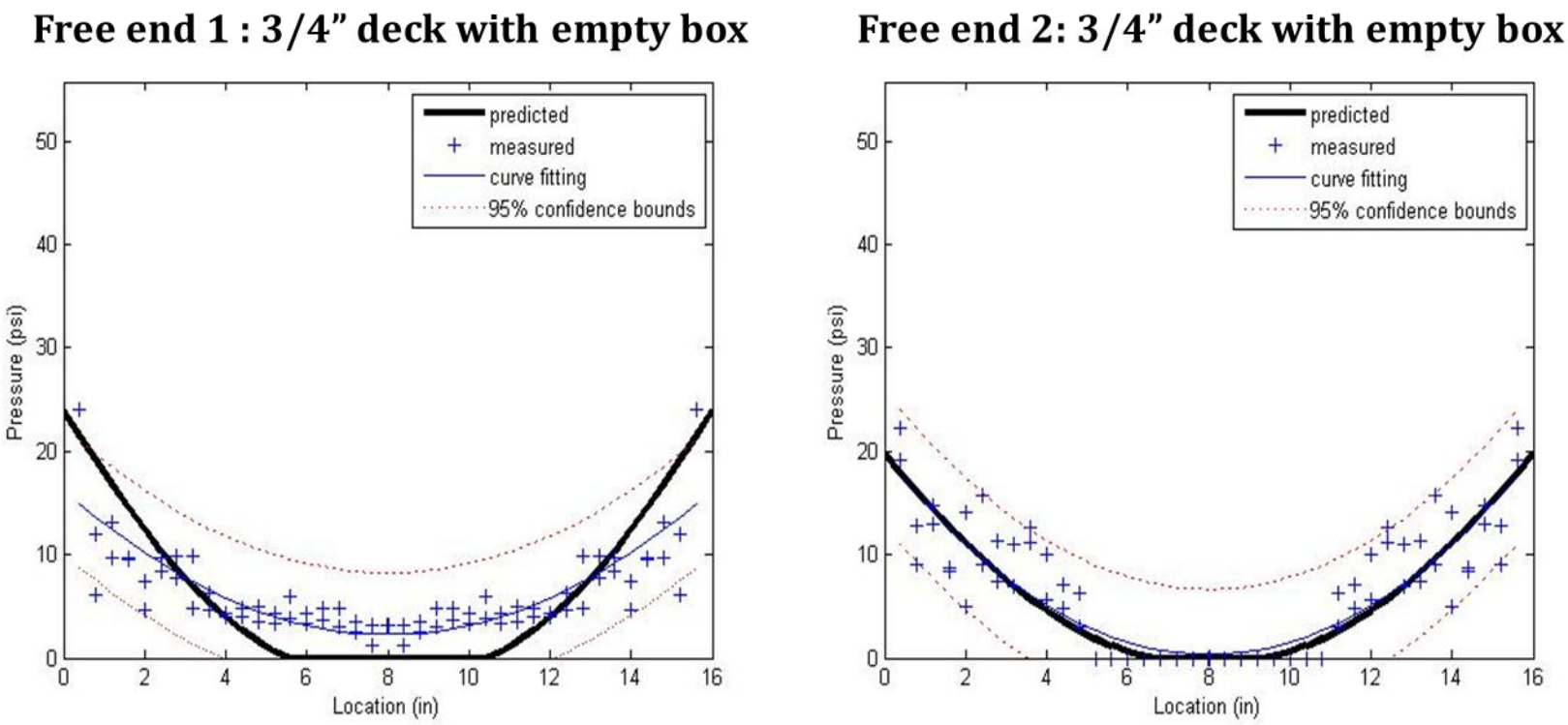

Figure 3. Validation of the predictive compressive stress distribution models for 3/4-inch free end deckboard with an empty box using second-order polynomial fit with 95% confidence bounds

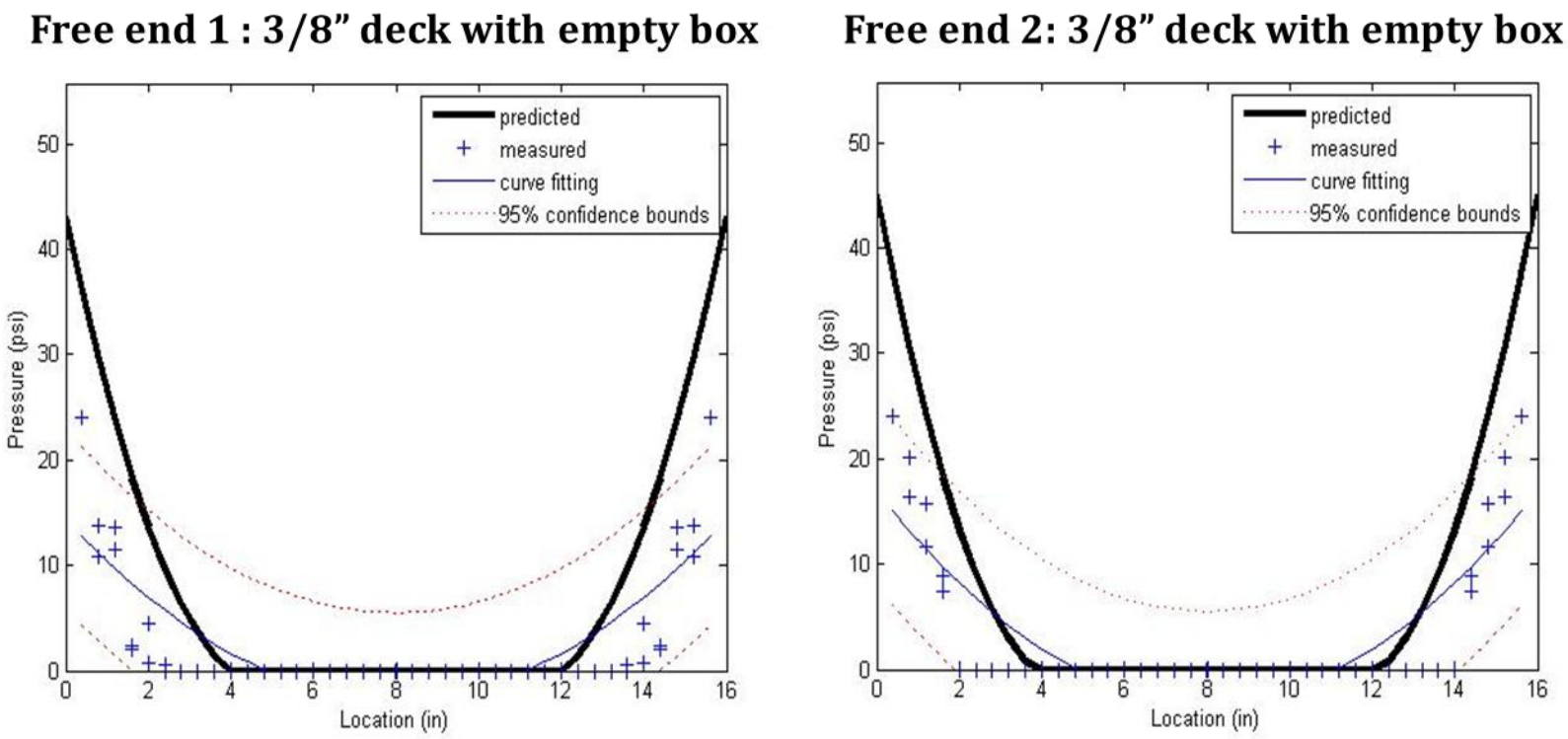

Figure 4. Validation of the predictive compressive stress distribution models for 3/8-inch free end deckboard with an empty box using second-order polynomial fit with 95% confidence bounds

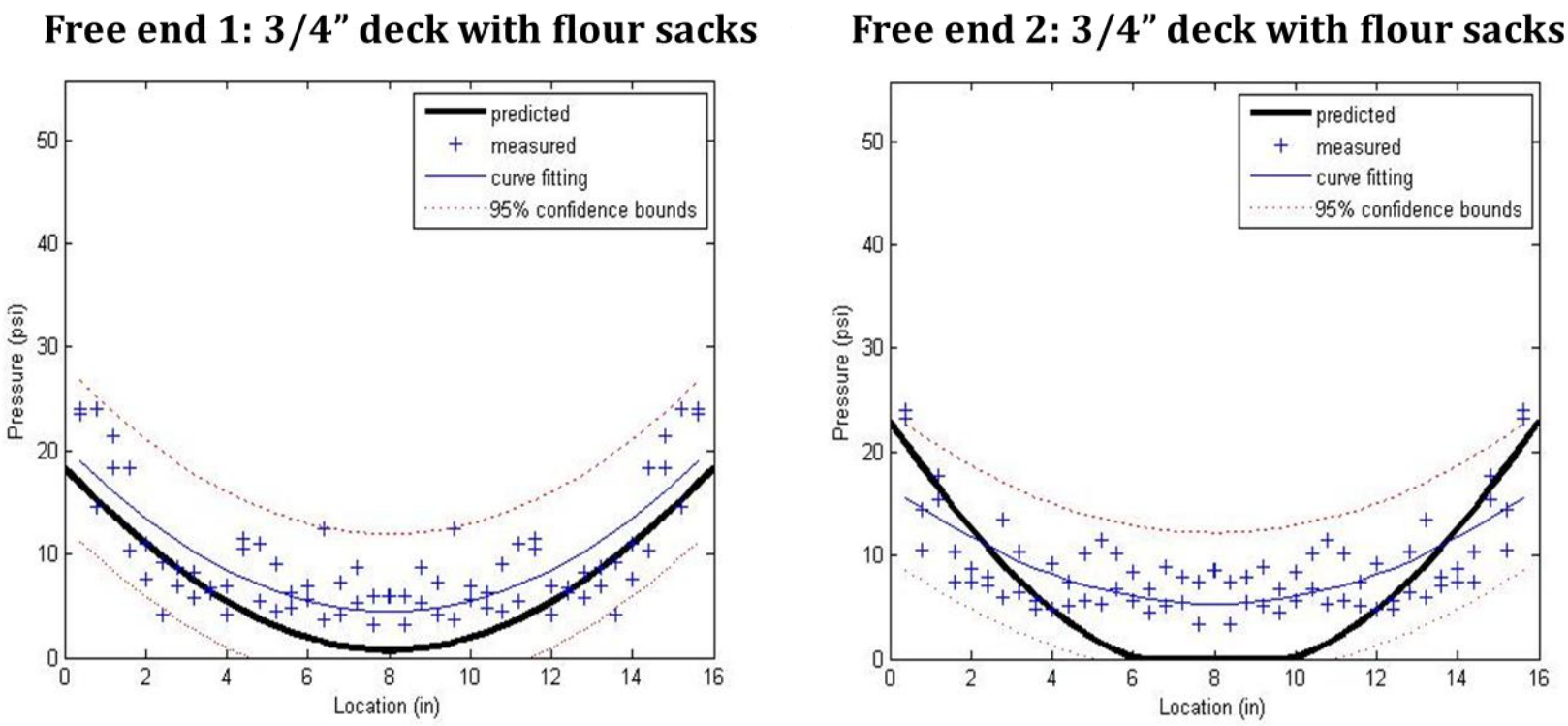

Figure 5. Validation of the predictive compressive stress distribution models for 3/4-inch free end deckboard with a box containing flour sacks using second-order polynomial fit with 95% confidence bounds

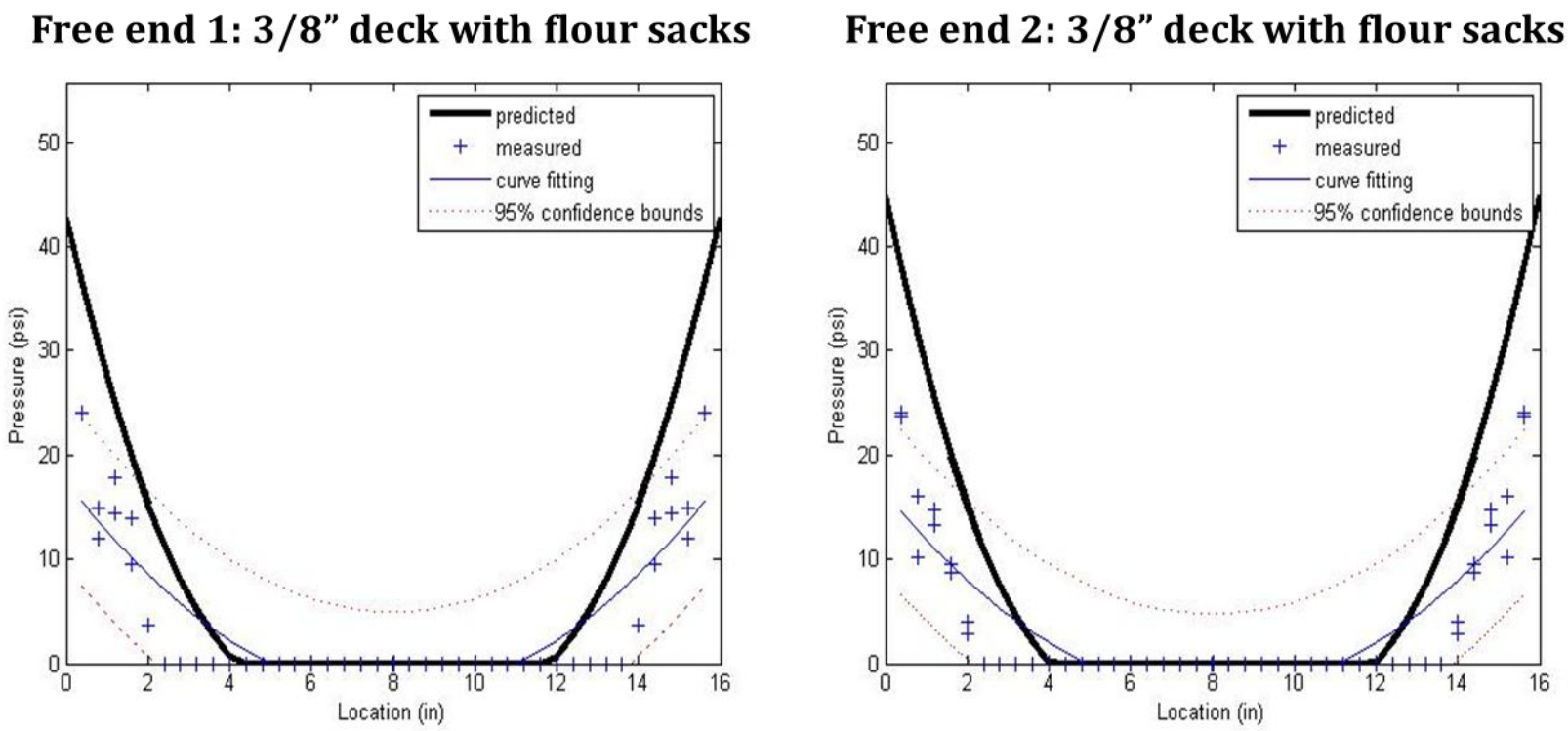

Figure 6. Validation of the predictive compressive stress distribution models for 3/8-inch free end deckboard with a box containing flour sacks using second-order polynomial fit with 95% confidence bounds

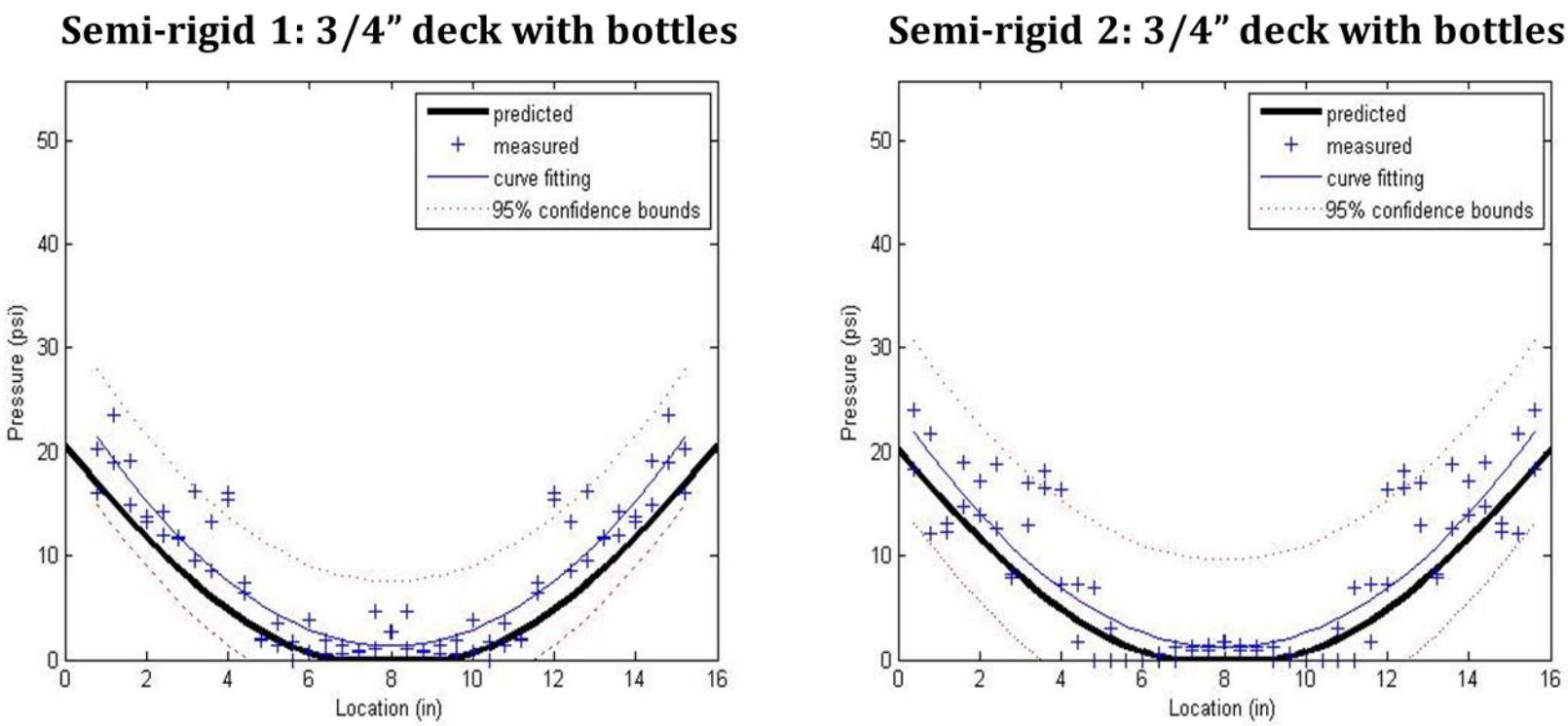

Figure 7. Validation of the predictive compressive stress distribution models for 3/4-inch semi-rigid joint deckboard with a box containing bottles using second-order polynomial fit with 95% confidence bounds

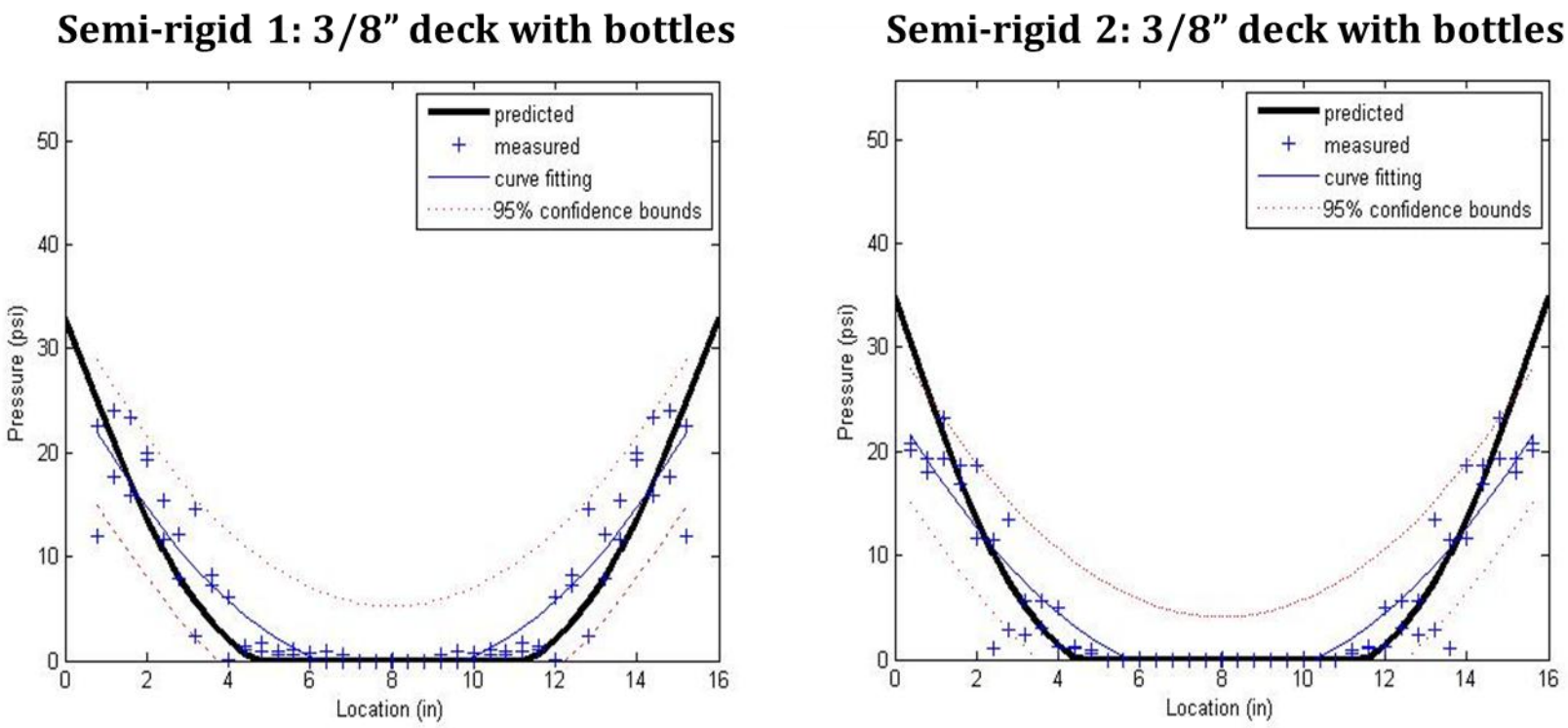

Figure 8. Validation of the predictive compressive stress distribution models for 3/8-inch semi-rigid joint deckboard with a box containing bottles using second-order polynomial fit with 95% confidence bounds

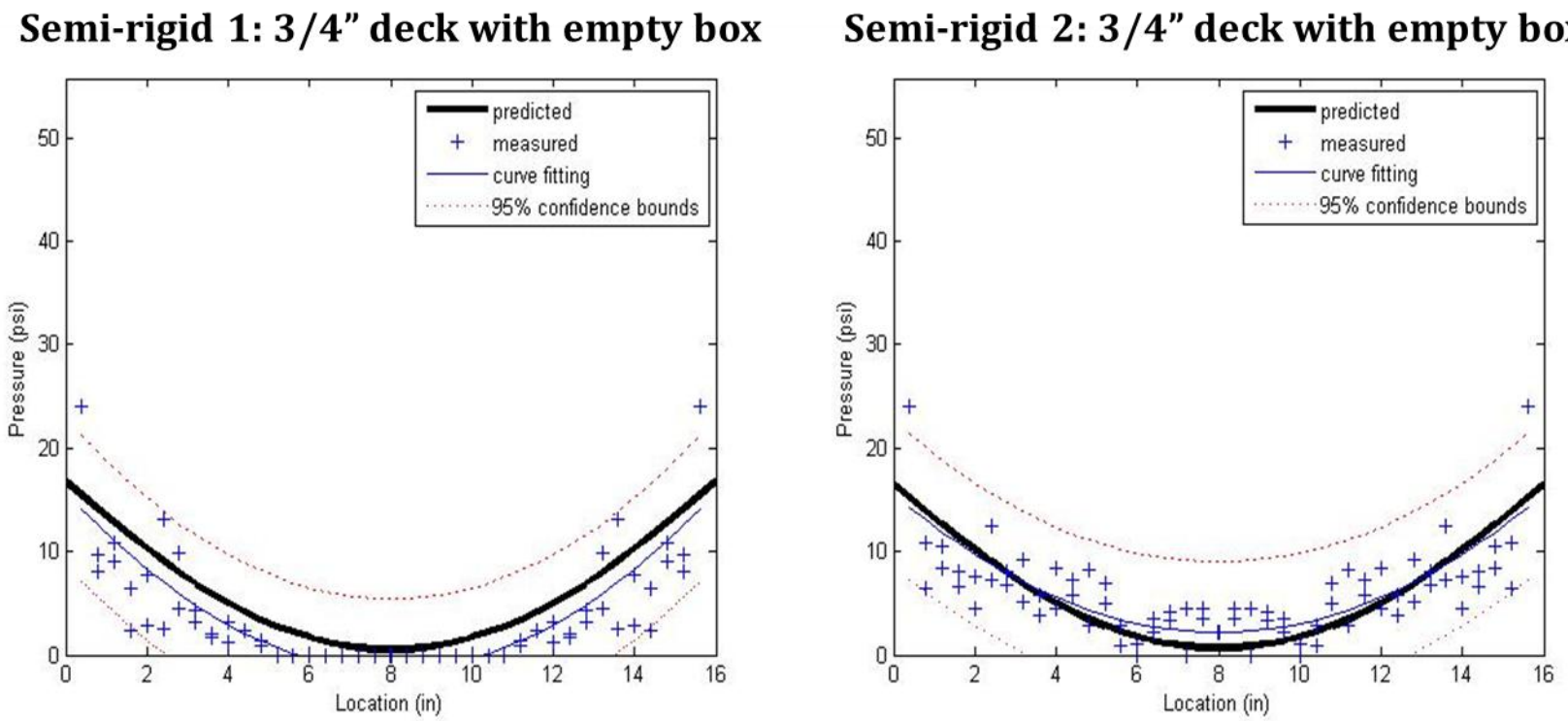

Figure 9. Validation of the predictive compressive stress distribution models for 3/4-inch semi-rigid joint deckboard with an empty box using second-order polynomial fit with 95% confidence bounds

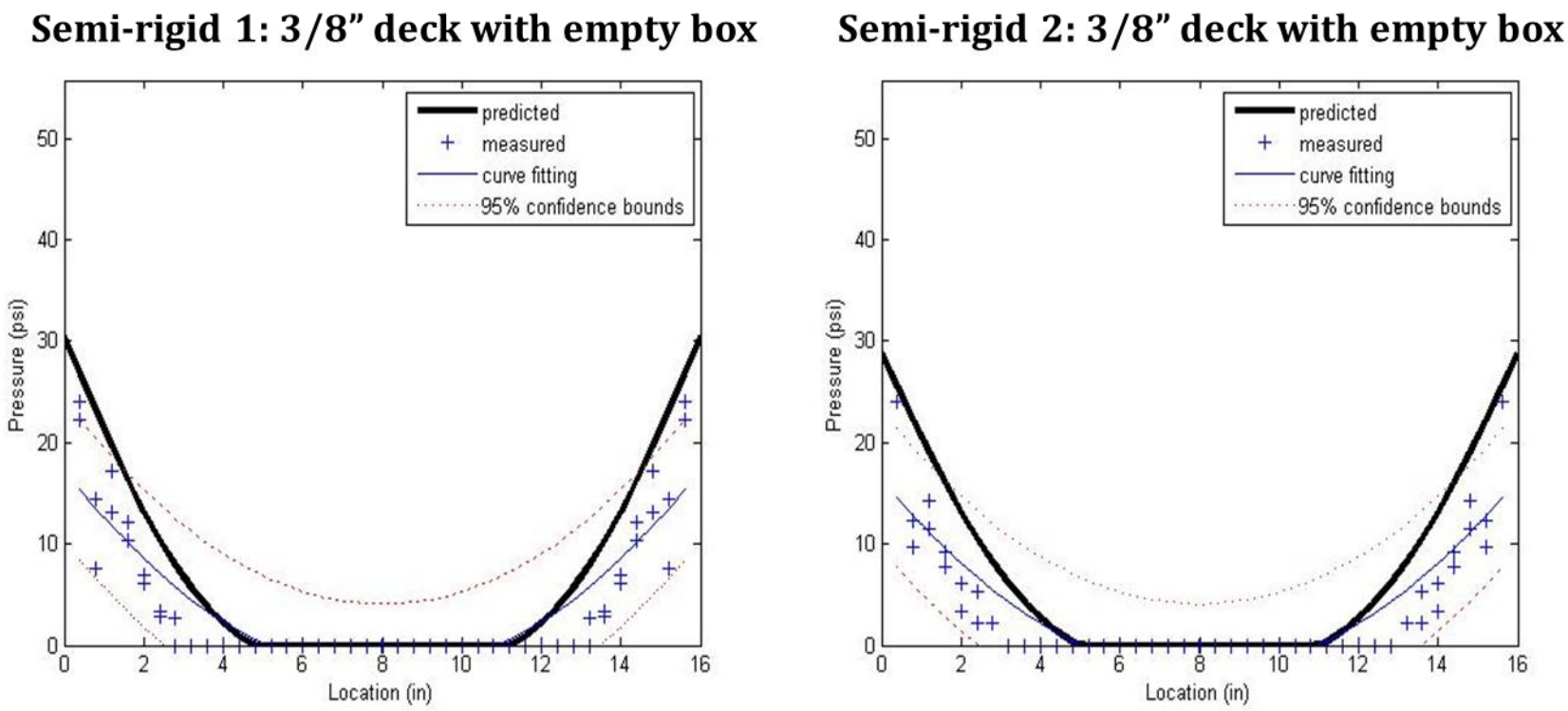

Figure 10. Validation of the predictive compressive stress distribution models for 3/8-inch semi-rigid joint deckboard with an empty box using second-order polynomial fit with 95% confidence bounds

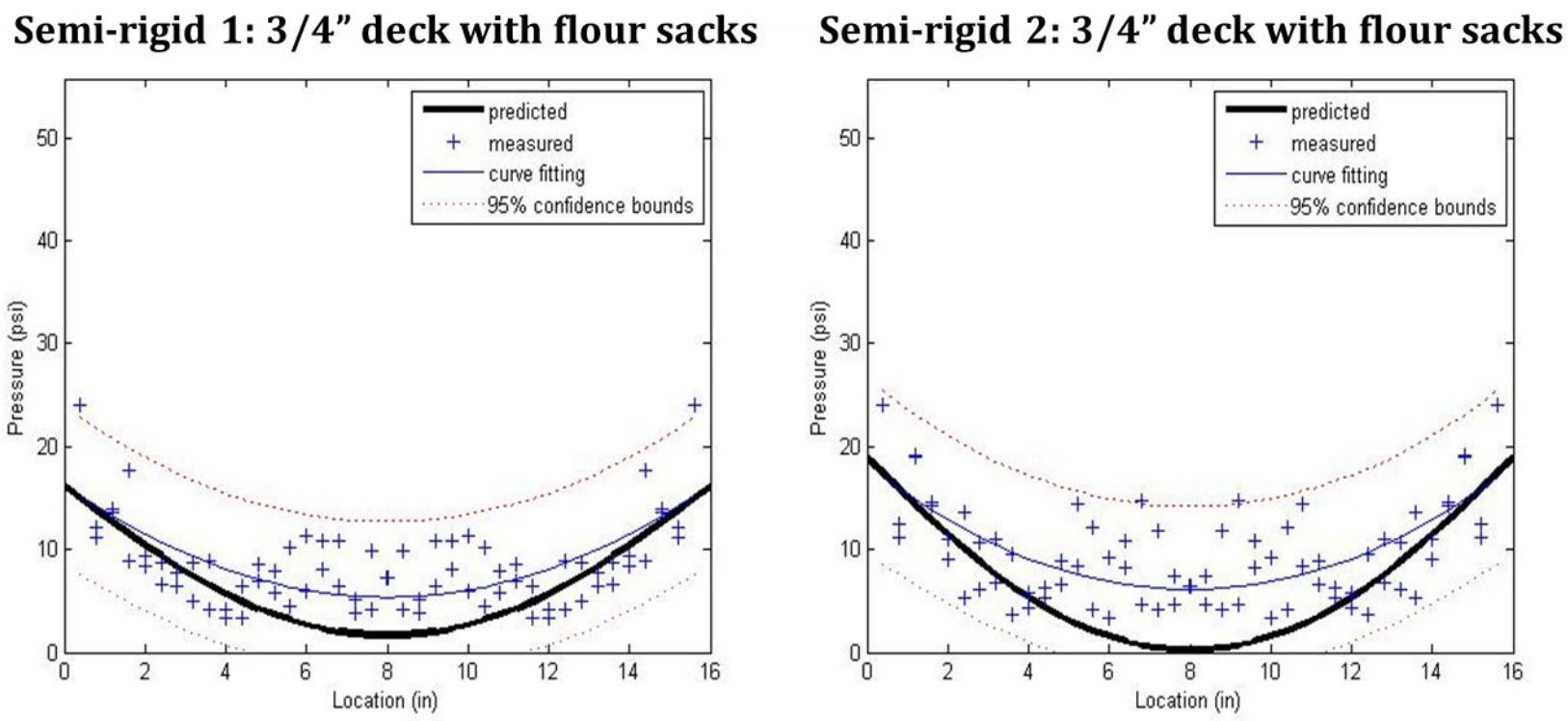

Figure 11. Validation of the predictive compressive stress distribution models for 3/4-inch semi-rigid joint deckboard with a box containing flour sacks using second-order polynomial fit with 95% confidence bounds

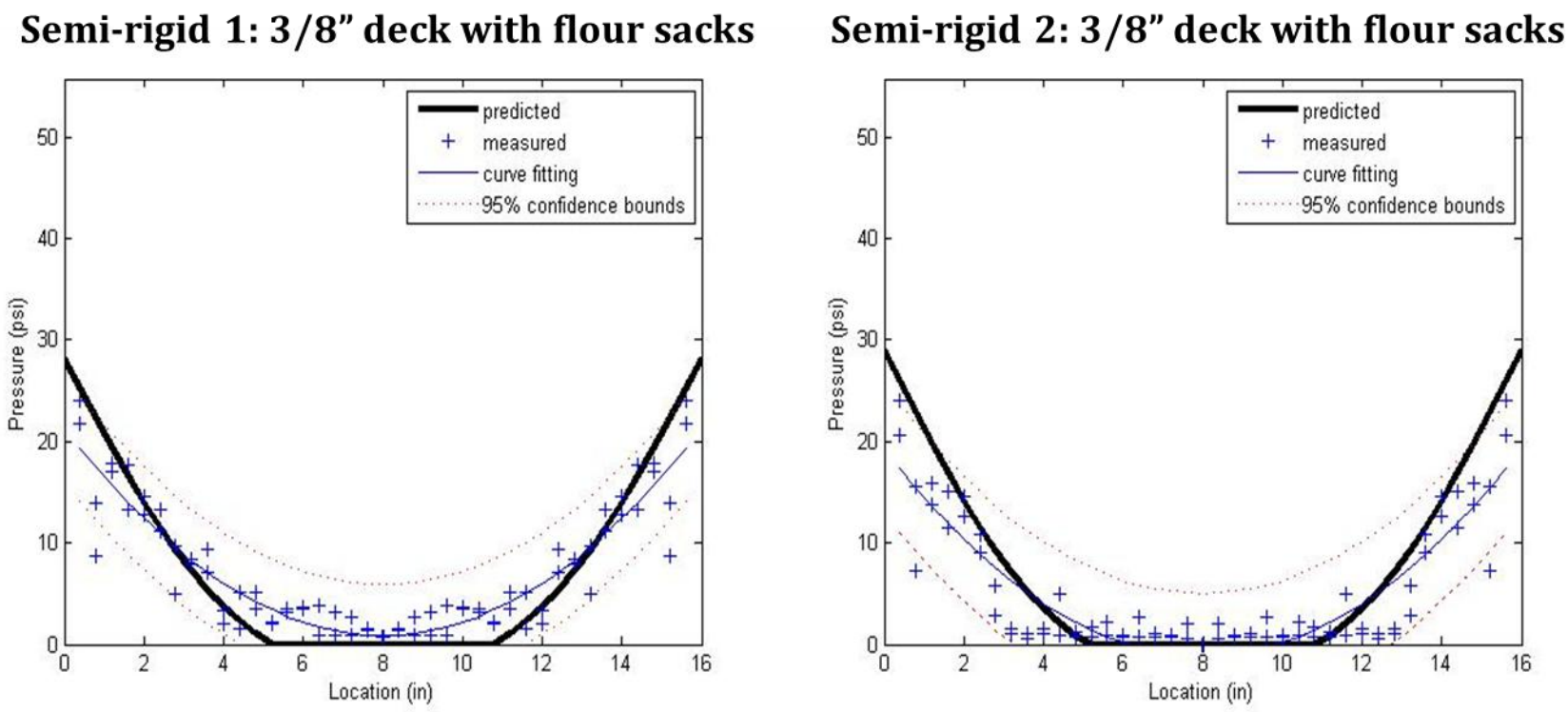

Figure 12. Validation of the predictive compressive stress distribution models for 3/8-inch semi-rigid joint deckboard with a box containing flour sacks using second-order polynomial fit with 95% confidence bounds

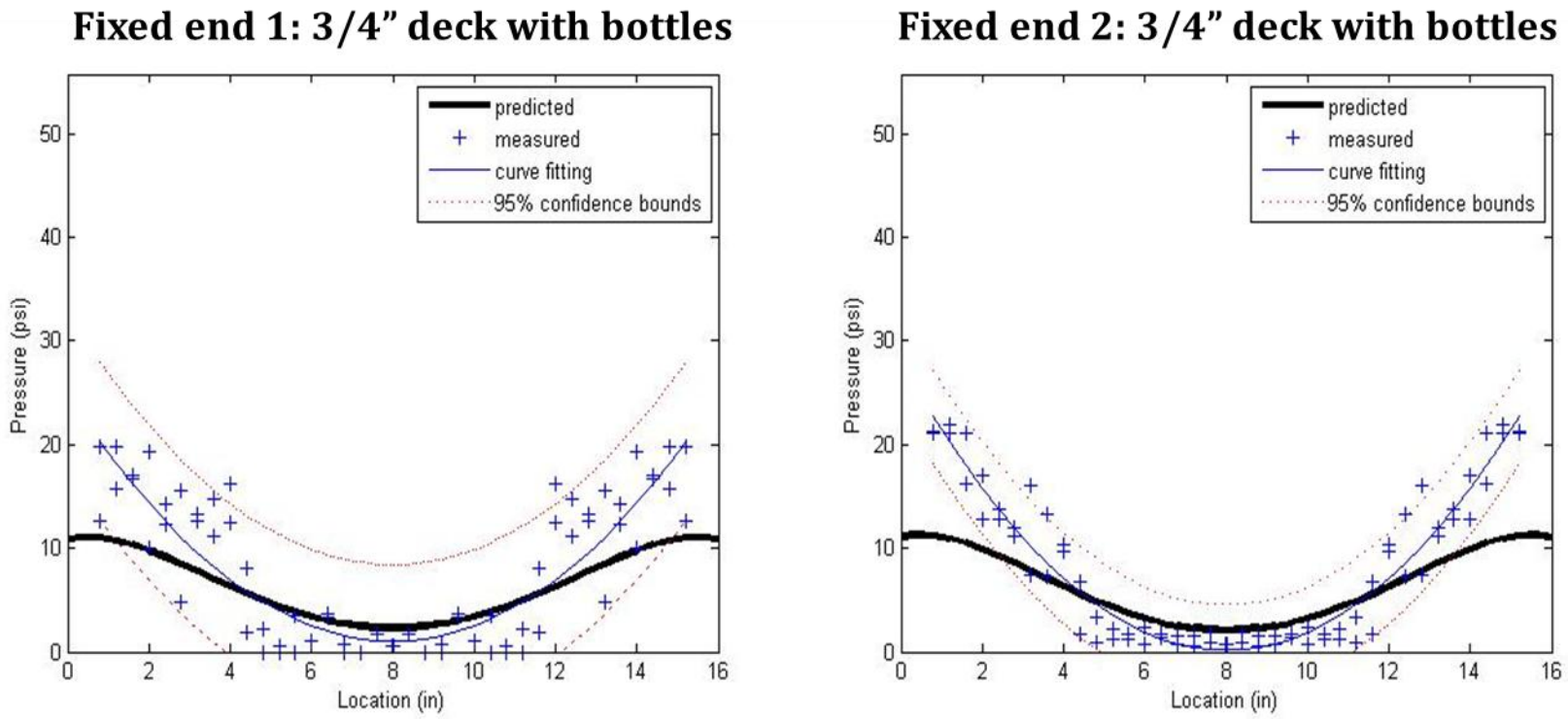

Figure 13. Validation of the predictive compressive stress distribution models for 3/4-inch fixed end deckboard with a box containing bottles using second-order polynomial fit with 95% confidence bounds

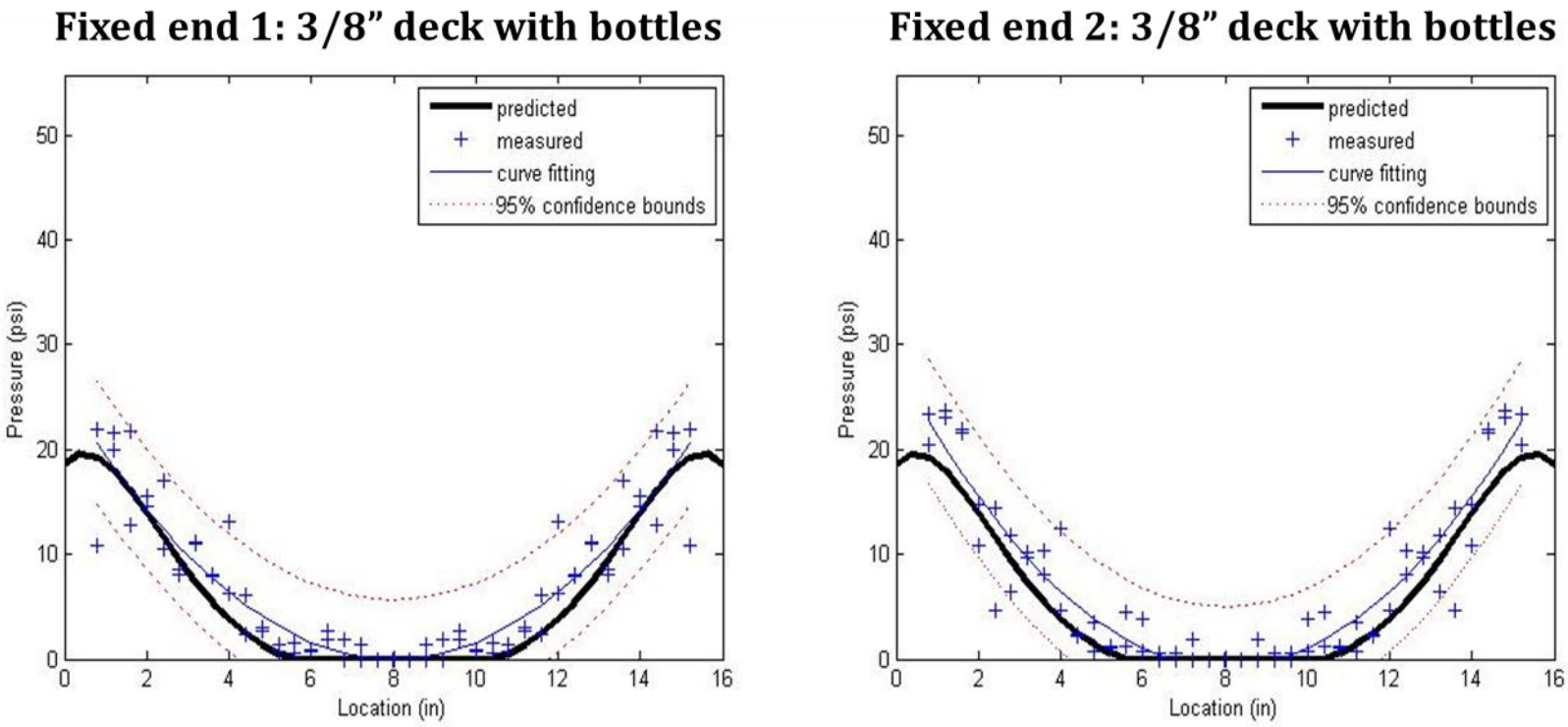

Figure 14. Validation of the predictive compressive stress distribution models for 3/8-inch fixed end deckboard with a box containing bottles using second-order polynomial fit with 95% confidence bounds

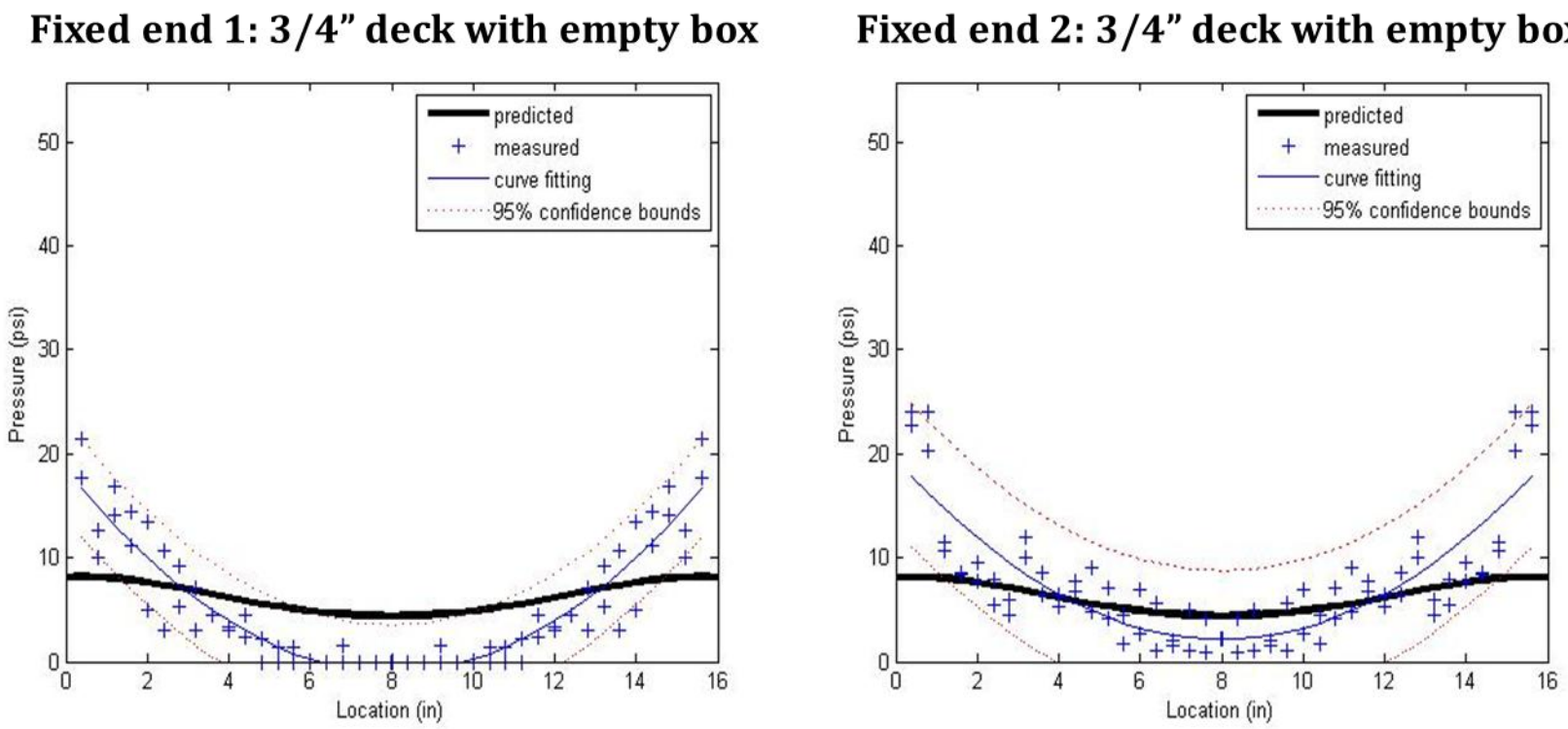

Figure 15. Validation of the predictive compressive stress distribution models for 3/4-inch fixed end deckboard with an empty box using second-order polynomial fit with 95% confidence bounds

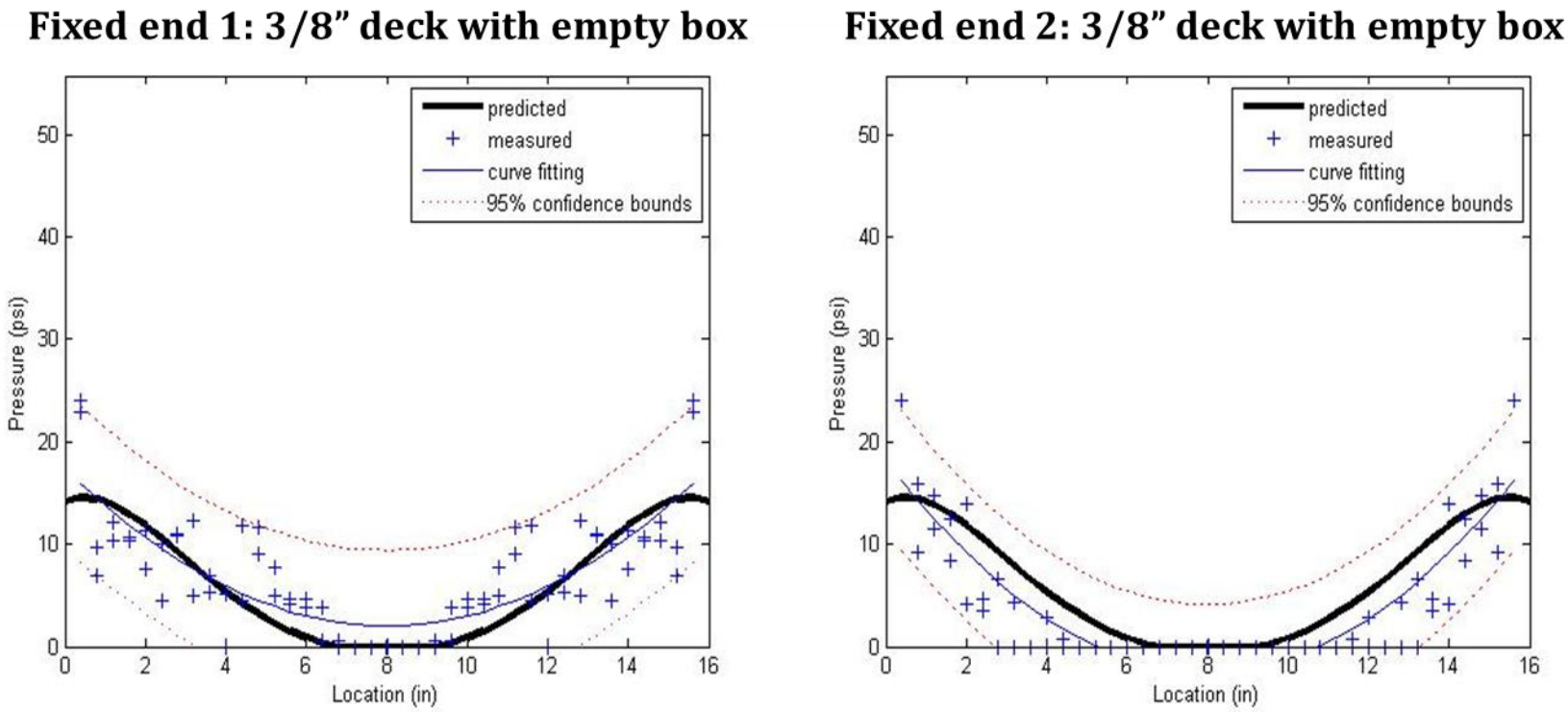

Figure 16. Validation of the predictive compressive stress distribution models for 3/8-inch fixed end deckboard with an empty box using second-order polynomial fit with 95% confidence bounds

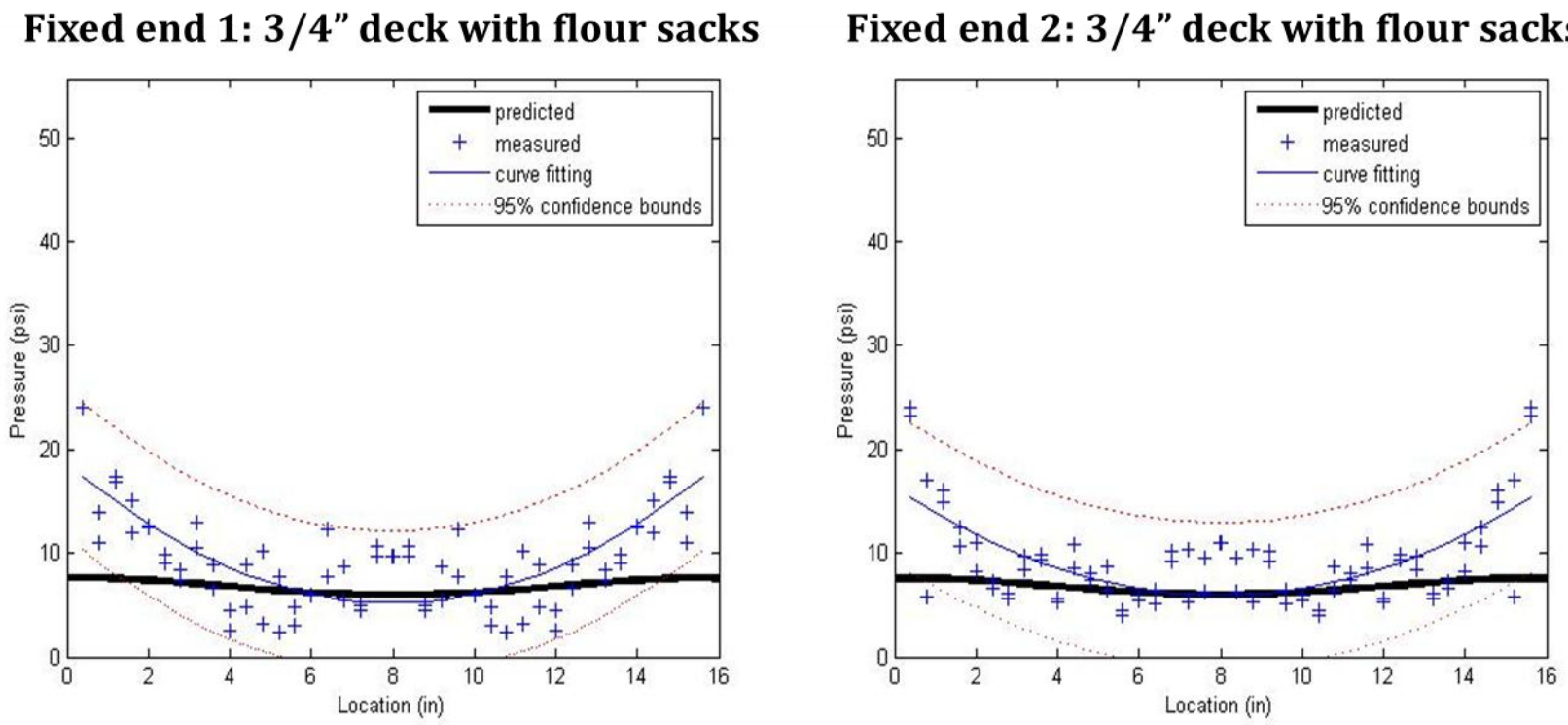

Figure 17. Validation of the predictive compressive stress distribution models for 3/4-inch fixed end deckboard with a box containing flour sacks using second-order polynomial fit with 95% confidence bounds

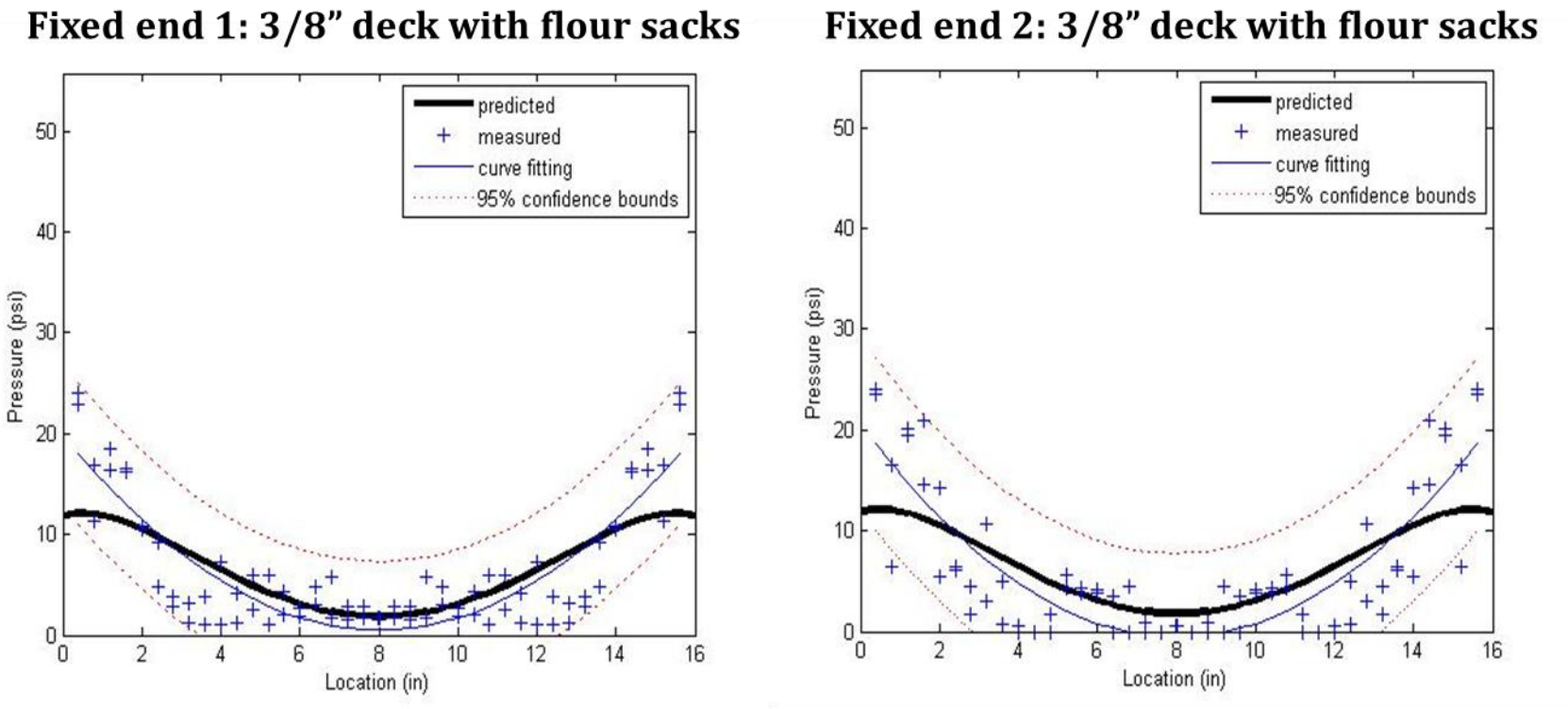

Figure 18. Validation of the predictive compressive stress distribution models for 3/8-inch fixed end deckboard with a box containing flour sacks using second-order polynomial fit with 95% confidence bounds